MOLECULAR DISSECTION OF SYNAPTIC REMODELING IN GABAERGIC NEURONS

By

Tyne Whitney Miller-Fleming

Dissertation
Submitted to the Faculty of the
Graduate School of Vanderbilt University
in partial fulfillment of the requirements
for the degree of
DOCTOR OF PHILOSOPHY
in
Neuroscience
May, 2017
Nashville, Tennessee

Approved:

Kendal S. Broadie, Ph.D.

David M. Miller, III Ph.D.

Donna J. Webb, Ph.D.

Randy D. Blakely, Ph.D.

Christopher V. Wright, D. Phil.

To my mother,

for her sacrifices, constant encouragement,

and unconditional love

ACKNOWLEDGMENTS

First, I would like to thank my mentor David Miller. Over the past six years, David has taught me not only to be a careful and thoughtful scientist, but also to be a kind and helpful colleague. His enthusiasm and curiosity are contagious and I can't imagine pursuing my degree in any other lab. I came into the Miller lab during a transitional period, and was able to overlap with several amazing people: Clay Spencer, Rachel Skelton, Cody Smith, Kathie Watkins, Tim O'Brien, Sarah Petersen, and Mallory Hacker all welcomed me into the lab in 2011. I thank you all for organizing our lab happy hours, teaching me all of the Miller lab traditions, and training me. I am so thankful for Siwei He and the following people that joined the lab over the next few years, including: my wonderful baymate Barbara O'Brien, our post-doc Lakshmi Sundararajan, and graduate students Andrea Cuentas-Condori, and Sierra Palumbos. I also thank my wonderful undergraduates (Allie Beers, Megan Gornet, Renzo Gutierrez, Stefanie Engert, and Patrick Meyers) and our lab technician Rebecca McWhirter. Lab movie nights, happy hours, and social events over these past few years have helped me keep my sanity. Before attending graduate school, I was a technician in Alissa Weaver's lab. This experience sparked my interest in research and convinced me that graduate school was the best option for my future. I thank Alissa and the the Weaver lab members for sharing their time and knowledge.

I thank the administrative staff of the Neuroscience Program, the Department of Cell and Development Biology, and the Program in Development Biology. Specifically, I want to acknowledge Roz Johnson, Mary Michael-Woolman, Beth Sims, Marc Wozniak, Susan Walker and Carol Johnson for all of their help throughout the years. The Program in Developmental Biology had the best weekly journal clubs and annual retreat, and I thank Chris Wright for devoting so much time to this program and the students in it. I am so thankful for my thesis committee members that were always asking the important questions and pushing me to be a better scientist,

Kendal Broadie, Randy Blakely, Donna Webb, and Chris Wright. I thank you all for not only serving on my committee, but for also being available and willing to meet and discuss my project. This research was driven by our amazing collaborators Janet Richmond and her student Laura Manning at the University of Illinois at Chicago, and Laura Bianchi and her graduate student Cristina Matthewman at the University of Miami. I thank you all for the extensive time and effort you contributed to this project. I immensely enjoyed our monthly Skype conversations. Additionally, I must acknowledge the NIH for my F31 funding and the Conte Center training grant, both of which made this research possible.

I want to acknowledge my friends from Evansville and Nashville. Graduate school has been difficult, but because of the love and support from those around me, this process has been made bearable. I thank my best friends from Indiana: Emily, Jenna, Catie, Belwood, Kellie, and Beth for always making me laugh. I also thank my wonderful friends from Nashville: Troy, Katie, and Collin. Happy hours with Allison and Mallory made the weeks feel shorter and I am thankful for their ongoing friendship.

Finally, I give my deepest gratitude to my family for all of their love throughout the years. My wonderful in-laws, Lisa and Phil, and my sister-in-law Natalie are so welcoming and I feel blessed to be a part of their family. I thank my Dad and stepmother, Bill and Anita, my grandparents Ralph, Donna, Robert, and my late grandmother Myrtie for their support. Also I thank my mother, Julia, for all of the sacrifices she made to guarantee that I had the best of everything in life. Lastly, I thank my husband, Nate, for showering me with love and support for the last eleven years. Thank you for being my best friend, for laughing at my corny jokes, and for letting me be the crazy dog lady that I always hoped to be. I look forward to our many adventures together.

TABLE OF CONTENTS

LIST OF TABLES

LIST OF FIGURES

CHAPTER I

INTRODUCTION

Introduction Overview

Neuronal circuits undergo extensive refinement during development, characterized by the formation and removal of synaptic connections. Stabilization of proper synaptic connections is critical for circuit architecture and information flow, and incorrect or redundant synapses are eliminated to produce the precise cellular connections that are characteristic of mature nervous systems. Studies of the vertebrate neuromuscular junction and central nervous system have defined some common characteristics in synapse refinement; the process is modulated by circuit activity and genetic programming; however, the molecular networks that connect circuit activity to refinement are largely unknown. Furthermore, synaptic refinement is also known to occur in invertebrate species, suggesting that the underlying mechanisms are conserved.

The work in this dissertation utilizes a genetically-controlled and activity-dependent synaptic remodeling paradigm in *C. elegans* to characterize novel pathways that mediate synapse stability and elimination. In the following **Introduction** sections, I provide a brief summary of neuronal circuit composition and plasticity. Next, I describe examples of synapse elimination from mammalian and invertebrate species, and introduce the Degenerin/Epithelial Sodium Channel (DEG/ENaC) family of proteins as regulators of synapse stability. In the final section, I present the GABAergic motor

neurons of *C. elegans* as a reliable and promising model to study conserved pathways that regulate synapse refinement.

Neural Circuit Refinement

Chemical synapses mediate neurotransmission

Neurons are highly polarized cells that receive information at dendrites and transmit signals via axons. Communication between two cells occurs when they make direct contact through gap junctions, termed electrical synapses, or at chemical synapses by secreting signals across a narrow extracellular cleft (Purves, Augustine, Fitzpatrick, Katz, LaMantia, McNamara & S. M. Williams 2001a). The presynaptic axons and postsynaptic cells have specialized protein machinery that mediates efficient communication. The presynaptic cell localizes synaptic vesicles (SVs) and dense core vesicles (DCVs), which contain neurotransmitters and neuropeptides, respectively (Purves, Augustine, Fitzpatrick, Katz, LaMantia, McNamara & S. M. Williams 2001a). Many proteins are required to mediate synaptic vesicle docking, priming, and fusion at the presynaptic membrane; including voltage-gated calcium channels (VGCCs) and SNARE proteins, which are described below (Südhof 2012). Juxtaposed to presynaptic compartments of the signaling cell, the receiving cell organizes receptor clusters to receive signals. Neurotransmitter-gated sodium and chloride channels, scaffold proteins, cell adhesion molecules, and signaling proteins (including kinases, phosphatases, and GTPases) are localized juxtaposed to sites of neurotransmitter release (Purves, Augustine, Fitzpatrick, Katz, LaMantia, McNamara & S. M. Williams 2001b; Purves, Augustine, Fitzpatrick, Katz, LaMantia, McNamara & S. M. Williams 2001a).

Coordination of pre- and postsynaptic function is required for efficient neurotransmission in conjunction with several trans-synaptic and extracellular proteins; however, this section will focus on the role of the presynaptic active zone.

The presynaptic density mediates synaptic vesicle release

Efficient neurotransmitter release requires a complex network of specialized proteins. The core proteins of the presynaptic active zone have been established and include Munc-13/UNC-13, RIM/UNC-10 (Rab3-interacting molecule), RIM binding proteins/RIM-BP, liprin(Lar-interacting-protein-related)-alpha/SYD-2, and ELKS/ELKS-1 (Augustin et al. 1999; Brose et al. 1995; Maruyama & Brenner 1991; Y. Wang et al. 1997; Y. Wang et al. 2000; Mittelstaedt & Schoch 2007; K. S. Y. Liu et al. 2011; Zhen & Jin 1999; Dai et al. 2006; Nakata et al. 1999; Monier et al. 2002; Ohtsuka et al. 2002; Y. Wang et al. 2002). These proteins are responsible for docking synaptic vesicles at the presynaptic membrane and mediating vesicle fusion. These core proteins control synaptic function by interacting with many other presynaptic proteins, including the vesicular and membrane-localized SNAREs (Soluble NSF Attachment Protein Receptors: including synatobrevin, syntaxin, and SNAP-25), local voltage-gated calcium channels, and the calcium sensor synaptotagmin (Malhotra et al. 1988; Bennett et al. 1992; Oyler et al. 1989; Südhof et al. 1989; Trimble et al. 1988; Perin et al. 1990; Brose et al. 1992; C. Li et al. 1995; Davletov & Südhof 1993; Geppert et al. 1994) In vertebrates, the Bassoon and Piccolo proteins are associated with active zones, whereas, invertebrates such as *C. elegans* and *Drosophila* encode SYD-1 (X. Wang et al. 1999; Fenster et al. 2000; Hallam et al. 2002; Patel et al. 2006; Owald et al. 2010)

Genetic and EM studies in vertebrate and invertebrates have provided clues into the organization of the core proteins into presynaptic active zone. The invertebrate rhoGAP (GTPase activating protein) SYD-1 is localized at the presynaptic membrane and mediates the localization of liprin-alpha/SYD-2 to the presynaptic density cell autonomously (Zhen & Jin 1999; Taru & Jin 2011; Yeh 2005; Watanabe et al. 2011). Active zone proteins RIM/UNC-10 and ELKS/ELKS-1 are recruited to the presynaptic density via this SYD-1/SYD-2 interaction (Dai et al. 2006; Patel & Shen 2009). RIM/UNC-10 proteins directly interact with the vesicular priming protein Munc-13/UNC-13 and bind to RAB-3 to dock synaptic vesicles (Weimer 2006; Gracheva et al. 2008). RIM/UNC-10 also recruits voltage-gated calcium channels to the active zone, and is therefore considered a central organizer of this complex (Kaeser et al. 2011; Südhof 2012). Direct interactions between RIM/UNC-10, RIM-binding proteins, and N- and P/Q-type voltage-gated calcium channels mediate calcium influx near docked vesicles to promote calcium-dependent fusion with the presynaptic membrane (Kaeser et al. 2011).

Although genetic work has revealed the core components that make up the presynaptic density, less is understood about how these proteins are trafficked to the synapse and how they are removed. Examination of individual active zone proteins was performed by mass spectrometry and FRAP analysis to determine the half-life of the proteins and the time spent in the active zone scaffolds, respectively (Cohen et al. 2013; Ziv & Fisher-Lavie 2014; Kalla et al. 2006; Tsuriel et al. 2009; Spangler et al. 2013). The half-life of both active zone and synaptic proteins was much longer than expected (hours to days); whereas, the duration of time these proteins spent in the active zone was shorter than expected (Petzoldt et al. 2016; Kalla et al. 2006; Spangler et al. 2013). These findings suggest that rather than eliminating the active zone proteins by

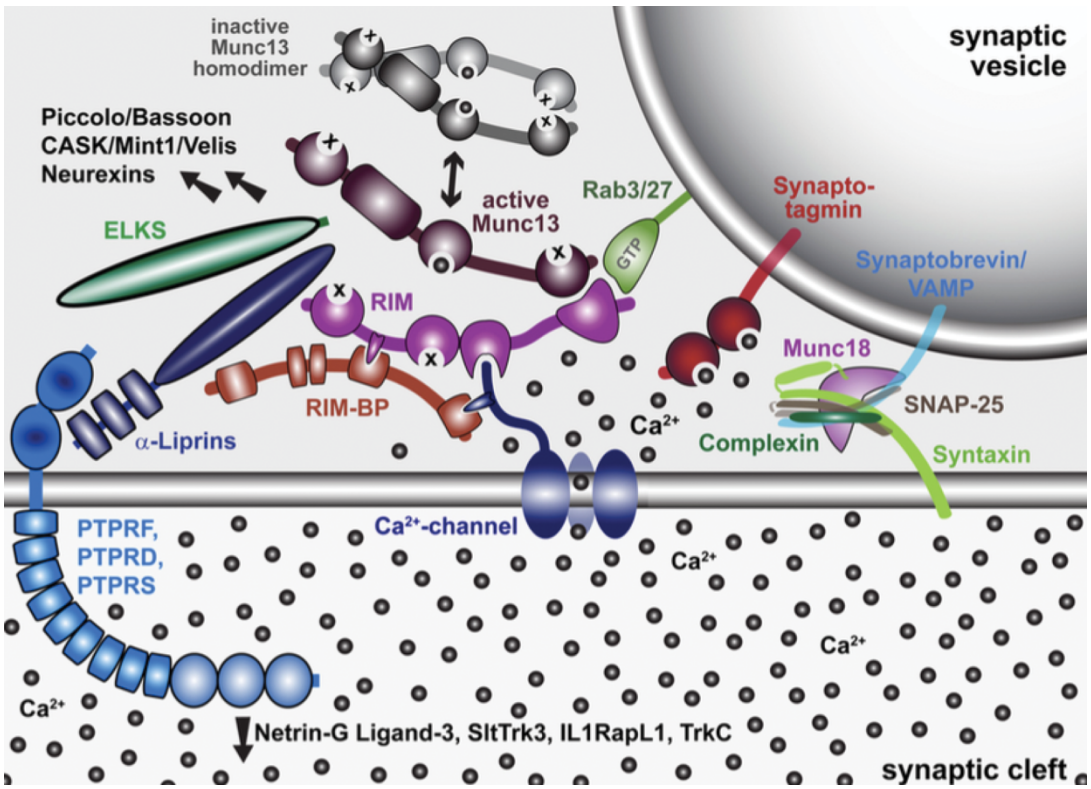

Figure 1.1: The Presynaptic Active Zone. The presynaptic density localizes synaptic vesicles near voltage-gated calcium channels with interactions between the core presynaptic density proteins, Munc-13/UNC-13, RIM/UNC-10, RIM-binding protein (RIM-BP), Liprin-alpha/SYD-2, and ELKS/ELKS-1. RIM directly interacts with the GTPase RAB-3 that is localized to the synaptic vesicles and this promotes vesicle docking. SNARE proteins (Synaptobrevin/SNB-1, Syntaxin/UNC-64, and SNAP-25/RIC-4) with interaction between Munc-18/UNC-18 and Complexin/CPX-1 mediate the zippering of the vesicular and presynaptic membrane upon activation of the calcium sensor synaptotagmin/SNT-5. **Original figure published by Thomas C. Sudhof *Neuron Review.* 2012.**

degradation, mechanisms likely exist to remove and recycle these proteins between a cytoplasmic pool.

The above experiments determining the turnover rate and occupancy rate of individual proteins in the presynaptic density were unable to address how these proteins are clustered into scaffolds. Work performed in *C. elegans* and *Drosophila* suggests that these clusters of protein scaffolds exist, as active zone scaffolds appear to be quantal (Kittelmann et al. 2013; Matkovic et al. 2013; Ehmann et al. 2015; Siebert et al. 2015). It is thought that two types of vesicles, PTVs (Piccolo-bassoon transport vesicles) and STVs (synaptic vesicle protein transport vesicles) migrate along axons to deliver presynaptic density and vesicular proteins to the active zone (Maeder & Shen 2011; Bury & Sabo 2016; Shapira et al. 2003; Dresbach et al. 2006; Maas et al. 2012; Ahmari et al. 2000; Sabo & McAllister 2003). Recent evidence suggests that these vesicular cohorts can also travel together and other trafficking vesicles may exist; therefore complicating our understanding of the components in each of these vesicles (Maas et al. 2012; Bury & Sabo 2011; Tao-Cheng 2007; Easley-Neal et al. 2013; Tang et al. 2013). Additional studies are needed to address which presynaptic density proteins are trafficked together and how turnover of individual proteins or scaffolded protein clusters are regulated during synapse maintenance and removal.

Identifying how the presynaptic active zone is regulated is critical for our understanding of synapse function. Both the size and molecular composition of the presynaptic active zone affect the functional output. Research in *Drosophila* shows that increasing the ELKS protein Bruchpilot strengthens evoked, rather than spontaneous neurotransmitter release (Peled et al. 2014). Consistent with this, postsynaptic currents are larger and faster when juxtaposed to presynaptic terminals expressing higher levels of ELKS, RIM proteins, or calcium channels (Paul et al. 2015; Matz et al. 2010; Holderith

et al. 2012). It remains unclear whether increasing the localization of these proteins is responsible for recruiting VGCCs to the active zone, thus leading to increases in calcium influx and vesicle release, or if the presynaptic proteins themselves are mediating enhanced neurotransmission (Petzoldt et al. 2016).

Functional output of the synapse is regulated not just by the quantity of presynaptic density proteins, but also by their type and localization. In *C. elegans* and *Drosophila,* the long and short isoforms of the vesicle priming protein UNC-13/Munc-13 (UNC-13L/Unc-13A and UNC-13S/Unc-13B, respectively) lead to functional differences depending on where they are localized at the synaptic terminal. UNC-13L drives fast neurotransmission; whereas, both UNC-13L and UNC-13S are required for slow release (Hu et al. 2013). The position of UNC-13 near VGCCs in the active zone regulates the timing and probability of synaptic vesicle fusion; furthermore, a recent study suggests that UNC-13L and UNC-13S are positioned at mature and immature synapses, respectively (Böhme et al. 2016). This localization is mediated by UNC-13L interacting with ELKS and Rim-binding proteins; whereas, UNC-13S is positioned at immature synapses by SYD-1 and SYD-2/liprin-alpha. Additionally, this study confirmed previous findings that differentially localized UNC-13L and UNC-13S affects neurotransmission; UNC-13L drives fast neurotransmission and is localized much closer to the VGCCs (K. Zhou et al. 2013; Böhme et al. 2016). Work at the *Drosophila* neuromuscular junction has also found that RIM-binding protein serves as a link between homeostatic plasticity and the release of synaptic vesicles (Müller et al. 2015). Collectively, these studies demonstrate a direct connection between the proteins localized to the presynaptic terminal and the functional output of the synapse.

Refinement is activity-dependent and controlled by genetic programs

Sculpting the nervous system requires the interplay between neuronal activity and genetic programming. Initial studies of synaptic pruning were performed at the vertebrate neuromuscular junction (NMJ), where individual muscle fibers initially receive inputs from several different axons. Competition between axons results in the pruning of less active inputs and stabilization of the most active input, resulting in each muscle fiber being innervated by a single axon. In one example of this, the biosynthetic enzyme required to generate acetylcholine, ChAT (choline acetyl-transferase) was genetically ablated in a subset of axons at the mouse NMJ. When competing with wild-type neuronal inputs, the ChAT-depleted inputs lost the competition to innervate (Buffelli et al. 2003). Interestingly, the competition of motor neurons is reversible and exogenous activation of weak inputs or blocking the strongest input can cause initially weaker motor neurons to be stabilized (Turney & Lichtman 2012; Walsh & Lichtman 2003; Antonini et al. 1998).

GABAergic signaling has been shown to play a critical role during the elimination of synapses in the brain. This was elegantly demonstrated in the visual system by Hubel and Wiesel 50 years ago. During development, inputs from both eyes are refined into segregated compartments in the visual cortex, called ocular dominance columns (Hubel & Wiesel 1963; Wiesel & Hubel 1963). Blocking the sensory input in one eye during a critical period of development, results in a loss of columns and blindness in the occluded eye. This outcome may only be reversed if the eye receives sensory input during the critical period (Hubel & Wiesel 1970). Additionally, it was found that this critical period, or time period of sensitivity, is mediated by GABA signaling; loss of the GABA biosynthetic enzyme suppresses the effects of monocular deprivation, likely because the critical

period does not initiate in the absence of GABA (Fagiolini & Hensch 2000; Hensch et al. 1998). Exogenous application of the ionotropic $GABA_A$ receptor agonist benzodiazepine rescues the effects of monocular deprivation (Fagiolini & Hensch 2000). Similar pruning defects are seen upon the loss of GABA synthesis and release in other models of plasticity; including in the cerebellum (Nakayama et al. 2012) and cortical interneurons (Wu et al. 2012), both of which result in the maintenance of redundant and improper connections.

Refinement of the visual circuitry is activity-dependent and occurs during defined stages of development; however, why certain circuits are sensitive to external stimuli and activity during critical periods is not well understood. Clues can be gathered from the work done in the mammalian visual system, which shows that in addition to GABA, other factors such as BDNF and Otx-2 initiate the onset of the critical period. BDNF, or brain neurotrophic factor is a growth factor that has been shown to induce precocious critical period onset by promoting the maturation of GABAergic neurons (Hanover et al. 1999; Z. J. Huang et al. 1999). A homeobox transcription factor otx-2 (orthodenticle homeobox-2) is thought to promote the initiation of plasticity by also promoting the maturation of GABAergic cells (Sugiyama et al. 2008). Although both BDNF and Otx-2 expression is activity-dependent, these proteins are widely expressed and therefore expression alone fails to explain how these proteins mediate refinement in specific brain regions (Lonze & Ginty 2002; Oray et al. 2004). This conundrum suggests that neuronal sensitivity to activity is likely driven by multiple temporally-regulated intrinsic cues, including transcription factors. In one example, UNC-55/COUP-TF (the chicken ovalbumin upstream promoter transcription factor), transcriptionally represses synapse remodeling in a subclass of GABAergic neurons in *C. elegans* (Shan et al. 2005; Walthall & Plunkett 1995; H. M. Zhou & Walthall 1998). Interestingly, the *Drosophila* and mammalian

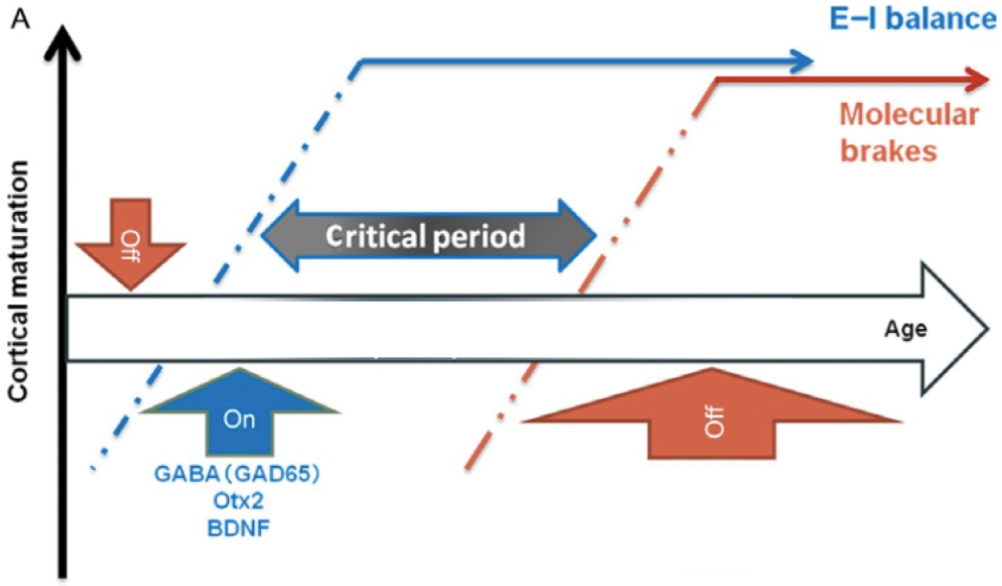

Figure 1.2: Synapse Refinement Occurs During Critical Periods of Plasticity. Onset of critical periods are blocked until postnatal development (red arrow, left). GABA signaling, BDNF, and Otx-2 expression drive the initiation of the critical period (blue arrow), which is thought to be achieved by promoting neuronal maturity and establishing a balance between excitation and inhibition (E-I balance). Expression of molecular brakes mediate the end of the critical period (red arrow, right). **Original figure published by: Anne E. Takesian and Takao K. Hensch *Progress in Brain Research.* 2013.**

homologs, Sevenup and COUP-TFI/COUP-TFII, also regulate the timing of neuronal development. COUP-TFI and COUP-TFII are expressed in subsets of GABAergic neurons and mediate the neuronal maturation and migration (Naka et al. 2008; Reinchisi et al. 2012); however, it remains unknown whether these proteins have conserved roles in regulating synapse stability.

Calcium signaling mediates synaptic strength

Alterations in pre- and postsynaptic neurotransmission require calcium signaling, such as long-term potentiation (LTP) and long-term depression (LTD) (Fukunaga 1993; Beattie et al. 2000). After an initial depolarization, postsynaptic NMDA (N-methyl-D-aspartate) receptors at excitatory synapses are activated, allowing the influx of sodium and calcium ions into the cell (Fukunaga 1993). If the presynaptic signal is stronger and more frequent, calcium and cAMP (cyclic adenosine monophosphate) can activate the kinases CaMKII (calcium/calmodulin-dependent protein kinase II) and PKA (protein kinase A), respectively, to mediate LTP (Fukunaga 1993). This results in the insertion of AMPA (alpha–amino–3–hydroxy–5–methyl–4–isoxazolepropionic acid) receptors into the postsynaptic membrane, which enhances neurotransmission and strengthens the synapse (Fukunaga 1993). Alternatively, low and less frequent calcium bursts activate the calcium and calmodulin dependent serine/threonine protein phosphatase calcineurin, which promotes the endocytosis of postsynaptic AMPA receptors and induces LTD (Beattie et al. 2000). Interestingly, CaMKII can also mediate LTD by phosphorylating T305/T306 on AMPA receptors (Pi et al. 2010), rather than T286, which facilitates LTP.

Calcium-mediated synaptic pruning has also been documented. In the mammalian cerebellum, several excitatory inputs from climbing fibers innervate each Purkinje cell, which are pruned during development to stabilize one synaptic connection

per cell (Hashimoto et al. 2011; Miyazaki et al. 2004). This process is GABA-dependent, and also requires the P/Q-type calcium channels (VGCCs) in the pre- and postsynaptic cells (Miyazaki et al. 2004; Hashimoto et al. 2011). Loss of the VGCC results in excess connections that result in behavioral deficits, suggesting that calcium influx through VGCCs mediates pruning (Miyazaki et al. 2004; Hashimoto et al. 2011). VGCC function is also important for mechanisms of homeostatic plasticity. Blocking postsynaptic glutamate receptors at the *Drosophila* neuromuscular junction drives enhanced vesicle release from the presynaptic neuron to maintain a steady level of neurotransmission (Frank et al. 2006). This effect requires expression of the presynaptic VGCCs and RIM-binding protein (Müller et al. 2012; Müller et al. 2015). These findings support a role for calcium influx through VGCCs and downstream calcium-mediated second messenger signaling pathways in synapse strengthening and elimination.

Synapse Elimination is a Conserved Feature of Neuronal Processes

Neural circuit refinement requires a balance between synaptic stabilization and elimination. Because neural circuits are typically established with too many connections, the pruning of redundant synapses is critical to build a functional nervous system. While much work has been done to uncover how synapses are formed, our understanding of synapse removal is still elementary; however, in humans it is thought that up to 40% of the initial connections made after birth are removed before adulthood, demonstrating the importance of synaptic pruning (Huttenlocher & de Courten 1987). Recent examples of synapse elimination are presented below, representing different models of synaptic plasticity. These distinct models share characteristics with the mechanism of GABAergic

plasticity we describe in this thesis, including a role for neuronal activity, the canonical cell death pathway, and the proteasome.

Cell death machinery and the proteasome drive synapse elimination

The cell death (CED) pathway eliminates unwanted cells in the developing nervous system; however, recent evidence suggests that apoptotic proteins may also regulate local synapse stability (Jiao & Z. Li 2011; Z. Li et al. 2010). CED activation can be induced by stimulation of a genetically encoded Mito-KillerRed, which results in the production of reactive oxygen species (Waldeck et al. 2011; Roy et al. 2010; Yang & Kimmelman 2011). Photo-activation of Mito-KillerRed in the cell soma of cultured rat hippocampal neurons triggers the apoptotic CED pathway and kills the neuron (Ertürk et al. 2014). Mito-KillerRed stimulation at hippocampal dendrites in these same cells restricts CED activation to the neurite process and triggers a local apoptotic response. Interestingly, this localized activation does not kill the neuron, rather it promotes elimination of dendritic spines (Ertürk et al. 2014). Local synapse elimination is mediated by the activation of the CED protein Caspase-3, consistent with the finding that Caspase-3 knock-out mice have more spines and enhanced synaptic strength (Ertürk et al. 2014). Additionally, local caspase activation appears to be restricted by proteasome activity; pharmacological block of the proteasome induces neuronal death in neurons where Mito-KillerRed is only activated in neurites distal to the cell soma (Ertürk et al. 2014). These studies provide a new role for apoptotic proteins and the proteasome during synapse elimination.

Studies in *C. elegans* have also established a role for the apoptotic pathway in synapse removal. Loss-of-function mutations in the CED pathway genes delay the

removal of GABAergic synapses from motor neurons (Meng et al. 2015). This pathway involves activation of the F-actin severing protein gelsolin via the canonical CED-3 (Meng et al. 2015). Furthermore, the Yan lab visualized fluorescently-tagged CED-3 and mitochondria at GABAergic synapses, consistent with the idea that local activation of the apoptotic pathway can mediate synapse turnover, without activating cell death (Meng et al. 2015). Because the Apaf-1 CED protein CED-4 and gelsolin bind calcium, and given the previously-established role for calcium in neurite pruning, the authors predict that calcium mediates this removal pathway (Hashimoto et al. 2011; Miyazaki et al. 2004; Yuan & Horvitz 1992; Z. Liu et al. 2011).

Local proteasome activity mediates synapse elimination

Although It is unclear what molecular mechanisms connect activity in the nervous system to the cellular constituents that physically dismantle synapses, one prediction involves the activity-dependent destabilization of synapses by the ubiquitin proteasome system (UPS) (Ehlers 2003; Colledge et al. 2003; Speese et al. 2003; Ding et al. 2007; Mabb & Ehlers 2010; Waites et al. 2005; Aravamudan & Broadie 2003). The proteasome regulates protein turnover by targeting proteins for proteasomal destruction by ubiquitin molecules. This process involves three enzymes: the ubiquitin-activating enzyme (E1), the ubiquitin-conjugating enzyme (E2), and the ubiquitin ligase (E3), which confers target specificity (Mabb & Ehlers 2010). Studies show that ubiquitination of both pre- and post-synaptic proteins occur at the synapse, and in certain instances this process requires neuronal activity (Colledge et al. 2003; Ehlers 2003; Speese et al. 2003; Ding et al. 2007; Mabb & Ehlers 2010; Waites et al. 2005; Aravamudan & Broadie 2003). A study in isolated vertebrate hippocampal neurons shows that in response to activity, the UPS

degrades PSD-95, a scaffolding protein in the postsynaptic cell and induces internalization of AMPA receptors, providing a connection between circuit activity, protein turnover, and molecular changes at the synapse (Colledge et al. 2003). Another study shows that Shank, GKAP and AKAP79/150 postsynaptic scaffolds selectively undergo activity-dependent ubiquitination (Ehlers 2003). Additionally, it was found that during synapse removal, distinct scaffolds of proteins are eliminated at different times, showing that differential regulation of groups of proteins play an important role in the process of disassembly (Culican et al. 1998). Examining the activity-dependent ubiquitination of presynaptic proteins has led to similar findings (Speese et al. 2003; Ding et al. 2007; Aravamudan & Broadie 2003). Studies at the *Drosophila* NMJ show that proteasome inhibitors strengthen synaptic transmission through up-regulation of a vesicular priming component DUNC-13 (Speese et al. 2003; Aravamudan & Broadie 2003).

A well-characterized model of proteasome-mediated synapse elimination occurs in *C. elegans.* The Hermaphrodite Specific Neurons (HSN) stimulate egg-laying by innervating vulval muscles (Shen & Bargmann 2003; Shen et al. 2004). During development, HSN forms redundant connections with muscle in “primary” and “secondary” synaptic regions. Prior to adulthood, the secondary synapses are removed, while the primary synapses are maintained (Shen & Bargmann 2003; Shen et al. 2004). Previous work found that the immunoglobulin superfamily proteins SYG-1 and SYG-2 are expressed in the HSN neuron and neighboring epithelial cells, respectively, and mediate the removal of secondary synapses (Shen & Bargmann 2003; Shen et al. 2004). The intracellular portion of SYG-1 was found to interact with the SKR-1 (Skp-1-Cullin-F-box) E3 ubiquitin ligase, which targets proteins to the proteasome for degradation (Ding et al. 2007). This finding is surprising because SYG-1 is enriched at

the primary synapse zone, suggesting that the SYG-1 interaction with SKR-1 protected primary synapses from elimination. It was determined that interaction of SYG-1 with SKR-1 at the primary synapse acts as a sink for SKR-1 activity, preventing it from interacting with the F-box adaptor protein SEL-10, and thus protecting this region from ubiquitination (Ding et al. 2007). Additionally, secondary synapses contain both SKR-1 and SEL-10, which mediate turnover of these synapses (Ding et al. 2007). In both the previously described cultured hippocampal neurons and in the HSN cells of *C. elegans*, the proteasome is utilized to restrict synapse elimination to distinct neurite regions (Ertürk et al. 2014; Ding et al. 2007). Interestingly, proteasome degradation in rat hippocampal cells degrades local caspases; whereas, the synaptic components themselves are thought to be targeted to the proteasome in the HSN cells. These findings confirm a conserved role for the proteasome during synapse elimination; however, they also raise the possibility that the proteasome is mediating removal by targeting different proteins in these different model systems.

Activity-dependent remodeling of active zone components

Neurotransmission can be strengthened and weakened by pre- and postsynaptic mechanisms. Typically, this is achieved by altering the amount and timing of synaptic vesicle release or by the insertion and removal of postsynaptic receptors, respectively (Ziv & Fisher-Lavie 2014). In the previous sections, evidence was provided that neuronal activity can regulate synaptic strength and the correlation between the molecular composition of the presynaptic complex and functional output was discussed. At *Drosophila* photoreceptor synapses, environmental cues have been shown to induce remodeling of specific active zone proteins, while other presynaptic density proteins are

unaffected (Sugie et al. 2015). In this paradigm, photoreceptors are exposed to low and constant light, which results in a loss of electron-dense T-bars, or presynaptic active zones by EM (Sugie et al. 2015). Interestingly, when the Tavosanis lab examined the localization of individual active zone proteins in these regions they found a loss of presynaptic Brunchpilot/ELKS-1, RIM-binding protein, and liprin-alpha; whereas, presynaptic voltage-gated calcium channels and SYD-1 were properly localized (Sugie et al. 2015). This mechanism required canonical Wnt signaling to destabilize presynaptic microtubules associated with Kinesin-3/UNC-104/Imac (Sugie et al. 2015). These findings are informative for two reasons: first, this study connects external environmental cues to the molecular stability of active zone proteins, which have a direct effect on synaptic output. Second, this work suggests that individual components of the presynaptic active zone are sensitive to activity-induced remodeling, while others are not. Because the organization and elimination of individual proteins in the active zone is not completely understood, these findings may help us begin to understand how the active zone is organized and stabilized.

Epithelial Sodium Channel (ENaC) Proteins in the Nervous System

Voltage-gated sodium channels are essential for the propagation of action potentials in the nervous system; however, less is understood about the role of neuronally-expressed voltage-independent sodium channels, such as the Degenerin/Epithelial Sodium Channels (DEG/ENACs). Here, I provide a brief summary of DEG/ENaC structure and function, and outline two examples in which these channels modulate synaptic stability.

Degenerin (DEG)/ENaC proteins are broadly expressed

DEG/ENaCs consist of homomeric or heteromeric trimers that are voltage-independent (Benson et al. 2002; Bianchi & Driscoll 2002; Jasti et al. 2007). This family includes diverse channel proteins that share a common structure, short intracellular N and C termini, two transmembrane domains and a large extracellular loop that is predicted to interact with the extracellular environment (Bianchi & Driscoll 2002). The term degenerin arises from the discovery that hyperactive DEG/ENaC proteins induce cell swelling and eventual neuron death. Degeneration in these cells can be rescued by blocking the channel by genetic manipulations or pharmacologically with the DEG/ENaC inhibitors Benzamil and Amiloride (Xiong et al. 2004; Zhang et al. 2008; Hong & Driscoll 1994). Initial studies of the degenerin channels were performed in *C. elegans*; however, these channels are found in both vertebrate and invertebrate species. In mammals, these channels are expressed broadly in epithelial tissues, including the kidney, respiratory, reproductive, and nervous systems (I. Hanukoglu & A. Hanukoglu 2016). ENaC function in the kidneys are thought to promote sodium resorption; whereas, ENaC expression in cilia mediate movement of gametes or mucus in the reproductive organs and during respiration, respectively (I. Hanukoglu & A. Hanukoglu 2016; Åstrand et al. 2015; Hernández-González et al. 2006; Darboux et al. 1998). Although ENaC proteins are expressed broadly in the nervous system, little is known about the function of these channels (Teruyama et al. 2012; Bianchi & Driscoll 2002).

Acid-sensing ion channels mediate neuronal plasticity

The DEG/ENaC protein family includes the acid-sensing ion channels, or ASICs, which are activated at low extracellular pH (Askwith et al. 2004; Benson et al. 2002).

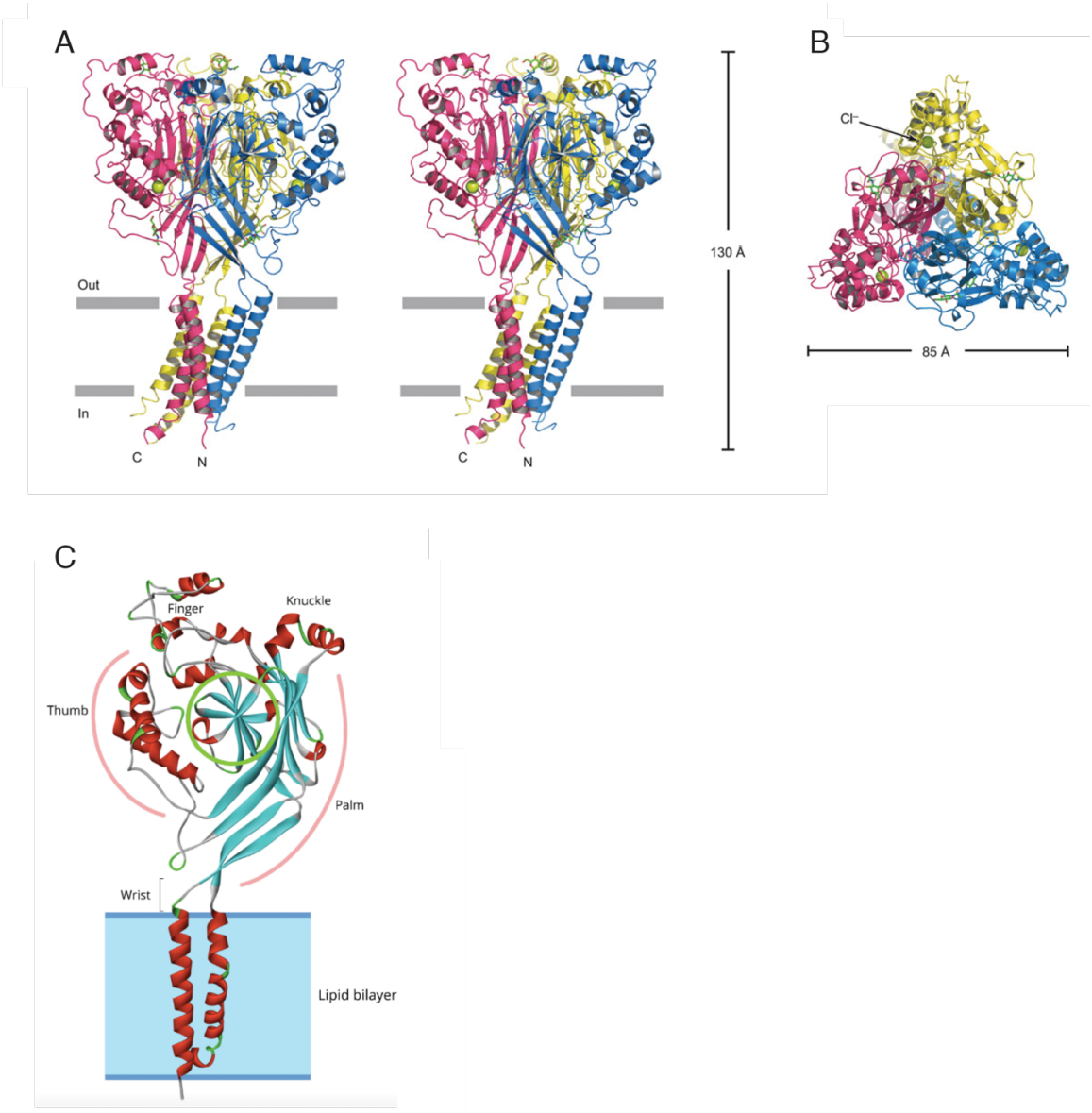

Figure 1.3: DEG/ENaC protein crystal structure. A. Side view of the chicken ASIC1 channel (crystal structure). Each of the three subunits of this homotrimeric protein are labeled in different colors (pink, yellow, and blue). **B.** Top view of the chicken ASIC1 channel, looking down on the extracellular side (subunits are pink, yellow, and blue). **Original figure panels A-B published by Jayasankar Jasti, Hiroyasu Furukawa, Eric B. Gonzales, and Eric Gouaux. *Nature.* 2007. C.** Ribbon diagram of the crystal structure of the chicken ASIC1 channel. Structural domains are listed (Thumb, Finger, Knuckle, Palm, and Wrist). These trimeric channels form a "clenched hand" structure. Alpha helices are red and beta-sheets are blue. **Original figure panel C published by Israel Hanukoglu and Aaron Hanukoglu. *Gene.* 2016.**

ASIC proteins are expressed throughout the nervous system and have been implicated in neuronal plasticity. Specifically, studies of ASIC1a mutant mice demonstrate learning deficits in tasks that are mediated by the hippocampus, amygdala, and cerebellum, suggesting that this channel may mediate plasticity in multiple brain areas (Wemmie et al. 2002; Wemmie et al. 2003; Ziemann et al. 2009).

The proposed mechanism for mammalian ASIC function during plasticity predicts that neurotransmitter release acidifies the synaptic cleft, activating postsynaptic ASIC proteins (Wemmie et al. 2006). Sodium and calcium influx through ASIC proteins propagates the presynaptic signal through depolarization of the postsynaptic membrane and by triggering downstream calcium-signaling, respectively (Wemmie et al. 2006). A similar mechanism was uncovered in *C. elegans*, in which the DEG/ENaC protein ASIC-1 is localized at presynaptic dopaminergic terminals and enhances neurotransmission in these cells (Voglis & Tavernarakis 2008). Sustained dopaminergic activity mediates an associative learning task, where animals avoid chemoattractants after learning to pair these chemosensory cues with starvation (Saeki et al. 2001; Voglis & Tavernarakis 2008). Loss of *asic-1* in the dopaminergic cells of these animals abolishes this response, suggesting that the role for ASIC proteins in mediating learning and memory is likely conserved across invertebrate and vertebrate species.

ENaC proteins in *Drosophila* promote plasticity

Synaptic strength is driven by the frequency and amplitude of presynaptic vesicle release and the number of postsynaptic receptors receiving these signals. Perturbations in either pre- or postsynaptic function can dramatically alter neurotransmission; therefore, to avoid permanent damage, neural circuits have established mechanisms to

adapt to these changes. One example of this is homeostatic plasticity, where presynaptic vesicle release in enhanced to compensate for the loss of postsynaptic function (Frank et al. 2006). A similar effect is seen when presynaptic vesicle release is decreased; upregulation of postsynaptic receptors compensates for the loss of presynaptic signals (Frank et al. 2006; Davis & Müller 2015). This phenomenon maintains a steady-state level of neurotransmission and supports a role for signaling across the synapse in both anterograde and retrograde directions. Homeostatic plasticity has been observed in several organisms, including *Drosophila,* mice, and humans, and can be maintained at individual synapses for weeks to years (Mahoney et al. 2014; Cull-Candy et al. 1980; Plomp et al. 1992; S. A. Petersen et al. 1997; Davis & C. S. Goodman 1998).

Maintenance of neurotransmission at the *Drosophila* neuromuscular junction requires the presynaptic expression and function of the degenerin/epithelial sodium channel (DEG/ENaC) proteins Pickpocket11 and Pickpocket16 (Younger et al. 2013). Loss of postsynaptic glutamate receptor function promotes the transcription of these pickpocket genes (Younger et al. 2013). The Davis lab proposes a model in which upregulation of presynaptic pickpocket channels depolarize the presynaptic membrane, resulting in activation of local voltage-gated calcium channels, which have previously been shown to mediate presynaptic homeostatic plasticity in this experimental paradigm (Frank et al. 2006; Younger et al. 2013). Calcium influx then mediates synaptic vesicle fusion through the calcium-dependent conformational change in synaptotagmin (Perin et al. 1990; Brose et al. 1992; Davletov & Südhof 1993; Geppert et al. 1994). These findings are the first to implicate DEG/ENaC family proteins in a presynaptic role driving neuronal plasticity. Additionally, these findings support the existence of the retrograde

signal endostatin from postsynaptic muscle cells, which is required for presynaptic homeostatic plasticity upon proteolytic cleavage (T. Wang et al. 2014).

The GABAergic Motor Circuit in *C. elegans* as a Model for Synaptic Remodeling

The nematode *C. elegans* is a small, transparent worm that has a simple well-defined nervous system consisting of 302 neurons. Work from the last 50 years has curated the *C. elegans* genome and neuronal connectome, providing the first model system with well-characterized synaptic connections that are preserved for every animal. Additionally, these animals are amendable to live imaging with the transgenic expression of fluorescent markers, allowing us to visualize dynamic synaptic connections in living animals. The neuromuscular junction in *C. elegans* includes the postsynaptic body wall muscles that receive excitatory input from the DA/DB and VA/VB classes of cholinergic neurons, which is balanced by inhibitory input from the GABAergic DD and VD neurons (White et al. 1986). A stringent balance between these systems is required for proper locomotion.

GABAergic Dorsal D (DD) motor neurons undergo a stereotypical synaptic remodeling process during early larval development (at first larval stage; L1). These cells have a ventrally-localized soma with a single process that runs anteriorly, crosses the body to form a commissure, and then runs posteriorly. Examination by electron microscopy revealed that DD neurons initially establish synaptic connections with ventral muscles, which are later removed and relocated to the dorsal nerve cord (White et al. 1986; Hallam & Jin 1998). Another class of GABAergic motor neurons, the Ventral D (VD) cells, do not remodel, suggesting there are intrinsic differences between these two

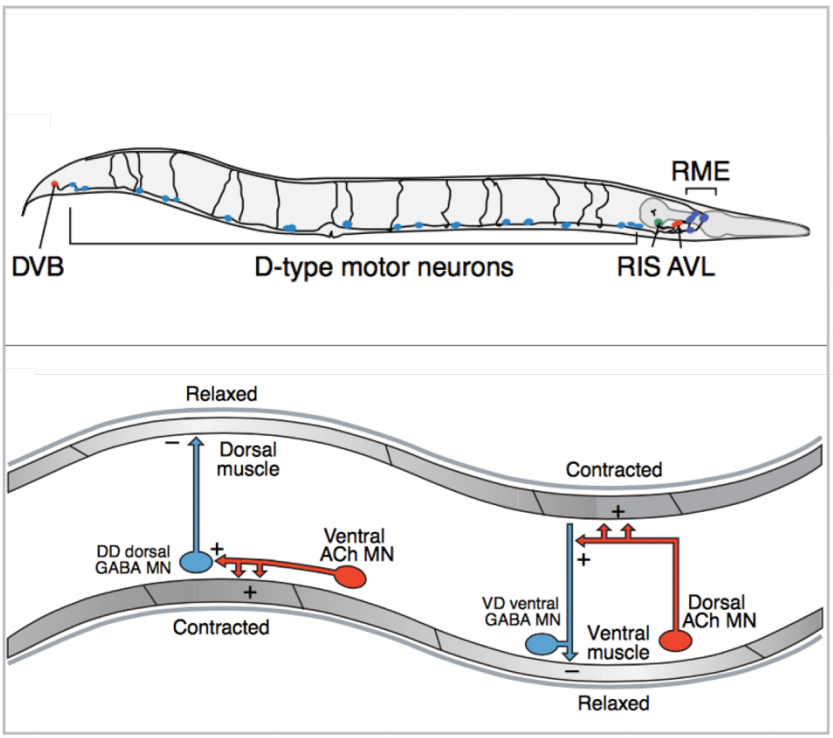

Figure 1.4: The *C. elegans* GABAergic Motor Circuit. Above: GABAergic D-type neurons are located along the ventral (ventral is down, anterior is to the right). DD and VD motor neurons and the GABAergic RIS head neurons are labeled in blue. Additional GABAergic head neurons, the RME and AVLs (excitatory) are labeled with purple and pink, respectively. The GABAergic DVB neuron is excitatory and located at the posterior end of the worm (pink). Below: Cholinergic and GABAergic motor neurons are required for coordinated locomotion in *C. elegans*. GABAergic neurons (blue) relax postsynaptic muscle cells, cholinergic neurons induce muscle depolarization and contraction on the opposite side of the animal. **Original figure published by: Kim Schuske, Asim A. Beg, and Erik Jorgensen. *Trends in Neurosciences.* 2004.**

cell types. The COUP/TFII (chicken ovalbumin upstream promoter) transcription factor UNC-55, which is most closely related to the Drosophila Seven-up protein, is expressed exclusively in VD GABAergic neurons (Shan et al. 2005). Loss-of-function mutations in *unc-55* result in ectopic VD remodeling, suggesting that the role of UNC-55 is to transcriptionally repress synaptic remodeling. This finding was verified by examining DD neurons ectopically expressing *unc-55*, which blocks DD remodeling (Shan et al. 2005; Walthall & Plunkett 1995; H. M. Zhou & Walthall 1998). Because of the disruption of the GABAergic/cholinergic balance, both of these mutations result in observable locomotor defects, including ventral coiling in *unc-55* loss-of-function animals; whereas, the *unc-55* gain-of-function animals coil dorsally (Walthall & Plunkett 1995). This plasticity paradigm can be used to identify novel regulators of synapse assembly and removal.

Genetic programs regulate GABAergic synapse reorganization

The Miller lab previously exploited the *unc-55* remodeling paradigm to detect novel regulators of synaptic remodeling (S. C. Petersen et al. 2011). Transcripts from wild type and *unc-55* mutant animals were immuno-precipitated and examined by microarray analysis. Transcripts that were enriched in *unc-55* mutants were predicted to be pro-remodeling genes and were further investigated by an RNAi suppression screen (S. C. Petersen et al. 2011). 19 conserved UNC-55 targets were validated, including the homeobox transcription factor Iroqouis/IRX-1. Homeodomain-containing proteins are required for patterning and embryonic development of the nervous system, among other organs (Gómez-Skarmeta & Modolell 2002; Cavodeassi et al. 2001). Knock down of *irx-1* delays DD remodeling and *irx-1* expression is sufficient to induce remodeling (S. C. Petersen et al. 2011).

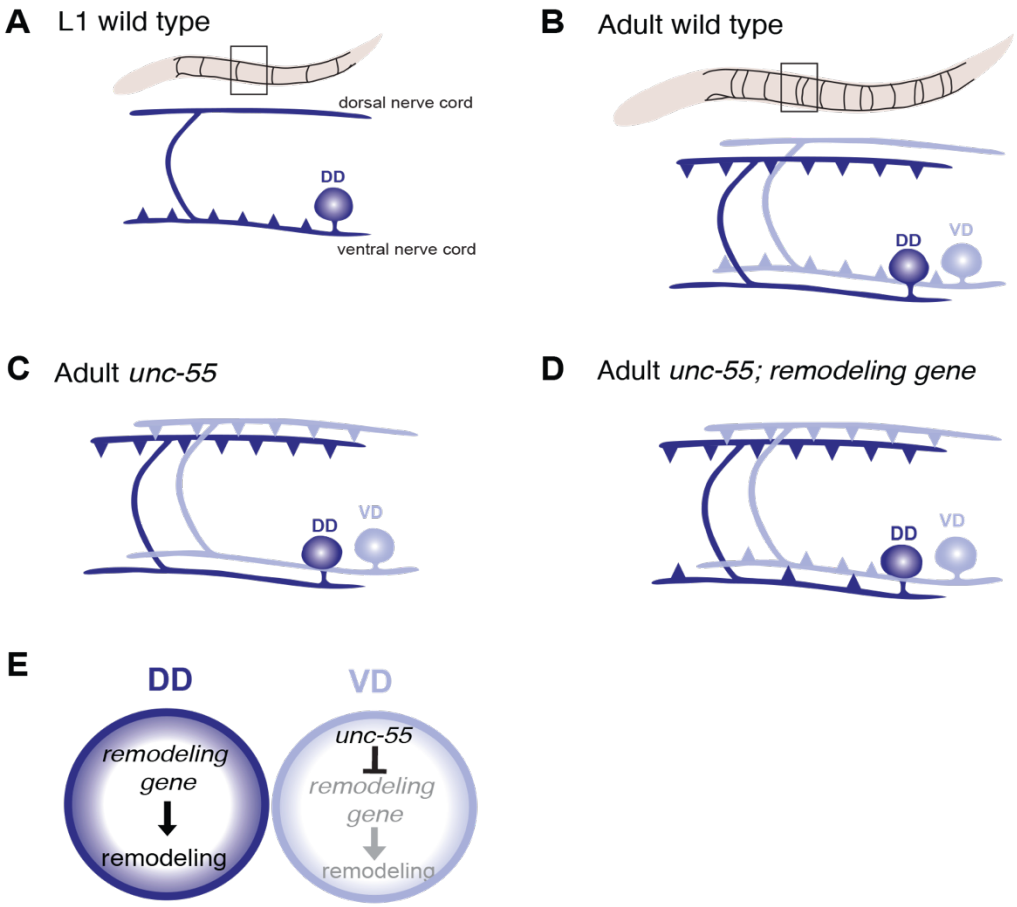

Figure 1.5: Synapse Remodeling in GABAergic Neurons. A. Dorsal D (DD) GABAergic motor neurons (dark blue) synapse with ventral muscles during embryonic development. **B.** DD synapses are relocated to dorsal muscles at the end of the first larval stage (L1). Ventral D (VD) GABAergic motor neurons (light blue) are generated in the late L1 and innervate ventral muscles. **C.** The COUP/TF transcription factor UNC-55 is expressed in VD neurons and blocks remodeling; VD neurons relocate synapses to the dorsal side in loss-of-function *unc-55* mutants. **D-E.** Expression of *remodeling genes* are negatively regulated by UNC-55 and RNAi knockdown of *remodeling genes* suppress ectopic VD remodeling in *unc-55* mutants. **Original figure by: Tyne Miller-Fleming and Sarah C. Petersen. *eLife.* 2016.**

In addition to IRX-1, several other transcription factors regulate the DD remodeling process. For example, the heterochronic gene *lin-14* dictates the onset of DD remodeling; *lin-14* mutants remodel precociously (Hallam & Jin 1998). In *C. elegans,* heterochronic genes like *lin*-14 function cell intrinsically to regulate the timing of development (Hallam & Jin 1998). HBL-1, the hunchback-like transcription factor, is also a heterochronic gene that has been implicated in DD remodeling downstream of the microRNA, *mir-84*. Hypomorphic *hbl-1* mutants delay DD remodeling and partially block *unc-55*-mediated ventral synapse removal (Thompson-Peer et al. 2012). Collectively, the *unc-55, irx-1*, *lin-14,* and *hbl-1* experiments demonstrate a crucial role for genetic programming in DD remodeling consistent with previous predictions that invertebrate models of plasticity are genetically hard-wired; however, in the subsequent sections of this dissertation, we provide evidence for neuronal activity in regulating DD remodeling as well (see Chapters 4 and 7).

Synaptic remodeling in *C. elegans* is activity-dependent

Mammalian models of synaptic plasticity have shown that neuronal activity works in conjunction with genetic programming to drive circuit rewiring. Genetic experiments analyzing the DD remodeling paradigm indicate this is also true in *C. elegans.* Loss-of-function mutations in the conserved synaptic vesicle fusion components UNC-13/Munc-13 and UNC-18/Munc-18 delay DD remodeling (Thompson-Peer et al. 2012). Additionally, the timing of DD remodeling is accelerated in the *tom-1*/tomosyn and *slo-1*/potassium channel loss-of-function mutants (Thompson-Peer et al. 2012). Under normal circumstances, TOM-1 antagonizes synaptic vesicle release, while SLO-1 potassium influx blocks postsynaptic depolarization (Fujita et al. 1998; Gracheva

et al. 2006; Kaczorowski et al. 1996; Gribkoff et al. 1997; Calderone 2002; Ghatta et al. 2006). Therefore, mutations in both of these proteins increase neuronal activity, and thus result in precocious DD remodeling (Thompson-Peer et al. 2012). These studies from the Kaplan lab establish a role for neuronal activity during remodeling, but do not identify the source of this activity. Animals with loss-of-function mutations in the GABA biosynthetic enzyme, glutamic acid decarboxylase (GAD/UNC-25) and the vesicular GABA transporter (VGAT/UNC-47) properly develop GABAergic synapses and have no effects on dorsal DD synapse formation, respectively (Thompson-Peer et al. 2012; Jin et al. 1999). However, these experiments failed to examine any effects on ventral DD synapse removal; therefore, GABA signaling cannot be completely ruled out. These findings demonstrate a common role for neuronal activity in driving synapse rewiring in vertebrates and invertebrates.

In recent studies, it was found that loss the the *nkcc-1* and *kcc-2* chloride transporters significantly delay DD remodeling (Han et al. 2015). The sodium-potassium-chloride- cotransporter-1 (NKCC-1) is expressed early in development and is thought to mediate the early depolarizing effects of GABA (Rivera et al. 1999). Later, expression of NKCC-1 is down-regulated and the potassium-chloride-cotransporter-2/KCC-2 is upregulated to promote hyperpolarization by GABA (Yamada et al. 2004). These transporters determine whether GABA signaling is excitatory or inhibitory by altering the intracellular and extracellular levels of chloride ions. During mammalian development, there is a switch in the outcome of GABA signals from excitatory to inhibitory, which coincides with the differential expression of chloride transporters (Rivera et al. 1999; Yamada et al. 2004; Blaesse et al. 2009). Although *C. elegans* also appear to exhibit this switch in chloride transporter expression, it is unclear whether GABA functions as an excitatory cue in early development (Han et al. 2015; Tanis et al. 2009; Bellemer et al.

2011). However, loss-of-function mutations in the *nkcc-1* and *kcc-2* chloride transporters do elicit DD remodeling delays, suggesting that GABA signals may regulate the timing of this process.

Circuit refinement at the developing vertebrate neuromuscular junction is thought to be partially mediated by competition between neighboring inputs (Lo & Poo 1991). Experiments at the frog and mouse neuromuscular junctions found that innervation of a single muscle fiber by multiple axons is reduced during development to stabilize a single input (Purves & Lichtman 1980; Lichtman & Purves 1983; Lo & Poo 1991; Turney & Lichtman 2012; Antonini & Stryker 1996). Researchers could drive a specific input to "win" by ablating acetylcholine release in that particular neurite, suggesting that the competition between inputs is resolved by the stabilization of the most-active axon and pruning of the least active neurites (Buffelli et al. 2003). Because the timing of GABAergic DD neuron remodeling coincides with the birth of VD neurons in *C. elegans*, it was hypothesized that DD remodeling could occur because of competition with neighboring VD neurons. Interestingly, DD neuron remodeling proceeds despite genetic ablation of VD neurons, suggesting that competition between the DD and VD cells is not a driving force for DD remodeling (Hallam & Jin 1998).

Distinct mechanisms regulate synapse removal and synapse assembly

In addition to the transcription factors that regulate DD remodeling, signaling proteins have also been shown to drive this process. Cyclin-dependent kinase-5/CDK-5 is a conserved enzyme implicated in brain development; including neuronal migration and synaptogenesis (Cheung et al. 2006; Cheung & Ip 2007). Additional studies demonstrate a role for CDK-5 in neuronal plasticity and neurotransmission (Seeburg et

al. 2008; Lai & Ip 2009). Work from the Shen lab found that mutations in *cdk-5* result in DD remodeling defects in *C. elegans*. Specifically, CDK-5 mediates the formation of dorsal DD synapses, while the removal of ventral DD synapses is regulated by the cyclin protein CYY-1in a different genetic pathway (M. Park et al. 2011). These findings not only describe the first signaling pathway to mediate DD remodeling, but also highlight two distinct mechanisms that drive synapse removal and subsequent synapse formation.

After the cyclin protein CYY-1 mediates the removal of ventral DD synapses, CDK-5 mediates the formation of nascent dorsal DD synapses through the conserved kinesin motor protein UNC-104/Kinesin-3. UNC-104 is an anterograde axonal motor for carrying synaptic vesicles along microtubules (Hall & Hedgecock 1991). Another motor protein, dynein/DHC-1, is also required for remodeling; however, this motor mediates retrograde trafficking along microtubules (M. Park et al. 2011). A role for these trafficking proteins during DD remodeling raised the possibility that formation of dorsal DD synapses may reincorporate some of the disassembled ventral synaptic components, rather than generating these new synapses *de novo*. The Shen lab tested this prediction and found that ventral vesicular components are recycled during the remodeling process. However, it remains unclear whether the ventral membrane-bound active zone components are also reused at the new dorsal synapses (M. Park et al. 2011).

In axons, synaptic vesicles are trafficked along stable microtubules, and the findings from the Shen lab suggest these synaptic vesicles are transported from newly disassembled ventral synapses to developing dorsal synapses (M. Park et al. 2011). Surprisingly, work from the Jin lab found that dynamic microtubules, rather than stable microtubules, are important during DD remodeling, suggesting that the cytoskeletal components that drive this process are not well understood (Kurup et al. 2015). Aside from the regulation of dynamic microtubules, actin structures are also important for DD

remodeling. Microarray analysis of *unc-55* target genes revealed that the Arp2/3 component, ARX-5/p21Arc (actin-related protein 2/3 complex subunit 3) is transcriptionally repressed in VD neurons (S. C. Petersen et al. 2011). An additional study showed that removal of ventral DD synaptic structures is facilitated by activation of gelsolin, an F-actin severing protein (Meng et al. 2015), suggesting that these synaptic structures are stabilized by actin networks.

Dissertation Overview

In the following chapters, I describe a new role for the DEG/ENaC protein UNC-8 during GABAergic synapse remodeling. In **Chapter 2**, I show that UNC-8 is expressed in DD neurons and promotes ventral GABAergic synapse removal. UNC-8 also promotes ventral synapse disassembly in *unc-55* mutants, in which both DD and VD neurons remodel. These experiments are outlined in **Chapter 3**, along with the findings that UNC-8 functions cell autonomously in GABAergic cells.

Interestingly, ectopic expression of UNC-8 in GABAergic motor neurons is sufficient to drive ventral synapse disassembly. This UNC-8-mediated removal mechanism is dissected in **Chapter 4**, where I outline findings that UNC-8 channel activity promotes the removal of several presynaptic proteins; including synatobrevin/SNB-1, RAB-3, endophillin/UNC-57, and liprin-alpha/SYD-2. This UNC-8 pathway requires calcium signaling through voltage-gated calcium channels, activation of the phosphatase calcineurin, and expression of the canonical cell death genes.

Consistent with previous findings from the Miller lab, the homeobox transcription factor, Iroqouis/IRX-1 also drives ventral synapse removal in a parallel pathway with UNC-8. In **Chapter 5**, I examine the differences between these two pathways and find

that IRX-1, but not UNC-8 is required to remove the synaptic vesicle priming protein UNC-13 from the GABAergic active zones.

In **Chapter 2** I show that UNC-8 is expressed in GABAergic and cholinergic motor neurons. The role of UNC-8 in cholinergic cells is further explored in **Chapter 6**. Previous findings that hyperactive UNC-8, like other DEG/ENaCs, induce neurodegeneration is confirmed. Specifically, constitutively active UNC-8 channels cause neuronal swelling and degeneration of the cholinergic, but not GABAergic neurons.

Building on the findings from **Chapter 4** suggesting that UNC-8 promotes synapse removal in an activity-dependent pathway, I examined the source of this activity. Using genetic and optogenetic approaches I found that GABA synthesis and release are required for ventral synapse removal. Additionally, the UNC-49 $GABA_A$ receptors antagonize remodeling, whereas the GBB-2 $GABA_B$ receptors promote removal. Depolarization of GABAergic, cholinergic, and muscle cells induces precocious remodeling and these findings are described in **Chapter 7**.

Ultimately, the work in this thesis describes a previously unknown molecular player in synapse elimination, UNC-8. Because DEG/ENaC proteins are conserved across species and are expressed in the mammalian brain, these findings may be informative for understanding human brain development and function. Although synapse elimination is a critical process during brain development, it can also have deleterious effects in neurodegenerative diseases, such as Alzheimer's Disease (Selkoe 2002; Stevens et al. 2007). A better understanding of the molecular regulators of synapse stability may help us understand these diseases and contribute to the identification of novel therapeutic targets.

CHAPTER II

THE DEG/ENAC PROTEIN UNC-8 PROMOTES DD SYNAPSE REMOVAL IN GABAERGIC MOTOR NEURONS

Summary

Neural circuits undergo significant changes during development to form a functional nervous system. New synapses are generated, while existing neuronal connections are pruned, and these processes are critical to direct information flow in the nervous system. Many previous studies have focused on the molecules directing synapse formation; however, less is known about how synapses are eliminated. The ability of the nervous system to dynamically create and destroy synapses has been widely observed among both vertebrate and invertebrate species, suggesting that the molecular mechanisms underlying these processes are conserved.

DD GABAergic motor neurons in *C. elegans* remodel during a specific period of larval development (Thompson-Peer et al. 2012; S. C. Petersen et al. 2011; White et al. 1978; Shan et al. 2005; Walthall & Plunkett 1995; Hallam & Jin 1998). This remodeling process involves the removal of ventral presynaptic densities and consequent formation of new synapses with dorsal muscles. Synaptic remodeling is repressed in VD GABAergic motor neurons by the COUP/TFII transcription factor, UNC-55; therefore, both DD and VD neurons remove their ventral synapses in *unc*-55 mutant animals (Thompson-Peer et al. 2012; S. C. Petersen et al. 2011; White et al. 1978; Shan et al. 2005; Walthall & Plunkett 1995; Hallam & Jin 1998). To identify genes that drive

GABAergic synapse removal, the Miller lab utilized a microarray strategy and RNAi screen (see **Introduction**, (S. C. Petersen et al. 2011)) to identify genes that are transcriptional targets of UNC-55. One candidate gene found in the screen, encodes a degenerin epithelial sodium channel (DEG/ENaC) protein, UNC-8.

DEG/ENaC family proteins form trimeric, voltage-independent cation channels. The DEG/ENaC family of proteins includes the acid-sensing ion channels, or ASIC proteins. Work from mammalian and invertebrate models has identified important roles for ASIC proteins in the nervous system in mediating fear and anxiety, neuronal injury, and synaptic plasticity (Vergo et al. 2011; Friese et al. 2007; Wemmie et al. 2002; Wemmie et al. 2003; Du et al. 2014). However, as described in the Introduction, little is known about the function of non-ASIC members of the DEG/ENaC family proteins, which are expressed in the nervous system.

Here we show that the DEG/ENaC subunit *unc-8* is expressed in remodeling DD GABAergic motor neurons. In *unc-55* mutants, *unc-8* expression is ectopically turned on in remodeling VD GABA neurons. Additionally, *unc-8* is expressed in cholinergic motor neurons and in the PVD sensory neuron, suggesting that this channel subunit may have roles in addition to the removal of GABAergic synapses (see **Chapter 6**). Results obtained with a newly generated *unc-8* null allele support our previous *unc-8 RNAi* studies, demonstrating that *unc-8* is required for complete removal of ventral synapses. Together, our findings have identified a novel role for non-ASIC members of the DEG/ENaC family of proteins during synapse removal.

Materials and Methods

Strains and Genetics

C. elegans strains were cultured at 20° C as previously described on standard nematode growth medium seeded with OP50 (Brenner 1974). The mutant alleles and strains used in this study are outlined in **Tables 2.1** and **2.2**.

Microscopy

Animals were immobilized on 2% agarose pads with 15mM levamisole as previously described(C. J. Smith et al. 2012). Timecourse analysis of L1 animals (**Figure 2.9**) were collected with a Zeiss Axioplan inverted microscope using ImageJ Micro-Manager software and a 63x oil objective (camera ORCA; Hammamatsu). L1 animals were synchronized by placing 100 gravid adult hermaphrodites onto plates and allowing them to lay eggs for one hour. The midpoint of the hour was considered T_0. After the hour all adults were removed and plates were incubated at 23° C unless stated otherwise. At 18 hours post-laying (T=18), L1 larval animals were imaged and analyzed. Synapse counts in adults (**Figure 2.11**) were collected on a Zeiss Axioplan inverted microscope using a 63x oil objective. Fluorescently-labeled synapses from GABAergic DD neurons were counted between DD1 and DD6 in L1 animals or VD3 to VD11 in adult animals. Z-stack images (**Figures 2.1, 2.2, 2.4, 2.5, 2.7,** and **2.11**) were collected on a Leica TCS SP5 confocal microscope using a 63X oil objective (0.5 µm/step), spanning the focal depth of the ventral nerve cord GABA neurons and synapses. Leica Application Suite Advanced Fluorescence (LAS-AF) software was used to generate maximum intensity projections. In **Figure 2.1**, DD and VD neurons were identified by the GABA-specific marker *pttr-*

39::mCherry. The cells were traced in ImageJ and background was subtracted. The *unc-8::GFP* fluorescence intensity was then normalized to the *pttr-39::mCherry* fluorescence intensity for each cell. Fluorescence intensity plots (**Figure 2.11**) were created by drawing a line through the ventral nerve cords of each animal and calculating the fluorescence intensity value in arbitrary units over the distance in micrometers with the ImageJ plot profile tool. The examiner was blinded to genotype.

Single molecule fluorescent *in situ* hybridization (smFISH)

Stellaris smFISH probes against *unc-8* transcripts were custom-designed and ordered from Biosearch Technologies. Synchronized adult animals expressing a cytosolic GFP GABAergic neuron marker were fixed and hybridized with a mix of 48 CAL Fluor Red 590 dye-fused oligonucleotides (Raj et al. 2008; C. J. Smith et al. 2013). Animals were imaged on a Leica TCS SP5 confocal microscope using a 100X oil objective (0.5 µm/step) and maximum intensity projections were generated (**Figure 2.2**).

Cloning and Molecular Biology

Recombineering UNC-8::GFP fosmid

The UNC-8::GFP fosmid (**Figures 2.4, 2.5, 2.6**) was recombineered as previously described (Tursun et al. 2009). The 30 kb fosmid WRM0635cA02 containing the *unc-8* genetic locus was obtained from GeneService and purified. Fosmid DNA was transformed into electrocompetent SW105 cells and was verified by PCR. A GFP-galK recombineering cassette was amplified with 50 kb homology arms from pBALU1 and gel-purified. The GFP-galK PCR product was transformed into electrocompetent, λRed recombinase-activated, fosmid-containing SW105 cells. Cells containing the fosmid and

GFP-galK were grown for more than 60 hours at 32°C and streaked on MacConkey and galactose plates with chloramphenicol to ensure insertion of recombineering cassette. To excise galK from the GFP intron, colonies were incubated with 0.1% arabinose to create an *unc-8::GFP* expression fosmid. This *unc-8::GFP* fosmid was then purified and confirmed by sequencing. The fosmid was injected into *unc-8(tm5052)* animals at 25 ng/µl with co-injection marker *pceh-22::*GFP at 15 ng/µl.

Construction of punc-25::UNC-8::GFP plasmid

UNC-8 cDNA was PCR-amplified from pSGEM/pTWM60 (Y. Wang et al. 2013) with primers that span the UNC-8 cDNA sequence and exclude the 3' stop codon. The primer sequences are: Forward 5'-ATGAGCGCAAGGAGTAGT-3' and Reverse 5'-TTTGCTCATTAACTCCTTTGT-3'. Primers include either 5'-AscI or 3'-SacII adaptors for inserting UNC-8 cDNA into pMLH260 (*punc-25::coq1cDNA::GFP::unc-54*) in place of the *coq-1* fragment (Earls et al. 2010). The resultant plasmid, pTWM62 (*punc-25::UNC-8::GFP*) was injected (10 ng/µl) with co-selectable marker *pmyo-2*::mCherry::*unc-54* (2.5 ng/µl) into *unc-8 (tm5052)* animals.

Fusion Protein Plasmid Construction

Plasmid vectors containing N-terminal MBP and HIS tags were obtained from the Vanderbilt Antibody and Protein Resource Core Facility. The UNC-8 extracellular domain was PCR amplified from pTWM62 and inserted into the vectors via 5' BamHI and 3'EcoRI restriction site adaptors or by overlap PCR with the In-Fusion Cloning Kit (Clontech). The resulting plasmids contain N-terminal His (pTWM108), MBP(pTWM103), or HiSMBP-tagged (pTWM115) directly upstream of the full *unc-8* extracellular domain and were confirmed by sequencing.

CRISPR/Cas9 Plasmid Construction

The empty sgRNA plasmid pDD162 was ordered from Addgene. Cas9 sgRNA target sites were identified in the *unc-8* genomic locus using APE software (M. Wayne Davis). Target sites were identified based on the following criteria (Dickinson et al. 2013): sequences starting with a G, followed by 19 nucleotides and ending in the PAM sequence NGG: $GN_{19}NGG$ (*unc-8* sgRNA 1 and 2). Additional Cas9 target sites for *unc-8* were identified using the following criteria (Farboud & Meyer 2015): 19-25 nucleotides followed by the PAM sequence NGG: $N_{19\text{-}25}NGG$ (*unc-8* sgRNA 3-6). Selected target sequences were confirmed to be specific by BLAST analysis against the *C. elegans* genome to prevent off-target binding. The 6 sgRNA target sequences were inserted into the pDD162 vector using the NEB Q5 site-directed mutagenesis kit as previously described (Dickinson et al. 2013).

Generation of the *unc-8 (tm5052)* allele

The *unc-8 (tm5052)* allele was generated by UV/TMP mutagenesis (Gengyo-Ando & Mitani 2000) and was identified by PCR amplification with primers spanning the deleted region. *tm5052* likely corresponds to an *unc-8* null allele because it deletes a portion of the fifth and entire sixth exon (197 base pairs) with the insertion of CT resulting in a premature stop codon prior to the first transmembrane domain.

Generation of the *unc-8 (tm2071)* allele

The *unc-8 (tm2071)* allele was generated by UV/TMP mutagenesis (Gengyo-Ando & Mitani 2000) and was identified by PCR amplification with primers spanning the deleted region. *tm2071* is an in-frame deletion that removes 130 amino acids from the extracellular loop (**Figure 3.14**). The *unc-8 (tm2071)* transcript is detectable by RT-PCR

analysis, suggesting that the truncated mRNA is expressed (data not shown, personal communication with Cristina Matthewman/Laura Bianchi at University of Miami).

Recombinant protein expression

The UNC-8 extracellular domain (ECD) fusion protein with an N-terminal MBP tag was grown in bacteria at 37˚ Celsius overnight until OD_{600} reached 0.8. Expression was induced by adding 400 μM IPTG as previously described (NEBBL21 protocol). After IPTG induction for 6 hours or overnight, the bacteria were lysed and sonicated in the presence of a protease inhibitor cocktail (#P8465 Sigma). Centrifugation steps (13K RPM for 5 minutes at 4˚C) were used to isolate the fusion peptide. Supernatent containing the fusion peptide was incubated with amylose resin (NEB #E8021S) at 4˚C for 1 hour. Resin was washed and protein was eluted by incubating resin with 10mM maltose (Sigma #47288). Presence of the MBP-UNC-8ECD fusion peptide was evaluated by Western blot analysis using an anti-MBP monoclonal antibody.

Table 2.1. Mutant alleles and genotyping primers used in this study.

Allele	Source	Genotyping Primer Sequences
unc-8 (tm5052) IV	NBRP	TGGGGCCCTAATAATTTCGA
		AGTGACAGTATGAAGCCAGG
unc-8 (tm2071) IV	NBRP	GCGGCACTCTTCATGTGCAT
		AGGCGTCTTCTGGGTAACTG
unc-55 (e1170) I	CGC	TAAGGACTACACGGATCCTG
		CCCAAGAAAGAAAAGAGAGGT

Table 2.2. Strains used in this study.

Strain	Genotype
NC2320	*pttr-39::mCherry V; otEx2876 [punc-8::GFP; elt-2::GFP]*
NC2321	*unc-55(e1170) I; pttr-39::mCherry V; otEx2876 [punc-8::GFP; elt-2::GFP]*
NC2585	*wyIs202 [pflp-13::GFP::RAB-3; pflp-13::mCherry]* X
NC2480	*unc-8(tm5052)* IV; *wyIs202* X
NC2861	*juIs137 [pflp-13::SNB-1::GFP]* II
NC2936	*unc-8(tm5052)* IV; *juIs137* II
NC2994	*unc-8 tm5052 IV*; wdEx960[*punc-25::UNC-8::GFP*]
FX05052	*unc-8 (tm5052) IV*
NC1123	*oxIs12[punc-47::GFP] X*
NC2387	*unc-8 (tm5052) juIs1 IV*
NC2388	*unc-55 (e1170) I; unc-8 (tm5052) juIs1 IV*
NC1909	*unc-8 (tm2071) IV*
NC2051	*unc-8 (tm2071) juIs1 IV*
NC2125	*unc-55 (e1170) I; unc-8 (tm2071) juIs1 IV*
NC2585	*wyIs202 [pflp-13::gfp::rab-3, pflp-13::mcherry; podr-1::dsRed] X*
NC2894	*unc-8 tm5052 IV; wpIs39 [punc-47::mCherry] X; wdEx944 [UNC-8::GFP fosmid; punc-25::mCherry::RAB-3; pceh-22::GFP]*
NC3010	*unc-55 (e1170)* I; *unc-8 (tm5052)* IV; *wdIs90 [punc-25::mCherry::RAB-3; ceh-22::GFP]*; *wdEx962 [UNC-8::GFP fosmid; pmyo-2::mCherry]*
N/A	*unc-8 (tm5052) IV; wdIs90[punc-25::mCherry::RAB-3; ceh-22::GFP]*
N/A	*unc-55 (e1170) I; wdIs90[punc-25::mCherry::RAB-3; ceh-22::GFP]*
NC3022	*unc-55 (e1170) I; unc-8[tm5052] IV; wdIs90[punc-25::mCherry::RAB-3; ceh-22::GFP]*

Results

unc-8 expression in GABAergic neurons is transcriptionally regulated

In a previous microarray experiment, we discovered that *unc-8* mRNA transcripts were enriched in *unc-55* mutant animals (S. C. Petersen et al. 2011). Building upon previous work that outlined a role for the transcription factor *unc-55* as a repressor of synaptic remodeling; i.e., acting to antagonize pro-remodeling genes, we predicted that *unc-55* blocks *unc-8* expression(S. C. Petersen et al. 2011; Thompson-Peer et al. 2012; Shan et al. 2005; H. M. Zhou & Walthall 1998). This prediction presumes that the DEG/ENaC subunit *unc-8* is expressed in wild type DD GABAergic motor neurons, while

it is repressed in VD motor neurons by *unc-55*. Additionally, we predicted that in *unc-55* mutant animals, *unc-8* should be strongly expressed in both DD and VD motor neurons. To test these predictions, we examined a fluorescent reporter for *unc-8* expression. A 1.6 kb genomic region upstream of the *unc-8* transcriptional start site was fused to GFP (**Figure 2.1A**, (Etchberger et al. 2007)). In wild type adult animals, this reporter (*punc-8::GFP*) exhibited strong fluorescence in DD GABAergic motor neurons; however, the fluorescence signal was not detectable in VD neurons. Using this same fluorescent reporter in *unc-55* mutant animals, we were able to see strong *punc-8::GFP* signal in both DD and VD GABAergic motor neurons (**Figure 2.1B**). These results validate the prediction that *unc-8* is expressed in remodeling GABAergic neurons and is transcriptionally regulated by *unc-55* (Miller-Fleming et al. 2016).

As an independent test of *unc-8* mRNA transcript levels, we examined RNA sequencing data acquired from wild type DD and VD neurons in developing animals. We see that *unc-8* mRNA is more highly expressed in DD, compared to VD motor neurons (data not shown, personal communication Andrea Cuentas Condori). Additionally, we find that *unc-8* mRNA transcripts are detectable in DD motor neurons using single molecule fluorescent *in situ* hybridization, or smFISH. Custom probes designed to target the *unc-8* transcript were fluorescently labeled and incubated with fixed animals. Weak fluorescent signal was detected in the gut and in multiple ventral cord neurons, including the DD GABAergic cells; however, little to no smFISH signal was detected in the VD GABAergic cell somas (**Figure 2.2**).

UNC-8 protein is present in DD GABAergic motor neurons

On the basis of our previous findings that *unc-8* transcripts are detectable in DD motor neurons, we next wanted to visualize endogenous UNC-8 protein in neurons. We

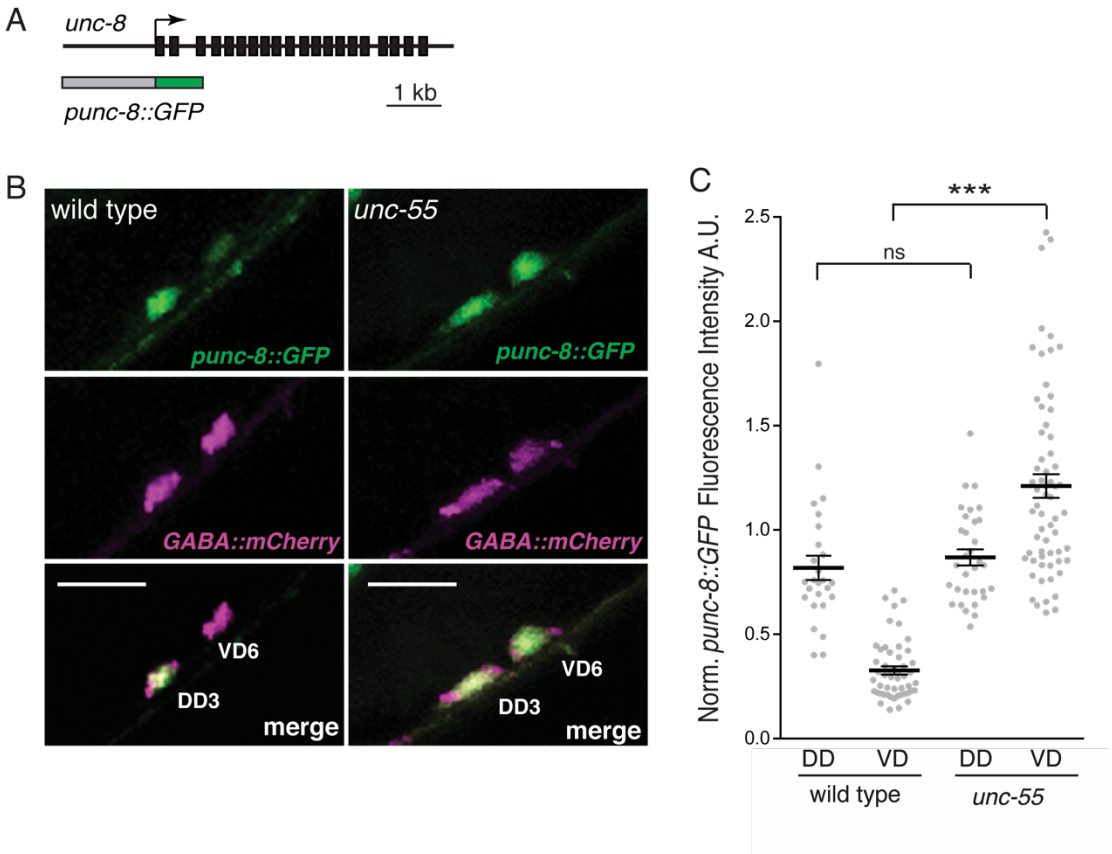

Figure 2.1: UNC-8 is expressed in remodeling GABAergic motor neurons and is repressed by the transcription factor UNC-55. A. *unc-8* expression in remodeling neurons is visualized with a *punc-8::GFP* reporter gene (*otEx2876*, see Methods). **B.** Strong *punc-8::GFP* (green) expression was observed in DD motor neurons in wild-type animals, but was repressed in wild type VD motor neurons. Loss of *unc-55* derepresses *unc-8* expression in VD neurons, visualized by strong GFP expression in *unc-55* VD neurons. GABAergic motor neurons are labeled with *pttr-39*::*mCherry* (magenta). Scale bar is 10 µm. **C**. Normalized fluorescence intensity is plotted on the Y-axis in arbitrary units (A.U.). *punc-8::GFP* expression is enhanced in VDs, but not DDs, in *unc-55* mutants (***$P < 0.001$, ns is not significant, One-Way ANOVA Bonferroni correction). $n \geq 26$ DDs and $n \geq 51$ VDs per genotype, data are mean ± SEM.

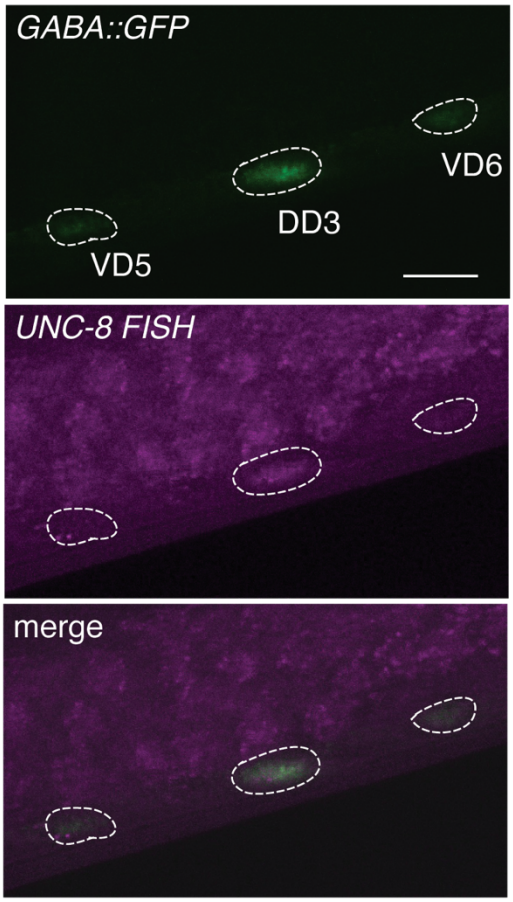

Figure 2.2: Single molecule fluorescent *in situ* hybridization (smFISH) detects *unc-8* transcripts in GABAergic motor neurons. smFISH targeted against the *unc-8* transcript shows weak fluorescence in the DD, but not VD GABAergic motor neurons (N = 12 animals). GABAergic cells were labeled with a genetically encoded cytosolic GFP protein, *punc-47::GFP*. Scale bar is 5 µm.

initially attempted to generate a monoclonal antibody against three variations of tagged-UNC-8 peptides (HIS, MBP, and HIS-MBP); however, we found that the extracellular domain of UNC-8 was highly insoluble and we were unable to purify enough protein for this approach (**Figure 2.3**). As an alternative, we acquired a large genomic clone containing 40 kb of the sequence spanning the *unc-8* gene. A fluorescent tag was recombineered to the C-terminus of *unc-8* as previously described (see **Methods**, (Miller-Fleming et al. 2016; Tursun et al. 2009)), to generate the UNC-8::GFP fosmid. Because this construct spans several kilo-bases upstream and downstream of *unc*-8, it is likely to include genomic regions required for endogenous *unc-8* expression patterns; including enhancer elements. Transgenic expression of the UNC-8::GFP fosmid resulted in fluorescent signal in multiple neurons and neuronal processes, including GABAergic DD cells and several cholinergic neurons. We confirmed that the UNC-8::GFP fosmid construct is functional by examining ectopic VD remodeling in *unc-55; unc-8* animals. As stated previously (see Introduction), both DD and VD motor neurons remodel their ventral synapses to dorsal muscle in *unc-55* animals, and this results in a significant loss of ventral synaptic puncta (refs). This effect requires *unc-8*; therefore, *unc-55; unc-8* mutants retain ventral synapses (see **Chapter 3**). Transgenic expression of the UNC-8::GFP fosmid in *unc-55; unc-8* animals restores ventral synapse removal, demonstrating that this fluorescently-labeled construct is functional (**Figure 2.5**).

unc-8 is expressed in cholinergic ventral cord motor neurons and PVD

Transcriptional and translational reporter constructs show that *unc-8* is expressed in DD GABAergic motor neurons, but we also see expression in other neuronal cells. Specifically, we see strong UNC-8::GFP fosmid expression in several cholinergic motor neurons in the ventral nerve cord (**Figure 2.4**). Transgenic expression

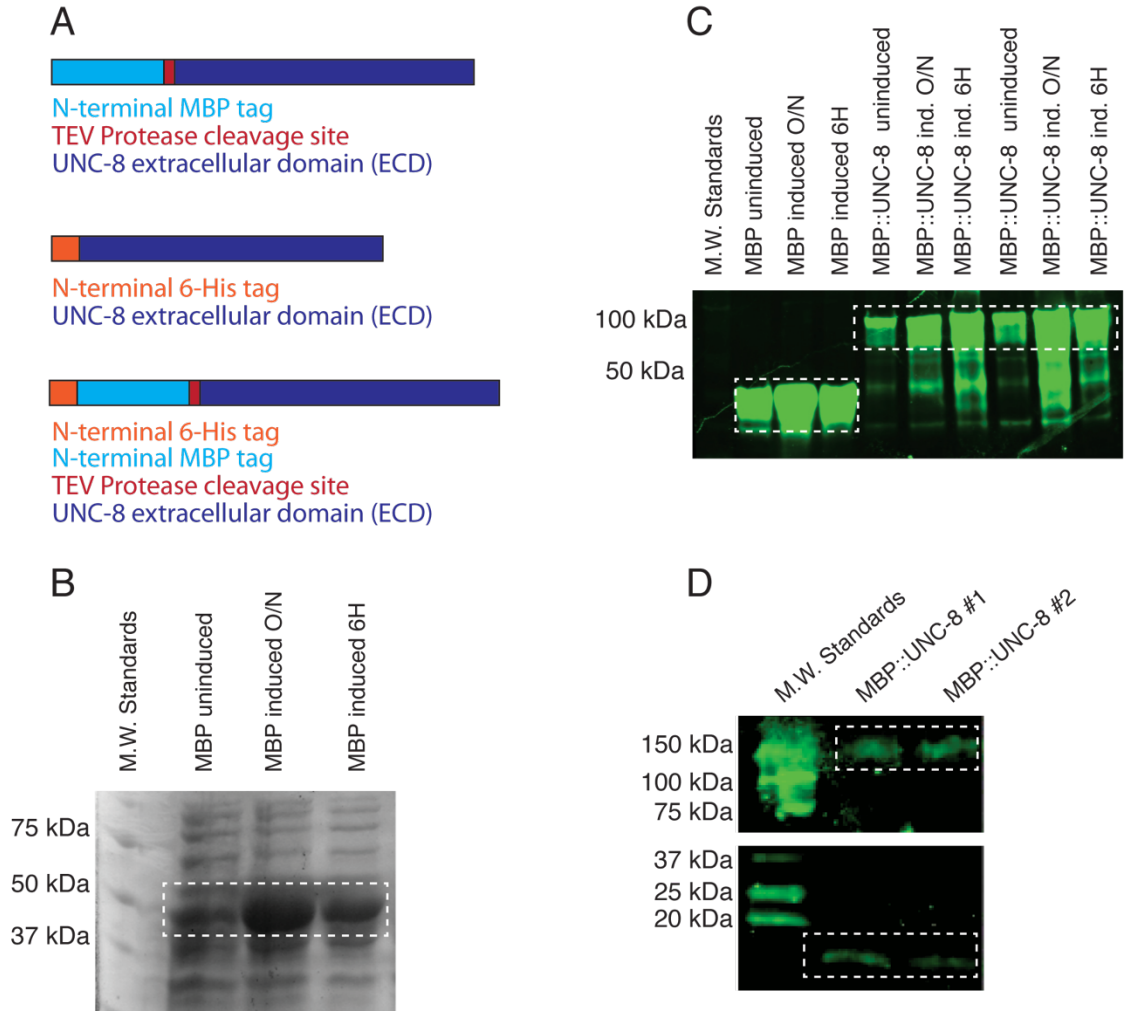

Figure 2.3: MBP-tagged UNC-8 fusion peptide is insoluble. A. Three strategies were used to generate an UNC-8 fusion peptide for monoclonal antibody production. N-terminal maltose binding protein (MBP), histidine (HIS), or HIS-MBP tags were cloned upstream of the UNC-8 extracellular domain (ECD, see Methods) **B.** The N-terminal MBP vector and MBP-UNC-8ECD were expressed in bacteria. Bacterial cells from uninduced and induced cultures (IPTG induction overnight (O/N) or for 6 hours (6H)) were examined on a Coomassie-stained protein gel. Induction of the MBP vector was observed (outlined above); however, no induction bands were seen for the MBP-UNC-8ECD expressing cells. **C.** To determine if induction was successful, MBP and MBP-UNC-8ECD expressing cells were tested for MBP expression using western blot analysis. Anti-MBP monoclonal antibody detected MBP expression (left box) and MBP-UNC-8ECD expression (right box) before and after IPTG induction. **D.** MBP-UNC-8ECD expressing bacteria were lysed and incubated with amylose resin to precipitate MBP-UNC-8ECD peptides. Pulldown of MBP-UNC-8ECD yielded very low intact protein (top box) and degraded protein (bottom box), when blotting against MBP. Further analysis at the Vanderbilt Antibody and Protein Resource (VAPR) concluded that this protein is highly insoluble.

of the UNC-8::GFP fosmid was mosaic; therefore, we quantified the frequency of UNC-8::GFP expression in GABAergic DD and cholinergic DA and DB motor neurons. In both larval and adult animals, UNC-8::GFP expression occurs more frequently in DA and DB cholinergic neurons as compared to GABAergic DD neurons (**Figure 2.6**). This result suggests that the *unc-8* subunit likely regulates additional processes in cholinergic neurons, and this idea is more thoroughly explored in Chapter VI. The UNC-8::GFP fosmid is also expressed in the PVD sensory neuron and SAB neurons as previously reported (data not shown,(Kratsios et al. 2015)). These findings support a diverse role for *unc-8* in regulating multiple processes among diverse cell types.

Fluorescently-tagged UNC-8 protein is localized to the ventral nerve cord of GABAergic motor neurons

We confirmed that the fluorescently-tagged UNC-8 protein is expressed in GABAergic DD and cholinergic DA/DB neurons in the ventral nerve cord. Furthermore, we also noted UNC-8::GFP puncta along the ventral nerve cord, where GABAergic and cholinergic neurites form synapses with multiple postsynaptic targets (**Figure 2.4,** (Miller-Fleming et al. 2016)). Interestingly, UNC-8::GFP fluorescence in the neurites is restricted to the ventral neuronal processes; however, using this construct, we cannot differentiate between ventral GABAergic and cholinergic neurites. To better understand where UNC-8::GFP is expressed in GABAergic neurons, we generated a cell-specific UNC-8::GFP construct under the control of a GABA motor neuron promoter (*punc-25::UNC-8::GFP*). This construct was lethal to animals; however, we were able to visualize GFP expression in a few surviving animals. Supporting the ventral localization observed for the UNC-8::GFP fosmid, punc-25::UNC-8::GFP puncta are also restricted

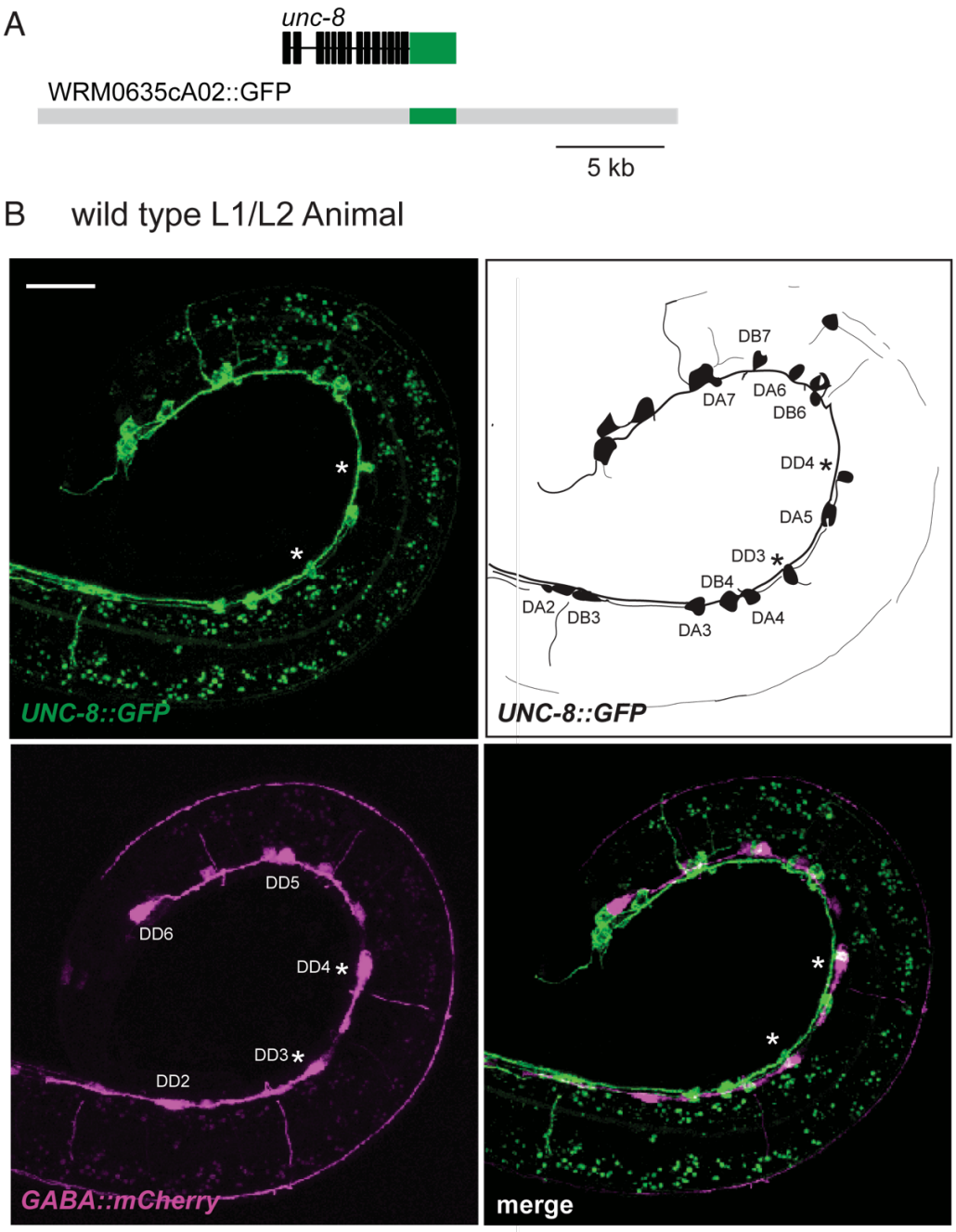

Figure 2.4: UNC-8::GFP fosmid is expressed in remodeling GABAergic motor neurons. A. The C-terminal GFP fusion with UNC-8 was generated by recombineering (see Methods). **B**. UNC-8::GFP is expressed in the ventral nerve cord (VNC) of early L2 animals in GABAergic DD neurons (asterisks) and in cholinergic DA and DB neurons (upper left). Schematic denotes VNC neurons that express UNC-8::GFP (upper right). The six DD neurons are labeled with *GABA::mCherry (punc-25::mCherry).* Cell bodies between the DD neurons are the newly born VD neurons (lower left). Merged image of UNC-8::GFP fosmid and *punc-25::mCherry* labeled GABA neurons (lower right). Asterisks indicate colocalization, scale bar is 20 µm.

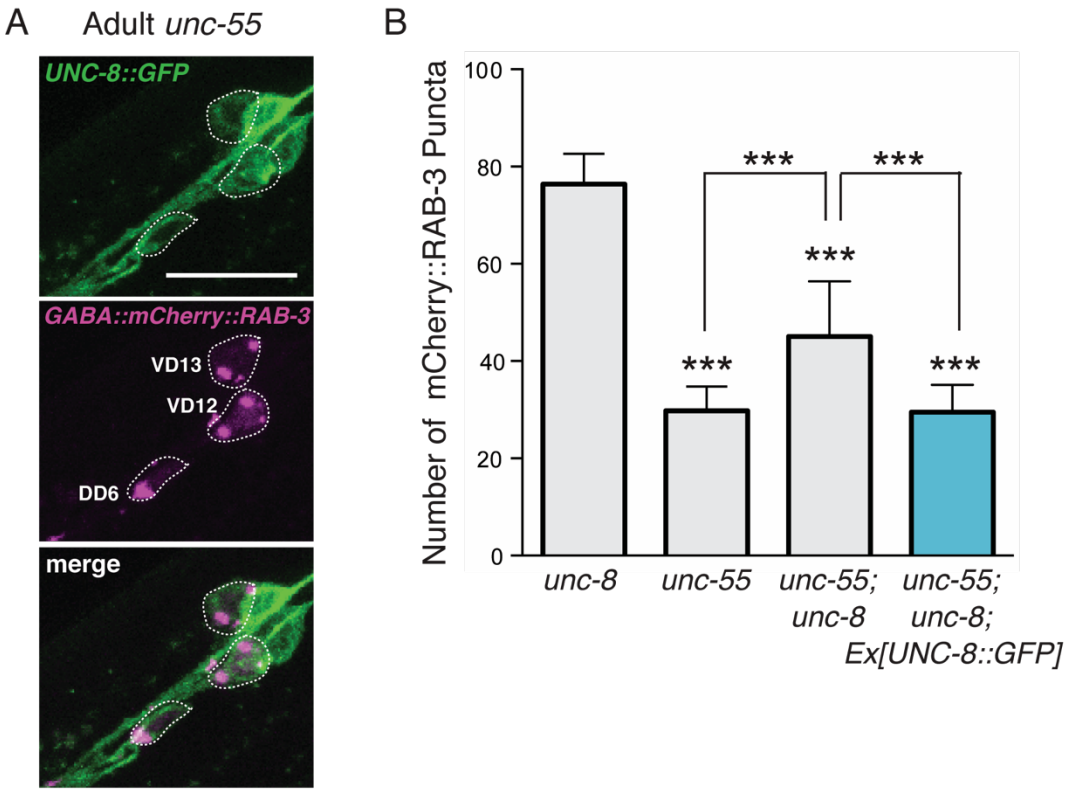

Figure 2.5: The UNC-8::GFP is functional. A. UNC-8::GFP is expressed in DD and VD neurons in *unc-55* mutants. GABA neurons are labeled with *wdIs90 [punc-25::mCherry::RAB-3].* UNC-8::GFP-expressing GABA neurons are outlined. Scale bar is 10 µm. **B.** Transgenic expression of UNC-8::GFP rescues the *unc-55* remodeling phenotype in *unc-55; unc-8* animals (***$P < 0.001$, $n \geq 20$ animals, One-Way ANOVA Bonferroni correction, data are mean ± SD).

to the ventral neurites and cell soma (**Figure 2.7**). Dorsal GFP puncta were not observed in animals expressing the *punc-25::UNC-8::GFP*, suggesting that UNC-8 function is likely restricted to the ventral compartments of GABAergic motor neurons.

unc-8 loss-of-function mutation delays DD synapse removal

Microarray and RNAi experiments identified *unc-8* as a pro-remodeling gene that is repressed by *unc-55*. As an independent test of this idea, we collaborated with Shohei Mitani's lab to generate *unc-8* mutant strains. Generation of the *unc-8 (tm5052)* allele was accomplished by mutagenesis and confirmed by sequencing. This mutation removes 197 base pairs encompassing the first transmembrane domain of *unc-8*. The *tm5052* deletion shifts the reading frame and inserts a premature stop codon just after the first transmembrane domain; therefore, we predict that this mutation is a null allele (**Figure 2.8**). We also generated an additional allele, *unc-8 (tm2071)*. This mutation results in an in-frame deletion of 390 nucleotides from the extracellular loop (Petersen dissertation). RT-PCR analysis confirmed that the *unc-8 (tm2071)* mRNA is detectable, suggesting that this allele may result in a stable truncated protein (personal communication Cristina Matthewman, Laura Bianchi lab, University of Miami). In support of this, GABAergic synapse removal was unaffected in *unc-8 (tm2071)* animals when examined in the *unc-55* background, suggesting that the (*tm2071)* allele may not completely abolish *unc-8* function during remodeling (**Figure 2.9**).

Additionally, we utilized the CRISPR/Cas9 genome editing system to generate six single-guide RNA constructs to target the *unc-8* genetic locus for knock-down (**Table 2.3,** Dickinson et al. 2013; Farboud & Meyer 2015). Unfortunately, transgenic expression of these constructs was lethal and we were not able to generate stable transgenic lines; therefore, the remainder of our studies used the *unc-8 (tm5052)* allele.

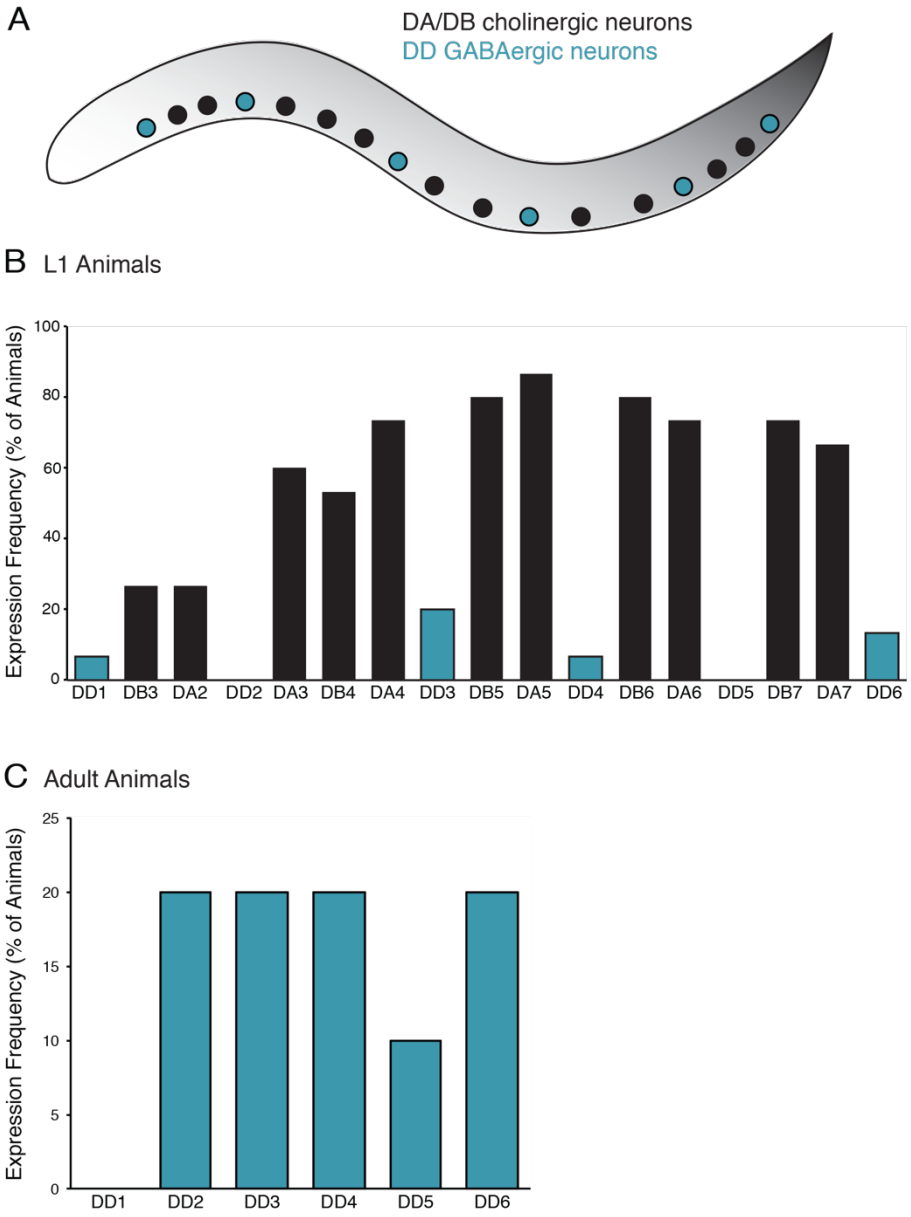

Figure 2.6: The UNC-8::GFP fosmid is expressed preferentially in cholinergic motor neurons. A. Expression of UNC-8::GFP was evaluated between DD1-DD6 in the ventral nerve cord. This region contains 6 GABAergic DD neurons (blue) and 11 cholinergic DA/DB neurons (black). **B.** In L1 animals, GFP expression is observed in most cholinergic neurons; however, there is a lower frequency of GFP expression in GABAergic DD neurons. **C.** Similar to larval animals, UNC-8::GFP expression in adult worms was apparent, but at a low frequency. (N > 10 animals).

We examined DD remodeling in wild type and *unc-8 (tm5052)* animals by monitoring the removal of ventral synapses and the formation of dorsal synapses labeled with a genetically-encoded fluorescent presynaptic protein (GFP::RAB-3). In wild type animals, ventral DD synapse removal initiates 16 hours after egg-laying and persists through 30 hours post-egg laying. Loss of *unc-8* delays this removal process; significantly more ventral DD synapses are detectable in *unc-8* mutants, compared to wild type controls (**Figure 2.10A,** Miller-Fleming et al. 2016). Surprisingly, *unc-8 (tm5052)* mutants had no effect on dorsal DD synapse formation, suggesting that *unc-8* specifically promotes synapse removal (**Figure 2.10B**). To confirm that the *unc-8* mutation does not delay overall development, we examined the timing of VD neuron birth over time in wild type and *unc-8* animals. We saw no overall developmental delay in the *unc-8* animals, supporting our results that *unc-8* is required to direct synapse removal (**Figure 2.10C**).

Table 2.3: CRISPR-targeting sites for *unc-8*.

Name	Target Sequence	Result
sgRNA1	aaagaaaccgccggttaca	No F_2 progeny
sgRNA2	aaccgttccctgatacatt	No F_1 progeny
sgRNA3	cgtgacacgtggcttaatc	No F_1 progeny
sgRNA4	acaaaatcttaggacgaaatccga	No F_1 progeny
sgRNA5	aataactgaaaccgaagaagcttt	No F_1 progeny
sgRNA6	gtcaatcttttctcagattttgg	No F_1 progeny

unc-8 mutants exhibit GABAergic synapse elimination defects that persist in adult animals

Based on our finding that *unc-8* delays ventral DD synapse removal, we anticipated that residual ventral DD puncta may be detectable in adult animals. Indeed

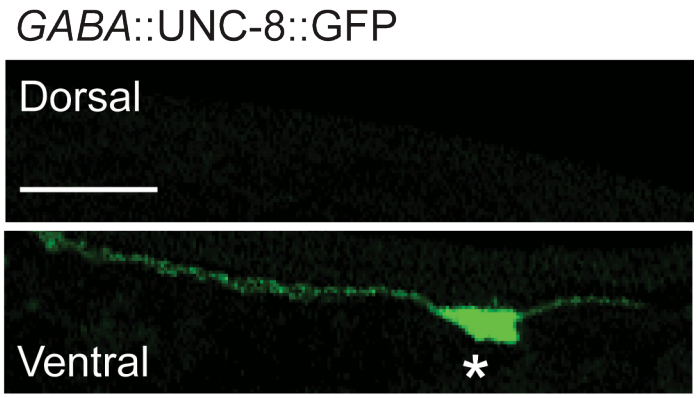

Figure 2.7: Expression of fluorescently-tagged UNC-8 in GABAergic motor neurons is ventrally localized. *punc-25::UNC-8::GFP* is localized specifically to the ventral nerve cord of young adult worms. Scale bar is 10 µm, asterisk denotes DD5 cell soma.

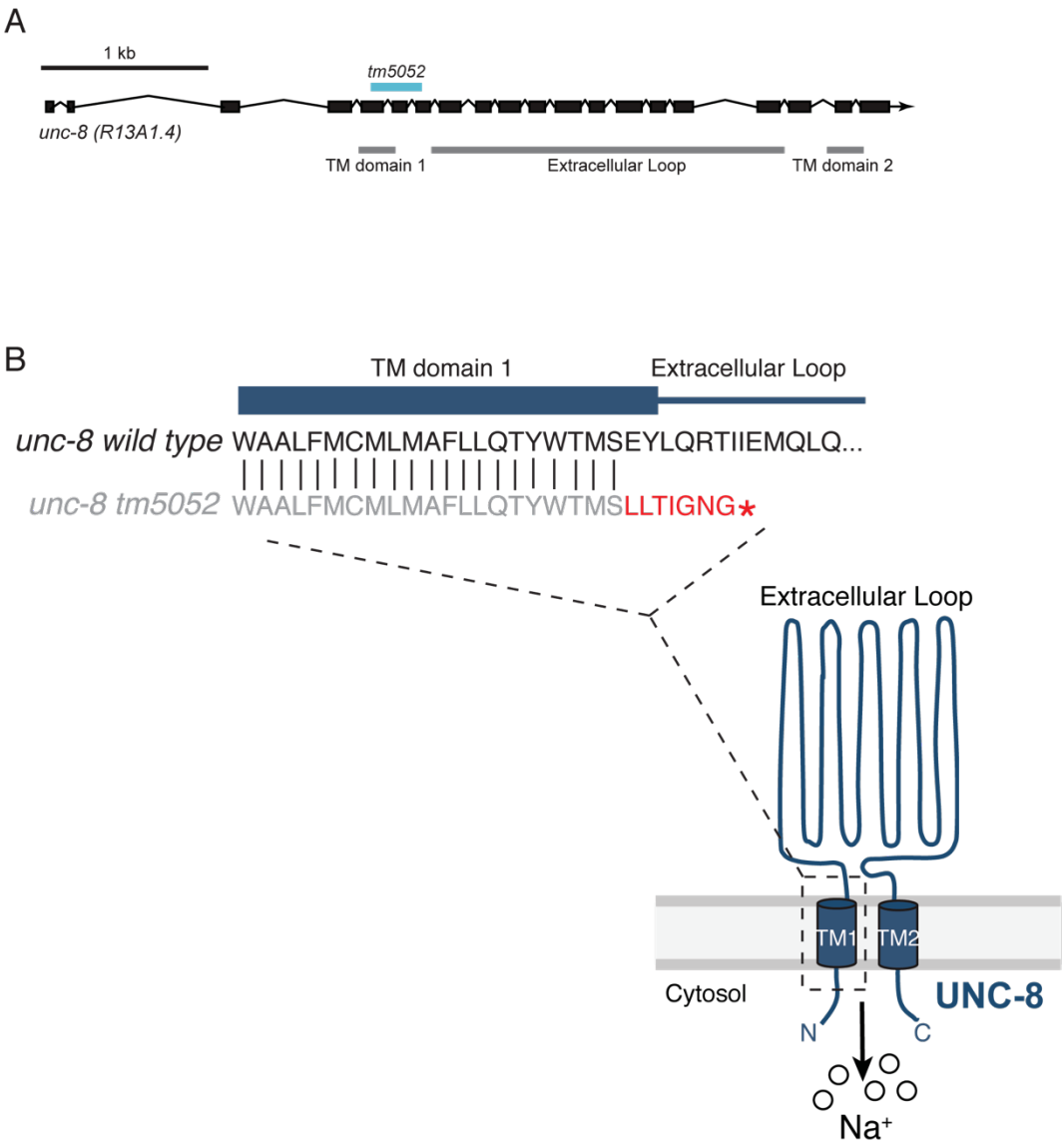

Figure 2.8: The *unc-8 (tm5052)* allele is a putative null mutation. A. Schematic of the *unc-8* gene and predicted UNC-8 protein. DEG/ENaC channel subunits contain two transmembrane domains (TM domains) and a large extracellular loop (gray bars). The *unc-8* deletion allele *tm5052* is annotated (blue bar). **B.** The *unc-8 (tm5052)* allele deletes 197 nucleotides and shifts the reading frame (red) to introduce a premature stop codon after the first transmembrane domain. This *unc-8(tm5052)* sequence should result in an unstable *unc-8* mRNA and likely null allele.

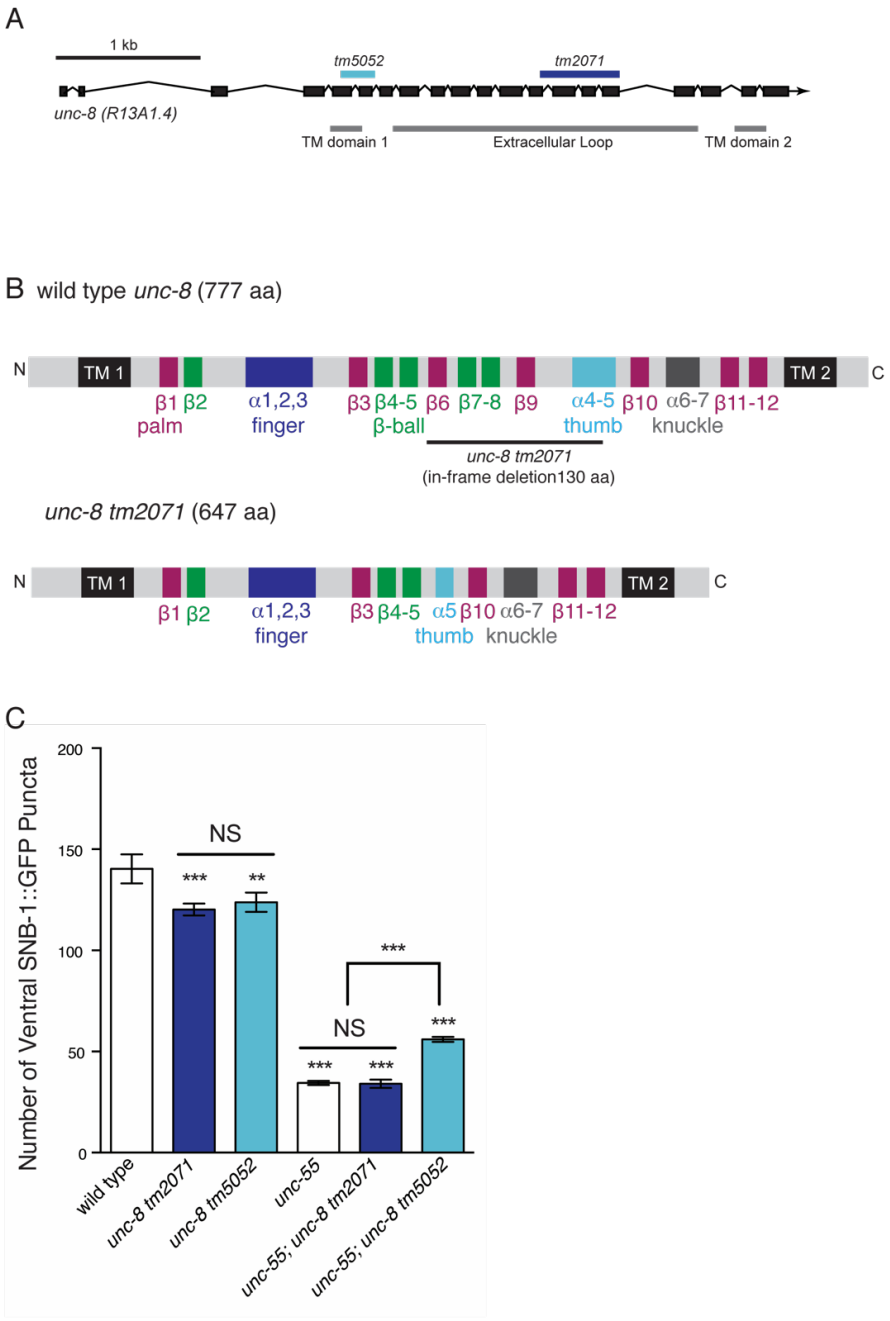

Figure 2.9: The in-frame *unc-8* deletion allele, *tm2071*, has no effect on GABAergic synapse remodeling. A. Schematic depicting the *unc-8* gene structure. The putative null allele *tm5052* and the in-frame deletion allele *tm2071* are annotated. **B.** Wild type and *unc-8 (tm2071)* protein schematics. The *tm2071* allele removes 130 amino acids from the extracellular domain of *unc-8*. **C.** SNB-1::GFP puncta are removed from ventral VD synapses in *unc-55* and this effect depends on *unc-8* (***p< 0.001, **p<0.01, NS is not significant, n ≥ 10) The *unc-8 (tm2071)* in-frame deletion allele has no effect on *unc-55* remodeling, whereas a significant fraction of ventral SNB-1::GFP puncta are not removed in the null allele, *unc-8 (tm5052)* (see **Chapter 3**).

we were able to visualize and quantify ventral DD puncta, labeled with the fluorescently-tagged presynaptic protein synaptobrevin-1 (DD::SNB-1::GFP), in adult *unc-8* animals (**Figure 2.11,** Miller-Fleming et al. 2016). These residual puncta persist several hours (~48) after the completion of DD synapse removal in wild type animals. Consistent with our previous results, we saw no effect on dorsal DD synapses in *unc-8* mutants compared to wild type controls. These data support the finding that *unc-8* promotes ventral DD synapse elimination.

Discussion

Synapse removal is a critical step for the maintenance of neuronal circuits; however, the molecules directing this process are not well understood. Here, we identify the DEG/ENaC protein UNC-8 as a novel regulator of GABAergic synapse removal. We demonstrate that *unc-8* is transcriptionally regulated by *unc-55* and is expressed in remodeling GABAergic motor neurons. UNC-8::GFP protein is primarily localized to the ventral nerve cord, and was not detected on the dorsal nerve cord. Additionally, we find that loss of *unc-8* antagonizes ventral DD synapse removal, whereas dorsal DD synapse formation is unaffected.

A novel role for DEG/ENaC proteins to eliminate synapses

As outlined in the Introduction, members of the DEG/ENaC family of proteins are broadly expressed in the nervous system (Giraldez & Domínguez 2013; Yamamura et al. 2004; Waldmann et al. 1995). The subfamily of acid-sensing ion channels (ASICs) of DEG/ENaC proteins has been studied extensively. Work in both mammalian and invertebrate neurons determined that postsynaptic ASIC proteins are gated by low pH, which typically coincides with the fusion and release of presynaptic vesicles (Askwith et

al. 2004; Benson et al. 2002). In this mechanism, ASIC proteins detect neurotransmitter release, to trigger channel activation and the flow of sodium ions into the postsynaptic cell. This ASIC-mediated depolarization of the postsynaptic membrane can activate downstream signals, including the voltage-gated calcium channels, VGCCs, thereby strengthening neurotransmission(Wemmie et al. 2006). Interestingly, we have found that reconstituted UNC-8 is inhibited at low pH, suggesting that this channel is likely gated by alternative mechanisms (see **Chapter 6**) and has the opposite effect of weakening synaptic connections, rather than strengthening them as observed for ASIC proteins (Miller-Fleming et al. 2016; Y. Wang et al. 2013).

unc-8 promotes synapse removal in a complex genetic pathway

Here, we find that *unc-8* mutant animals show a significant delay in synapse removal; however, *unc-8* mutants are still able to properly remove the majority of their ventral DD synapses. This result supports the hypothesis that DD synapse remodeling is likely complex and includes at least one additional parallel-acting genetic pathway (see **Chapter 5**). Previous microarray experiments from our lab and others have identified several targets of *unc-55*, including multiple transcription factors, cytoskeletal components, and signaling proteins (see **Chapter 5**, Thompson-Peer et al. 2012; He et al. 2015; S. C. Petersen et al. 2011). Additionally, several proteins have been identified to regulate DD remodeling independently of *unc-55* regulation (M. Park et al. 2011; Kurup et al. 2015; Han et al. 2015), underscoring the extensive gene networks regulating this process.

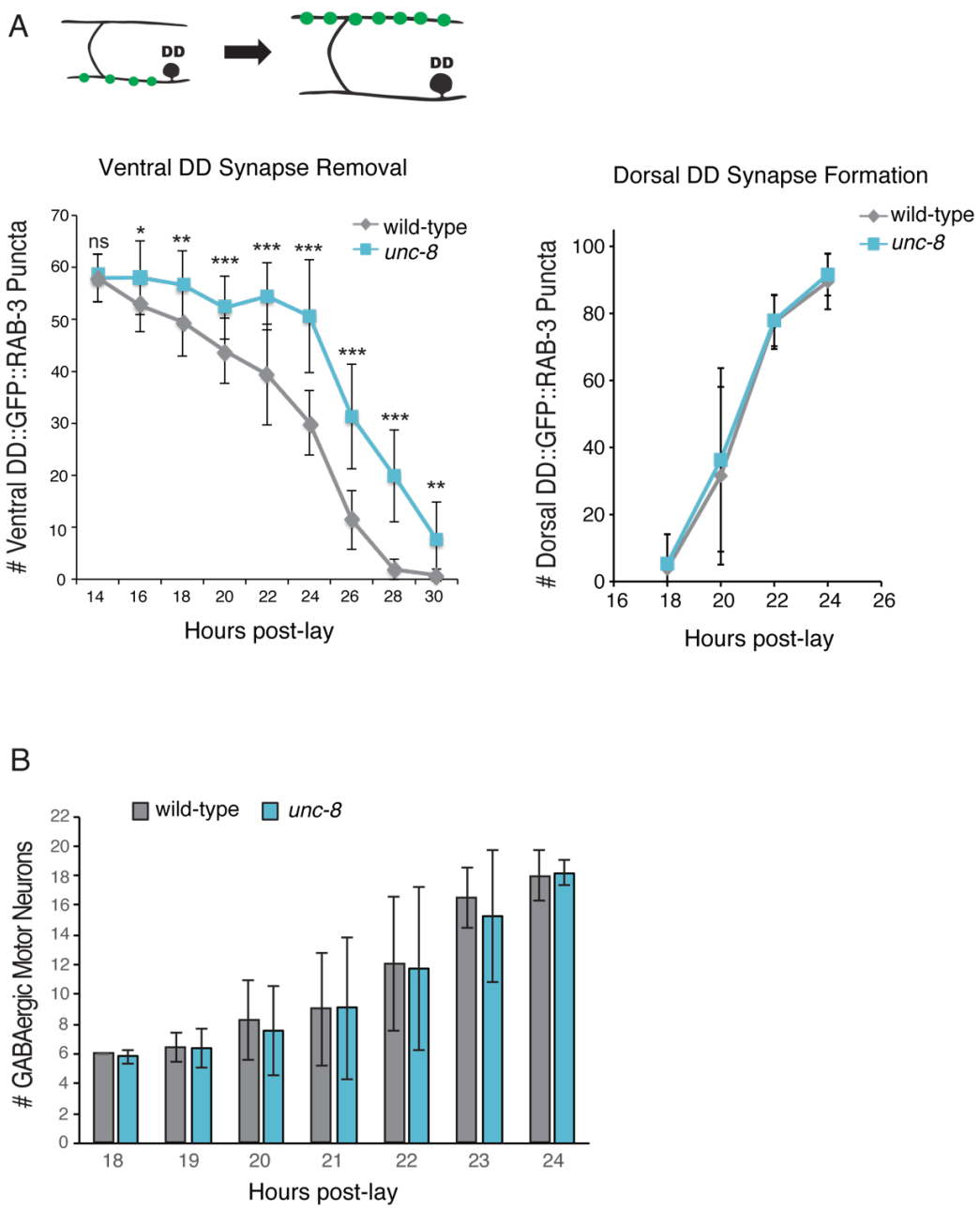

Figure 2.10: UNC-8 promotes ventral GABAergic synapse removal. A. DD GABAergic synapses with ventral muscles (green circles) are relocated to the dorsal side during development. DD-specific GFP-tagged RAB-3 (*pflp-13::GFP::RAB-3)* was used to quantify synapses over the duration of larval development. Removal of ventral DD synapses is significantly delayed in *unc-8* animals (left panel, NS is not significant, $^{*}P < 0.05$, $^{**}P < 0.01$, $^{***}P < 0.001$ Student's *t*-test, data are mean ± SD); however, dorsal synapse formation is unaffected (right panel, Student's *t*-test, data are mean ± SD). Results were pooled from 3 independent experiments. **B.** GABA neuron development is not delayed in *unc-8* mutants. GABA neurons in the ventral cord, marked with GABA::SNB-1::GFP, were counted in developing wild-type and *unc-8* mutant larvae (Student's *t*-test, data are mean ± SD).

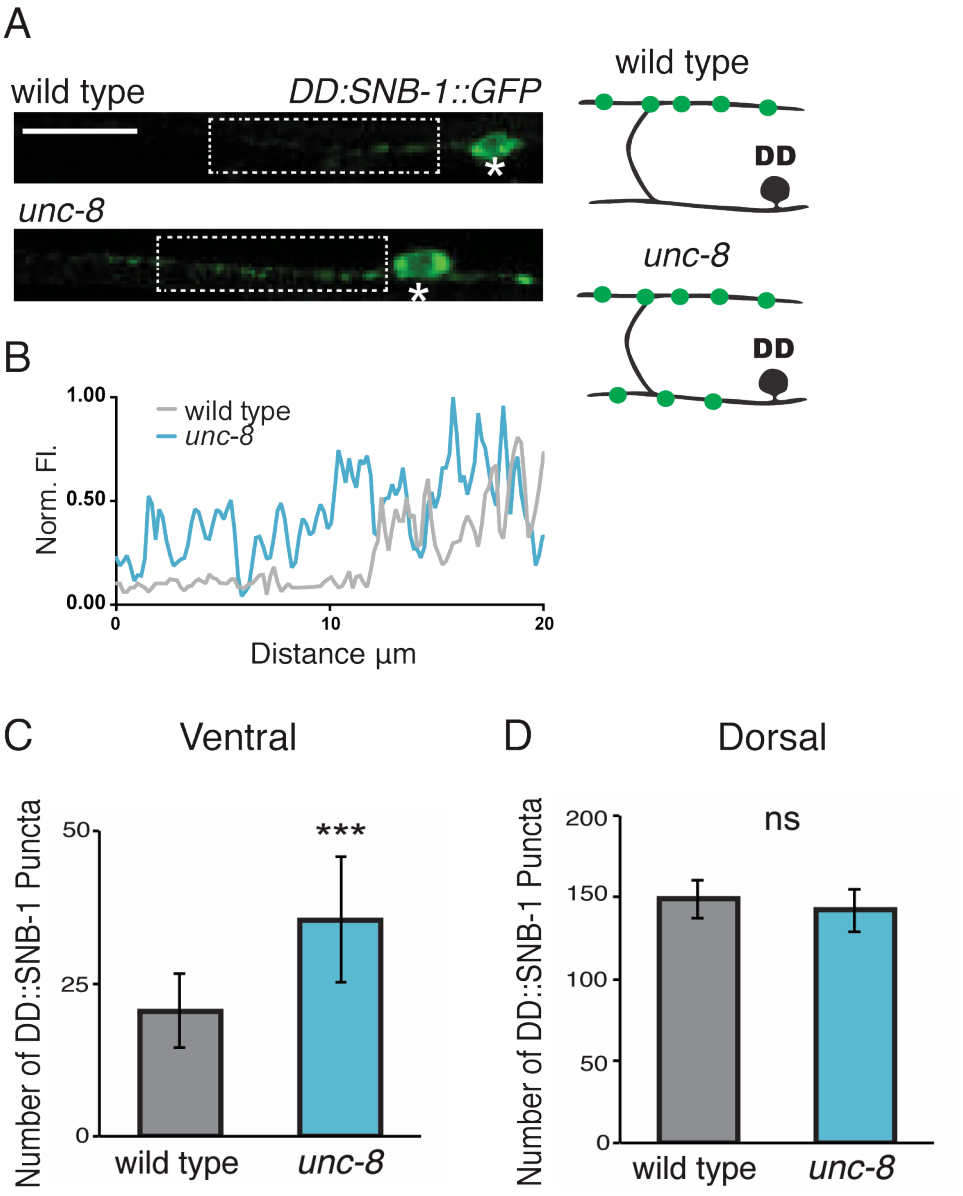

Figure 2.11: Synapse removal defects persist in the adult *unc-8* animals. A. Representative images of wild-type and *unc*-8 adult VNCs (asterisk denotes DD5 soma). Ventral DD::SNB-1::GFP puncta are retained in *unc-8* mutant adult animals. Scale bar is 10 µm. Inset shows pixel intensity over a 20 µm region (indicated by dashed boxes) of the VNC in wild-type and *unc-8* animals. (E) Removal of *pflp-13::SNB-1::GFP* puncta is defective in *unc-8* mutant adults; however, dorsal DD synaptic assembly is not affected (***$P < 0.001$, $n \geq 20$, ns is not significant, Student's *t*-test, data are mean ± SD).

UNC-8 protein is asymmetrically localized in neurons

We utilized two strategies to visualize fluorescently-labeled UNC-8 protein in GABAergic motor neurons. The UNC-8::GFP fosmid was detectable in the cell bodies of GABAergic and cholinergic neurons, in addition to ventral neuronal processes. Transgenic expression of fluorescently-tagged UNC-8 cDNA in GABA neurons, (*punc-25::UNC-8::GFP*) also resulted in bright cell soma expression and punctate labeling along the ventral nerve cord. These results indicate that UNC-8 localization is asymmetrically localized, potentially near the ventral DD synapses that undergo elimination. Interestingly, when we examined adult animals expressing the UNC-8::GFP fosmid, localization was still restricted to the ventral nerve cord (data not shown). This finding suggests that although the ventral presynaptic apparatus is dismantled and reassembled on the dorsal side, additional mechanisms may anchor UNC-8 to the ventral nerve cord, thus preventing its dorsal relocation.

Author Contributions

The microarray and RNAi experiments that identified *unc-8* as an *unc-55* target gene were performed by previous graduate student, Sarah C. Petersen. The images in **Figure 2.1** were collected by Sarah C. Petersen, and the UNC-8::GFP fosmid and *unc-8 tm5052 juIs1* recombinant strain was constructed by Sarah C. Petersen. The time course in **Figure 2.9** was initially collected by Sarah C. Petersen and was completed by Tyne Miller-Fleming. Undergraduate student Will Johnston assisted with the *unc-8* smFISH protocol. Rotation student Leif Neitzel assisted with the MBP::UNC-8ECD fusion peptide plasmid construction. Undergraduate students Patrick Meyers and Renzo Gutierrez helped construct the *unc-8* sgRNA plasmids. The remaining experiments

(strain construction, image collection, and synapse quantifications) in this chapter were performed by Tyne Miller-Fleming.

Acknowledgments

We thank O. Hobert for *otEx2876[punc-8::GFP; elt-2::GFP].* We thank S. Mitani and S. Hori for generating the *unc-8 tm5052* and *unc-8 tm2071* alleles. Some strains used in this study were provided by the CGC, which is funded by the NIH Office of Research Infrastructure Programs (P40 OD010440). We also received strains from the Japanese National BioResource Project. This work was supported by NIH grants 5R01NS081259 (DMM), and 1F31NS084732 (TWM). **Figures 2.1, 2.4, 2.5, 2.7, 2.8, 2.10**, and **2.11** were adapted from a manuscript published in *eLife* (Miller-Fleming et al. 2016).

CHAPTER III

UNC-8 PROMOTES SYNAPSE REMOVAL IN REMODELING GABAERGIC NEURONS

Summary

We identified the DEG/ENaC protein UNC-8 as a regulator of synapse removal in DD GABAergic motor neurons. Loss of function *unc-8* mutants show defects in synapse removal, as visualized by the retention of fluorescently-labeled presynaptic proteins in the ventral nerve cord. Data collected with the *punc-8::GFP* transcriptional reporter and the translational UNC-8::GFP fosmid construct show GFP expression in DD neurons and in *unc-55* mutant VD neurons. This result raises the possibility that UNC-8 channels also regulate GABAergic neuron remodeling in *unc-55* mutants, in which both DD and VD motor neurons remove their ventral connections.

Wild type DD motor neurons remove their ventral synapses during larval development to form nascent dorsal connections, while VD motor neurons generate ventral synaptic connections which are stabilized and do not remodel (see **Figure 1.5**, (White et al. 1978; Hallam & Jin 1998). The COUP/TF transcription factor UNC-55 represses remodeling in VD motor neurons; thus in *unc-55* mutants both DD and VD ventral synapses are removed and relocated to the dorsal nerve cord (Walthall & Plunkett 1995; H. M. Zhou & Walthall 1998; Shan et al. 2005). In this case, VD ventral synapse elimination occurs later during larval development than DD synapse removal. However, multiple lines of evidence indicate that these remodeling processes are comparable. For example, ectopic expression of UNC-55 in DD motor neurons blocks

synapse remodeling (Shan et al. 2005). Additionally, in *unc-55* mutants, VD motor neurons initially generate ventral synapses that are gradually removed during larval development, similar to wild-type DD neurons and these re-established dorsal synapses are functional (S. C. Petersen et al. 2011; Thompson-Peer et al. 2012). Most importantly, *unc-55* regulated genes such as *irx-1*, *hbl-1*, and *oig-1* also control DD remodeling (S. C. Petersen et al. 2011; He et al. 2015; Thompson-Peer et al. 2012).

Here we examine a role for UNC-8 in remodeling GABAergic neurons (DD and VD) in *unc-55* animals. As expected, we find that UNC-8 is required for synapse removal in wild-type DD neurons, in addition to *unc-55* mutant VD cells. UNC-8 expression functions cell-autonomously in GABAergic neurons and is sufficient to induce synapse removal. We find that UNC-8 is required for the elimination of multiple presynaptic proteins, including synaptobrevin-1, RAB-3, alpha-liprin, and endophilin. Furthermore, loss of *unc-8* restores presynaptic densities in electron micrographs collected from *unc-55* animals, suggesting that UNC-8 is required to disassemble multiple components of the presynaptic apparatus.

Materials and Methods

Strains and Genetics

C. elegans strains were cultivated at 20° C as previously described on standard nematode growth medium seeded with OP50 (Brenner 1974). The mutant alleles and strains used in this study are outlined in **Tables 3.1** and **3.2**.

Microscopy

Staging and Synapse Quantification

For time-course experiments, 100 adult hermaphrodites from each genotype were picked to fresh 60 mm plates and allowed to lay eggs for one hour. The mid-point at which the eggs were laid is considered T_0. All adults were removed from the plates after 1 hour. Plates were maintained at 23°C until assayed. Puncta arising from localization of fluorescent presynaptic markers were counted with a Zeiss Axiovert microscope (63X oil objective) in immobilized animals. For the timecourse experiment (**Figure 3.1**), puncta were counted between DD1 and DD6 in larvae and VD3 to VD11 in adults. In young adults, labeled puncta were counted in the ventral nerve cord region between VD3 and VD11 (**Figures 3.1, 3.3, 3.7, 3.11, 3.14**). For experiments featuring mosaic expression of either *unc-8 csRNAi* (**Figure 3.4**) or *unc-8cDNA* (**Figures 3.5, 3.6**), puncta were counted from individual DD and VD neurons. The examiner was blinded to genotype.

Confocal Microscopy and Image Analysis

Animals were immobilized on 2% agarose pads with 15mM levamisole as previously described (C. J. Smith et al. 2012; Miller-Fleming et al. 2016). Timecourse analysis and synapse counts of animals (**Figures 3.1, 3.4-3.7, 3.11,** and **3.14**) were collected with a Zeiss Axioplan inverted microscope using ImageJ Micro-Manager software and a 63x oil objective (camera ORCA; Hammamatsu). Z-stack images (**Figures 3.1, 3.2, 3.4-3.8, 3.12** and **3.13**) were collected on a Leica TCS SP5 confocal microscope using a 63X oil objective (0.5 µm/step), spanning the focal depth of the ventral nerve cord GABA neurons and synapses. Leica Application Suite Advanced Fluorescence (LAS-AF) software was used to generate maximum intensity projections. Images in **Figure 3.2**

were collected from 10 animals of each genotype. Ventral nerve cord images between VD4 and VD5 were straightened using an ImageJ plug-in and aligned in rows. Fluorescence intensity values in **Figure 3.3** were generated in ImageJ by determining the mean gray value or the average number of pixels normalized by the length of regions of interest drawn around the ventral presynaptic puncta. These values were corrected for background fluorescence. Fluorescence intensity plots (**Figure 3.2**) were created by drawing a line through the ventral nerve cords of each animal and calculating the fluorescence intensity value in arbitrary units over the distance in micrometers with the ImageJ plot profile tool. Fluorescence intensity plots in **Figure 3.8** were created with the ImageJ plot profile tool, analyzing the same region of the ventral nerve cord in both GFP and RFP channels. Fluorescence intensity values were normalized for each channel. The coefficient of determination (r^2) in **Figures 3.8, 3.12,** and **3.13** were calculated in ImageJ using the Manders coefficients macro, from at least 3 animals for each genotype. r^2 values were averaged and presented as mean ± SEM. An r^2 value of 0 represents no co-localization, whereas $r^2 = 1$ represents complete co-localization. The examiner was blinded to genotype.

Electron Microscopy

All electron microscopy experiments were performed by Laura Manning, a graduate student in Janet Richmond's lab at University of Illinois at Chicago.Young adult hermaphrodites of each strain were prepared for high-pressure freeze (HPF) fixation as described(Rostaing et al. 2004; Miller-Fleming et al. 2016). 10–15 animals were loaded into a specimen chamber filled with *E. coli.* The specimens were frozen rapidly in a high-pressure freezer (Bal-Tec HPM010) at -180°C and high pressure. Freeze substitution was performed on frozen samples in a Reichert AFS machine (Leica, Oberkochen,

Germany) with 0.1% tannic acid and 2% OsO_4 in anhydrous acetone. The temperature was kept at -90°C for 107 h, increased at 5°C/h to -20°C, and kept at -20°C for 14h. The temperature was then increased by 10°C/h to 20°C. Fixed specimens were embedded in Epon resin after infiltration in 50% Epon/acetone for 4h, 90% Epon/acetone for 18h, and 100% Epon for 5 hours. Embedded samples were incubated for 48h at 65°C. All specimens were prepared in the same fixation procedure and labeled with anonymous tags so that the examiner was blinded for genotype. Ultra thin (40 nm) serial sections were cut using an Ultracut 6 (Leica) and collected on formvar- covered, carbon-coated copper grids (EMS, FCF2010-Cu). Grids were counterstained in 2% aqueous uranyl acetate for 4 min, followed by Reynolds lead citrate for 2 min. Images were obtained on a Jeol JEM-1220 (Tokyo, Japan) transmission electron microscope operating at 80 kV. Micrographs were collected using a Gatan digital camera (Pleasanton, CA) at a magnification of 100k. Images were quantified using NIH ImageJ software. Dorsal and ventral cords were distinguished by size and morphology. GABAergic synapses were identified by previously established criteria, including position in the cord as well as the morphology of the synapse (White et al. 1986; Jin et al. 1999). GABAergic synapses are larger than their cholinergic motor neuron counterparts, and the active zones in these synapses form a direct, perpendicular angle with muscle arms. On the other hand, the presynaptic density in cholinergic synapses orient at an acute angle to the muscle, generally 30-45° and are often dyadic. Some images were collected at 30k to aid in identifying synaptic identity based on terminal position in the cord. Two colleagues with expertise in EM reconstruction of the *C. elegans* ventral nerve cord independently reviewed synapse images from each strain to verify identification. Each profile represents an image taken of a 40 nm section. A synapse was defined as a set of serial

sections containing a presynaptic density and flanking sections from both sides without presynaptic densities. Synaptic vesicles were identified as spherical, light gray structures with an average diameter of ~30 nm. At least two animals were analyzed for each genotype. Numbers of profiles analyzed for each genotype were: wild type = 502, *unc-8* = 322, *unc-55* = 246, *unc-55; unc-8* = 304 for ventral GABAergic synapse evaluation; wild type = 502, *unc-8* = 322, *unc-55* = 246, *unc-55; unc-8* = 304 for ventral cholinergic synapse evaluation.

Cloning and Molecular Biology

Construction of pttr-39::UNC-8 plasmid

UNC-8 cDNA was PCR-amplified from pSGEM/pTWM60 with primers that span the UNC-8 cDNA sequence(Y. Wang et al. 2013). The primer sequences are: Forward 5'-ATGAGCGCAAGGAGTAGT-3' and Reverse 5'- TTTGCTCATTAACTCCTTTGT-3'. Primers include either 5'-AscI or 3'-EcoRI adaptors for inserting UNC-8 cDNA into pTWM35 (*pttr39::arx-5::GFP::unc-54*) in place of the ARX-5::GFP fragment. The resultant plasmid, pTWM92 (*pttr-39::*UNC-8cDNA) was injected (25 ng/µl) with co-selectable markers *pmyo-2*::*mCherry*::*unc-54* (2 ng/µl) and *punc-25::mCherry::RAB-3* (5 ng/µl) into *unc-55; unc-8 (tm5052) juIs1* or *juIs1* animals.

Table 3.1: Mutant alleles and genotyping primers used in this study.

Allele	Source	Genotyping Primer Sequences
unc-8 (tm5052) IV	NBRP	TGGGGCCCTAATAATTTCGA
		AGTGACAGTATGAAGCCAGG
unc-55 (e1170) I	CGC	TAAGGACTACACGGATCCTG
		CCCAAGAAAGAAAAGAGAGGT

Table 3.2: Strains used in this study.

Strain	Genotype
CZ333	*juIs1[punc-25::SNB-1::GFP; lin-15+]* IV
NC2387	*unc-8(tm5052) juIs1* IV
NC1851	*unc-55(e1170)* I; *juIs1* IV
NC2388	*unc-55(e1170)* I*; unc-8(tm5052) juIs1* IV
NC2319	*unc-55(e1170)* I; *unc-119(ed3)* III; *juIs1* IV; *wdEx658* [*punc-25::mCherry, unc-119(+)*]
NC2601	*unc-55(e1170)* I; *unc-119(ed3)* III; *juIs1* IV; *wdIs86*[*pttr-39::unc-8; unc-119+; punc-25::mCherry; pttr-39::unc-8 antisense*]
NC3064	*unc-55*; *unc-8 juIs1*; *wdEx*969[*pttr-39::UNC-8; punc-47::mCherry*]
	juIs1; UNC-8 cDNA
KP5348	*nuIs279[punc-25::UNC-57::GFP;punc-25::mCherry::RAB-3]*
NC2870	*unc-8(tm5052)* IV; *nuIs279*
NC2984	*unc-55(e1170)* I; *nuIs279*
NC2873	*unc-55(e1170)* I; *unc-8(tm5052)* IV; *nuIs279*
ZM54	*hpIs3[punc-25::SYD-2::GFP; lin-15+]* X
NC2875	*unc-8(tm5052)* IV; *hpIs3* X
NC1849	*unc-55(e1170)* I; *hpIs3* X
NC2874	*unc-55(e1170)* I; *unc-8(tm5052)* IV; *hpIs3* X
EG5052	*oxIs351[punc-47:ChR2::mCherry; lin-15+ LITMUS 38i]* X
NC2857	*unc-8(tm5052)* IV; *oxIs351* X
NC2211	*unc-55(e1170)* I; *oxIs351* X
NC2807	*unc-55(e1170)* I; *unc-8(tm5052)* IV; *oxIs351* X
NC3063	*pflp-13::mCherry::RAB-3 ;unc-55; unc-8 juIs1 IV*
NC3167	*wdEx961[punc-25::mCherry::RAB-3; ceh-22::GFP] ; oxIs22[punc-49::UNC-49B::GFP; lin-15+] II*
NC3168	*unc-8 (tm5052) IV; wdEx961; oxIs22 II*
NC3169	*unc-55 (e1170) I wdEx961; oxIs22 II*
NC3170	*unc-55(e1170) I; unc-8 (tm5052) IV; wdEx961; oxIs22 II*

Results

UNC-8 promotes synapse removal in remodeling GABAergic motor neurons

Based on the findings in **Chapter 2** that UNC-8 promotes synapse removal in DD motor neurons, we next examined the effects of *unc-8 tm5052* in *unc-55* animals where both DD and VD synapses are removed. We confirmed that ventral GABAergic

synapses (from both DD and VD neurons) labeled with fluorescently-tagged synaptobrevin (*SNB-1::GFP*) are depleted in *unc-55* animals, as previously shown (S. C. Petersen et al. 2011; Thompson-Peer et al. 2012). As anticipated, *unc-8 (tm5052)* suppresses *unc-55*-mediated synapse removal; significantly more ventral synapses are retained in the *unc-55; unc-8* animals (**Figure 3.1A-B,** Miller-Fleming et al. 2016). These effects are first observed in the third and fourth larval stages (36-48 hours post-lay), after VD motor neurons have initiated removal in *unc-55* animals and significantly more ventral synapses are retained and persist into adulthood (**Figure 3.1C**).

In addition to counting the number of SNB-1::GFP puncta in *unc-55* and *unc-55; unc-8* animals, we performed fluorescence intensity measurements to independently confirm our findings. Regions of interest were drawn (boxes) around the entire ventral nerve cord, excluding cell somas. We calculated both the average fluorescence intensities (average mean gray value) and average number of pixels (normalized to the length of the area measured) for the ventral nerve cords of wild-type, *unc-8, unc-55,* and *unc-55; unc-8* animals. Consistent with the independent quantification of changes in synaptic number, this approach determined that *unc-55* mutants show significantly less ventral fluorescence and that his effect is suppressed in the *unc-55; unc-8* strain (**Figure 3.2**). To eliminate potential variability, we also calculated fluorescence intensity in a specific region of the ventral nerve cord, between VD4 and VD5. Again, this approach also determined that ventral fluorescence intensity is reduced in *unc-55* animals due to GABAergic synapse removal and that *unc-8* is required for this effect (**Figure 3.2,** Miller-Fleming et al. 2016).

The marker used to label the presynaptic regions (*GABA::SNB-1::GFP*) in the experiments described above detects synaptic puncta arising from both DD and VD motor neurons. To determine the separate contributions of both DD and VD neurons,

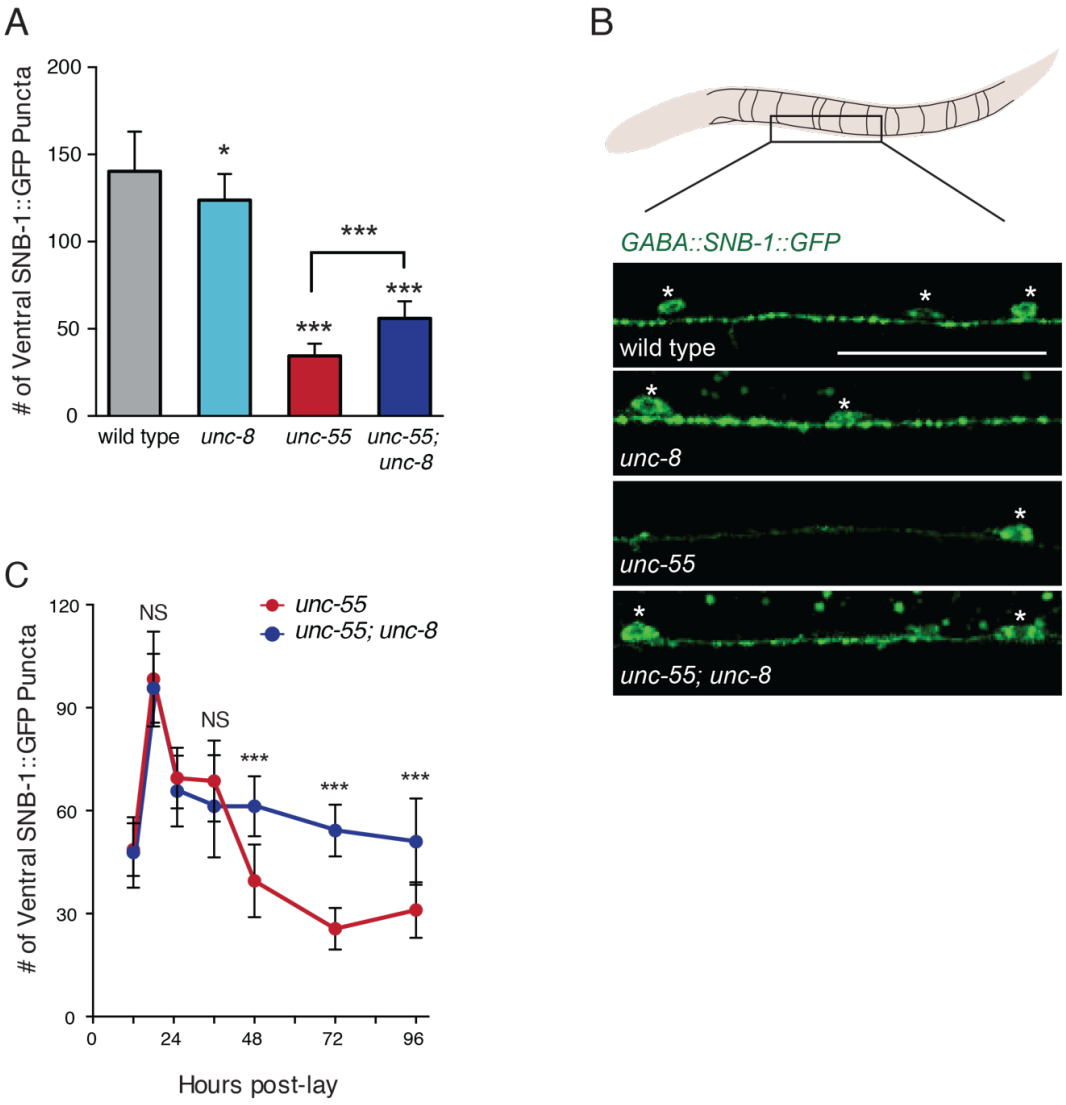

Figure 3.1: UNC-8 is required for synapse removal in remodeling GABAergic motor neurons. A. Ventral GABA synapses were labeled with the fluorescently-tagged presynaptic protein synaptobrevin (SNB-1::GFP). GFP-labeled puncta are removed from ventral synapses in *unc-55* and this effect requires *unc-8* (***$P < 0.001$, *$P < 0.05$, $n \geq 10$). One-Way ANOVA with Bonferroni correction, data are mean ± SD. **B.** Representative images of ventral SNB-1::GFP. Loss of *unc-55* results in the removal of ventral DD and VD synapses, visualized by a significant loss of SNB-1::GFP puncta. UNC-8 is required for complete synapse removal; loss of *unc-8* in the *unc-55* animals results in the retention of ventral SNB-1::GFP puncta. Scale bar is 25 μm, asterisks denote cell somas. **C.** *unc-55* animals remodel DD and VD synapses over the course of develop. Synapse removal is defective in the *unc-55; unc-8* animals and this effect persists in adult animals (***$P < 0.001$, NS is not significant, Student's *t*-test, $n \geq 78$ animals per genotype, data are mean ± SD).

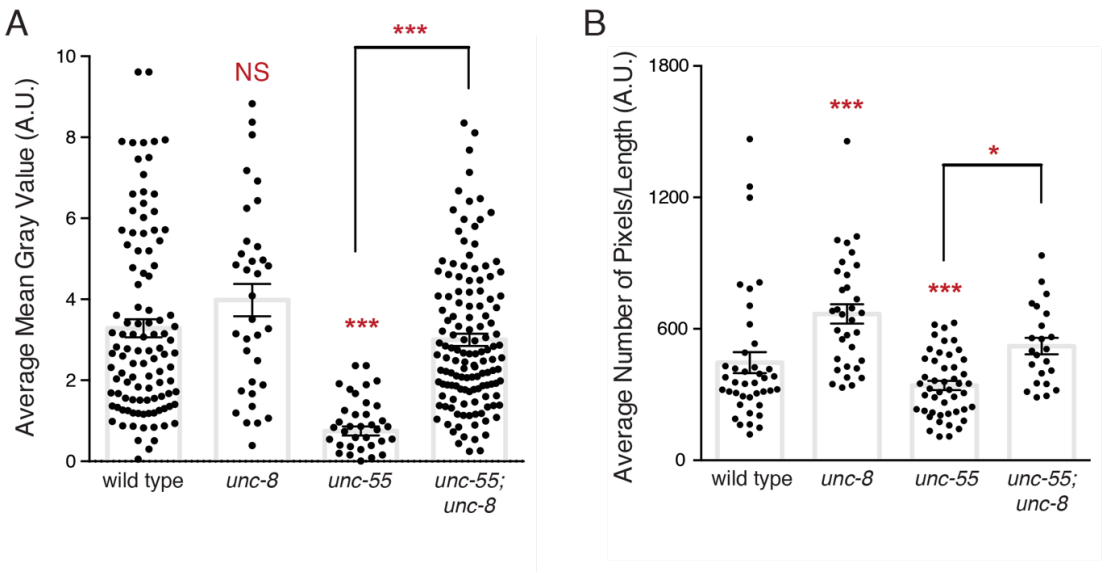

Figure 3.2: Loss of *unc-8* restores ventral fluorescent puncta to *unc-55* animals. A/B. Fluorescent SNB-1::GFP puncta are restored in *unc-55; unc-8* animals when measuring average fluorescence values (A) and average fluorescence normalized by nerve cord length (B). Data are average ± SEM (***P< 0.001, *P<0.05, NS is not significant, One-Way ANOVA with Bonferroni Correction, N ≥ 34).

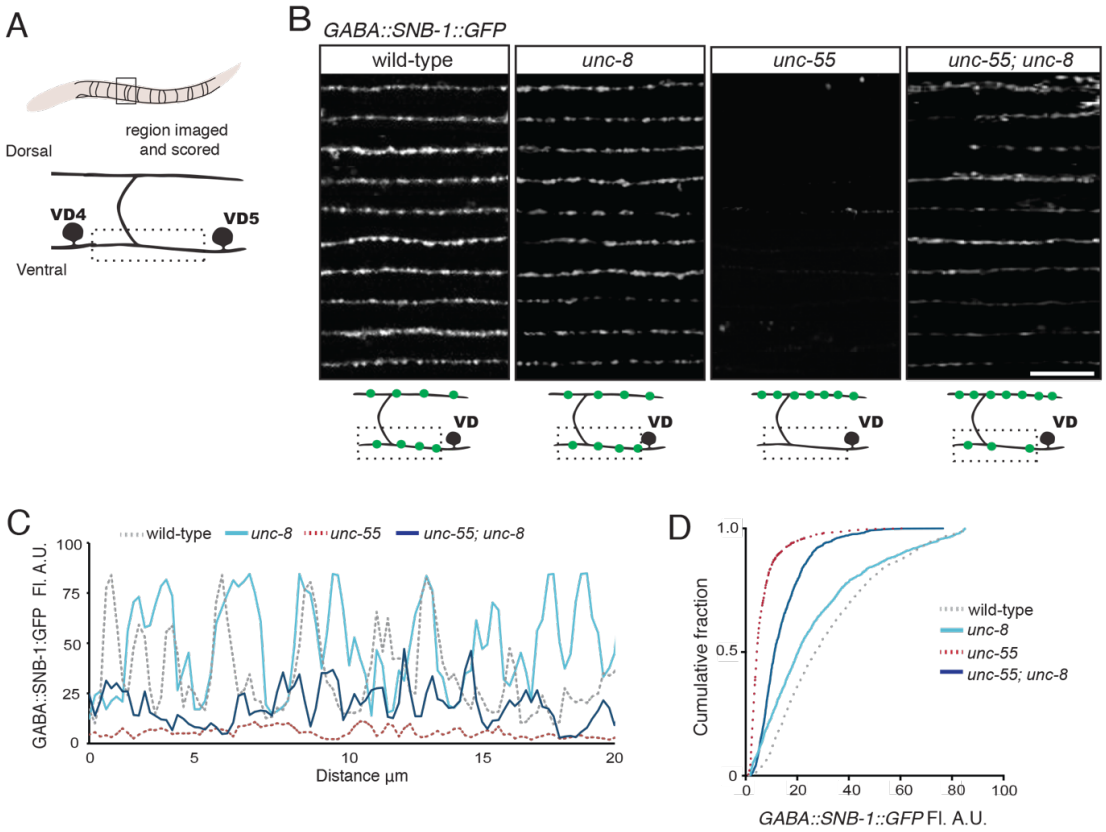

Figure 3.3: *unc-8* mutants demonstrate defects in ventral synapse removal. A. Data were collected from the VNC between VD4 and VD5. **B.** Ventral GABA synapses labeled with GFP-tagged synaptobrevin (*punc-25::SNB-1::GFP*) shown for 10 adult animals. Wild-type and *unc-8*(*tm5052*) show similar distributions of SNB-1::GFP puncta. Ventral SNB-1::GFP is depleted from *unc-55* due to VD remodeling, but partially restored in *unc-55; unc-8* animals. **C.** SNB-1::GFP fluorescent intensity measurements from each genotype. Each line represents the pixel intensity over a 20 µm region of the VNC from a single representative animal. **D.** Cumulative frequency curves for SNB-1::GFP fluorescence intensity for each genotype ($n > 10$ animals). *unc-55* animals show a significant loss of ventral SNB-1::GFP fluorescence ($P < 0.0001$ vs wild-type). SNB-1::GFP fluorescence is partially restored in the *unc-55; unc-8* animals, demonstrating the necessary role of UNC-8 in remodeling ($P < 0.0001$ vs *unc-55*). *P* values calculated with Kruskal-Wallis and Dunn's post-test.

GABAergic synapses were co-labeled with *GABA::SNB-1::GFP* and a DD-specific presynaptic label (*pflp-13::mCherry::RAB-3*). In this strain VD specific puncta (GFP) can be distinguished from DD presynaptic domains (GFP and mCherry). This experiment revealed that 40% of residual *unc-55; unc-8* puncta arise from DD neurons, whereas the remaining 60% are contributed by VD neurons (**Figure 3.4**). This result confirms the finding that loss of *unc-8* results in defective synapse removal in both DD and VD GABAergic motor neurons.

UNC-8 functions cell autonomously to promote synapse removal

We established in **Chapter 2** that *unc-8* is expressed in GABAergic motor neurons, in addition to several other cholinergic ventral cord cells (**Figure 2.6**). Despite the broad expression of *unc-8*, we predicted that synaptic removal requires UNC-8 function in GABAergic neurons. To test whether *unc-8* regulates GABAergic synapse removal in a cell-autonomous manner, we first used cell-specific RNA interference (csRNAi) to knock down *unc-8* expression in GABA neurons (S.C. Petersen 2011). As predicted, *unc-55* animals expressing control RNAi (empty vector RNAi) are depleted of ventral GABA synapses. In contrast, *unc-55* animals expressing *unc-8 csRNAi* retain significantly more ventral GABA synapses, therefore supporting a cell-autonomous role for UNC-8 in GABAergic synapse removal (**Figure 3.5**).

As an independent test of this model, we expressed wild-type *unc-8 cDNA* in the GABA motor neurons in *unc-55; unc-8* animals. This treatment rescued synapse removal, thereby confirming our hypothesis that UNC-8 drives synapse elimination cell-autonomously in GABAergic cells (**Figure 3.6,** Miller-Fleming et al. 2016).

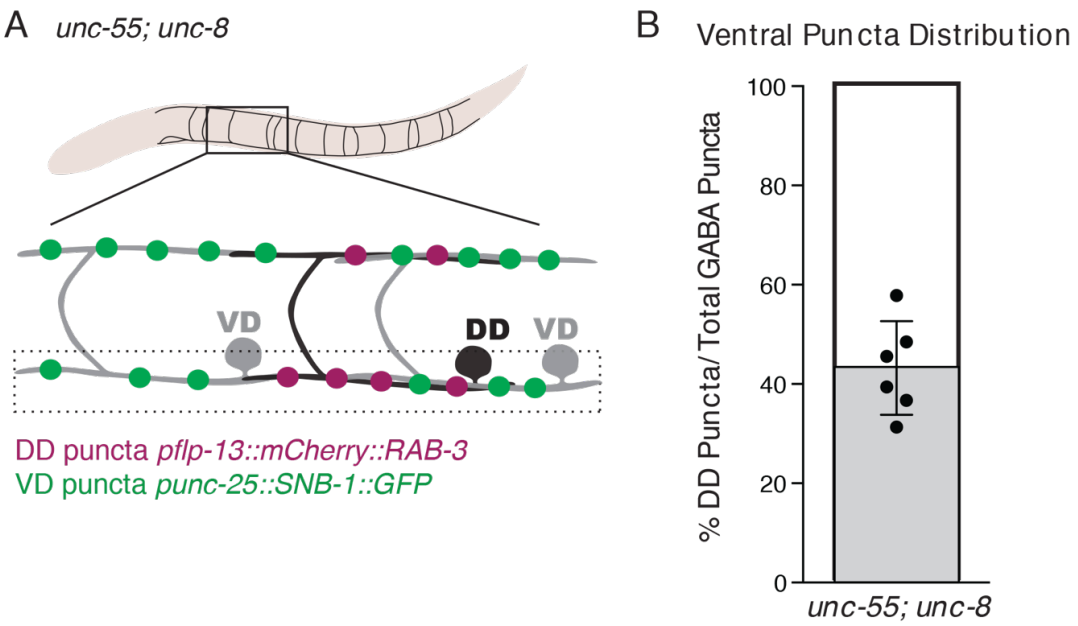

Figure 3.4: Residual ventral GABAergic puncta arise from the defective removal of remodeling DD and VD neurons in *unc-55; unc-8* animals. A. Ventral GABA synapses in *unc-55; unc-*8 animals were co-labeled with *punc-25::SNB-1::GFP,* which marks all synapses (DD and VD) and *pflp-13::mCherry::RAB-3,* which labels DD synapses only. **B.** The proportion of ventral DD synapses (labeled with *pflp-13::mcherry::RAB-3*) in *unc-55; unc-8* adults is shown in gray as a percentage of total ventral synapses (N= 6, data are mean ± SD).

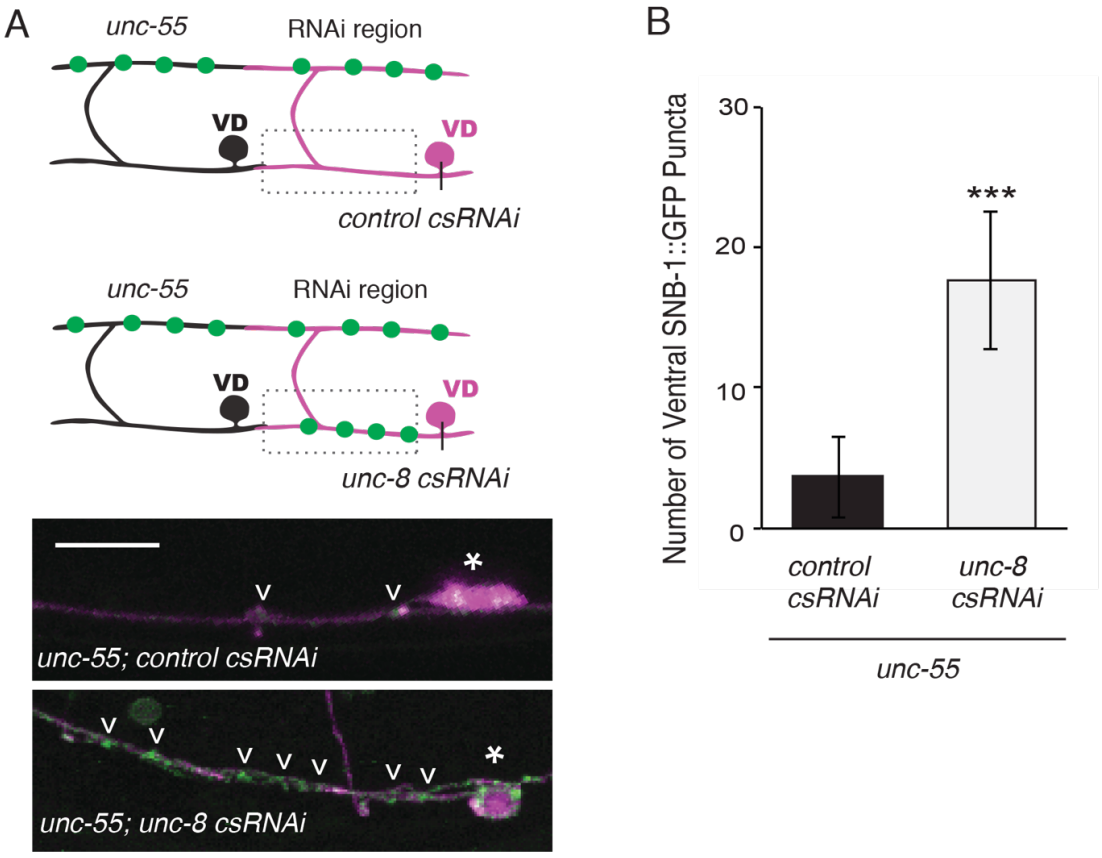

Figure 3.5: Cell-specific knockdown of *unc-8* perturbs ventral synapse removal. A. Knockdown of *unc-8* by GABA neuron-specific RNAi [*unc-8(csRNAi)*] restored SNB-1::GFP puncta to the VNC of *unc-55; juIs1* animals vs control animals expressing empty vector RNAi. GABAergic neurons are labeled with *punc-25*::*mCherry* (magenta). Asterisks denote GABA neuron cell bodies and arrowheads point to SNB-1::GFP-labeled ventral synapses. **B.** Ventral synapses anterior to each cell body expressing the RNAi construct were scored ($n \geq 60$ animals). Knockdown of *unc-8* in *unc-55* mutant GABA neurons significantly suppresses synaptic remodeling (***$P < 0.001$, Student's *t*-test. Data are mean ± SD). Scale bars are 10 µm.

UNC-8 overexpression induces synapse elimination

Because we found that UNC-8 is required for complete synapse removal and that these effects are mediated cell-autonomously in GABAergic neurons, we predicted that forced expression of UNC-8 might induce synapse removal in wild-type VD neurons. To test this idea *unc-8 cDNA* was overexpressed in wild-type GABA neurons. Mosaic expression of the *unc-8 cDNA* transgene provided an internal control to assess the role of *unc-8* in synapse removal in individual GABAergic neurons. For example, VD neurons expressing the *unc-8 cDNA* construct (co-labeled with a red fluorescent marker) were compared to neighboring VD neurons that do not express *unc-8 cDNA*. This experiment revealed that forced expression of *unc-8 cDNA* induces ventral synapse elimination, while neighboring VD neurons that do not express the *unc-8cDNA* transgene maintain their ventral connections (**Figure 3.7,** Miller-Fleming et al. 2016). These results demonstrate that UNC-8 alone is sufficient to drive ventral synapse disassembly in neurons that otherwise maintain stable, functional connections.

UNC-8 promotes the removal of the presynaptic apparatus

Based on our findings that *unc-8* promotes the removal of fluorescently-labeled synaptobrevin (SNB-1::GFP) and RAB-3 (mCherry::RAB-3) proteins, we next investigated the possibility that UNC-8 removes other key components of the presynaptic apparatus. To test this idea, we used the fluorescently-tagged presynaptic proteins endophilin (UNC-57::GFP) and liprin-alpha (SYD-2::GFP), which show a punctate distribution similar to that of SNB-1::GFP and mCherry::RAB-3 (**Figure 3.8**). Consistent with our previous findings, all of the ventral presynaptic markers that we examined were lost in *unc-55* animals and restored in *unc-55; unc-8* mutants (**Figure**

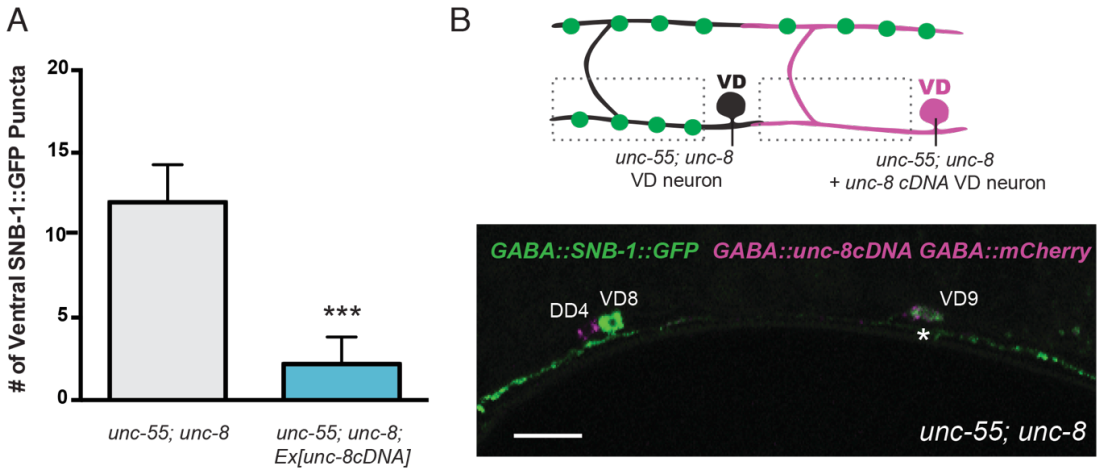

Figure 3.6: Expression of UNC-8 in GABAergic motor neurons rescues ventral synapse removal. A. UNC-8 function is cell-autonomous. Ventral synapses were counted in *unc-55; unc-8* animals injected with *GABA::UNC-8cDNA* and the GABA marker *punc-25::mCherry* (left). Asterisk denotes cell expressing *UNC-8cDNA* and *punc-25::mCherry,* scale bar is 10 µm. **B.** GABA neurons expressing *UNC-8cDNA* showed fewer ventral puncta than neighboring *unc-55; unc-8* neurons that do not express the *UNC-8cDNA* transgene, indicating that UNC-8 functions in GABA neurons to promote remodeling (***$P < 0.001$, $n \geq 15$ animals, Student's *t*-test, data are mean ± SD).

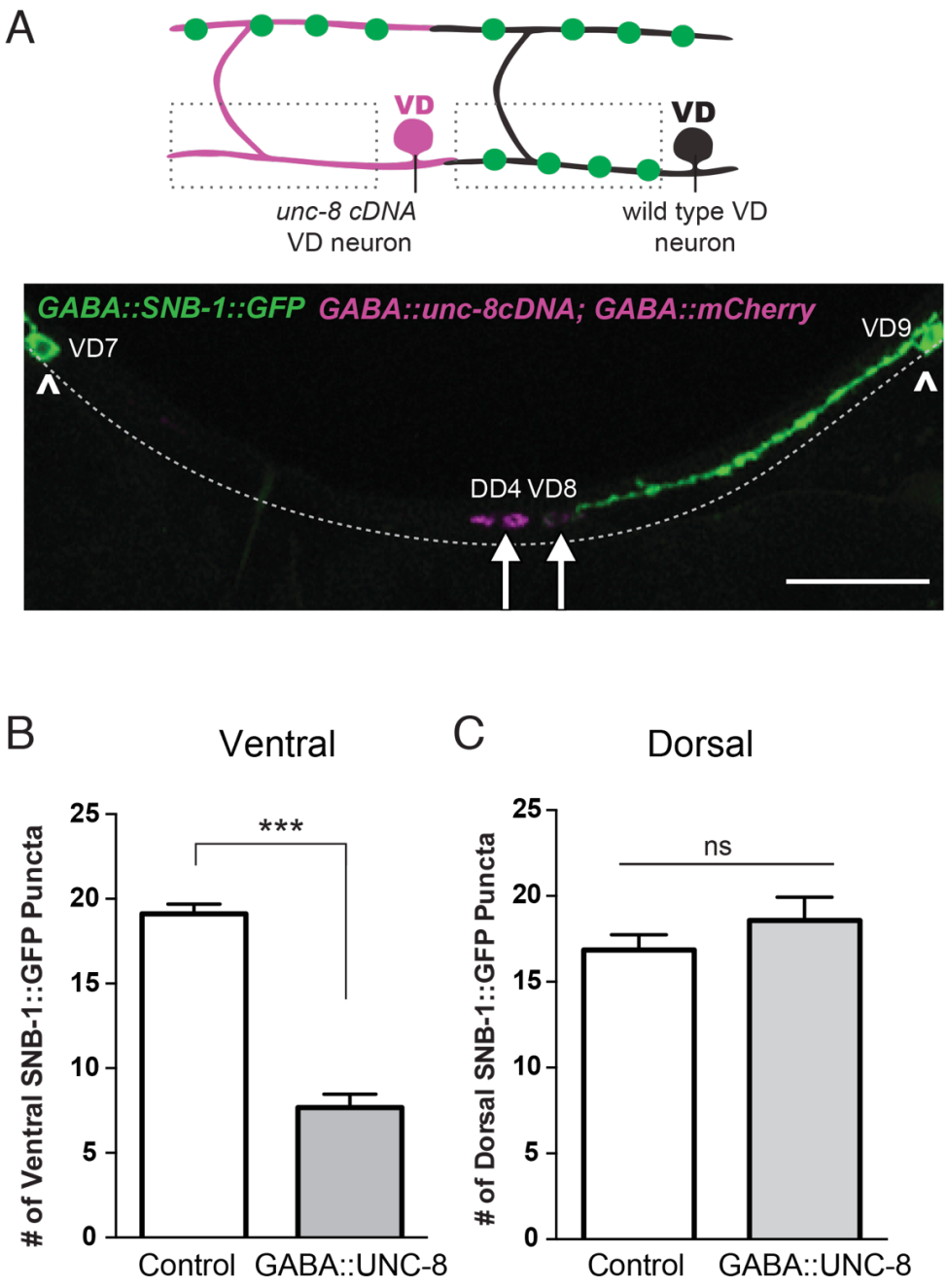

Figure 3.7: Expression of UNC-8 in GABAergic motor neurons is sufficient to remove ventral synapses. Ectopic expression of *unc-8cDNA* in GABA neurons induces ventral synapse removal. VD neurons expressing *unc-8cDNA* (co-labeled with GABA::mCherry, VD8 denoted with arrow) show significantly fewer ventral SNB-1::GFP (*punc-25::SNB-1::GFP*) puncta than neighboring VD neurons that do not express *unc-8cDNA* which are unaffected (e.g., VD9 denoted with arrowhead). Anterior to left. Ectopic expression of *unc-8cDNA* in VD neurons has no effect on dorsal synapses (***$P < 0.001$, ns is not significant, Student's *t*-test, $n \geq 51$ VDs (ventral) and $n = 7$ VDs (dorsal), data are mean ± SEM).

3.8). These results confirm that UNC-8 removes multiple presynaptic proteins during synapse elimination.

Because UNC-8 removes presynaptic markers that localize to both vesicles (SNB-1, RAB-3, UNC-57) and to the presynaptic membrane (UNC-57 and SYD-2), we tested the prospect that UNC-8 dismantles the entire presynaptic apparatus (Dai et al. 2006; Schuske et al. 2003). We simultaneously imaged mCherry::RAB-3 and UNC-57::GFP in *unc-55; unc-8* animals to monitor the organization of the residual presynaptic domains. As expected, mCherry::RAB-3 and UNC-57::GFP are strongly co-localized at ventral synapses in wild-type animals. Interestingly, although fewer presynaptic clusters are detected at ventral synapses in *unc-55; unc-8* mutants, residual mCherry::RAB-3 and UNC-57::GFP presynaptic domains are comparably co-localized (**Figure 3.9,** Miller-Fleming et al. 2016). This finding suggests that the residual ventral puncta in *unc-55; unc-8* animals may be organized presynaptic structures.

As an additional test of the prediction that UNC-8 dismantles the presynaptic apparatus we performed electron microscopy (EM) to examine the structure of the residual GABAergic synapses in *unc-55; unc-8* animals. Both GABAergic and cholinergic presynaptic densities are visible by EM, but can be distinguished by morphological criteria (see **Methods**). Consistent with our fluorescent marker data, ventral GABAergic synapses were detected in wild type, *unc-8*, and *unc-55; unc-8* animals (wild type = 6 synapses/20.08 µm, n = 3 animals, *unc-8* = 5 synapses/12.88 µm, n = 2 animals, *unc-55; unc-8* = 2 synapses/12.16 µm, n = 2 animals, **Figures 3.10** and **3.11**). We did not detect ventral GABAergic presynaptic densities in *unc-55* animals as expected; however, ventral cholinergic presynaptic densities were preserved. Taken together, our findings validate a role for UNC-8 in the disassembly of the presynaptic apparatus.

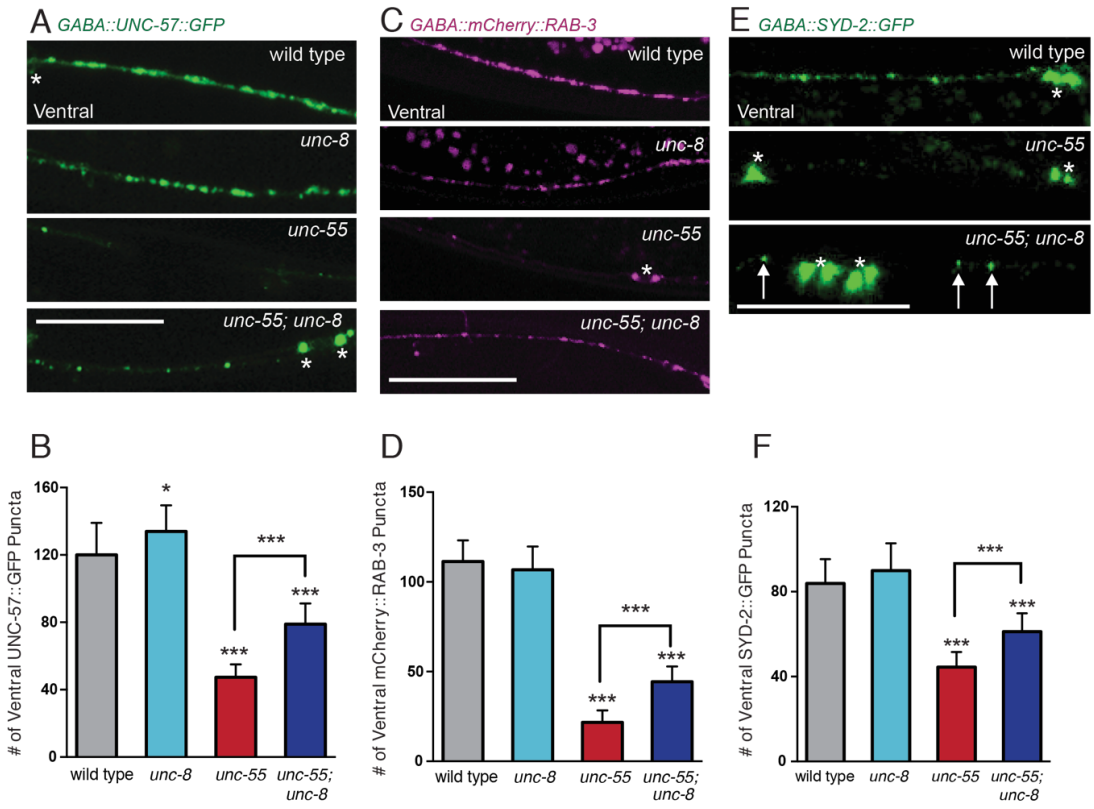

Figure 3.8: UNC-8 orchestrates the removal of multiple proteins that make up the presynaptic apparatus. A/B. Representative images (A) and quantification (B) of endophilin/UNC-57 indicate that *unc-8* is required for the removal of UNC-57::GFP from ventral synapses in remodeling neurons (*$P < 0.05$, ***$P < 0.001$, $n \geq 25$). **C/D.** Removal of the presynaptic G protein RAB-3 fails in *unc-55; unc-8* animals (***$P < 0.001$, $n \geq 21$). **E/F.** Efficient removal of the presynaptic density protein α-liprin/SYD-2 from ventral synapses in *unc-55* requires *unc-8* (***$P < 0.001$, $n \geq 21$). Scale bars are 10 µM, asterisks denote cell somas, SYD-2::GFP puncta denoted by arrows. One-Way ANOVA with Bonferroni correction, data are mean ± SD.

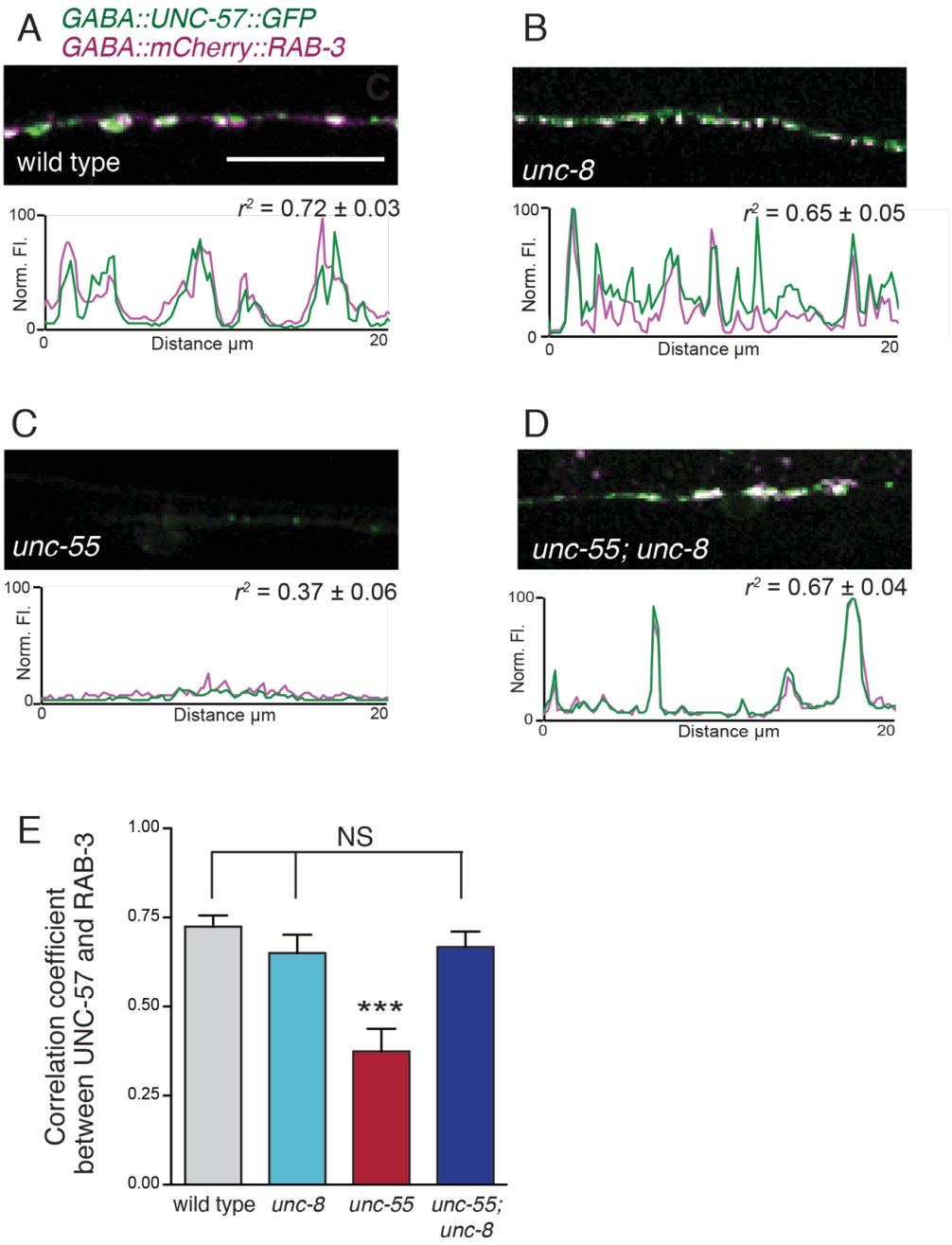

Figure 3.9: Restored ventral presynaptic proteins are colocalized in *unc-55; unc-8 animals*. A-D. GFP-tagged endophilin (*punc-25::UNC-57::GFP*) and mCherry::RAB-3 (*punc-25::mCherry::RAB-3*) are co-localized in GABA neurons of wild-type, *unc-8,* and *unc-55;unc-8* animals. Representative images and normalized fluorescence intensity plots for a 20 µm region of the ventral nerve cord are shown. Scale bar is 10 µm. r^2 is Pearson's correlation coefficient ($n \geq 10$, mean ± SEM). Presynaptic components are co-localized in wild type ($r^2 = 0.72 \pm 0.03$), *unc-8* ($r^2 = 0.65 \pm 0.05$) and *unc-55;unc-8* ($r^2 = 0.67 \pm 0.04$); however, puncta are less colocalized in *unc-55* animals ($r^2 = 0.37 \pm 0.06$). Average r^2 value for *unc-55;unc-8* is not statistically different from the average r^2 value for wild type and *unc-8* (***$P < 0.001$, Mann-Whitney test).

Discussion

The *unc-55*-mediated VD remodeling pathway mirrors the endogenous DD remodeling pathway

Based on previously published studies, we predicted that the remodeling pathway initiated by a loss of *unc-55* in VD motor neurons utilizes shared mechanisms with the endogenous remodeling pathway in wild-type DD motor neurons (S. C. Petersen et al. 2011; Thompson-Peer et al. 2012; Shan et al. 2005). In support of this hypothesis, we determined that *unc-8* is required for ventral GABAergic synapse removal in both VD and DD cells (**Figure 3.4**). This finding validates the observation in **Chapter 2** that *unc-8* promotes synapse removal. We previously exploited the Unc-55 remodeling phenotype to uncover novel regulators of synapse removal (i.e., genes that are enriched in *unc-55* mutant GABA neurons versus wild type). This approach yielded 19 conserved genes, suggesting that synaptic remodeling may require multiple components and that *unc-8* specifically regulates synapse removal in one of these pathways.

UNC-8 disassembles multiple components of the presynaptic apparatus

We validated a role for *unc-8* in GABAergic synapse removal by using fluorescent markers of several presynaptic proteins. Vesicular components including the vesicular SNARE protein synaptobrevin (SNB-1) and the G-protein RAB-3 are removed by the UNC-8-dependent pathway. Additionally, we found that UNC-8 eliminates the membrane protein alpha-liprin (SYD-2) and the membrane bending molecule endophilin

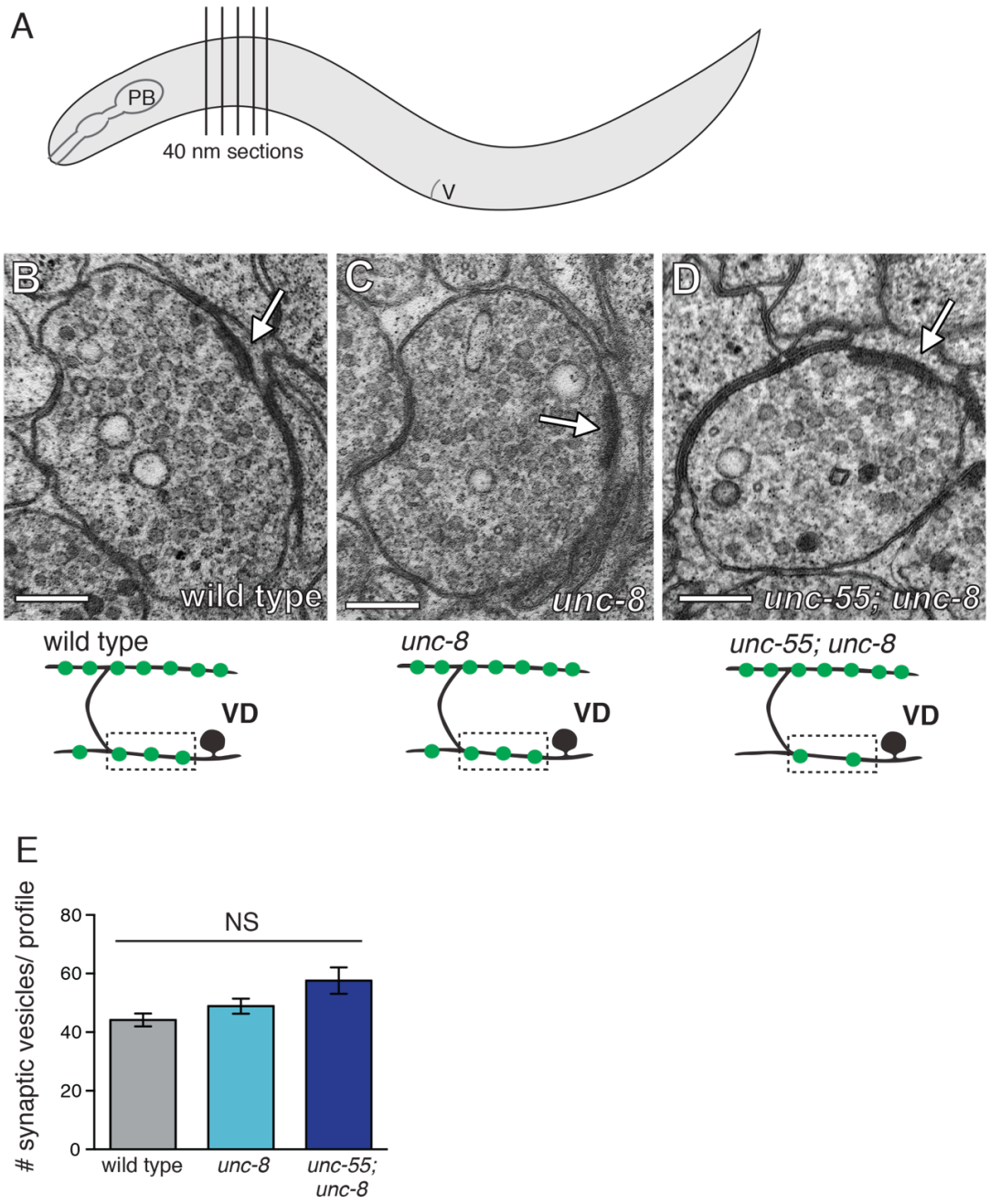

Figure 3.10: UNC-8 promotes ventral GABAergic synapse removal. A. Electron micrograph images were collected from animals that underwent high pressure freezing and were sliced into 40 nm sections from the posterior bulb of the pharynx (PB) to the vulva (V). **B-D.** Electron micrographs of GABA synapses with ventral muscles in (**B**) wild type, (**C**) *unc-8* and (**D**) *unc-55; unc-8*. No ventral GABA presynaptic densities were detected in *unc-55*. Arrows point to presynaptic density, scale bars are 200 nm. (**E**) Synaptic vesicles were quantified in ventral GABAergic synapses. Synapses in wild-type, *unc-8* and *unc-55;unc-8* animals contain comparable numbers of synaptic vesicles (N > 5 for each genotype, ns is not significant). EM images were collected by Laura Manning.

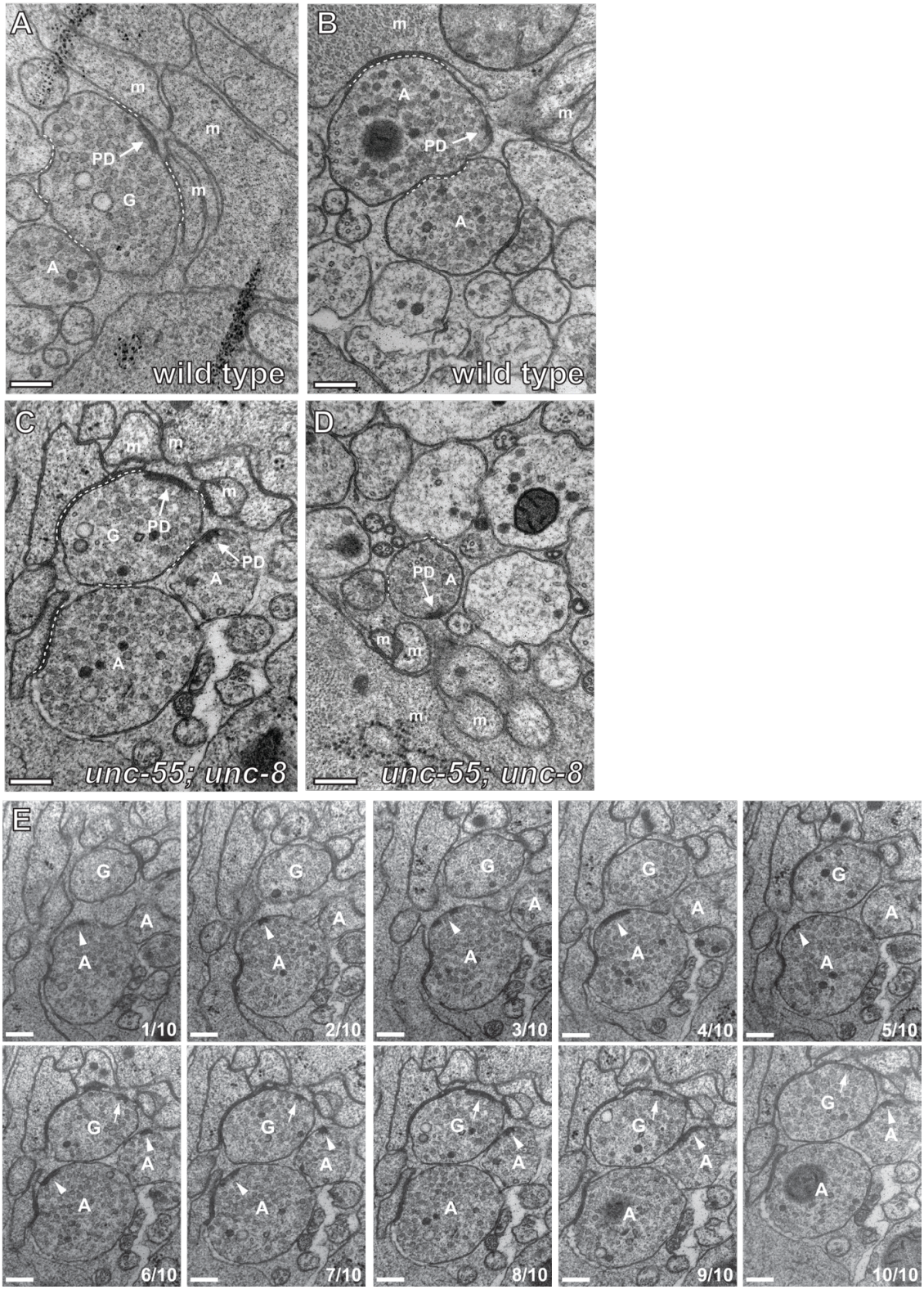

Figure 3.11: Ventral GABAergic and cholinergic synapses are detectable in electron micrographs of wild-type and *unc-55; unc-8* animals. A-B. Ventral GABAergic (A) and cholinergic (B) presynaptic densities are visible in electron

micrographs from wild-type animals. **C-D**. Ventral GABAergic (C) and cholinergic (C/D) presynaptic densities were also detected in *unc-55; unc-8* animals, suggesting that wild-type *unc-8* function is required for the complete removal of ventral GABA synapses in *unc-55* mutants. Arrows denote presynaptic densities, PD (presynaptic density), G (GABAergic neuron), A (cholinergic neuron), m (muscle arm), dotted lines are adherens or gap junctions. **E**. Serial slices from the ventral nerve cord of the *unc-55; unc-8* animals. 10 serial slices span a region with GABAergic neuron terminal (denoted by G) and cholinergic neuron terminal (denoted by A). Each micrograph slice number is listed in lower right corner. Cholinergic (arrowhead) and GABAergic (arrow) presynaptic densities are labeled. GABAergic and cholinergic neuron synapses were distinguished by previously established criteria (see **Methods**). Scale bars are 200 nm. Images were collected by Laura Manning.

(UNC-57) from the ventral presynaptic region (Miller-Fleming et al. 2016). Analysis of electron micrographs from *unc-55; unc-8* animals contained detectable presynaptic densities and synaptic vesicles in GABAergic neurons, suggesting that without *unc-8*, presynaptic components that would normally be eliminated by the remodeling program are incorrectly maintained. Therefore, localization of fluorescently-tagged presynaptic proteins and EM analysis confirm that *unc-8* is required for proper removal of the presynaptic density in GABAergic cells. Consistent with our fluorescent reporter data, retained ventral synapses in *unc-55; unc-8* GABA neurons were detected much less frequently than synapses in wild-type and *unc-8* animals (2 synapses over 12.16 µm examined for *unc-55 unc-8*, compared to 6 synapses over 20.08 µm for wild type and 5 synapses over 12.88 µm for *unc-8*, Miller-Fleming et al. 2016).

UNC-8 is sufficient for synapse removal

Experiments reported here identified a necessary role for *unc-8* in the disassembly of ventral GABAergic presynaptic domains. Additionally, we discovered that forced expression of UNC-8 protein in VD neurons induces synapse removal. Because VD synapses normally do not remodel, this finding tells that UNC-8 is sufficient to trigger synapse elimination and suggests that the machinery needed to remove GABA presynaptic components is normally present in VD cells. This finding also highlights our proposal that transcriptional upregulation of *unc-8* acts as a genetic switch that drives removal of the presynaptic signaling apparatus in GABAergic cells.

Author Contributions

The control and *unc-8 csRNAi* plasmids were generated by previous graduate student Sarah C. Petersen. Undergraduate student Renzo Gutierrez helped construct the *punc-25::mCherry::RAB-3* strain. All of the electron microscopy was performed by graduate student Laura Manning under the guidance of Janet Richmond at University of Illinois at Chicago. The remaining experiments (plasmid and strain construction, image collection, and quantifications) in this chapter were performed by Tyne Miller-Fleming.

Acknowledgments

We thank M. Francis for the *pflp-13::mCherry::RAB-3* strain in **Figure 3.11**. We also thank J. Kaplan and M. Zhen for the *nuIs279* and *hpIs3* strains, respectively. Some strains used in this study were provided by the CGC, which is funded by the NIH Office of Research Infrastructure Programs (P40 OD010440). We also received strains from the Japanese National BioResource Project. This work was supported by NIH grants 5R01NS081259 (DMM), and 1F31NS084732 (TWM). **Figures 3.1, 3.2**, and **3.4-3.12** were adapted from a manuscript published in *eLife* (Miller-Fleming et al. 2016).

CHAPTER IV

UNC-8 PROMOTES GABAERGIC SYNAPSE ELIMINATION IN AN ACTIVITY-DEPENDENT PATHWAY

Summary

Developing neural circuits are pruned by a combination of genetic programs and neuronal activity. Neuronal connections are removed in some locations and stabilized in others to produce a functional nervous system. The wiring of the nervous system occurs during specific developmental windows, or critical periods when genetic programs sensitize the nervous system to activity from the external environment. In one example the visual system is established by light exposure during a critical period of development. This time window of plasticity was determined by occluding one eye from light, which antagonizes proper circuit formation, and results in monocular blindness. Interestingly, reversal of the eye occlusion before the critical period ends allows for proper neural connectivity and vision (Wiesel & Hubel 1963; Hubel & Wiesel 1970). Critical periods of plasticity are seen in other regions of the brain as well. For example, each Purkinje cell of the mammalian cerebellum is initially innervated by several incoming axonal projections called climbing fibers (Miyazaki et al. 2004; Hashimoto et al. 2011). Loss of calcium signaling via the P/Q-type voltage-gated calcium channels (VGCCs) impedes synapse removal in this system, such that Purkinje cells maintain multiple inputs from climbing fibers in this mutant background (Miyazaki et al. 2004; Hashimoto et al. 2011). Despite a critical role for both transcriptional regulation and

activity to shape neural circuits, the interactions between these two pathways are not well understood.

Here, we describe a mechanism for the DEG/ENaC protein UNC-8 that mediates the intersection of genetically-regulated and activity-dependent pathways to drive synapse removal. We find that *unc-8* promotes GABAergic synapse removal in a pathway with the VGCC subunit UNC-2. Additionally, we find that the calcium-activated phosphatase calcineurin (TAX-6) promotes synapse removal upstream of the UNC-8-dependent pathway, consistent with the conserved role of calcineurin in synaptic stability. Finally, we connect the upstream calcium-dependent pathway and UNC-8 channel activity to a synaptic removal process that requires activation of canonical cell death (CED) components. Activation of the CED pathway in GABAergic neurons has been shown to dismantle presynaptic complexes via gelsolin-dependent severing of F-actin filaments (Meng et al. 2015). Therefore, we propose a model in which UNC-8 triggers synapse elimination by the intersection of the UNC-55-regulated genetic program and a calcium-signaling pathway that promotes neurotransmission.

Materials and Methods

Strains and Genetics

C. elegans strains were cultured at 20° C as previously described on standard nematode growth medium seeded with OP50 (Brenner 1974). The mutant alleles and strains used in this study are outlined in **Tables 4.1** and **4.2**.

Microscopy

Staging and Synapse Quantification

Puncta arising from localization of fluorescent presynaptic markers were counted with a Zeiss Axiovert microscope (63X oil objective) in immobilized animals. In young adults, labeled puncta were counted in the ventral nerve cord region between VD3 and VD11 (**Figures 4.1, 4.2, 4.4-4.7, 4.9, 4.11-4.13**). The examiner was blinded to genotype. For the timecourse experiment (**Figure 4.8**), puncta were counted between DD1 and DD6 in larvae. For the time-course experiment, 100 adult hermaphrodites from each genotype were picked to fresh 60 mm plates (control or 3mM Benzamil) and allowed to lay eggs for one hour. The mid-point at which the eggs were laid is considered T_0. All adults were removed from the plates after 1 hour. Plates were maintained at 23°C until assayed.

Confocal Microscopy and Image Analysis

Animals were immobilized on 2% agarose pads with 15mM levamisole as previously described (C. J. Smith et al. 2012). Timecourse analysis and synapse counts of animals were collected with a Zeiss Axioplan inverted microscope using ImageJ Micro-Manager software and a 63x oil objective (camera ORCA; Hammamatsu). Z-stack images (**Figures 4.1, 4.4, 4.6, 4.7, 4.11** and **4.12**) were collected on a Leica TCS SP5 confocal microscope using a 63X oil objective (0.5 µm/step), spanning the focal depth of the ventral nerve cord GABA neurons and synapses. Leica Application Suite Advanced Fluorescence (LAS-AF) software was used to generate maximum intensity projections. Fluorescence intensity plots (**Figure 4.1** and **4.4**) were created by drawing a line through the ventral nerve cords of each animal and calculating the fluorescence intensity value in arbitrary units over the distance in micrometers with the ImageJ plot profile tool.

Molecular Biology

Generation of the fluorescently-tagged utrophin strain

The *pttr-39::GFP::utrophin* plasmid (pTWM1) was generated by replacing the PVD-specific promoter *F49H12.4* in plasmid pCSJ91 (*pF49H12.4::GFP::utrophin*) with the GABA neuron specific promoter *pttr-39* from plasmid pSA47 (*pttr-39::IRX-1 csRNAi F*). Promoters from each plasmid were flanked by SphI and AscI restriction sites. 8 μg of this constructed was transformed into *pha-1 e2123* mutant animals with the *pha-1* rescuing plasmid (pBx) using microparticle bombardment as previously described (Spencer et al. 2011; S. C. Petersen et al. 2011). Animals eliciting *pha-1*-rescued lethality at 25°C were maintained and examined for GFP expression.

Feeding RNA Interference Experiments

Bacteria producing either double-stranded *cca-1, arx-5, ubc-1, ubc-23* RNA or containing the RNAi empty vector were seeded on NGM plates and stored at 4°C for up to 1 week. Four L4 *unc-55; eri-1* animals were grown on each single RNAi plate at 23°C until progeny reached the L4 stage, or about 3-4 days. Progeny were picked to fresh RNAi plates and the ventral synapses were quantified (**Figures 4.5, 4.12,** and **4.13**). *eri-1* is a conserved RNAse in *C. elegans* that impedes the processing of RNA interference. Including this mutation in the genetic background of our strain sensitizes the animals to RNAi (Kennedy et al. 2004).

Pharmacology

Amiloride hydrochloride hydrate (Sigma, #A7410) stock solution was prepared in sterile water (50 mg/ml) and stored at -20°C. A final concentration of 3 mM Amiloride diluted in OP50 bacteria was seeded on NGM plates. Control NGM plates contained the same

volume of sterile water added to OP50. Benzamil hydrochloride hydrate (Sigma, #B2417) stock solution was prepared in sterile water (1 mg/ml) and stored at 4°C. A final concentration of 3 mM Benzamil diluted in OP50 bacteria was seeded on NGM plates. Control NGM plates contained the same volume of sterile water added to OP50. Plates were stored at 4°C for up to one week. Five adult *unc-55; juIs1* animals were placed on either Amiloride, Benzamil, or control plates at room temperature and progeny examined at the young adult stage (**Figure 4.1** and **4.2,** (Miller-Fleming et al. 2016)). Adult *tax-6(d); wyIs202* animals were grown on Benzamil or control plates and their larval progeny were collected on control or Benzamil plates for timecourse assays (**Figure 4.8**). The examiner was blinded to genotype and treatment condition.

Oocyte electrophysiology

These experiments were performed by Crisitna Matthewman in the Bianchi lab at Univerity of Miami. UNC-8(G387E) cRNA was synthesized using T7 mMESSAGE mMACHINE kit (Ambion). cRNA was purified and examined on a denaturating agarose gel to confirm correct size and integrity. cRNA quantification was performed spectroscopically. Stage VI defolliculated oocytes from *Xenopus Laevis* were purchased from Ecocyte Bioscience US LLC (Austin, Texas). Oocytes were injected with 10 ng/oocyte of cRNA and incubated in OR2 solution (82.5 mM NaCl, 2.5 mM KCl, 1 mM $CaCl_2$, 1 mM $MgCl_2$, 1 mM Na_2HPO_4, 0.5 g/liter polyvinyl pyrolidone, and 5 mM HEPES, pH 7.2, supplemented with penicillin and streptomycin (0.1 mg/ml) and 2 mM Na-pyruvate) plus 500 μM amiloride (to prevent channel hyperactivation-dependent cell death) at 20°C for 2–3 d before recordings. Currents were measured using a two-electrode voltage-clamp amplifier (GeneClamp 500B; Axon Instruments) at room temperature. Electrodes (0.2–0.5 MΩ) were filled with 3 M KCl, and oocytes were

perfused with a physiological NaCl solution (100 mM NaCl, 2 mM KCl, 1 mM $CaCl_2$, 2 mM $MgCl_2$, and 10 mM HEPES, pH 7.2) and divalent cation free plus EGTA NaCl solution (110 mM NaCl, 2 mM KCl, 1 mM EGTA, and 10 mM HEPES, pH 7.2). pH was adjusted at the indicated values using NaOH. The oocyte membrane was clamped at –30 mV and stepped from –160 to +100 mV. Benzamil was added to the solutions from a stock of 10 mM. A saturating concentration of benzamil (1mM) was added at the end of each experiment to confirm that endogenous/leak currents were similar in amplitude to non-injected oocytes within each oocyte batch. Oocytes that had larger endogenous/leak currents were not further analyzed. We used the pCLAMP suite of programs (Axon Instruments) for data acquisition and analysis. Currents were filtered at 200 Hz and sampled at 1 kHz. We used OriginPro 8 (OriginLab Corporation) to generate graphs, K_i, and for statistical analysis.

Table 4.1. Mutant alleles and genotyping primers used in this study.

Allele	Source	Genotyping Primer Sequences
unc-8 tm5052 IV	NBRP	TGGGGCCCTAATAATTTCGA
		AGTGACAGTATGAAGCCAGG
unc-55 e1170 I	CGC	TAAGGACTACACGGATCCTG
		CCCAAGAAAGAAAAGAGAGGT
unc-2 e55 X	CGC	TGTCCGACACTGAAATTGGA
		TGCGTGATGTTACCCACCTA
egl-19 n582 IV	CGC	GTACGGTCAAACCGATTCCA
		TATTCTCCACGGCATTCTGC
eri-1 mg366 IV	CGC	CATGCAATTTCAATGCCTTTTA
		TGCATCATCCAATCCACTATGT
tax-6 jh107 IV	CGC	CCGTAATCCCTTCAAATCCCAATGGG
		GCCATAGTGCATTTGCGCATGACAA
cnb-1 ok276 V	CGC	CCATGGTTGACATAACACCAGGTCTA
		ATGTCGATGGCTCAGGCTCACT
ced-4 n1162 III	CGC	TCATCCACGACTTTGAACCA
		TGATATTTCGTGACGCTTGC
unc-43 n498 IV	CGC	CTATGGACAATTCCACGCTG
		GTTTCTGAAAGTCACGAGCG

Table 4.2. Strains used in this study.

Strain	Genotype
CZ333	*juIs1[punc-25::SNB-1::GFP; lin-15+]* IV
NC2387	*unc-8(tm5052) juIs1* IV
NC1851	*unc-55(e1170)* I; *juIs1* IV
NC2388	*unc-55(e1170)* I*; unc-8(tm5052) juIs1* IV
NC2443	*unc-55(e1170)* I; *unc-2(e55)* X; *juIs1* IV
NC2834	*unc-55(e1170)* I; *unc-2(e55)* X; *unc-8(tm5052) juIs1* IV
NC1852	*unc-55 (e1170) I; eri-1 (mg366) juIs1 IV*
KP5348	*nuIs279[punc-25::UNC-57::GFP;punc-25::mCherry::RAB-3]*
NC2870	*unc-8(tm5052)* IV; *nuIs279*
NC2984	*unc-55(e1170)* I; *nuIs279*
NC2873	*unc-55(e1170)* I; *unc-8(tm5052)* IV; *nuIs279*
NC2711	*egl-19 (n582) IV; pha-1 (e2123ts) III; wdEx889[punc-25::mCherry::RAB-3; pha-1+]*
NC2712	*unc-55 (e1170) I; egl-19(n582) IV; pha-1 (e2123ts) III; wdEx889*
NC2710	*unc-55(e1170); pha-1 (e2123ts) III; wdEx889*
NC3065	*tax-6 (p675) IV; nuIs279*
NC3066	*unc-55 (e1170) I; tax-6 (p675) IV; nuIs279*
NC3067	*hqIs5[ptax-6::tax-6::GFP]; punc-47::mCherry X*
NC3069	*cnb-1 (ok276) V; juIs1 IV*
NC3070	*unc-55 (e1170) I; cnb-1 (ok276) V; juIs1 IV*
NC3071	*unc-55 (e1170) I; cnb-1 (ok276) V; unc-8 (tm5052) juIs1 IV*
NC3068	*tax-6 (jh107) IV; wyIs202 X*
NC2585	*wyIs202[pflp-13::GFP::RAB-3; pflp-13::mCherry]* X
NC3080	*ced-4 (n1162) III; juIs1 IV*
NC3081	*ced-4 (n1162) III; unc-55 (e1170) I; juIs1 IV*
NC3082	*ced-4 (n1162) III; unc-55 (e1170) I; unc-8 (tm5052) juIs1 IV*
N/A	*unc-43 (n498) IV; unc-55 (e1170) I; nuIs279*
NC2538	*pha-1 (e2123) III; wdEx849[pttr-39::GFP::utrophin; pha-1+]*

Results

UNC-8 channel activity drives GABAergic synapse elimination

Although proteins in the DEG/ENaC family can be permeable to sodium, potassium, and calcium ions, we found that a constitutively active UNC-8 channel expressed in *Xenopus* oocytes preferentially gates sodium ions (Y. Wang et al. 2013).

We predicted that sodium influx through the DEG/ENaC protein UNC-8 mediates synapse removal. To test this hypothesis, we treated *unc-55* animals with the pharmacological DEG/ENaC inhibitors, Amiloride and Benzamil. These drugs function as diuretics in humans due to strong inhibition of DEG/ENaC channel activity in the kidney that blocks sodium reabsorption (Kleyman & Cragoe 1988). *unc-55* animals were maintined on growth plates containing either vehicle (water) or 3 mM Benzamil. Examination of the ventral GABAergic synapses revealed that treatment with Benzamil significantly antagonizes synapse removal in comparison to *unc-55* animals grown on control plates (**Figure 4.1,** Miller-Fleming et al. 2016). Similar results were observed for *unc-55* animals treated with 3 mM Amiloride. Moreover, these drug treatments phenocopied the effects of the *unc-8 (tm5052)* loss-of-function mutation. Finally, we showed that the inhibition of synaptic removal by these pharmacological treatments was not enhanced by the *unc-8 (tm5052)* mutation. These results suggest that UNC-8 channel activity promotes synapse elimination in GABAergic neurons.

We performed control experiments to confirm that the effects observed with the pharmacological treatments and Amiloride and Benzamil are specific to UNC-8 activity. Indeed, we found that treatment of *unc-8* animals has no effects on ventral synapse number (**Figure 4.2A**). Critically, we found that treatment of *unc-55; unc-8* animals with Amiloride or Benzamil does not enhance the effects seen when *unc-55* animals are treated with the drugs. This control is important because it confirms that the synapse removal defects observed in *unc-55* animals treated with Benzamil or Amiloride are in a shared pathway with *unc-8* (**Figure 4.2B and C**).

Expression of the constitutively active UNC-8 protein, UNC-8 G387E, in *Xenopus* oocytes elicits an Amiloride-sensitive current (Y. Wang et al. 2013). These currents are

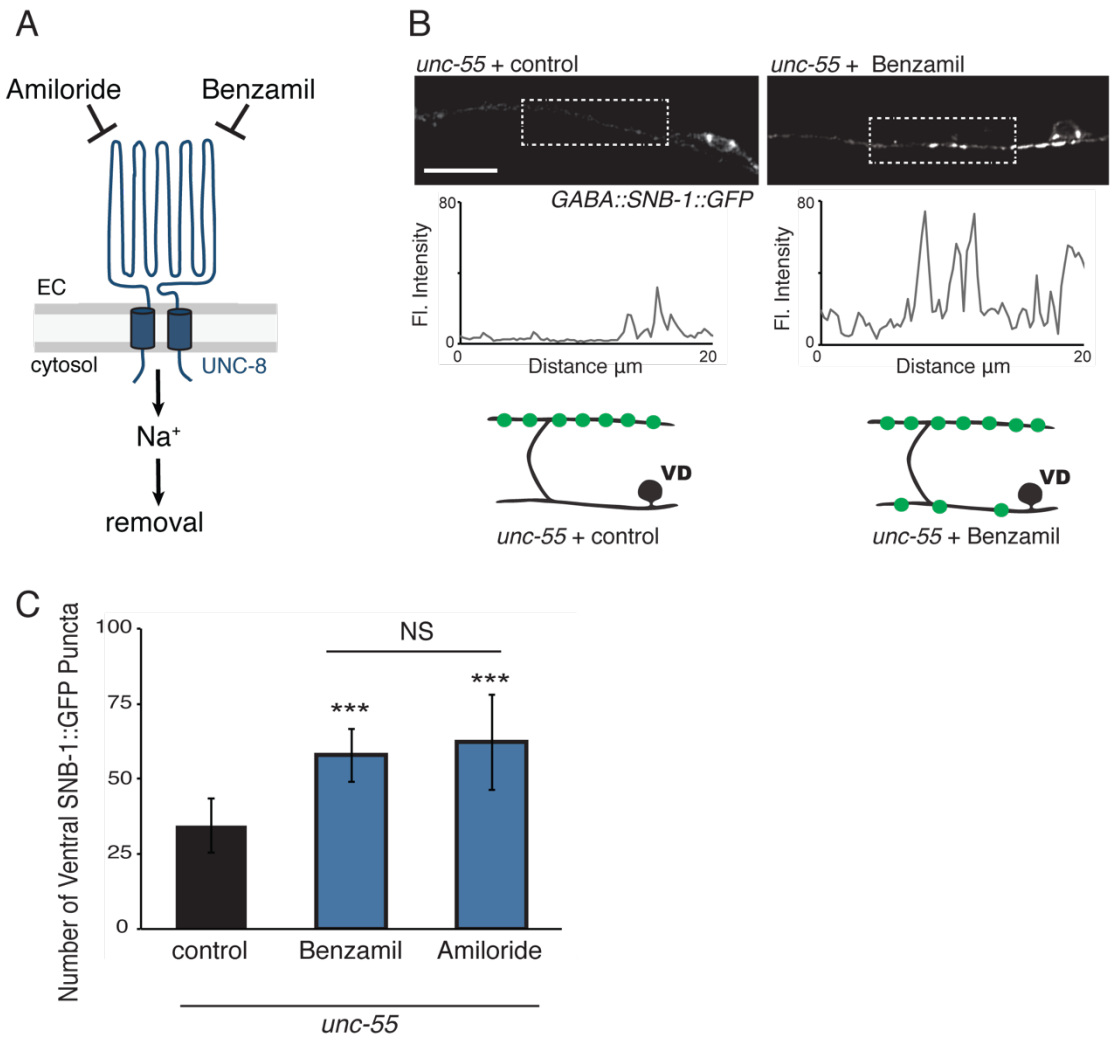

Figure 4.1: UNC-8 channel activity promotes synapse removal. A. Amiloride and Benzamil block DEG/ENaC channel activity. **B.** Representative images and fluorescence intensity plots (generated from 20 µm dashed region) of SNB-1::GFP-marked ventral GABA neuron synapses in *unc-55* animals treated with either 3 mM Benzamil or water (control). Scale bar is 10 µm. **C.** Benzamil and Amiloride antagonize the removal of ventral GABA synapses in *unc-55* mutant animals. Ventral GABA neuron synapses were quantified by counting SNB-1::GFP puncta (***$P < 0.001$, ns is not significant, $n \geq 25$ animals, data are mean ± SD, One-Way ANOVA Bonferroni correction).

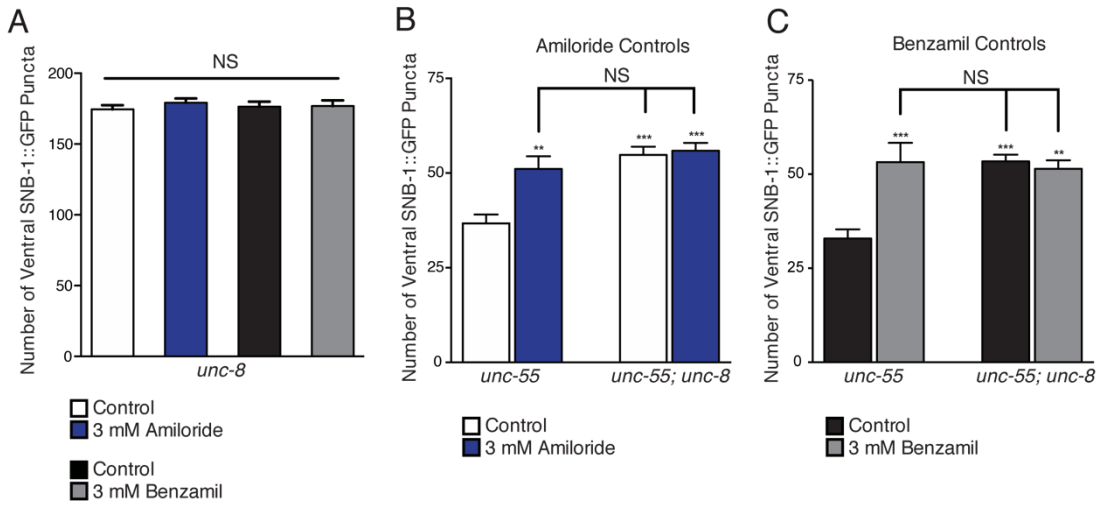

Figure 4.2: Benzamil and Amiloride perturb synapse removal in the UNC-8-dependent pathway. A. Treatment of *unc-8* or *unc-5; unc-8* animals with either 3 mM Amiloride or 3 mM Benzamil has no effect on remodeling. Vehicle control for Amiloride and Benzamil treatment is water ($n \geq 10$, $^{**}P < 0.01$, $^{***}P < 0.001$, ns is not significant, mean ± SEM, One-Way ANOVA Bonferroni correction).

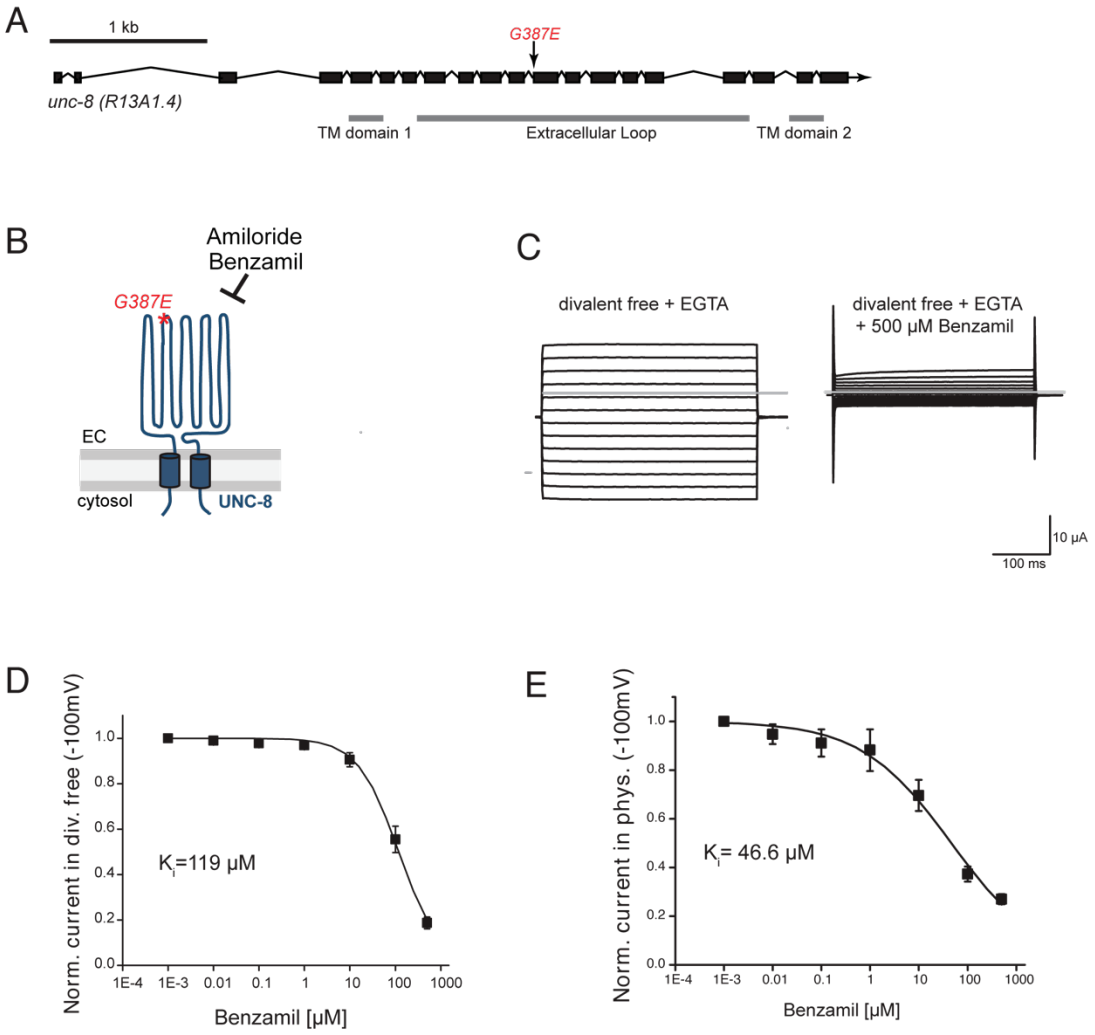

Figure 4.3: Benzamil blocks UNC-8 currents in a heterologous expression system. **A.** Schematic of the *unc-8* gene. The G387E point mutation (red) renders the UNC-8 channel constitutively active. **B.** Amiloride and Benzamil are pharmacological inhibitors of DEG/ENaC channel activity. **C.** Benzamil blocks UNC-8(G387E) current in *Xenopus* oocytes. Representative currents from oocyte expressing UNC-8(G387E) in a bath of divalent cation-free solution plus EGTA. Currents elicited by 20mV voltage steps from -160mV to +100mV. The holding potential was -30mV. The gray line represents the zero current level (left). The same oocyte exposed to 500μM Benzamil (right). **D**. Benzamil dose-response curve in divalent cation-free bath solution. Currents recorded with Benzamil were normalized against recordings in divalent cation-free bath solution plus EGTA at -100mV. Data were fitted to the Boltzman equation to derive K_i = 119 μM (*n* = 10 oocytes). Data are mean ± SEM. **E.** UNC-8(G387E) currents recorded in physiological solution plus the potent DEG/ENaC inhibitor Benzamil at -100mV were normalized against currents recorded in physiological solution at -100mV. Data were fitted with the Boltzman equation for Ki = 46.6 µM (*n* = 10 oocytes). Data are mean ± SEM. The graphs in panels C-E were generated by Cristina Matthewman.

significantly enhanced when the calcium chelator EGTA is added to the recording solution, suggesting that this UNC-8 protein is inhibited by extracellular calcium. As expected, we confirmed that UNC-8 G387E channel activity is strongly blocked by Benzamil treatment ($K_i \sim 119\ \mu M$, **Figure 4.3C and D**). Furthermore, we found that in the presence of extracellular calcium ions, Benzamil is a more potent inhibitor of UNC-8 G387E activity ($K_i \sim 46.6\ \mu M$, **Figure 4.3E**). These findings are consistent with the hypothesis UNC-8-dependent sodium influx promotes disassembly of the presynaptic apparatus.

Calcium signaling promotes synapse removal in the *unc-8* pathway

Previous studies found that DD remodeling is activity-dependent; mutations that decrease neurotransmission delay dorsal DD synapse formation; whereas, dorsal DD synapses appear prematurely in animals with enhanced neurotransmitter release (Thompson-Peer et al. 2012). We predicted that neuronal activity could also regulate synapse removal in remodeling GABAergic neurons. Voltage-gated calcium channels (VGCCs) are expressed near sites of synaptic vesicle fusion and calcium influx through these channels is critical for neurotransmitter release. The P/Q-type calcium channel subunit, UNC-2 is localized at presynaptic regions and drives neurotransmitter release (Gracheva et al. 2010; Saheki & Bargmann 2009). The *unc-2* gene in *C. elegans* encodes the CaV2 alpha-1 pore-forming subunit of the channel and is therefore critical for channel function. Using the strong loss-of-function allele *unc-2 (e55)*, we found that abrogation of calcium signaling suppresses *unc-55*-mediated synapse removal. *unc-55; unc-2* animals exhibit a synaptic removal defect that is comparable to that of *unc-55; unc-8* animals. Furthermore, loss of *unc-2* in the *unc-55; unc-8* animals does not

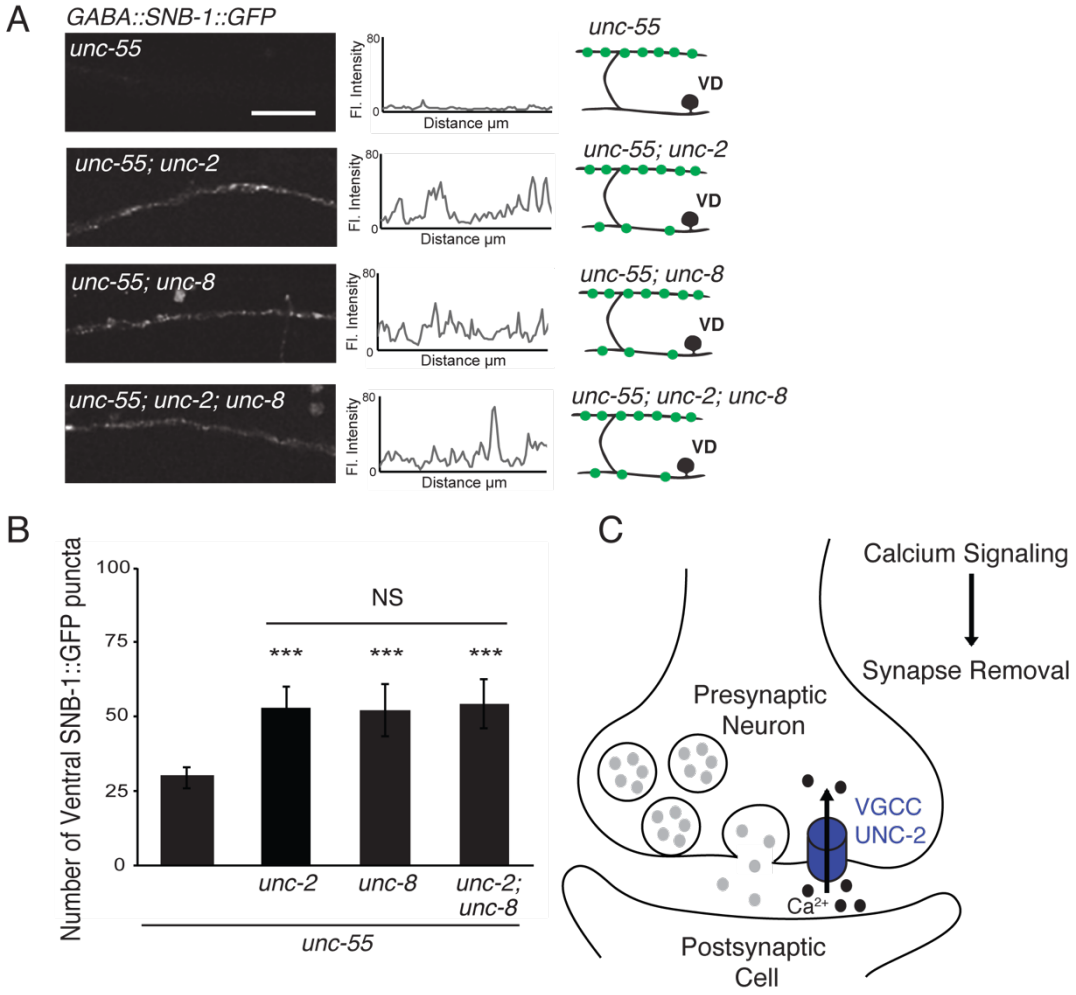

Figure 4.4: UNC-8 disassembles synapses in a common pathway with neurotransmitter release. A. Loss-of-function mutations in either *unc-2* (P/Q-type VGCC subunit) or *unc-8* impairs removal of ventral SNB-1::GFP in *unc-55* animals. The *unc-8* mutation does not enhance the *unc-55;unc-2* removal defect. Representative images and insets show fluorescence intensity plots over a 20 µm region of the ventral nerve cord for each genotype. Scale bar is 5 µm. **B.** Quantification of ventral fluorescent puncta in *unc-55; unc-2; unc-8* animals is not significantly different than *unc-55; unc-8* or *unc-55; unc-2* mutants, demonstrating that UNC-2/VGCC and UNC-8/DEG/ENaC function in a common pathway to promote GABA synapse removal (***$P < 0.001$ vs *unc-55*, One-Way ANOVA Bonferroni correction, data are mean ± SD, $n \geq 17$). **C.** Calcium signaling via the VGCC UNC-2 promotes GABAergic synapse removal.

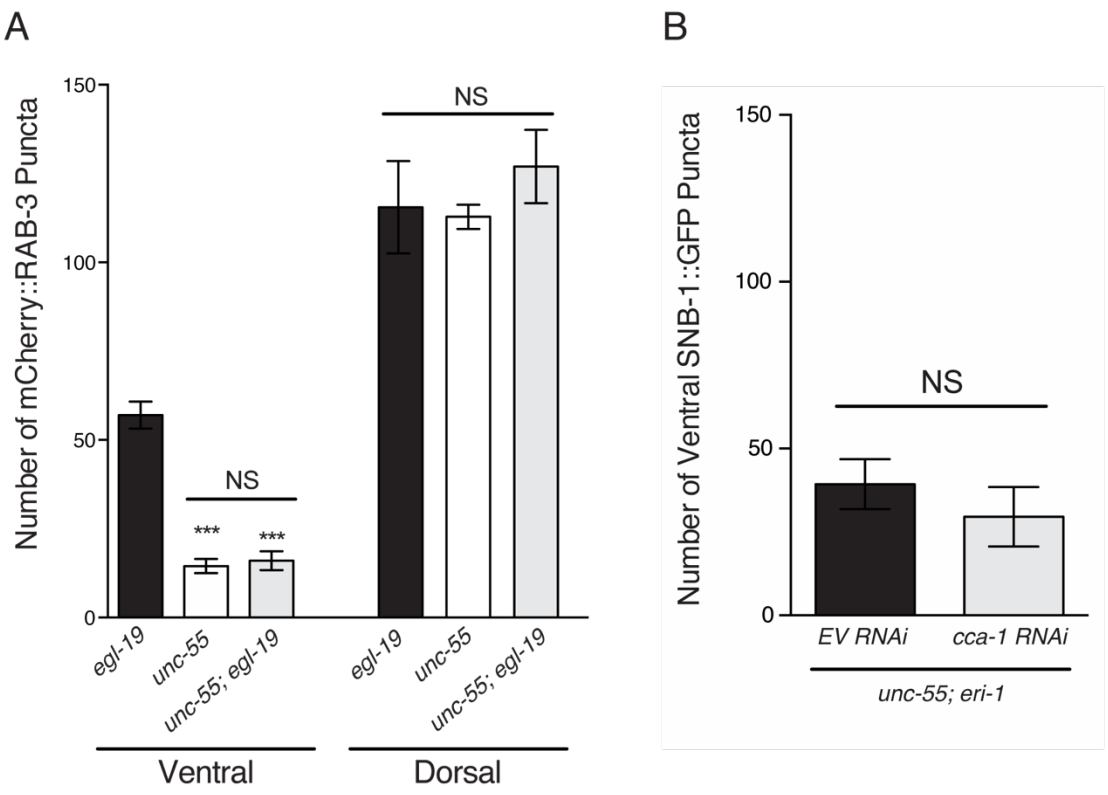

Figure 4.5: The L-type and T-type calcium channel subunits, EGL-19 and CCA-1 respectively, are not required for synapse removal. A. Mutations in the N-type calcium channel subunit *egl-19* have no effect on ventral synapse removal or dorsal synapse assembly (***$P < 0.001$, NS is not significant, One Way ANOVA with Bonferroni Correction, $N \geq 10$). **B.** Knock down of the T-type calcium channel subunit *cca-1* by feeding RNAi has no effect on ventral synapse removal (NS is not significant, Student's t-test, $N \geq 10$).

enhance the removal defect, therefore suggesting that UNC-2/VGCC and UNC-8/DEG/ENaC function in a common genetic pathway (**Figure 4.4**, Miller-Fleming et al. 2016). As mentioned above (see **Introduction**), this finding is intriguing because it parallels the requirement for calcium signaling via P/Q-type VGCCs during synapse elimination in the mammalian cerebellum.

Based on our finding that the P/Q-type calcium channel subunit UNC-2 promotes remodeling in the UNC-8 pathway, we next wanted to determine whether this effect could also be mediated by other types of calcium channels. While P/Q-type UNC-2 VGCC proteins are expressed exclusively in neurons, the *C. elegans* L-type VGCC subunit EGL-19 is expressed in pharyngeal and body wall muscles (R. Y. Lee et al. 1997; Garcia et al. 2001). We found that the partial loss-of-function *egl-19 (n582)* allele had no effect on ventral synapse removal or dorsal synapse formation in GABAergic neurons (**Figure 4.5A**). Additionally, we tested the T-type VGCC subunit CCA-1, which is expressed in pharyngeal muscle and several neurons. Knock down of *cca-1* by RNAi had no effect on ventral synapse removal (**Figure 4.5B**). These findings support the possibility that calcium signaling, specifically through the P/Q-type calcium channels, regulates synapse removal in GABAergic motor neurons.

Calcineurin eliminates GABAergic synapses upstream of UNC-8 channel activity

Experiments described above indicate that calcium influx promotes synapse disassembly. To understand this pathway, we tested known components that function downstream of calcium signaling. Calcineurin is a calcium/calmodulin-dependent phosphatase that is expressed in the nervous system and has been implicated in

activity-dependent processes that regulate synapse stability, promoting long-term depression (LTD) and antagonizing long-term potentiation (LTP) ((Winder et al. 1998; H. K. Lee et al. 1998; Sanderson et al. 2012) (Mulkey et al. 1994). Two protein components are required for the phosphatase activity of calcineurin, including the catalytic subunit calcineurin A and the regulatory subunit calcineurin B (TAX-6 and CNB-1, respectively in *C. elegans*) (**Figure 4.6A**). We found that fluorescently-tagged TAX-6 protein is broadly expressed in the *C. elegans* nervous system and body wall muscles. Detectable TAX-6::GFP was identified in GABAergic motor neurons, which were co-labeled with a GABA-specific marker (*punc-47::mCherry*, **Figure 4.6B**).

We evaluated the number of ventral synapses in *unc-55; tax-6* animals and detected significantly more ventral puncta than in *unc-55* animals (**Figure 4.6C,** Miller-Fleming et al. 2016). This result confirms that calcineurin activity promotes synapse removal. Validating this result, we determined that a loss-of-function allele of the calcineurin B subunit, *cnb-1* suppresses ventral synapse removal. Additionally, we found that the *cnb-1* mutation did not enhance the *unc-55; unc-8* synaptic removal defect, thereby suggesting that calcineurin promotes synapse elimination in a common genetic pathway with UNC-8/DEG/ENaC and UNC-2/VGCC (**Figure 4.7,** Miller-Fleming et al. 2016).

Based on our findings that calcineurin activity promotes synapse disassembly, we predicted that a constitutively active mutation in *tax-6* (aka *tax-6d*) would induce precocious synapse removal in DD neurons. We monitored DD-specific presynaptic puncta (DD::GFP::RAB-3) during remodeling and found that indeed, *tax-6d* mutants exhibit a precocious loss of ventral DD synapses. In addition, dorsal DD synapses are formed prematurely in *tax-6d* compared to wild-type controls. This result is consistent with hypothesis that calcineurin drives ventral synapse removal. To delineate this

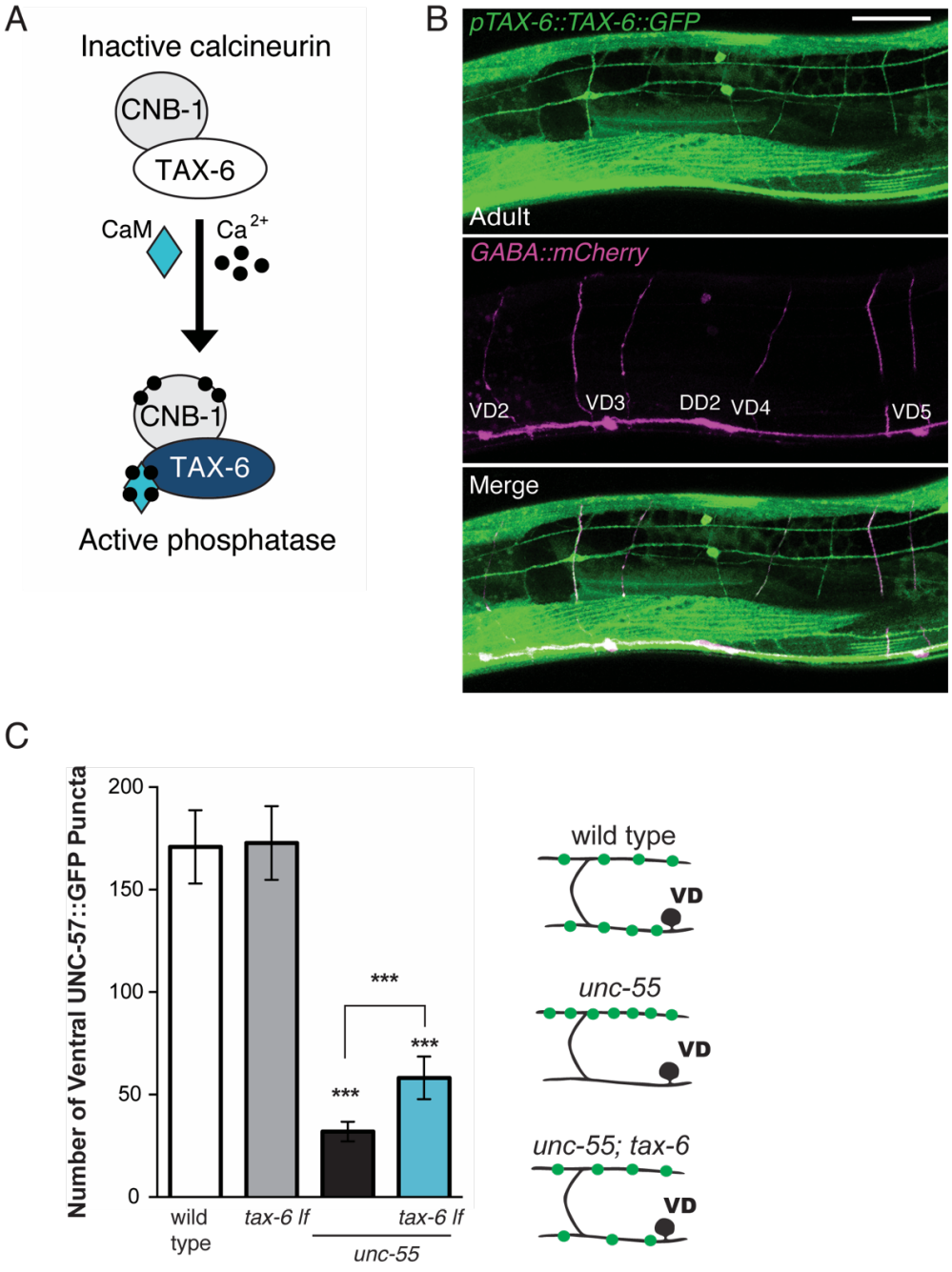

Figure 4.6: Calcineurin promotes GABA synapse elimination. A. Calcineurin A and B subunits (TAX-6 and CNB-1, respectively) require calcium and calmodulin (CaM) to activate phosphatase activity. **B**. GFP-tagged TAX-6 under the control of the *tax-6* promoter region (*ptax-6::TAX-6::GFP)* is expressed in GABA neurons (*punc-47::mCherry*). Scale bar is 20 µm. **C.** Loss of *tax-6* partially suppresses the *unc-55* remodeling phenotype in GABA neurons (***$P < 0.001$, One-Way ANOVA Bonferroni correction, data are mean ± SD, $n \geq 25$). Thus, calcineurin activity promotes ventral synapse removal.

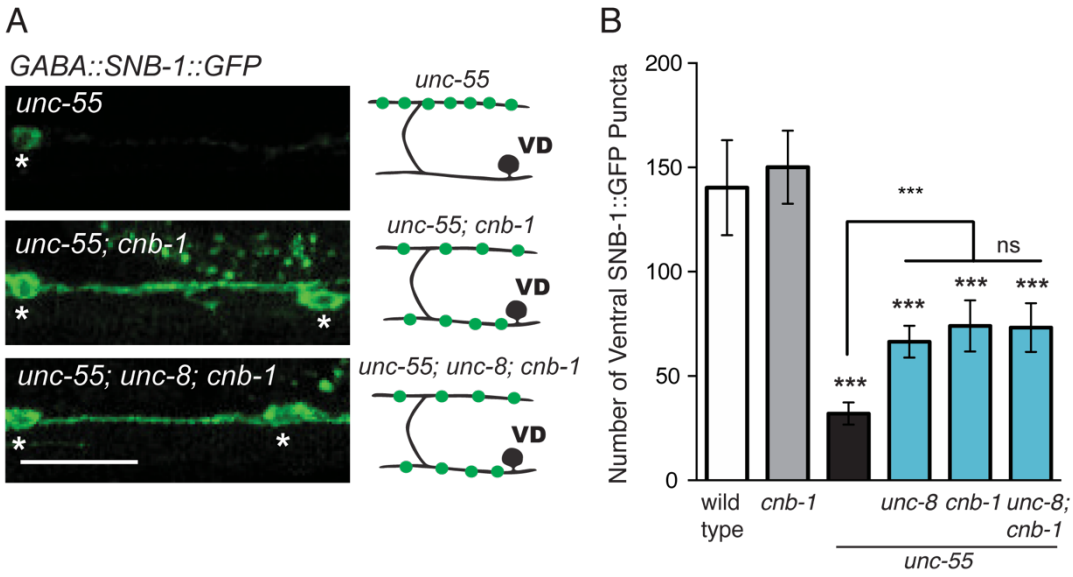

Figure 4.7: The calcium/calmodulin-dependent phosphatase calcineurin promotes GABA synapse removal in the UNC-8 pathway. A. CNB-1 is required for remodeling in *unc-55* animals. Representative images of ventral nerve cords in *unc-55, unc-55; cnb-1* and *unc-55; unc-8; cnb-1* animals. Asterisks denote GABA neuron soma, scale bar is 20 µm. **B.** The *cnb*-1 mutation significantly suppresses synapse removal in *unc-55* animals; however, loss of *cnb-1* function does not enhance the *unc-55; unc-8* remodeling defect. These results suggest that calcineurin and UNC-8 promote synapse removal in a common genetic pathway (***$P < 0.001$, ns is not significant, One-Way ANOVA with Bonferroni Correction, data are mean ± SD, wild type $n = 10$, mutants $n = 20$).

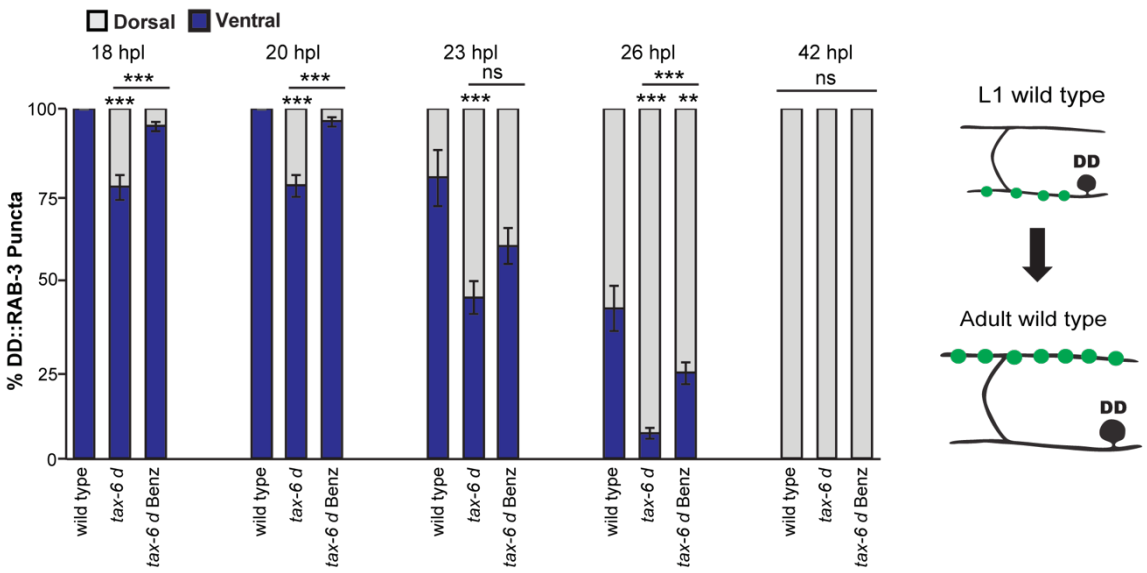

Figure 4.8: Calcineurin activity drives synapse removal upstream of UNC-8. Gain-of-function *tax-6* (*tax*-6*d*) mutants remodel precociously and this effect is suppressed by Benzamil. Percentage of ventral (blue) vs dorsal (gray) DD synapses (*pflp-13::GFP::RAB-3*, $^{**}P < 0.01$, $^{***}P < 0.001$, ns is not significant, One-Way ANOVA Bonferroni correction, $n \geq 8$ animals per timepoint, data are mean ± SEM). Results for *tax-6d* and for the *tax-6d* control for Benzamil treatment (see Methods) are combined because they were not significantly different. Benz denotes 3mM DEG/ENaC inhibitor Benzamil.

genetic pathway, we treated *tax-6d* animals with the DEG/ENaC inhibitor Benzamil to block UNC-8 channel activity. We posited that if this treatment suppressed precocious remodeling in *tax-6d* animals, then UNC-8 channel function likely promotes synapse removal downstream of calcineurin. Treatment of *tax-6d* animals with Benzamil suppressed the precocious removal phenotype observed in *tax-6d* animals grown on control plates, confirming that calcineurin drives synapse removal upstream of UNC-8 channel activity (**Figure 4.8,** Miller-Fleming et al. 2016).

Additionally, we find that a gain-of-function allele in the calcium/calmodulin-dependent protein kinase II ortholog, *unc-43gf*, impedes synapse removal in GABAergic neurons. This finding suggests that UNC-43/CaMKII normally functions to antagonize synapse removal, in opposition to the pro-removal effects of calcineurin/TAX-6 (**Figure 4.9**). This finding provides confirmation of previously published reports of opposing roles for calcineurin and CaMKII in regulating the plasticity of neuronal connections (Mulkey et al. 1994; Giese et al. 1998; Lisman et al. 2002; Silva, Wang, et al. 1992; Silva, Paylor, et al. 1992; Zeng et al. 2001; Torii et al. 1995). The observation that TAX-6/calcineurin functions upstream of UNC-8 channel activity, and in opposition to UNC-43/CamKII to regulate synapse removal raises the possibility that UNC-8 may function as a shared substrate for these two proteins (**Figure 4.9C**).

A model for UNC-8-mediated synapse removal involves the activation of the canonical cell death pathway

Previous work has shown that the apoptotic pathway promotes ventral synapse removal in remodeling DD neurons. In this mechanism, the adaptor protein CED-4/Apaf1 and its downstream effector, CED-3/caspase activate the actin-severing protein gelsolin

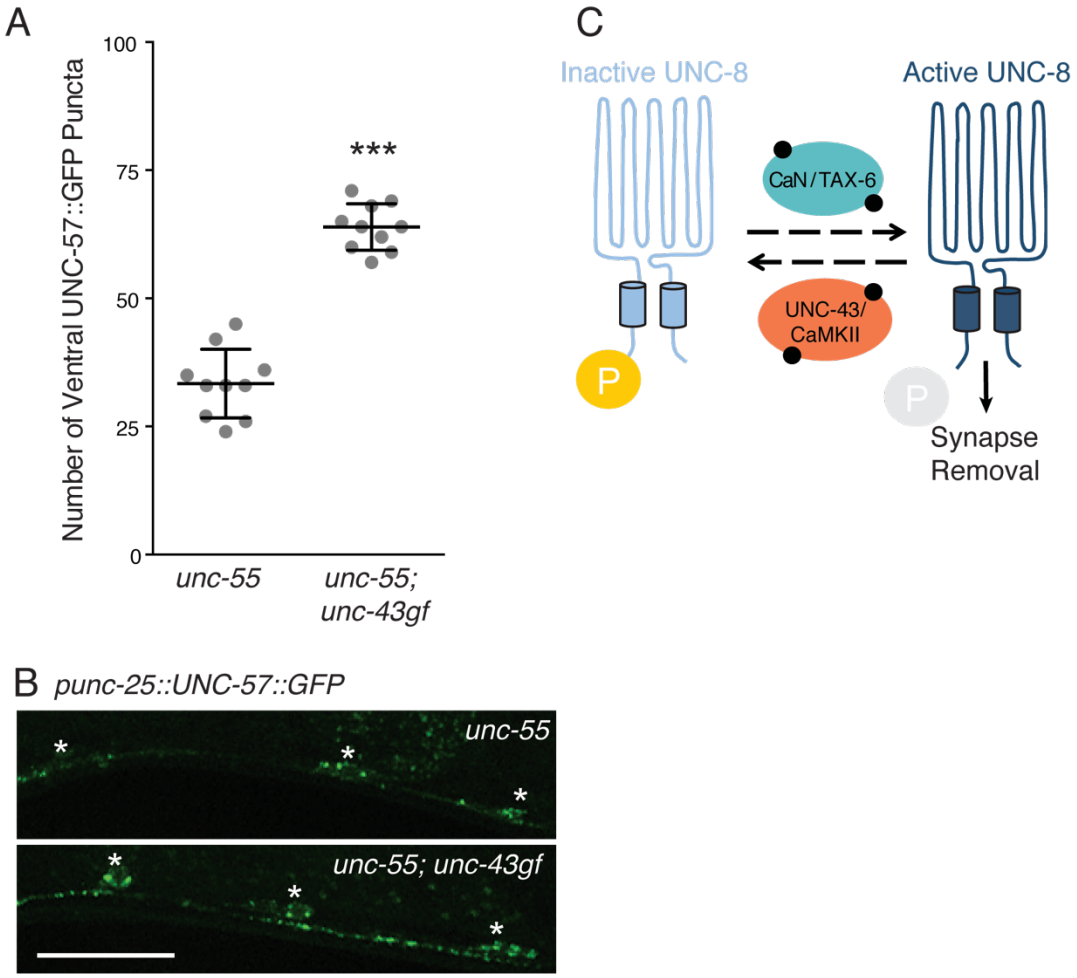

Figure 4.9: The calcium/calmodulin-dependent protein kinase II (CaMKII/UNC-43) antagonizes synapse removal. A. Constitutive activation of the CaMKII/*unc-43* gene suppresses *unc-55*-mediated synapse removal (***P < 0.001, Student's t-test, N = 10). Data are mean ± SEM. **B.** Representative images of *unc-55* and *unc-55; unc-43 gf* animals. Presynaptic regions are labeled with UNC-57::GFP (endophillin::GFP). Asterisks denote cell bodies, scale bar is 20 µm. **C.** Model for UNC-8 regulation by the calcium-dependent proteins CaMKII/UNC-43 (teal) and the calcineurin/TAX-6 (orange), black circles represent calcium ions. Phosphorylation (yellow circle) of UNC-8 by UNC-43 may inactivate channel activity; whereas, TAX-6 promotes UNC-8 by dephosphylation.

to destabilize a presynaptic F-actin network during synapse elimination (Meng et al. 2015). Based on our findings that UNC-8 promotes synapse removal downstream of calcineurin, we considered the possibility that these components function in a common pathway. To test this idea, we examined a loss-of-function *ced-4* mutation in *unc-55* animals. *unc-55; ced-4* animals retain significantly more ventral synapses compared to *unc-55,* suggesting that the cell death pathway promotes synapse elimination in remodeling GABAergic cells (**Figure 4.10**, (Meng et al. 2015; Miller-Fleming et al. 2016)). The *unc-55; ced-4* synaptic removal defect is comparable to that of *unc-55; unc-8* double mutants. Furthermore, the *unc-55; unc-8; ced-4* triple mutants did not enhance the restoration of ventral synapses over that of *unc-55; unc-8* or *unc-55; ced-4* animals(Miller-Fleming et al. 2016). Together, these results suggest that the DEG/ENaC protein UNC-8 functions in a common pathway with *ced-4* to eliminate ventral GABA synapses.

We propose a model in which UNC-8 functions at the presynaptic membrane to dismantle ventral GABAergic synapses in a common pathway with calcium signaling and the cell death machinery. Neuronal depolarization activates VGCCs and increases intracellular calcium, potentially stimulating local calcineurin. We found that UNC-8 channel activity promotes synaptic removal downstream of calcineurin, and therefore predict that UNC-8 channels may be activated by calcineurin-dependent dephosphorylation. Influx of sodium ions by UNC-8 channels would further depolarize the presynaptic membrane, thus functioning as a feed-forward mechanism to enhance VGCC activity and calcium signaling. We hypothesize that the consequent elevation of intracellular calcium above a critical threshold through the cyclical activation of UNC-8 and UNC-2, the cell death pathway triggers F-actin disassembly, and thus destabilizes the presynaptic complex (**Figure 4.11,** (Miller-Fleming et al. 2016)). Current evidence

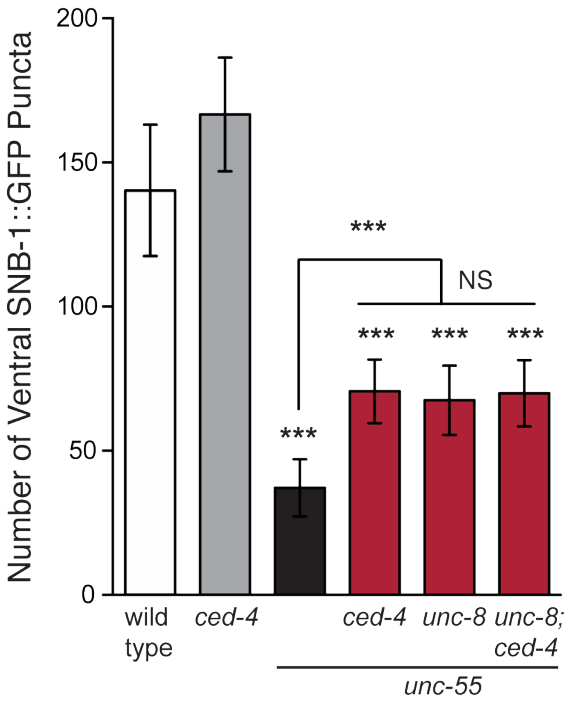

Figure 4.10: The cell death pathway promotes GABAergic synapse elimination in the UNC-8-dependent pathway. Loss of the pro-apoptotic gene *ced-4* partially suppresses GABA synapse removal in *unc-55* animals. Genetic ablation of *unc-8* in the triple mutant *unc-55; ced-4; unc-8* mutants does not enhance the remodeling defect and thus suggests that UNC-8 and CED-4 promote synapse elimination in a common pathway (***$P < 0.001$, ns is not significant, One-Way ANOVA with Bonferroni Correction, data are mean ± SD, wild type $n = 10$, mutants $n \geq 20$).

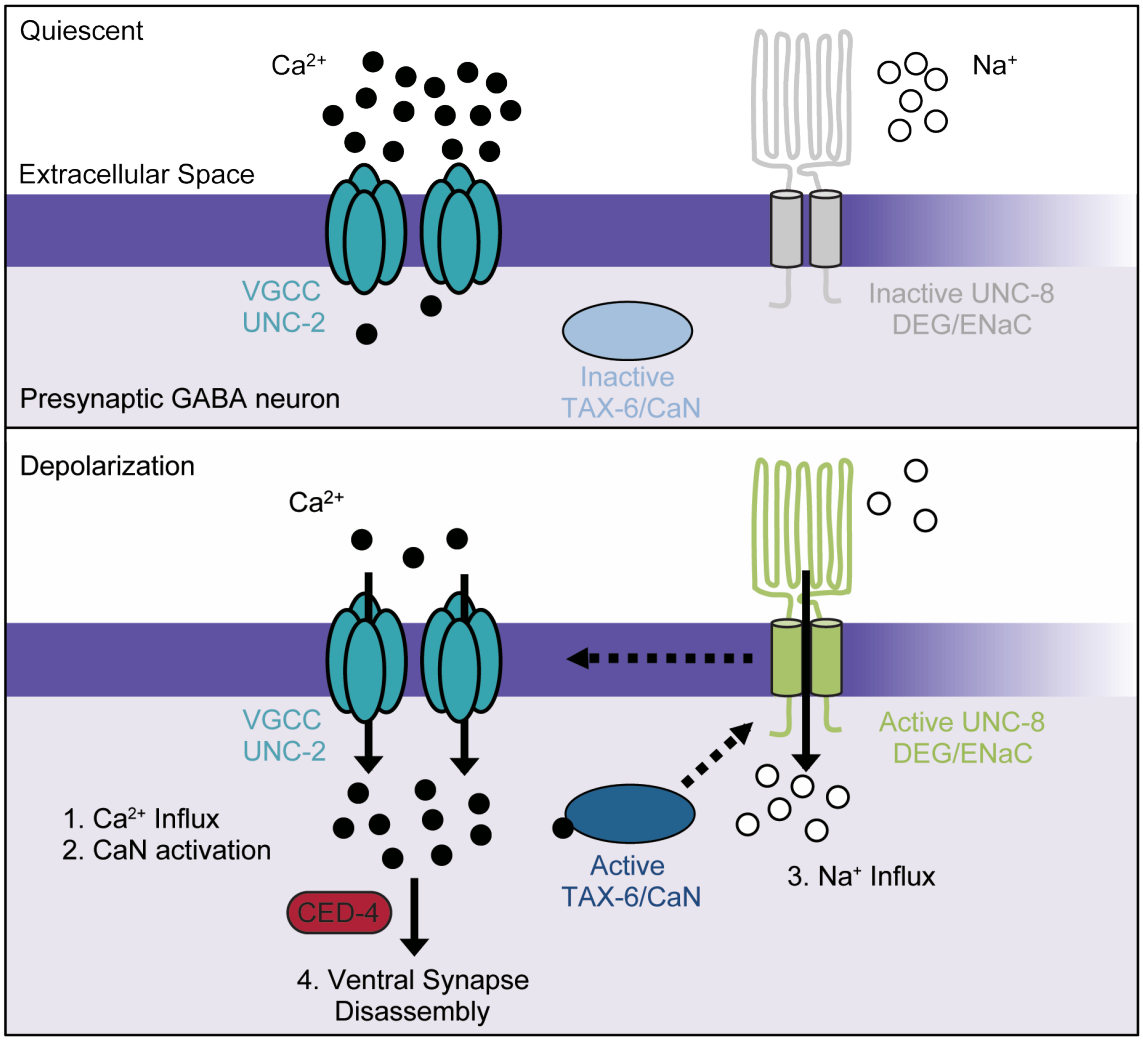

Figure 4.11: Predicted model for UNC-8-mediated synapse disassembly. A DEG/ENaC channel containing UNC-8 is not active (gray) in quiescent GABA motor neurons (top panel). (1) GABA neuron depolarization activates the voltage-gated calcium channel (VGCC), UNC-2, to allow calcium entry (black circles bottom panel). (2) Intracellular calcium activates the calcium/calmodulin-dependent phosphatase, calcineurin (CaN/TAX-6). (3) CaN phosphatase may activate UNC-8, which results in the movement of sodium ions (white circles) into the presynaptic GABA neuron, further depolarizing the presynaptic membrane and activating VGCCs. This positive feedback loop is predicted to further elevate intracellular calcium. (4) Our results show that UNC-8 drives the removal of presynaptic components and functions in a common genetic pathway with calcium signaling and with the apoptotic protein CED-4. Therefore, we hypothesize that selective expression of UNC-8 in remodeling GABA neurons effectively boosts the level of intracellular calcium to activate a CED-4-dependent pathway for removal of the presynaptic apparatus.

suggests that the F-actin capping protein gelsolin is activated by calcium; however, there is also a possibility that sodium influx via UNC-8 could activate the cell death pathway directly (Klaavuniemi et al. 2008; Banasiak et al. 2004).

Actin regulators and the ubiquitin proteasome complex may regulate ventral synapse disassembly

Candidate remodeling genes in GABAergic neurons were identified by exploiting the *unc-55* remodeling phenotype. In *unc-55* mutants, both DD and VD neurons remove ventral synapses and establish new connections with dorsal muscles. Cell-specific microarray profiling of remodeling GABAergic neurons detected multiple mRNA transcripts that are negatively regulated by the UNC-55 COUP/TF transcription factor. One target gene, *arx-5* encodes the p21Arc component of the Arp2/3 complex. This seven-subunit complex is a major cytoskeletal component that stimulates branched actin assembly (Kelleher et al. 1995; Mullins et al. 1998). Interestingly, the only Arp2/3 component identified in our screen was *arx-5*, suggesting that this component might be differentially regulated to modulate Arp2/3 activity. To confirm our microarray result, we used RNAi to knock down *arx-5* in *unc-55* animals to test for a role in synapse removal. This experiment suggests that *arx-5* is required for efficient synapse elimination; *unc-55; arx-5 RNAi* animals retain significantly more synapses compared to *unc-55* animals treated with control RNAi (**Figure 4.12A**). Thus, these findings suggest that branched actin promotes synapse removal. This is a puzzling result, given the observation that F-actin disassembly due to the activity of gelsolin also drives synapse elimination (Meng et al. 2015). Interestingly, gelsolin and Arp2/3 have been reported to cooperate with one another during actin polymerization, highlighting a potential role for actin assembly

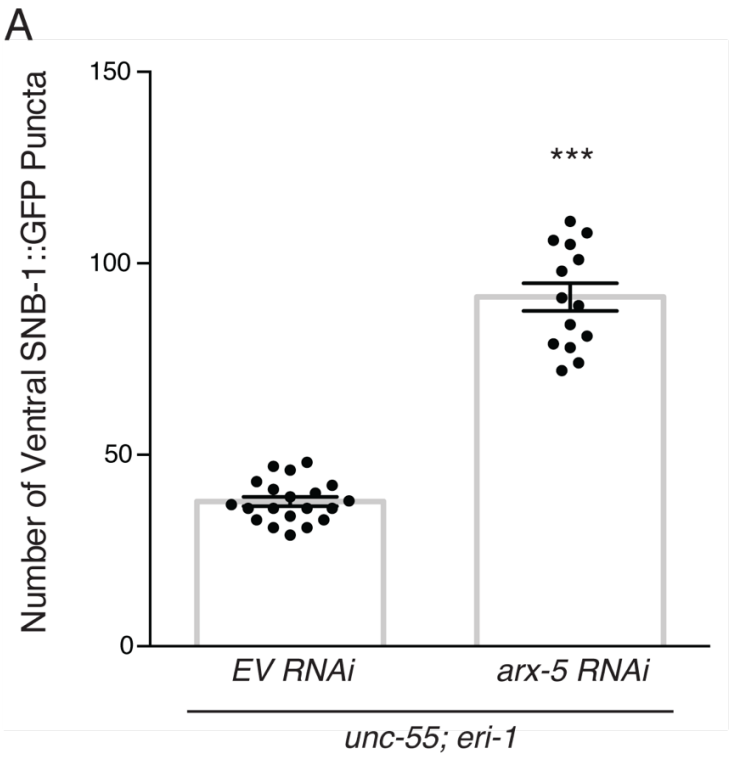

Figure 4.12: Branched actin promotes ventral synapse removal. A. Knock down of the Arp-2/3 component, *arx-5*, by feeding RNAi suppresses *unc-55* synapse removal (***P < 0.001, Student's t-test, N ≥ 14 animals). Data are mean ± SEM. **B.** Representative image of the GFP-labeled F-actin binding protein utrophin in GABAergic cells (*pttr-39::GFP::utrophin*). Actin is detectable throughout the entire GABAergic neuron, including the cell soma, ventral nerve cord, and dorsal nerve cord. Scale bar is 20 µm.

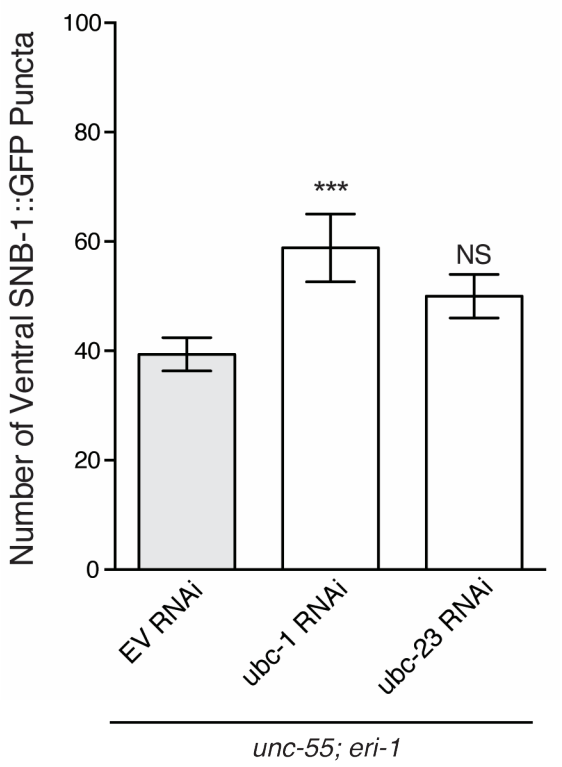

Figure 4.13: The ubiquitin proteasome pathway may regulate synapse removal. Knock down of the E2 ubiquitin conjugating enzyme, *upc-1*, by feeding RNAi suppresses *unc-55*-mediated synapse removal. However, loss of the E2 ubiquitin conjugating enzyme, *upc-23*, has no effect (***P < 0.001, NS is not significant. N ≥ 10, One Way ANOVA with Bonferroni Correction). Data are mean ± SD.

during synapse turnover (Falet et al. 2002; Ressad et al. 1999). Additionally, we find that expression of the fluorescently-tagged F-binding protein utrophin localizes to GABAergic neurons (**Figure 4.12B**). These findings are consistent with a role for both branched and filamentous actin during synapse removal through mechanisms that are not yet understood.

Consistent with our finding that UNC-8 promotes synapse elimination in remodeling GABAergic motor neurons, dendritic spines are also pruned by a caspase-3-dependent mechanism (Ertürk et al. 2014). In this paradigm, the cell death pathway is spatially restricted to the region of synaptic elimination by proteasome activity; therefore, inhibition of proteasome activity in these neurons induces cell death. To determine whether the proteasome mediates GABAergic synapse removal, we treated *unc-55* animals with RNAi against two E2 ubiquitin conjugating enzymes, *ubc-1* and *ubc-23*. Knock down of *ubc-1* significantly suppressed *unc-55* synapse removal, whereas *ubc-23* had no effect (**Figure 4.13**). These results require further investigation and support the possibility that synapse removal in GABAergic neurons is also regulated by the proteasome.

Discussion

Here, we elucidate a synaptic removal pathway that depends on concurrent function of transcriptional expression of the DEG/ENaC protein UNC-8 and calcium-mediated neurotransmission. We find that the VGCC subunit UNC-2 and the calcium-dependent phosphatase calcineurin (TAX-6) function upstream to regulate UNC-8 channel activity, thus driving synapse elimination in GABAergic motor neurons. Based on our genetic data, we predict that UNC-8 mediates synapse turnover through

regulation of the actin cytoskeleton via the canonical cell death pathway (Miller-Fleming et al. 2016). This model demonstrates a unique role for DEG/ENaC proteins in the dismantling the presynaptic apparatus in GABAergic neurons.

DEG/ENaC activity regulates synaptic stability through calcium signaling

We found that pharmacological inhibition of UNC-8 channel function obstructs ventral synapse removal in GABAergic neurons, suggesting that sodium ion influx through UNC-8 channels promotes synapse destabilization. Additionally, work from the Drosophila nervous system has identified a role the DEG/ENaC protein pickpocket during homeostatic plasticity (Younger et al. 2013). In this system, partial pharmacological blockade of postsynaptic receptors elicits a consequential increase in presynaptic neurotransmitter release to maintain a constant level of neurotransmission (Frank et al. 2006). This homeostatic effect is mediated by expression of the pickpocket channel in the presynaptic neuron that is thought to increase synaptic vesicle release through VGCC activation (Younger et al. 2013). Pickpocket is predicted to depolarize the presynaptic membrane, activating local VGCCs, and triggering synaptic vesicle fusion (Younger et al. 2013). One major disparity between the UNC-8 and Pickpocket models is the ultimate outcome of local DEG/ENaC activity; pickpocket activity strengthens the synaptic connection, whereas UNC-8 activity appears to destroy it. These findings raise the interesting possibility that different DEG/ENaC proteins may exert diverse roles in sculpting neuronal circuitry.

Calcineurin regulates UNC-8 channel activity

The calcium-dependent phosphatase calcineurin is an established regulator of neuronal plasticity; blocking calcineurin activity abolishes long term depression and overexpression of calcineurin inhibits long-term potentiation (Mulkey et al. 1994; Mansuy et al. 1998; Hodgkiss & Kelly 1995). Here we demonstrate a role for calcineurin in GABAergic neurons in *C. elegans*. Loss of function calcineurin mutants partially block synapse removal, whereas constitutive activation of calcineurin induces precocious synapse elimination. Our genetic results show that UNC-8 channel activity functions downstream of calcineurin. We predict that calcineurin may directly activate UNC-8 through dephosphorylation. There is precedence for this prediction; ASIC1a, a member of the DEG/ENaC family is activated by phosphorylation via CaMKII ((Gao et al. 2005). Additionally, we found that a gain-of-function mutation in the CaMKII protein UNC-43, impedes synapse removal. Therefore, our results suggest there is a calcium-driven balance of phosphorylation and dephosphorylation that may dictate UNC-8 channel activity; however, our current results cannot distinguish between a direct or indirect relationship between these proteins. Future experiments will focus on determining whether UNC-8 is a direct target of calcineurin and CaMKII.

Actin reorganization drives synapse removal in the UNC-8 pathway

Previous work in *C. elegans* identified a role for cytoskeletal dynamics during synaptic remodeling in GABAergic neurons (Kurup et al. 2015; Meng et al. 2015). Dynamic microtubules promote synaptic remodeling in DD neurons through kinesin-1-mediated transport (Kurup et al. 2015). Additionally, the Yan lab found that synapse elimination in GABAergic neurons is partially achieved by activation of the F-actin

severing protein gelsolin. This process is mediated by the canonical cell death proteins, which we found to function in a common pathway with UNC-8. In an RNAi screen of candidate *unc-55* target genes, we found that the Arp2/3 component *arx-5* also promotes synapse removal. Taken together, these findings are intriguing because they suggest that severing F-actin (gelsolin) and driving branched actin assembly (Arp2/3) both promote the synaptic removal process. Importantly, gelsolin functions as an actin-capping protein in addition to its roles in severing F-actin. Several reports have shown that the Arp2/3 complex and gelsolin function in a common pathway to drive branched actin nucleation (Falet et al. 2002; Ressad et al. 1999). Therefore, it is possible that gelsolin and Arp2/3 may be functioning in a common pathway in *C. elegans* to drive synapse removal by regulating the branched actin network. In support of this prediction, one study found that loss of Arp2/3 can promote aberrant synaptic connections in mammalian neurons (Kim et al. 2015).

Author Contributions

Graduate student Cristina Matthewman (Laura Bianchi lab- University of Miami) performed the oocyte experiments in **Figure 4.3**. Former undergraduate student Megan Gornet constructed the *unc-2* and *egl-19* strains (**Figures 4.4** and **4.5**). Undergraduate student Allie Beers constructed the *tax-6* loss-of-function and *unc-43* gain-of-function strains (**Figures 4.6** and **4.11**). The remaining experiments performed in this chapter (strain construction, image collection, and synapse quantifications) were completed by Tyne Miller-Fleming.

Acknowledgments

We thank M.Q. Dong for *hqIs2 and hqIs5[ptax-6::TAX-6::GFP].* Some strains used in this study were provided by the CGC, which is funded by the NIH Office of Research Infrastructure Programs (P40 OD010440). We also received strains from the Japanese National BioResource Project. This work was supported by NIH grants 5R01NS081259 (DMM), and 1F31NS084732 (TWM). The data in Figures **4.1-4.4**, and **4.6-4.10** were published in *eLife* (Miller-Fleming et al. 2016).

CHAPTER V

DISASSEMBLY OF THE GABAERGIC PRESYNAPTIC ACTIVE ZONE IS CONTROLLED BY UNC-8 AND IRX-1 VIA DISTINCT PATHWAYS

Summary

Information flow in the nervous system relies on the efficient and expeditious communication between neurons and their target cells at junctions, or chemical synapses. The asymmetric pre- and postsynaptic membranes contain specialized clusters of proteins that mediate the exchange of information and appear as electron dense regions by electron microscopy (EM). Active zone proteins are critical to mediate neurotransmission through the docking and priming of synaptic vesicles and by recruiting and tethering voltage-gated calcium channels (Südhof 2012). Additionally, studies have shown that regulating the size and composition of the active zone has profound effects on the functional output of the neuron (Peled et al. 2014; Matz et al. 2010; Holderith et al. 2012; Paul et al. 2015; Zhen & Jin 1999; Dai et al. 2006). Although fluorescent imaging and biochemical analysis of the active zone proteins has been difficult, genetic studies have identified several major protein components including: UNC-10/RIM, UNC-13/Munc-13, RIM-binding protein, SYD-1, SYD-2/liprin-alpha, and ELKS-1/ELKS (Südhof 2012).

Genetic dissection and EM studies in *C. elegans* have shown that the rho-GAP protein SYD-1 localizes SYD-2, the liprin-alpha homolog (Lar-interacting-protein-related), at the presynaptic active zone (Dai et al. 2006). This structure is required for the proper

targeting of additional active zone proteins including UNC-10/RIM and ELKS-1/ELKS (Dai et al. 2006). UNC-10 can then directly bind to the synaptic vesicle priming protein UNC-13/MUNC-13 (Dai et al. 2006; Patel & Shen 2009), localizing it to the presynaptic density. UNC-10/RIM additionally mediates the interactions between vesicle-bound RAB-3, thus acting as a tether to dock synaptic vesicles (Fukuda 2003). These studies predict that the active zone components arrive and are stabilized in a particular order, which has led to the speculation that *de novo* formation and growth of active zones may be the result of pre-assembled scaffolds that are trafficked and stabilized at synapses. The molecular composition of these scaffolds has been difficult to delineate, although it is predicted that distinct populations likely exist and are trafficked along axons (Petzoldt et al. 2016; Maeder & Shen 2011; Bury & Sabo 2016; Shapira et al. 2003; Dresbach et al. 2006; Maas et al. 2012; Ahmari et al. 2000; Sabo & McAllister 2003). First, it was found that active zones likely arise from quantal units (Kittelmann et al. 2013; Ehmann et al. 2015; Matkovic et al. 2013). This finding was further supported when a serine/threonine kinase mutant, SRPK79D, was shown to prevent these quantal scaffold units from co-assembling, thereby resulting in ectopic pre-assembled protein clusters along the axon (Siebert et al. 2015; Nieratschker et al. 2009; Johnson et al. 2009). Interestingly, these protein clusters were a similar size and composition to the predicted quantal units previously identified. Second, dense core vesicles and synaptic vesicles are thought to travel along axons to deliver cargos of active zone proteins or synaptic vesicle proteins to synaptic sites, respectively. (Shapira et al. 2003; Dresbach et al. 2006; Maas et al. 2012; Ahmari et al. 2000). Although these distinct population of vesicles exist, both are co-transported along axons and it has been difficult to isolate either population (Tao-Cheng 2007; Bury & Sabo 2011); therefore, it is unclear which active zone proteins are trafficked together. These findings are further complicated by

the contribution of active zone proteins by local translation machinery and the potential exchange of presynaptic components by neighboring active zones (Tsuriel et al. 2009; Spangler et al. 2013).

Even less is known about the mechanism of active zone disassembly. Current studies demonstrate a role for the apoptotic pathway and the proteasome complex in synapse elimination; however, it has not been shown whether active zone proteins are eliminated in a specific order (Meng et al. 2015; Ertürk et al. 2014; J.-Y. Wang et al. 2014). A recent study in *Drosophila* found that constant light exposure promoted presynaptic active zone removal in photoreceptors. In this paradigm SYD-2/DLiprin-alpha, ELKS-1/Brp/ELKS and DRBP (*Drosophila* RIM-binding protein)are reduced, but SYD-1/DSyd-1 and voltage-gated calcium channels (VGCCs/Cac) in the active zone were unaffected (Sugie et al. 2015). These findings suggest that distinct components of the active zone scaffolds are sensitive to activity-dependent disassembly, while others are not. Here, we report similar findings at the GABAergic neuromuscular junction of *C. elegans.* We previously identified two transcriptional targets of UNC-55 that promote ventral GABAergic synapse removal, the transcription factor IRX-1 and the DEG/ENaC protein UNC-8 (S. C. Petersen et al. 2011; Miller-Fleming et al. 2016). Genetic dissection of these components reveals that UNC-8 and IRX-1 promote synapse disassembly via parallel, or distinct, pathways. EM analysis confirmed that the loss of *irx-1* or *unc-8* restores visible active zone structures (including membrane and vesicular proteins) to the ventral nerve cords of *unc-55* animals; however, *unc-55; unc-8* synapses are not functional. We found that ventral synapses in *unc-55; unc-8* animals are missing the synaptic vesicle priming protein UNC-13, while ventral UNC-13 is retained in *unc-55; irx-1* mutants, suggesting that IRX-1 regulates tha removal of UNC-13. Furthermore,

these findings support the idea that individual components of the presynaptic active zone can be regulated by distinct genetic or activity-dependent mechanisms.

Materials and Methods

Strains and Genetics

C. elegans strains were cultured at 20° C as previously described on standard nematode growth medium seeded with OP50 (Brenner 1974). The mutant alleles and strains used in this study are outlined in **Tables 4.1** and **4.2.**

Microscopy

Staging and Synapse Quantification

Puncta arising from localization of fluorescent presynaptic markers were counted with a Zeiss Axiovert microscope (63X oil objective) in immobilized animals. In young adults, labeled puncta were counted in the ventral nerve cord region between VD3 and VD11 (**Figures 5.9** and **5.10**). The examiner was blinded to genotype.

Confocal Microscopy and Image Analysis

Animals were immobilized on 2% agarose pads with 15mM levamisole as previously described (C. J. Smith et al. 2012). Synapse counts of animals were collected with a Zeiss Axioplan inverted microscope using ImageJ Micro-Manager software and a 63x oil objective (camera ORCA; Hammamatsu). Z-stack images (**Figures 5.1, 5.2, 5.5, 5.6, 5.7, 5.9, and 5.10**) were collected on a Leica TCS SP5 confocal microscope using a 63X oil objective (0.5 µm/step), spanning the focal depth of the ventral nerve cord GABA neurons and synapses. Leica Application Suite Advanced Fluorescence (LAS-AF)

software was used to generate maximum intensity projections. Ventral nerve cord images were straightened using an ImageJ plug-in. Fluorescence intensity values in **Figure 5.2, 5.5,** and **5.9** were generated in ImageJ by determining the mean gray value of a region of interest drawn around sections of the ventral nerve cord or by drawing a line through the ventral nerve cord. The coefficient of determination (r^2) in **Figures 5.6** and **5.7** were calculated in ImageJ using the Manders coefficients macro, from at least 3 animals for each genotype. r^2 values were averaged and presented as mean ± SEM. An r^2 value of 0 represents no co-localization, whereas r^2 = 1 represents complete co-localization. The heat maps in **Figures 5.2** and **5.10** were generated with the HeatMap Histogram macro on ImageJ (Samuel Péan).

Electron Microscopy

All EM images were collected by Laura Manning, a graduate student from Janet Richmond's lab at the University of Illinois at Chicago. Young adult hermaphrodites of each strain were prepared for high-pressure freeze (HPF) fixation as described (Rostaing et al. 2004; Miller-Fleming et al. 2016). 10–15 animals were loaded into a specimen chamber filled with *E. coli.* The specimens were frozen rapidly in a high-pressure freezer (Bal-Tec HPM010) at -180°C and high pressure. Freeze substitution was performed on frozen samples in a Reichert AFS machine (Leica, Oberkochen, Germany) with 0.1% tannic acid and 2% OsO_4 in anhydrous acetone. The temperature was kept at -90°C for 107 h, increased at 5°C/h to -20°C, and kept at -20°C for 14h. The temperature was then increased by 10°C/h to 20°C. Fixed specimens were embedded in Epon resin after infiltration in 50% Epon/acetone for 4h, 90% Epon/acetone for 18h, and 100% Epon for 5 hours. Embedded samples were incubated for 48h at 65°C. All

specimens were prepared in the same fixation procedure and labeled with anonymous tags so that the examiner was blinded for genotype. Ultra thin (40 nm) serial sections were cut using an Ultracut 6 (Leica) and collected on formvar- covered, carbon-coated copper grids (EMS, FCF2010-Cu). Grids were counterstained in 2% aqueous uranyl acetate for 4 min, followed by Reynolds lead citrate for 2 min. Images were obtained on a Jeol JEM-1220 (Tokyo, Japan) transmission electron microscope operating at 80 kV. Micrographs were collected using a Gatan digital camera (Pleasanton, CA) at a magnification of 100k. Images were quantified using NIH ImageJ software. Dorsal and ventral cords were distinguished by size and morphology. GABAergic synapses were identified by previously established criteria, including position in the cord as well as the morphology of the synapse (White et al. 1986; Jin et al. 1999). GABAergic synapses are larger than their cholinergic motor neuron counterparts, and the active zones in these synapses form a direct, perpendicular angle with muscle arms. On the other hand, the presynaptic density in cholinergic synapses orient at an acute angle to the muscle, generally 30-45° and are often dyadic. Some images were collected at 30k to aid in identifying synaptic identity based on terminal position in the cord. Two colleagues with expertise in EM reconstruction of the *C. elegans* ventral nerve cord independently reviewed synapse images from each strain to verify identification. Each profile represents an image taken of a 40 nm section. A synapse was defined as a set of serial sections containing a presynaptic density and flanking sections from both sides without presynaptic densities. Synaptic vesicles were identified as spherical, light gray structures with an average diameter of ~30 nm. Synaptic vesicles were considered docked if they touched the membrane. At least two animals were analyzed for each genotype. Numbers of profiles analyzed for each genotype were: wild type = 502, *unc-8* = 322, *unc-55* = 246, *unc-55; unc-8* = 304 for ventral GABAergic synapse evaluation; wild type

= 502, *unc-8* = 322, *unc-55* = 246, *unc-55; unc-8* = 304 for ventral cholinergic synapse evaluation.

Electrophysiology

Electrophysiology experiments were performed by Janet Richmond at the University of Illinois at Chicago. The *C. elegans* dissection and electrophysiological methods were as previously described (Richmond & Jorgensen 1999; Miller-Fleming et al. 2016). Animals were immobilized along the dorsal axis with Histoacryl Blue glue, and a lateral cuticle incision was made with a hand-held glass needle, exposing ventral medial body wall muscles. Muscle recordings were obtained in the whole-cell voltage-clamp mode using an EPC-10 patch-clamp amplifier and digitized at 1 kHz. The extracellular solution consisted of 150 mM NaCl, 5 mM KCl, 5 mM CaCl2, 4 mM MgCl2, 10 mM glucose, 5 mM sucrose, and 15 mM HEPES (pH 7.3, ~340 mOsm). The low Cl intracellular patch pipette solution used to isolate outward GABA minis at a 0 mV holding potential was composed of 115 mM KGluconate, 25 mM KCl, 0.1 mM CaCl2, 1 mM BAPTA and 50 mM HEPES. GABAergic hyperosmotic responses were acquired at a holding potential of -60 mV by pressure-ejecting extracellular saline containing an additional 500 mOsm of sucrose. The intracellular solution consisted of 120 mM KCl, 4 mM KOH, 4 mM MgCl2, 5 mM (N-tris[Hydroxymethyl] methyl-2-aminoethane-sulfonic acid), 0.25 mM CaCl2, 4 mM Na2ATP, 36 mM sucrose, and 5 mM EGTA (pH 7.2, ~315 mOsm). 10 mM d-tubocurare was added to both the extracellular solution and the pressure ejection pipette to block cholinergic hyperosmotic currents. Data were acquired using Pulse software (HEKA, Southboro, Massachusetts, United States) run on a Dell computer. Subsequent analysis and graphing was performed using Pulsefit (HEKA), Mini analysis (Synaptosoft Inc., Decatur, Georgia, United States) and Igor

Pro (Wavemetrics, Lake Oswego, Oregon, United States). For **Figure 5.5C**, a 100 ms pulse of 5x10-4 M GABA in extracellular solution was pressure ejected onto the patch-clamped muscle under constant bath perfusion. GABAergic hyperosmotic responses were acquired at a holding potential of -60 mV by pressure-ejecting extracellular saline containing an additional 500 mOsm of sucrose. 10 M d-tubocurare was added to both the extracellular solution and the pressure ejection pipette to block cholinergic hyperosmotic currents. Data were acquired using Pulse software (HEKA, Southboro, Massachusetts, United States) run on a Dell computer. Subsequent analysis and graphing was performed using Pulsefit (HEKA), Mini analysis (Synaptosoft Inc., Decatur, Georgia, United States) and Igor Pro (Wavemetrics, Lake Oswego, Oregon, United States).

Molecular Biology

Generation of the fluorescently-tagged UNC-13 strain

We used the In-Fusion cloning kit (ClonTech) to amplify the cDNA of the long isoform of UNC-13 from a plasmid provided by J. Kaplan (pTWM88). This fragment was ligated into a vector containing the *punc-25* GABA promoter and a C-terminal GFP tag. The resulting plasmid pTWM90 was injected into *unc-13 e51* null mutants at 25 ng/μl with the co-injection marker *pmyo-2::mCherry* (2 ng/ μl). This transgenic array was integrated by x-ray irradiation to generate stable transgenic lines for analysis.

Feeding RNA Interference Experiments

Bacteria producing either double-stranded *irx-1* RNA or containing the RNAi empty vector were seeded on NGM plates and stored at 4°C for up to 1 week. Four L4 *unc-55* or *unc-55; unc-8* animals were grown on each single RNAi plate at 23°C until progeny

reached the L4 stage, or about 3-4 days. Progeny were picked to fresh RNAi plates and the ventral synapses were quantified (**Figure 5.2,** S. C. Petersen et al. 2011).

Table 5.1. Mutant alleles and genotyping primers used in this study.

Allele	Source	Genotyping Primer Sequences
unc-8 tm5052 IV	NBRP	TGGGGCCCTAATAATTTCGA
		AGTGACAGTATGAAGCCAGG
unc-55 e1170 I	CGC	TAAGGACTACACGGATCCTG
		CCCAAGAAAGAAAAGAGAGGT
eri-1 mg366 IV	CGC	CATGCAATTTCAATGCCTTTTA
		TGCATCATCCAATCCACTATGT

Table 5.2. Strains used in this study.

Strain	Genotype
CZ333	*juIs1[punc-25::SNB-1::GFP; lin-15+]* IV
NC1851	*unc-55(e1170)* I; *juIs1* IV
NC2388	*unc-55(e1170)* I*; unc-8(tm5052) juIs1* IV
NC3052	*unc-55(e1170)* I*; unc-8(tm5052) juIs1* IV; *wdEx686[pttr-39::irx-1csRNAi F; unc-119+; punc-25::mCherry; pttr-39::irx-1 csRNAi R]*
NC1852	*unc-55 (e1170) I; eri-1 (mg366) juIs1 IV*
KP5348	*nuIs279[punc-25::UNC-57::GFP;punc-25::mCherry::RAB-3]*
NC2984	*unc-55(e1170)* I; *nuIs279*
NC2873	*unc-55(e1170)* I; *unc-8(tm5052)* IV; *nuIs279*
NC3167	*wdEx961[punc-25::mCherry::RAB-3; ceh-22::GFP] ; oxIs22[punc-49::UNC-49B::GFP; lin-15+] II*
NC3168	*unc-8 (tm5052) IV; wdEx961; oxIs22 II*
NC3169	*unc-55 (e1170) I wdEx961; oxIs22 II*
NC3170	*unc-55(e1170) I; unc-8 (tm5052) IV; wdEx961; oxIs22 II*
ZM54	*hpIs3[punc-25::SYD-2::GFP; lin-15+]* X
NC2875	*unc-8(tm5052)* IV; *hpIs3* X
NC1849	*unc-55(e1170)* I; *hpIs3* X
NC2874	*unc-55(e1170)* I; *unc-8(tm5052)* IV; *hpIs3* X
EG5052	*oxIs351[punc-47:ChR2::mCherry; lin-15+ LITMUS 38i]* X
NC2857	*unc-8(tm5052)* IV; *oxIs351* X
NC2211	*unc-55(e1170)* I; *oxIs351* X
NC2807	*unc-55(e1170)* I; *unc-8(tm5052)* IV; *oxIs351* X
NC2212	*unc-55 (e1170)* I; *oxIs351* X; *wdEx686[irx-1 csRNAi]*
NC1910	*unc-55 (e1170)* I; *eri-1 (mg366)* IV; *hpIs3* X
NC1852	*unc-55 (e1170)* I; *juIs1 eri-1 (mg366)* IV
EG1653	*oxIs22[punc-49::UNC-49B::GFP; lin-15+]* II
NC2122	*unc-55 (e1170)* I; *oxIs22* II
NC2117	*unc-55 (e1170)* I; *unc-8 (tm5052) IV; oxIs22* II
ZM1344	*hpIs61[punc-25::UNC-10::GFP]* II
NC2872	*unc-55 (e1170)* I; *hpIs61* II
NC2991	*unc-55 (e1170)* I; *unc-8 (tm5052)* IV; *hpIs61* II
NC3216	*unc-55 (e1170)* I; *wdIs97*
NC3217	*unc-55 (e1170)* I; *unc-8 (tm5052)* IV; *wdIs97*
NC3219	*unc-55 (e1170)* I; *wdIs97; wdEx[IRX-1csRNAi]*

Results

UNC-8 and IRX-1 drive ventral GABAergic synapse elimination in parallel genetic pathways

The Miller lab previously identified UNC-55 target genes that promote GABAergic synapse removal (S. C. Petersen et al. 2011). Two of these targets, the DEG/ENaC protein UNC-8 and the homeobox transcription factor IRX-1 are required for the complete removal of ventral presynaptic proteins, including the vesicular SNARE protein, SNB-1 (S. C. Petersen et al. 2011; Miller-Fleming et al. 2016). To determine whether the loss of *unc-8* or knock down of *irx-1* restores the presynaptic complex to *unc-55* animals, we used electron microscopy to visualize the presynaptic active zones. As predicted, we identified electron-dense GABAergic presynaptic active zones in wild-type, *unc-55; unc-8*, and *unc-55; irx-1 csRNAi* animals (**Figure 5.1A-C,** wild type = 6 synapses/20.08 µm, n = 3 animals, *unc-55; unc-8* = 2 synapses/12.16 µm, n = 2 animals, *unc-55;irx-1 RNAi* = 5 synapses/13.68 µm, n = 2 animals). No ventral GABAergic synapses were identified in the *unc-55* animals. Additionally, we quantified the number of synaptic vesicles at GABAergic synapses in wild type, *unc-55; unc-8*, and *unc-55; irx-1 csRNAi* animals and saw no significant differences (**Figure 5.1F**). These EM data are consistent with our findings that fluorescently-labeled SNB-1 (synaptic vesicle marker) and SYD-2 (active zone marker) are absent in *unc-55* mutants, but loss of *unc-8* or *irx-1* activity rescues this effect (**Figure 5.1D-E,** Miller-Fleming et al. 2016; S. C. Petersen et al. 2011). Additionally, the GABAergic synapses detected in the *unc-55; unc-8* and *unc-55; irx-1 csRNAi* animals appear to be morphologically normal.

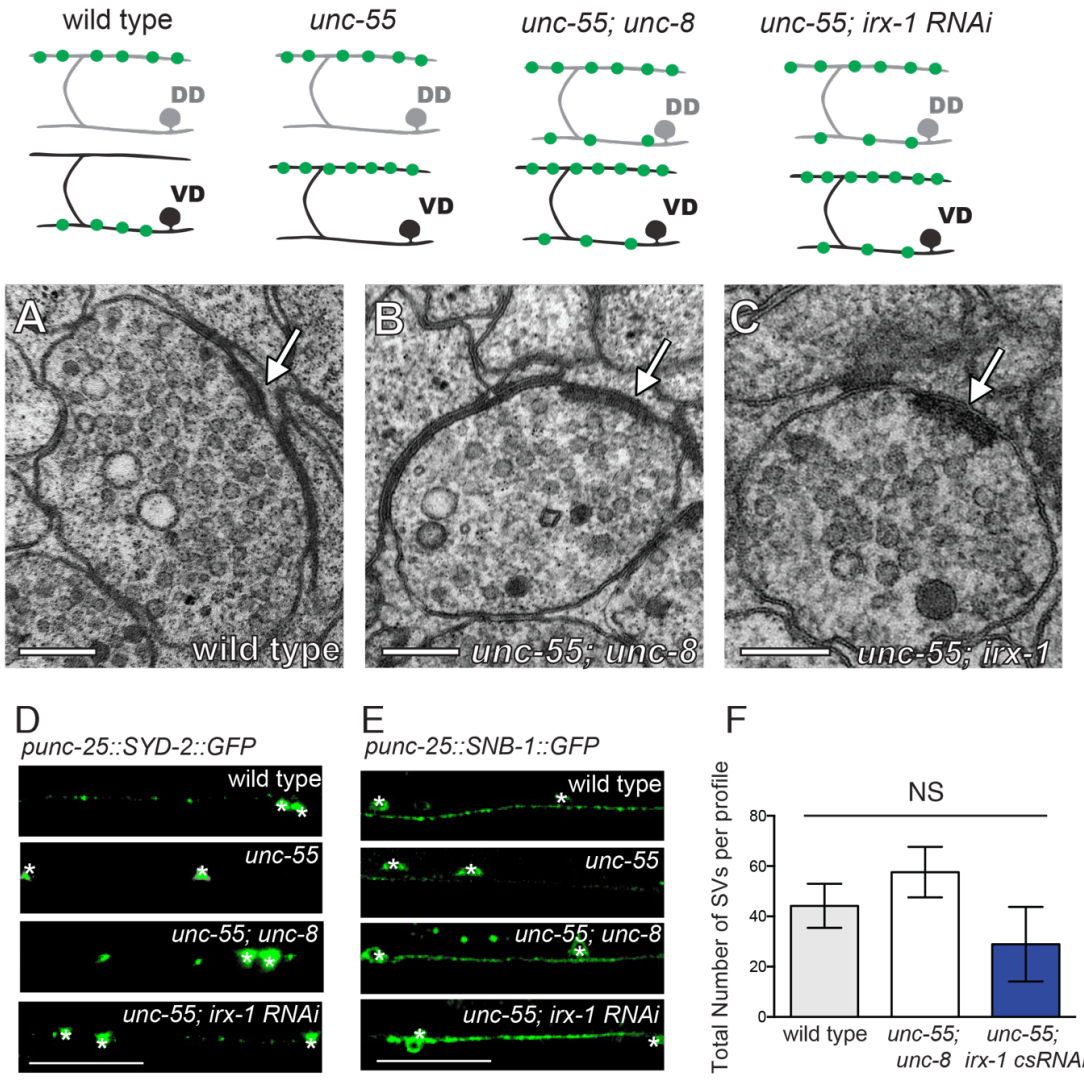

Figure 5.1: UNC-8 and IRX-1 promote ventral GABAergic synapse elimination. A-C. Representative electron micrographs of GABA neuron synapses with ventral muscles for wild-type (A), *unc-55; unc-8* (B), and *unc-55*; *irx-1 csRNAi* (C). Arrow points to presynaptic density, scale bar is 200 nm. **D.** Loss of *unc-8* and *irx-1* restore the active zone marker SYD-2::GFP to the ventral nerve cords of *unc-55* animals. **E.** UNC-8 and IRX-1 are required *unc-55*-mediated SNB-1::GFP removal. Scale bars are 10 µm. **F.** Quantification of ventral GABAergic synaptic vesicles by EM is consistent with the fluorescent marker data; synaptic vesicles are seen in wild-type, *unc-55; unc-8* and *unc-55; irx-1 csRNAi* ventral synapses (NS is not significant, N ≥ 5, data are mean ± SEM, One-Way ANOVA Bonferroni correction).

To determine whether UNC-8 and IRX-1 promote synapse removal in a common genetic pathway, we treated *unc-55* and *unc-55; unc-8* animals with RNAi targeted against *irx-1* or empty vector control. We quantified the SNB-1::GFP fluorescence intensity along the ventral nerve cord. We confirmed our previous findings that significantly more fluorescent puncta are retained in the ventral nerve cords of *unc-55*; *unc-8* and *unc-55; irx-1* animals compared to *unc-55* mutants. Additionally, we find that knock down of *irx-1* in *unc-55; unc-8* animals enhanced the removal defects observed in both *unc-55; unc-8* and *unc-55; irx-1* animals, suggesting that UNC-8 and IRX-1 promote synapse elimination in parallel pathways (**Figure 5.2**).

Ventral GABAergic synapses in *unc-55; unc-8* animals are not functional

Based on our findings in Chapter 3 showing that UNC-8 is required for the complete removal of several presynaptic proteins (SNB-1, SYD-2, RAB-3, UNC-57) and the finding that loss of *unc-8* restores the presynaptic density to *unc-55* animals (**Figure 5.1B**), we predicted that the *unc-55; unc-8* GABA synapses would restore function. As an initial test of this prediction, we examined backward locomotion. *unc-55* animals promote synapse remodeling in both DD and VD neurons, leading to a loss of ventral and excess dorsal GABAergic input and as a result, *unc-55* animals coil ventrally went tapped on the head (Walthall & Plunkett 1995; Shan et al. 2005). Loss of the pro-remodeling genes *irx-1* or the hunchback transcription factor homolog *hbl-1* rescues *unc-55*-mediated ventral coiling, suggesting that this assay can be used as a read-out for GABAergic synapse function(S. C. Petersen et al. 2011; Thompson-Peer et al. 2012). To determine whether *unc-55; unc-8* animals regain backward locomotion, we performed a tapping assay with wild-type, *unc-8*, *unc-55*, and *unc-55; unc-8* animals. *unc-55* and *unc-*

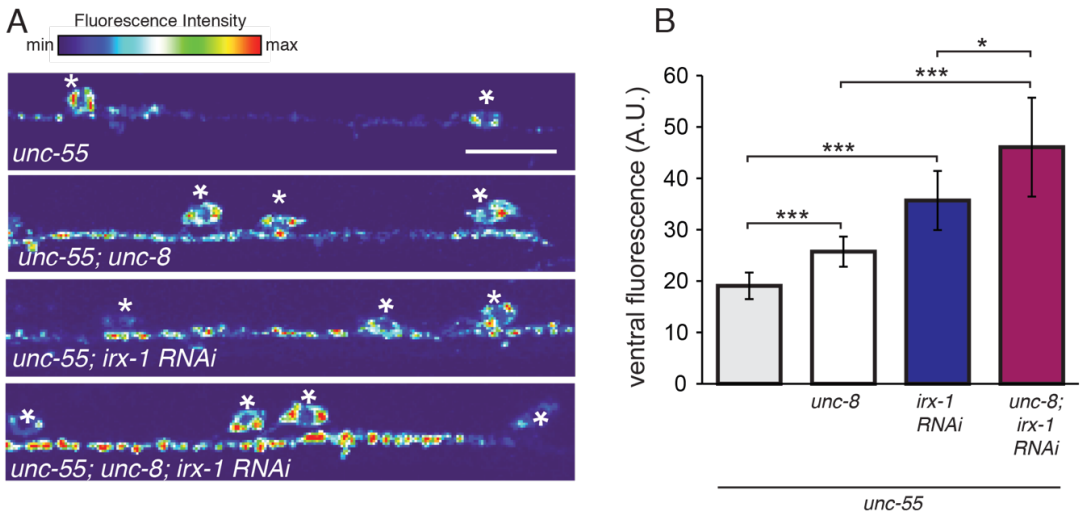

Figure 5.2: UNC-8 and IRX-1 dismantle the GABAergic presynaptic complex via distinct genetic pathways. A. Representative images of SNB-1::GFP labeled VD GABA neuron synapses in the ventral nerve cord. Scale bar is 10 µm and asterisks denote cell bodies. **B.** SNB-1::GFP fluorescence intensity was quantified for each genotype. *unc-55;unc-8* and *unc-55;irx-1(RNAi)* animals show more ventral SNB-1::GFP-marked synapses than *unc-55*. This effect is enhanced in *unc-55;unc-8;irx-1(RNAi)* animals, suggesting that UNC-8 and IRX-1 promote remodeling in parallel pathways (*p<0.05, ***p<0.001, One-Way ANOVA Bonferroni correction, error bars are SD, n ≥ 6 animals).

55; unc-8 animals have severe defects in backward locomotion, suggesting that the ventral GABAergic synapses observed in *unc-55; unc-8* animals may not be functional (**Figure 5.3**).

As a more direct test of this possibility, we recorded spontaneous inhibitory postsynaptic current (iPSCs) arising from GABA release onto ventral body muscles (see **Methods**). Robust, iPSCs were detected for wild-type animals (**Figure 5.4A**). Ventral iPSCs were not produced in *unc-55* mutants as expected since these animals lack GABAergic synapses in the ventral nerve cord (S. C. Petersen et al. 2011; Thompson-Peer et al. 2012). Interestingly, ventral iPSCs were restored in *unc-55; irx-1 csRNAi* animals, but not in *unc-55; unc-8* animals (**Figure 5.4A-C**) despite the presence of organized clusters of fluorescent presynaptic proteins, electron dense active zones, and abundant synaptic vesicles (**Figure 5.1**). Total ventral activity (cholinergic and GABAergic) was measured to confirm that spontaneous ventral cholinergic activity was unaffected by the *unc-55, irx-1*, and *unc-8* mutations (**Figure 5.4D-E**). These findings are consistent with the behavioral data and suggest that although IRX-1 and UNC-8 promote synapse elimination, restored synapses in *unc-55; unc-8* and *unc-55; irx-1 csRNAi* animals are not functionally identical.

Postsynaptic $GABA_A$ receptors are localized and functional in *unc-55; unc-8* animals

Our findings that ventral GABAergic electron-dense active zones are retained in *unc-55; unc-8* animals, but are not functional, raised the possibility that postsynaptic $GABA_A$ receptors are defective in these mutants. We visualized the expression of the postsynaptic fluorescently-tagged ionotropic $GABA_A$ receptor, UNC-49. Wild-type, *unc-*

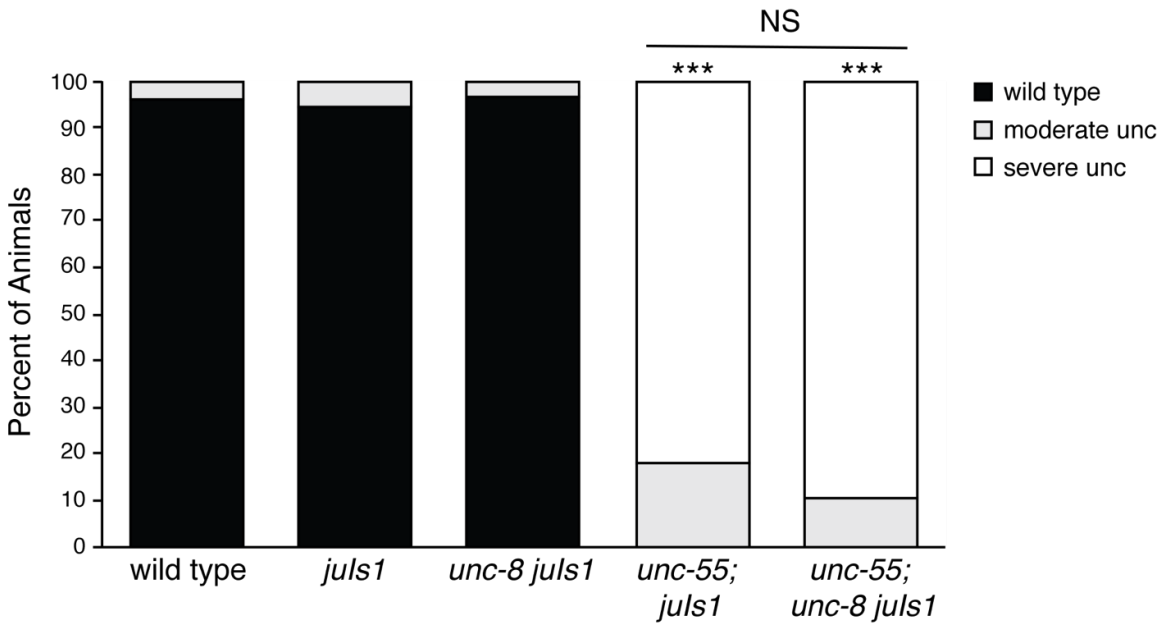

Figure 5.3: Loss of *unc-8* does not rescue backward locomotion in *unc-55* animals. Animals were tapped on the head to evoke backward movement and scored for either wild-type (black) vs uncoordinated (moderate or severe, gray or white, respectively) backward locomotion. *unc-55* and *unc-55; unc-8* animals coil ventrally with head tap. (***p<0.001, NS is not significant, Fisher's Exact Test, n ≥ 20 animals per genotype). Loss of *unc-8* restores ventral presynaptic domains to *unc-55* animals, but does not rescue backward locomotion.

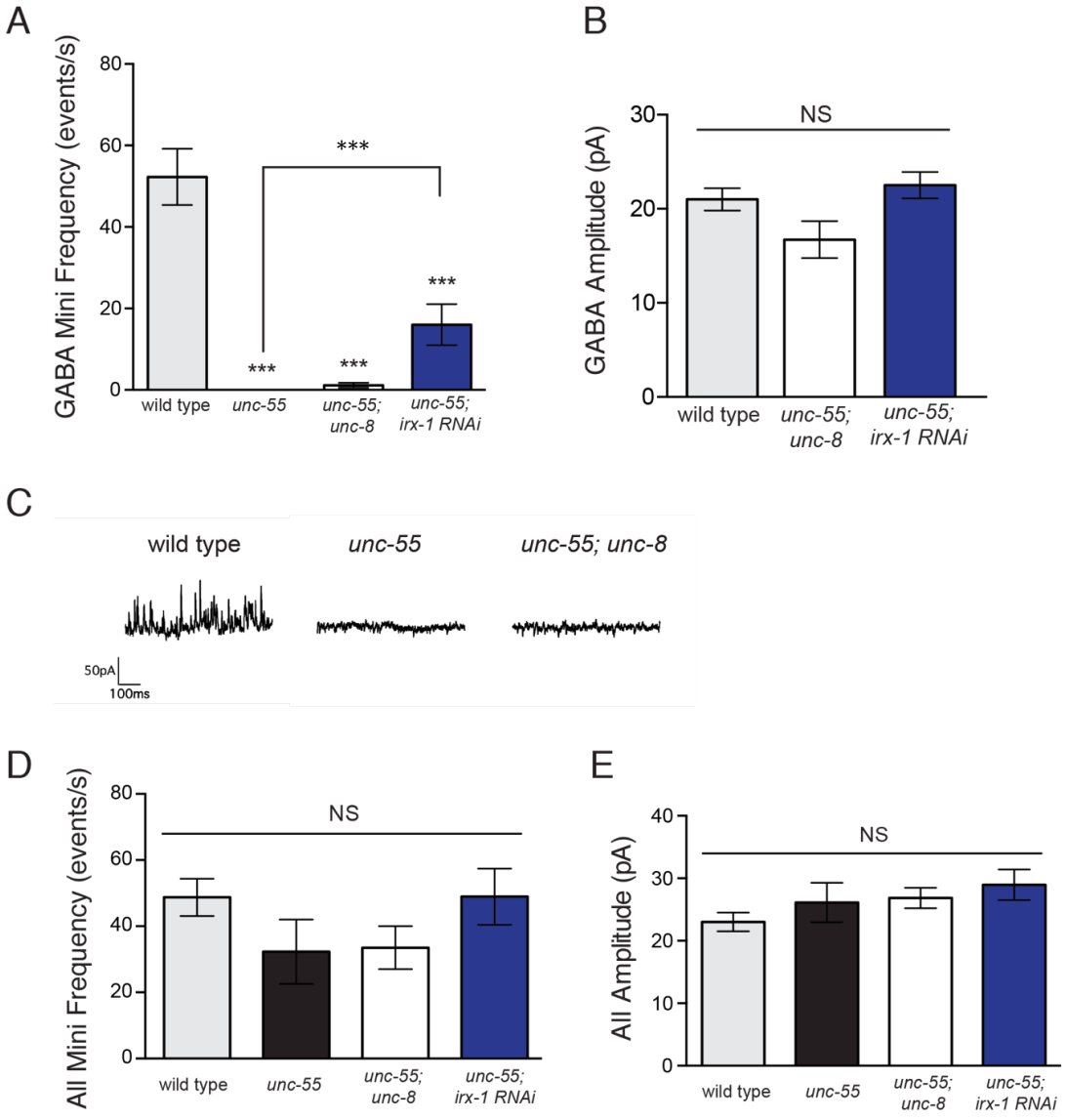

Figure 5.4: Genetic ablation of *irx-1*, but not *unc-8*, restores ventral GABA synaptic function to *unc-55* mutants. A. Ventral iPSCs were detected in wild-type and in *unc-55; irx-1 csRNAi* animals, but not in *unc-55* or *unc-55;unc-8* **B.** iPSC amplitude was not affected in *unc-55; irx-1* and *unc-55; unc-8* compared to wild type (ns is not significant, N ≥ 5, data are mean ± SEM, One-Way ANOVA Bonferroni correction). **C.** Representative traces of ventral mini-iPSCs from each genotype. **D./E.** Mini frequency and amplitude of all events (GABAergic and cholinergic) were indistinguishable in wild type, *unc-55*, *unc-55; unc-8*, and *unc-55; irx-1*, suggesting that the effects we observed were GABA-specific type (NS is not significant, N ≥ 5, data are mean ± SEM, One-Way ANOVA Bonferroni correction).

55, and *unc-55; unc-8* animals showed comparable levels of GFP label on muscle cells and discrete UNC-49::GFP puncta along the ventral nerve cords (**Figure 5.5A**). Fluorescence intensity measurements revealed no differences in GFP levels among these genotypes, suggesting that UNC-49 is properly expressed in *unc-55; unc-8* animals (**Figure 5.5B**). To confirm that UNC-49::GFP is correctly localized in these mutants, we co-labeled the presynaptic active zone with mCherry::RAB-3 and the postsynaptic complex with UNC-49::GFP. This experiment confirmed that these pre- and postsynaptic components are co-localized in wild-type, *unc-8*, *unc-55*, and *unc-55; unc-8* animals. As expected, mCherry::RAB-3 and UNC-49::GFP are not co-localized in *unc-55* mutants, due to ectopic remodeling of ventral GABAergic presynaptic complexes (**Figures 5.6** and **5.7,** Miller-Fleming et al. 2016). These findings confirm that the correct localization of postsynaptic UNC-49::GFP in muscle in juxta-position to the presynaptic complex of GABAergic motor neurons is maintained in *unc-55; unc-8* animals and rule out a model in which mislocalization UNC-49 accounts for the absence of postsynaptic iPSCs in *unc-55; unc-8* animals (**Figure 5.4**).

As a more direct measurement of postsynaptic $GABA_A$ receptor function, GABA was perfused onto patch-clamped ventral muscles of wild-type, *unc-8*, *unc-55,* and *unc-55; unc-8* animals for recording postsynaptic GABA responses. Consistent with the UNC-49::GFP expression and co-localization studies, strong GABA responses were elicited from all of these genotypes (**Figure 5.5C**). Collectively, these findings rule out a postsynaptic defect in the *unc-55; unc-8* animals arising from dysfunction of the postsynaptic UNC-49 GABA receptor.

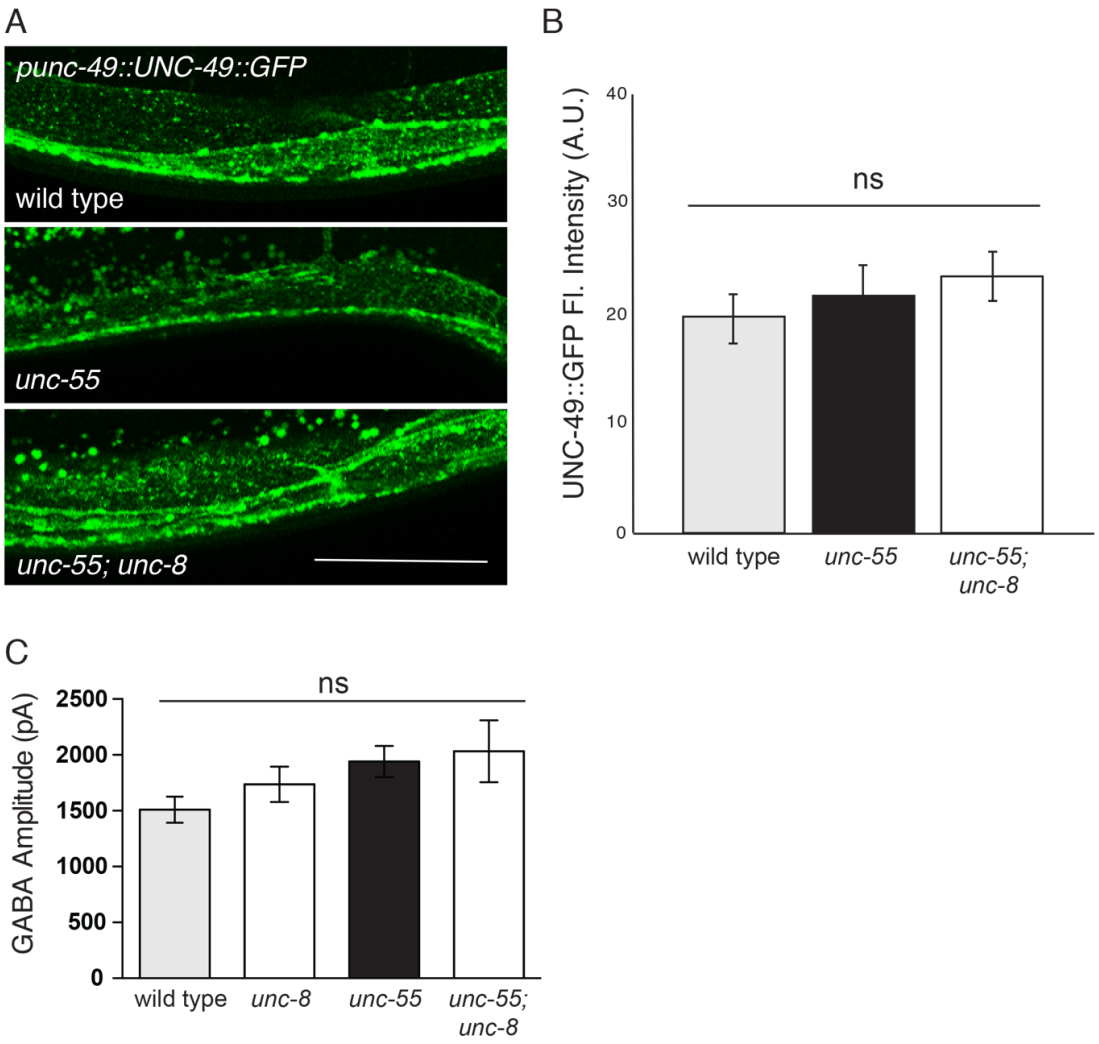

Figure 5.5: The postsynaptic UNC-49 $GABA_A$ receptors are expressed and functional in *unc-55; unc-8* animals. **A.** Representative images of UNC-49::GFP in wild type, *unc*-55, and *unc-55; unc-8* animals. Fluorescently-tagged UNC-49 (ionotropic $GABA_A$ receptor) is expressed in *unc-55* and *unc-55; unc-8* animals at levels that are indistinguishable from wild type. Scale bar is 15 μm. **B.** Fluorescent intensity measurements of ventral UNC-49::GFP are not significantly different in any of the genotypes (NS is not significant, One-Way ANOVA with Bonferroni correction, data are mean ± SD, N ≥ 5 animals). **C.** Exogenous application of GABA to the ventral nerve cords of wild type, *unc-8*, *unc-55*, and *unc-55; unc-8* animals results in a robust postsynaptic GABA response. GABA amplitude from the mutants was not different from wild type (NS is not significant, N ≥ 3 preparations, data are mean ± SEM, One-Way ANOVA with Bonferroni correction). These findings suggest that the GABAergic functional defect observed in *unc-55; unc-8* animals is likely due to presynaptic dysfunction; postsynaptic $GABA_A$ receptors in *unc-55; unc-8* animals are localized and functional.

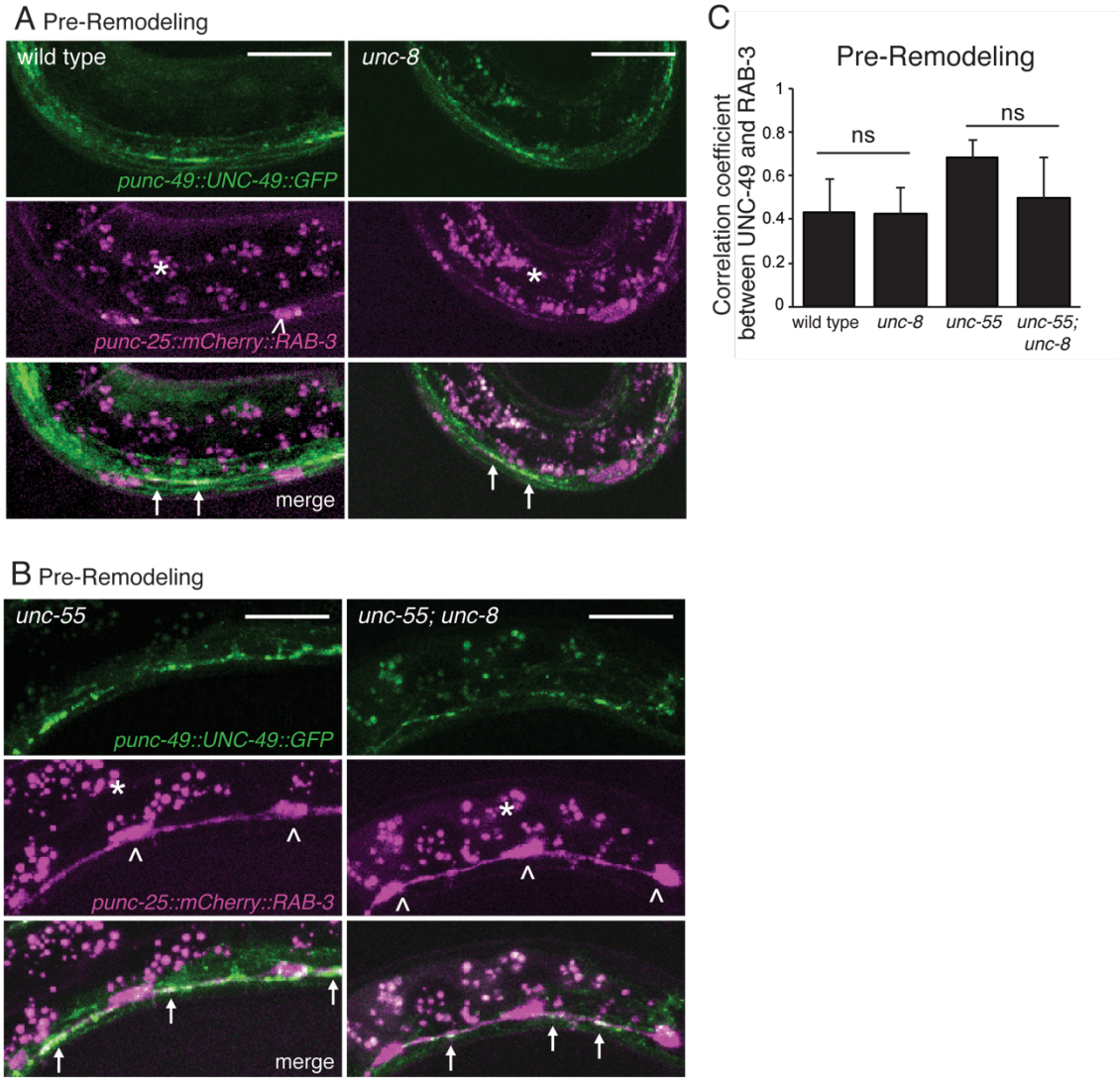

Figure 5.6: The postsynaptic UNC-49 $GABA_A$ receptor co-localizes with the presynaptic domains of GABAergic neurons before remodeling. Presynaptic regions (GABAergic neurons) are labeled with *mCherry::RAB-3* (magenta) and the postsynaptic compartment (body muscle) is marked with UNC-49::GFP (green); arrows denote regions of co-localization. Arrowheads point to GABA neuron cell soma. Asterisks mark intestinal auto-fluorescent granules. **A.** Pre-remodeling DD synapses with ventral muscles (early L1 larva, 2-hours post hatch). **B.** Pre-remodeling VD synapses with ventral muscles (L2 larva, 18-hours post hatch), show co-localization of *mCherry::RAB-3* and *UNC-49::GFP* in both *unc-55* and *unc-55; unc-8* animals before remodeling. Scale bars are 10 µm. **D.** Average correlation coefficient for ventral *UNC-49::GFP* and *mCherry::RAB-3* puncta before remodeling. *unc-8* is not significantly different from wild type ($P > 0.05$, n ≥ 3 L1 larvae, NS is not significant) and *unc-55; unc-8* is not significantly different from *unc-55* ($P > 0.05$, N ≥ 5 L2 larvae, NS is not significant, data are mean ± SD, Mann-Whitney test).

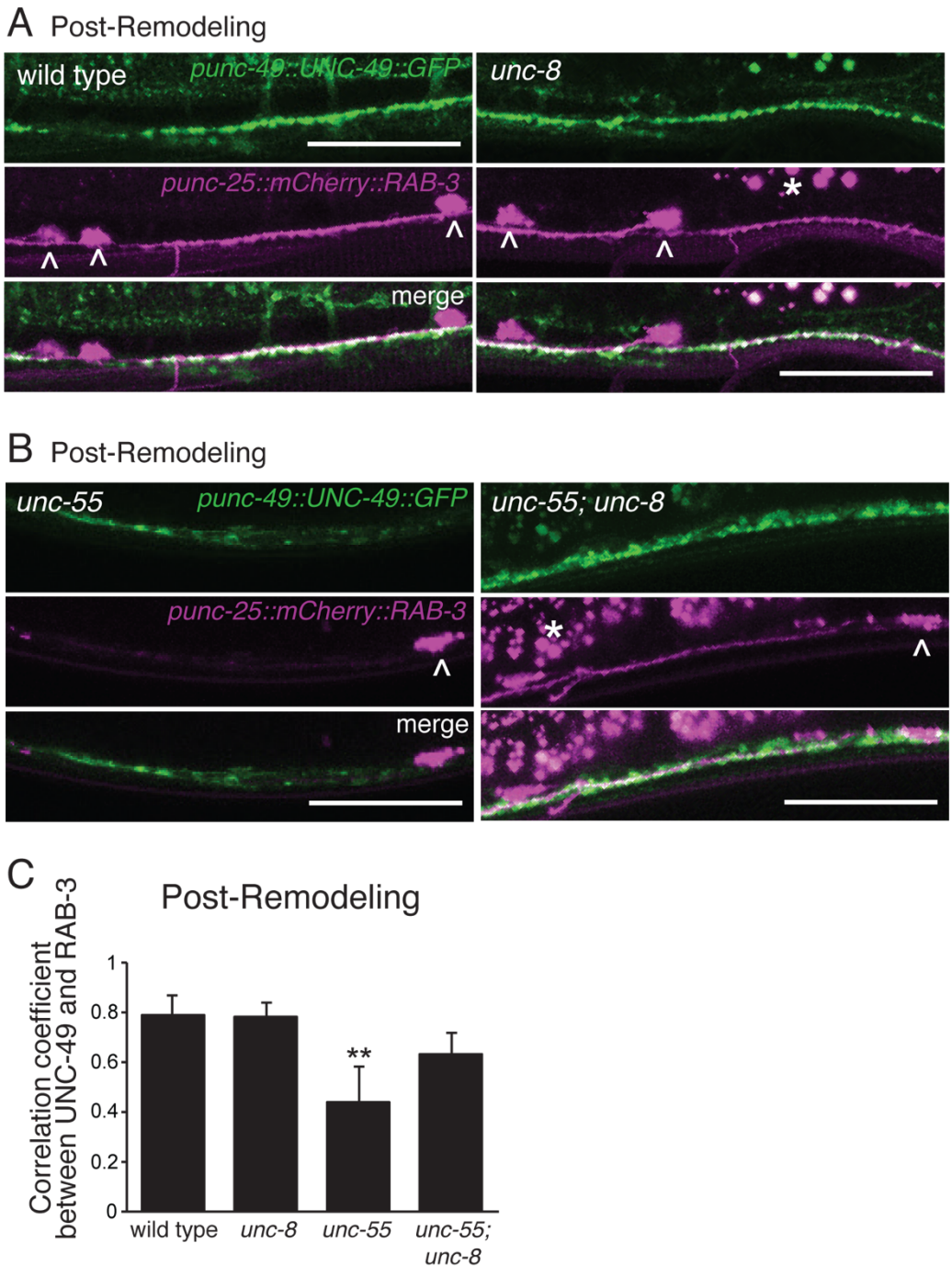

Figure 5.7: The postsynaptic UNC-49 $GABA_A$ receptor co-localizes with the presynaptic domains of GABAergic neurons after remodeling. Presynaptic regions (GABAergic neurons) are labeled with *mCherry::RAB-3* (magenta) and the postsynaptic compartment (body muscle) is marked with UNC-49::GFP (green), arrowheads point to GABA neuron cell soma. Asterisks mark intestinal autofluorescent granules. **A-B.** Ventral GABAergic synapses in young adults. Few ventral *mCherry::RAB-3*-marked presynaptic domains are detected in the *unc-55* mutant background due to ectopic

remodeling, but are abundant in both *unc-8* and *unc-55; unc-8*. Scale bars are 25 µm. **C.** Average coefficients of determination for ventral *UNC-49::GFP* and *mCherry::RAB-3* puncta after remodeling are not significantly different among wild-type, *unc-8* and *unc-55; unc-8* animals. *unc-55* shows significantly lower values likely due to the relative depletion of *mCherry::RAB-3* vs *UNC-49::GFP* (** $P < 0.01$, NS is not significant, $N \geq 5$ young adults, data are mean ± SD, Kruskal-Wallis with Dunn's multiple comparisons test).

unc-55; unc-8 animals exhibit a presynaptic vesicle fusion defect

Based on our findings that *unc-55; unc-8* animals show properly localized and functional postsynaptic complexes, we predicted that these animals exhibit a presynaptic defect. To test this hypothesis, we treated animals with a hyperosmotic sucrose solution to induce neurotransmitter release from primed synaptic vesicles (Niles & D. O. Smith 1982). In this case, GABAergic activity was isolated by recording from ventral muscles in the presence of d-tubocurare (dTBC) to block cholinergic signaling (S. C. Petersen et al. 2011). As predicted, wild-type and *unc-55; irx-1 csRNAi* animals show a robust response to hyperosmotic stimulation, whereas ventral muscles in *unc-55* mutants are unresponsive. In contrast, hyperosmotic treatment of *unc-55;unc-8* animals does not evoke ventral GABA release suggesting that these animals are likely defective in synaptic vesicle fusion (**Figure 5.8A**). Prior to this hyperosmotic test, preparations of all four of the genotypes exhibited spontaneous cholinergic activity that could be abolished by dTBC treatment. Only wild-type and *unc-55; irx-1 csRNAi* animals then showed robust GABAergic activity, confirming that the samples used for the hyperosmotic experiments were healthy (data not shown). These data support the prediction that ventral GABAergic synapses in *unc-55; unc-8* animals exhibit defects in synaptic vesicle fusion. The presence of docked synaptic vesicles in the EM images of wild-type, *unc-55; irx-1 csRNAi,* and *unc-55; unc-8* animals, suggest that docked vesicles in *unc-55; unc-8* animals are unable to fuse with the presynaptic membrane (**Figure 5.8B**). These results are consistent with the presence of a presynaptic defect in *unc-55; unc-8* animals.

Because previous work has shown that localization of the vesicular GTPase protein RAB-3 and the RAB-3-interacting protein UNC-10/RIM-1 at the presynaptic active zone is sufficient to prime and dock synaptic vesicles, we examined the ventral

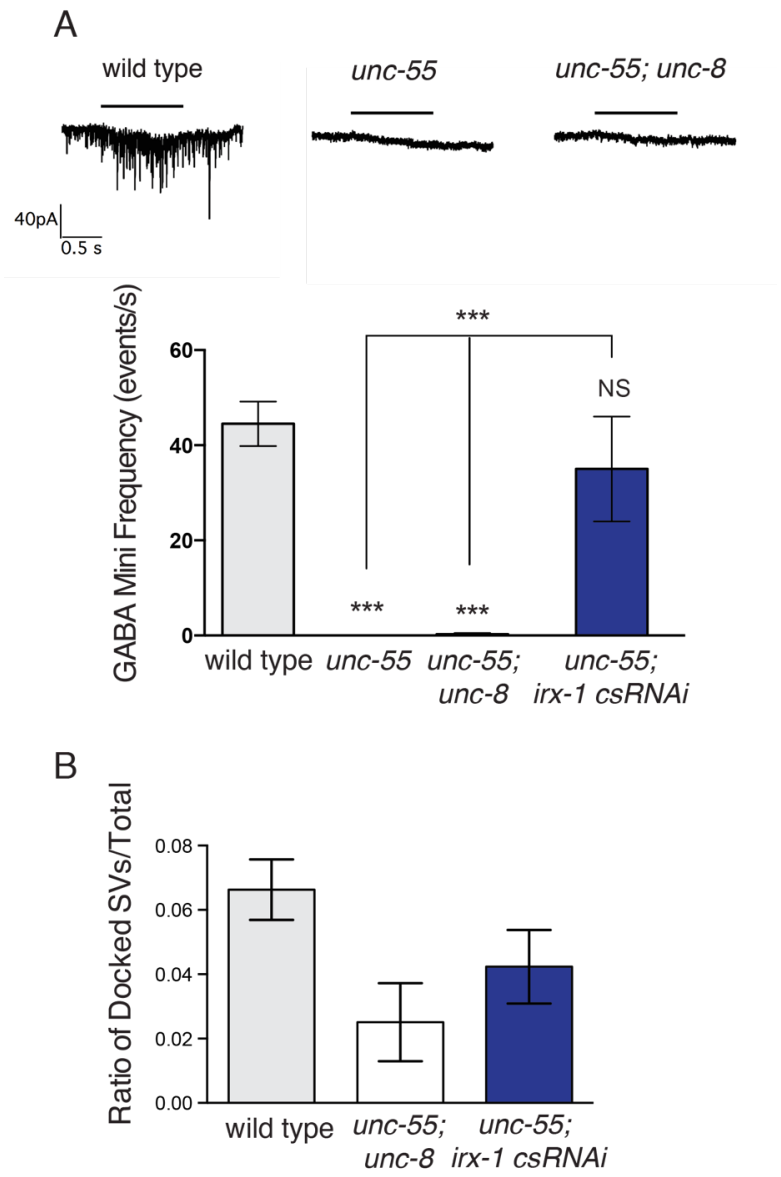

Figure 5.8: Synaptic vesicle fusion is defective in *unc-55; unc-8* animals. A. Representative hyperosmotic responses. Black bar represents application of sucrose solution. Treatment with hypertonic sucrose solution evokes a robust response at wild-type and *unc-55; irx-1 csRNAi* ventral GABA synapses, but not in *unc-55* or *unc-55; unc-8* (*p < 0.05, ns is not significant, N ≥ 3, data are mean ± SEM, One-Way ANOVA Bonferroni correction). **B.** Quantification of docked synaptic vesicles was calculated by counting the number of synaptic vesicles touching the plasma membrane, normalized by the total number of synaptic vesicles per profile (N ≥ 5, data are mean ± SEM, One-Way ANOVA with Bonferroni correction, no significant differences were observed). Docked synaptic vesicles were observed in wild type, *unc-55; unc-8,* and *unc-55; irx-1; csRNAi*; however, only the vesicles in wild type and *unc-55; irx-1 csRNAi* are fusion-competent.

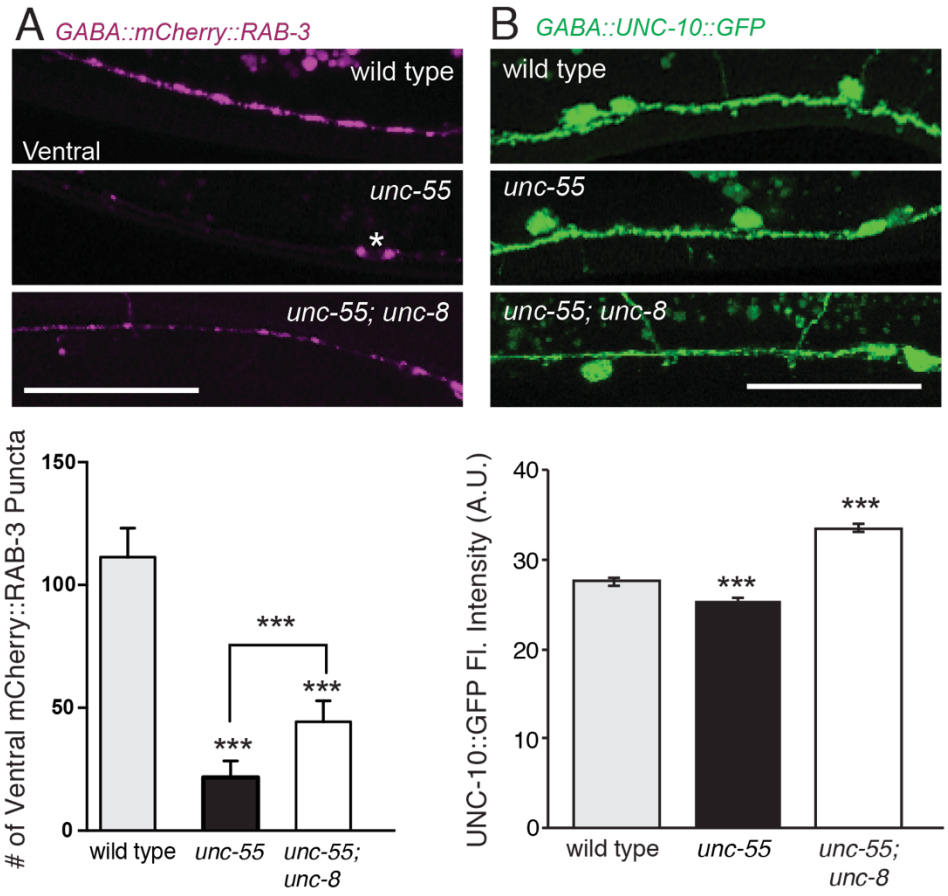

Figure 5.9: The synaptic vesicle docking proteins UNC-10/RIM-1 and RAB-3 are localized at the ventral nerve cord in *unc-55; unc-8* animals. A. Representative images (top) and quantification (below) of the presynaptic G protein RAB-3 indicate that *unc-8* is required for the removal of mCherry::RAB-3 from ventral synapses (***P < 0.001, N ≥ 21 animals). Scale bar is 10 µM, asterisks denote cell somas. One-Way ANOVA with Bonferroni correction, data are mean ± SD. These data were reported in Chapter 3 Figure 3.8. **B.** Fluorescently-labeled UNC-10/RIM-1 is localized to the ventral nerve cords of wild type, *unc-55*, and *unc-55; unc-8* animals and does not remodel. (***P < 0.001, N ≥ 6 animals, data are mean ± SEM, One-Way ANOVA with Bonferroni correction). Scale bar is 10 µM.

localization of fluorescently-labeled RAB-3 and UNC-10/RIM-1 proteins in GABAergic neurons. Consistent with our EM and electrophysiology data, this confirmed that wild-type animals express RAB-3 and UNC-10/RIM-1 in punctate patterns along the ventral nerve cord (**Figure 5.9**). RAB-3 is largely absent from ventral nerve cords of *unc-55* animals as a result of ectopic VD remodeling; however, UNC-10/RIM-1 is retained, suggesting that it does not remodel in *unc-55* mutants (**Figure 5.9B**). The additional finding that both RAB-3 and UNC-10/RIM-1 puncta are localized to the ventral nerve cord of *unc-55; unc-8* animals is consistent with EM results showing normal levels of docked vesicles in these animals (**Figure 5.9**).

IRX-1, but not UNC-8, removes the synaptic vesicle priming protein UNC-13 from the presynaptic active zone

Previous results indicate that presynaptic UNC-13/MUNC-13 is required for synaptic vesicle fusion, but not for docking (Varoqueaux et al. 2002). Because synaptic vesicles appear to be docked, but are incapable of fusion in *unc-55; unc-8* animals, we predicted that UNC-13::GFP could be missing from ventral GABAergic synapses in these animals. To test this idea, we generated a strain expressing GFP-tagged UNC-13 protein in GABA neurons. As noted for other presynaptic proteins, UNC-13::GFP is restricted to the ventral nerve cord prior to DD remodeling in early L1 larvae, but is detectable post-remodeling UNC-13::GFP is detectable in both the dorsal and ventral nerve cords in adults (**Figure 5.10A-B**). We quantified the number of UNC-13::GFP puncta along the ventral nerve cord and found that UNC-13::GFP is retained in wild-type animals, but is removed in *unc-55* animals. Loss of *unc-8* is not sufficient to restore ventral UNC-13::GFP puncta to *unc-55* animals, confirming our prediction that UNC-13

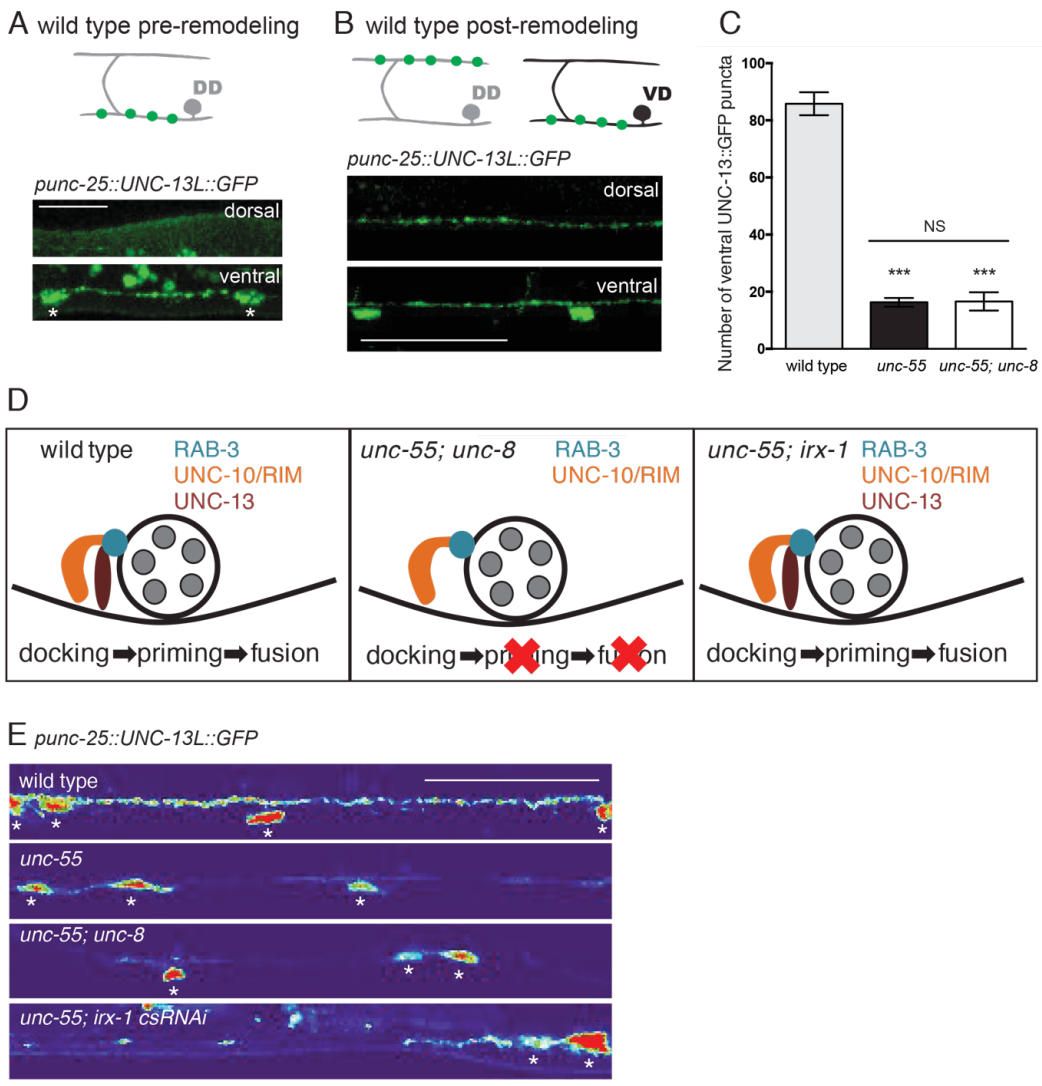

Figure 5.10: The synaptic vesicle priming protein UNC-13 is removed from ventral GABA synapses by IRX-1, but not UNC-8. A/B. Fluorescently-tagged UNC-13 *(punc-25::UNC-13L::GFP)* is strictly localized to the ventral nerve cord before remodeling (in L1 animals); however, UNC-13::GFP is visible on both the dorsal and ventral nerve cords after remodeling. **C.** Quantification of the number of UNC-13::GFP puncta along the ventral nerve cord of wild type, *unc-55*, and *unc-55; unc-8* animals reveals that *unc-55* and *unc-55; unc-8* animals have dramatically fewer puncta (***$P < 0.001$, NS is not significant, N ≥ 10 animals, data are mean ± SEM, One-Way ANOVA with Bonferroni correction). **D.** These results support the model that wild type and *unc-55; irx-1 csRNAi* ventral synapses restore function because they have ventrally-localized RAB-3 and UNC-10/RIM-1 to dock synaptic vesicles, and UNC-13 for vesicle priming. *unc-55; unc-8* animals are able to dock vesicles with ventrally localized RAB-3 and UNC-10/RIM-1; however, docked vesicles cannot be released due to the lack of ventral UNC-13. **E.** Consistent with our model, we see that UNC-13::GFP ventral puncta are missing in *unc-55* and *unc-55; unc-8* animals, but are restored in *unc-55; irx-1 csRNAi* animals. Scale bar is 15 µM.

is missing from these ventral synapses (**Figure 5.10C**). This finding suggests that although the ventral presynaptic active zone in *unc-55; unc-8* GABAergic neurons appears normal by EM, UNC-13 is not properly localized at these terminals and thus these synapses are not functional.

Because knock down of *irx-1* in *unc-55* mutants is sufficient to restore backward locomotion and ventral GABAergic function (S. C. Petersen et al. 2011), we predicted that UNC-13::GFP would be restored to the ventral nerve cords of *unc-55; irx-1 csRNAi* animals (**Figure 5.10D**). Indeed, we find that ventral UNC-13::GFP puncta are detectable in both wild-type and *unc-55; irx-1 csRNAi* animals, in contrast to the absence of UNC-13::GFP puncta in *unc-55* and *unc-55; unc-8* ventral nerve cords (**Figure 5.10E**). This finding is interesting because is suggests that different genetic pathways dismantle the remodeling presynaptic apparatus in GABAergic neurons by targeting specific active zone components.

Discussion

Here, we demonstrate that the transcription factor IRX-1/Iroquois and the UNC-8 DEG/ENaC protein function in separate pathways to dismantle the presynaptic apparatus of remodeling GABAergic neurons. Our evidence indicates that IRX-1 promotes the removal of the presynaptic apparatus in parallel to UNC-8; the combined activity of both IRX-1 and UNC-8 is required for efficient destruction of the presynaptic complex. In addition, we found that IRX-1, but not UNC-8, is specifically required for removing ventral UNC-13 from the presynaptic active zone in remodeling GABAergic neurons.

Activity-dependent and genetic regulation of active zone proteins

Work in the *Drosophila* nervous system showed that constant exposure to light resulted in the selective removal of a subset of presynaptic density proteins (SYD-2, RIM, DRBP) from photoreceptors, whereas, other active zone components were not affected (VGCCs and SYD-1, Sugie et al. 2015). We observe a parallel effect in remodeling GABAergic neurons in *C. elegans* in which the removal of selected presynaptic components is also activity-dependent. We have previously found that UNC-8 dismantles components of the presynaptic active zone in an activity-dependent pathway (see **Chapter 4,** Miller-Fleming et al. 2016), suggesting that UNC-8-mediated removal of SNB-1/synaptobrevin, SYD-2/liprin-alpha, UNC-57/endophillin, and RAB-3 requires neurotransmission, whereas UNC-13 removal requires the transcription factor IRX-1.

The composition and size of the active zone regulate its functional output (Peled et al. 2014; Matz et al. 2010; Holderith et al. 2012; Paul et al. 2015; Zhen & Jin 1999; Dai et al. 2006); therefore, a deeper knowledge of how assembly and removal of presynaptic proteins are regulated can advance our understanding of synaptic dysfunction and disease. Studies of UNC-13 in *C. elegans* have shown that both the long (UNC-13L) and short isoforms (UNC-13S) mediate the timing of synaptic vesicle release; UNC-13L promotes rapid neurotransmitter release, whereas UNC-13L and UNC-13S are required for slow neurotransmission (Hu et al. 2013). The position of UNC-13 and nearby voltage gated calcium channels (VGCCs) in the active zone regulate the timing and probability of synaptic vesicle fusion (K. Zhou et al. 2013). Recent work in *Drosophila* has shown that UNC-13S/UNC-13B is positioned at immature synapses by SYD-1 and SYD-2/liprin-alpha; whereas, the UNC-13L/UNC-13A is localized at mature synapses with ELKS and

Rim-binding proteins. Additionally, this study found that UNC-13L is localized much closer to VGCCs as compared to UNC-13S and that this differential localization affects neurotransmission (Böhme et al. 2016). Our findings may be useful in understanding the upstream transcriptional mechanisms regulating UNC-13L localization to the active zone and thus future studies will evaluate how IRX-1 promotes UNC-13L removal from GABAergic synapses. Previous work in *Drosophila* suggests that the proteasome regulates UNC-13 localization; therefore, in our future studies we can test whether IRX-1 regulates proteasome function (Aravamudan & Broadie 2003; Speese et al. 2003).

Author Contributions

Graduate student Laura Manning (Janet Richmond lab- University of Illinois at Chicago) performed the electron microscopy experiments in **Figures 5.1** and **5.8**. Janet Richmond performed the electrophysiology recordings in **Figures 5.4, 5.5,** and **5.8**. Former graduate student Sarah Petersen collected the images and performed the initial analysis in **Figure 5.2**. The remaining experiments performed in this chapter (strain construction, image collection, and synapse quantifications and tapping assays) were completed by Tyne Miller-Fleming.

Acknowledgments

We thank J. Kaplan for the UNC-13L plasmid. We thank M. Zhen for *hpIs3 and hqIs61* and E. Jorgensen for *oxIs22* and *oxIs351.* Some strains used in this study were provided by the CGC, which is funded by the NIH Office of Research Infrastructure Programs (P40 OD010440). We also received strains from the Japanese National BioResource Project. This work was supported by NIH grants 5R01NS081259 (DMM), and

1F31NS084732 (TWM). The data in **Figures 5.1, 5.4, 5.6, 5.7** and **5.9** were published in *eLife* (Miller-Fleming et al. 2016).

CHAPTER VI

CONSTITUTIVE ACTIVATION OF UNC-8 PROMOTES SELECTIVE DEGENERATION OF CHOLINERGIC MOTOR NEURONS

Summary

The DEG/ENaC protein family includes the degenerins, such as MEC-4, and the mammalian epithelial sodium channels. These channel subunits combine into homomeric as well as heteromeric trimers to form voltage-independent cation channels in epithelial cells, neurons, and glia (Canessa et al. 1993; Bianchi & Driscoll 2002; Y. Wang et al. 2008; Hitomi et al. 2009; Calavia et al. 2010; García-Añoveros et al. 1995). Prolonged activation of DEG/ENaC proteins either through genetic mutation or chronic proton exposure can result in neurodegeneration (Driscoll & Chalfie 1991; Xiong et al. 2004; García-Añoveros et al. 1995). This effect is thought to arise from enhanced cation influx through hyperactivated DEG/ENaCs, which induces cell swelling and eventual necrotic cell death (Driscoll & Chalfie 1991; Shreffler et al. 1995). Calcium plays a critical role in this process by activating cathepsin enzymes and calpain proteases; some DEG/ENaCs, such as MEC-4 and ASIC1a, are calcium permeable, while sodium influx through others can trigger calcium release from the ER to induce necrosis (Xu et al. 2001; Syntichaki et al. 2002).

In collaboration with the Bianchi lab at the University of Miami, we expressed a constitutively active form of the UNC-8 channel (UNC-8 G387E) in *Xenopus* oocytes. Initial experiments performed in physiological saline resulted in limited cation transport (1 μA/100mV, (Y. Wang et al. 2013)). Interestingly, addition of the calcium chelator EGTA

resulted in significantly larger current (10 μA/100mV), suggesting that the UNC-8 G387E channel is blocked by extracellular calcium. We confirmed that the UNC-8 G387E current is Amiloride and Benzamil-sensitive (**Chapter 4,** Y. Wang et al. 2013). Expression of UNC-8 G387E channels with low extracellular calcium was toxic *in vitro* and this toxicity was suppressed when the oocytes were treated with Amiloride (Y. Wang et al. 2013). These findings suggested that UNC-8 G387E encodes a hyperactive DEG/ENaC channel that induces cell death through channel activation. Additionally, we found that UNC-8 G387E is permeable to sodium ions, bot not calcium. These *in vitro* results gave us the tools to elucidate UNC-8 G387E channel properties, and we next sought to validate our findings *in vivo.*

In this chapter, we revisit the *unc-8 (n491)* allele, which encodes the constitutively active UNC-8 G387E sodium channel (Brenner 1974; E. C. Park & Horvitz 1986; Shreffler et al. 1995). Consistent with previous findings, we observed severe neuronal swelling and uncoordinated locomotion in *unc-8d* animals. Upon further analysis, we found that the DA and DB cholinergic neurons in the ventral nerve cord are likely responsible for the uncoordinated phenotype, because these cells swell in larval animals and around 35% of the neurons degenerate by adulthood. Additionally, we found that the neighboring GABAergic neurons that express *unc-8* were unaffected by the *unc-8d* mutation. GABAergic neuronal remodeling was only minimally affected in the *unc-8d* animals, and regulators of UNC-8d channel activity have no effect on synapse removal. These results support the prediction that wild-type UNC-8 channels and hyperactive UNC-8 G387E channels may function through unique mechanisms in different cell types.

Materials and Methods

Strains and Genetics

C. elegans strains were cultured at 20° C as previously described on standard nematode growth medium seeded with OP50 (Brenner 1974). The mutant alleles and strains used in this study are outlined in **Tables 6.1** and **6.2**.

Microscopy

Animals were immobilized on 2% agarose pads with 15mM levamisole as previously described (C. J. Smith et al. 2012). Images of L1 animals (**Figure 6.1**) were collected with a Zeiss Axioplan inverted microscope using ImageJ Micro-Manager software and a 100x oil objective (camera ORCA; Hammamatsu). L1 animals were synchronized by placing 100 gravid adult hermaphrodites onto plates and allowing them to lay eggs for one hour. The midpoint of the hour was considered T_0. After the hour all adults were removed and plates were incubated at 23° C. At 18 hours post-laying (T=18), L1 larval animals were imaged and analyzed. For L1 synapse counts (**Figure 6.6**), the number of dorsal and ventral synapses were counted for each animal and normalized to the number of GABAergic motor neurons in the ventral nerve cord. This normalization was performed to control for the overall developmental delay in the *unc-8d* animals. Images of young adults (**Figure 6.2**) were collected on a Leica SP5 confocal microscope using a 40x oil objective (1 um/step). Single-plane projections were generated with the Leica Application Suite Advanced Fluorescence software (LAS-AF). Insets of the ventral nerve cords in Figure 6.2 were generated with the ImageJ plug-in “straightened curved objects” (Kocsis 1991). Cholinergic DA/DB neurons and GABAergic DD/VD neurons were counted between DD1 and DD6 in young adult animals using the 63X objective on a

Zeiss Axioplan inverted microscope. Young adult synaptic counts (**Figures 6.7 and 6.8**) were performed using the same equipment, by noting the number of fluorescent puncta from VD3 to VD11. Some results were pooled from three separate experiments and the examiner was blinded to genotype.

Movement Assay

Wild-type, *unc-8d (n491),* and *unc-8d/+* animals in **Figure 6.1C** were assayed for previously described locomotion defects (E. C. Park & Horvitz 1986; Shreffler et al. 1995) by tapping individual animals on the head (S. C. Petersen et al. 2011). Four hermaphrodite adults from each genotype were placed on OP50 plates and allowed to lay eggs for 3-4 days. Young adult progeny were tapped on the head with a platinum wire pick. Animals were binned into three categories: “coordinated” (move backwards following head tap), “moderately uncoordinated” (attempt backward locomotion, but are unable to complete backward body bend), and “severely uncoordinated” (coil immediately upon head tap). For data presented in **Figures 6.1C** and 6.4C moderately and severely uncoordinated categories were combined into a singe “uncoordinated” category. Movement assays in **Figure A.4C** were performed as above, with the exception that four *unc-8d* and *unc-8d/+* hermaphrodite worms were placed on OP50 (control) or 500 µM EGTA plates.

EGTA Assay

Control and 500 uM EGTA plates were made as previously described (Earls et al. 2010). After autoclaving the agar, 19 milligrams of EGTA was added per 1 liter of Nematode Growth Media (NGM). Plates were poured, cooled, and seeded with OP50 as previously described (Earls et al. 2010). Adult hermaphrodite worms from each genotype were

added to plates 48 hours later. Young adult progeny were assayed for cell death and movement.

Stomatin Gene Expression

Expression profiles of stomatin genes in Figure 6.5A are from the open-access Wormviz database (http://www.vanderbilt.edu/wormdoc/wormmap/WormViz.html) (Spencer et al. 2011).

Table 6.1. Mutant alleles used in this study.

Allele	Source	Genotyping Primer Sequences
unc-8 (n491)	CGC	GCTACCCAACTTCCGTATGG
		TGCCGTATTCAGGATCAACG
sto-2 (tm1475)	NBRP	GACTGATGCAGCATCACGCA
		GGAGTAATCCACGTCGTCAG
sto-4 (tm1638)	NBRP	TATCGCCGGACACATACGCT
		GTGCGGCTTGCATTTGCATA
sto-6 (tm1610)	NBRP	GGTCGCTGGGTGCACTTGAA
		CATGGCAGACAACAACCGAT
cnb-1 (ok276)	CGC	CCATGGTTGACATAACACCAGGTCTA
		AGTGAGCCTGAGCCATCGACAT
ced-4 (n1162)	CGC	TCATCCACGACTTTGAACCA
		GCAAGCGTCACGAAATATCA
asic-1 (ok415)	Blakely Lab	GCCGTGCTCTAGCCGTAATACAG
		GCCCAGCTTCTGGCCATATGTA

Table 6.2. Strains used in this study.

Strain	Genotype
CZ1200	*juIs76 [punc-25::GFP; lin-15+] II*
MT1085	*unc-8 (n491) IV*
NC2782	*unc-8 (n491) IV; juIs76 II*
RP1	*trIs10 [pmyo-3::MB::YFP; pmyo-2::YFP; pceh-23::HcRed; punc-25::DsRed; punc-129::nsp::CFP] I*
NC2799	*unc-8 (n491) IV; trIs10 I*
NC2788	*sto-2 (tm1475) X*
NC2785	*sto-4 (tm1638) X*
NC2789	*sto-6 (tm1610) X*
NC2805	*sto-2 (tm1475) X; unc-8 (n491) IV; trIs10 I*
NC3187	*sto-4 (tm1638) X; unc-8 (n491) IV; trIs10 I*
NC2806	*sto-6 (tm1610) X; unc-8 (n491) IV; trIs10 I*
MP84	*mec-6 (lb84) dpy-5 (e61) I; unc-8 (n491) IV*
CZ333	*juIs1 [punc-25::GFP; lin-15+] IV*
NC1714	*unc-8 n491 juIs1 [punc-25::SNB-1::GFP; lin-15+] IV*
NC3072	*unc-8 n491 juIs1 IV; cnb-1 ok276 V*
NC3179	*ced-4 (n1162) III; unc-8 (n491) juIs1 IV*
NC2860	*unc-8 (n491) IV; wpIs36 [punc-47::mCherry] I; wyIs202 [pflp-13::mCherry::RAB-3] X*
NC2852	*unc-55 (e1170) I mec-6 (lb84) I*
NC1851	*unc-55 (e1170) I; juIs1 [punc-25::SNB-1::GFP] IV*
NC2878	*unc-55 (e1170) I mec-6 (lb84) I; juIs1 IV*
NC2723	*asic-1 (ok415) I; juIs1 IV*
NC2781	*asic-1 (ok415) unc-55 (e1170) I*
NC2780	*asic-1 (ok415) unc-55 (e1170) I; juIs1 IV*

Results

Constitutively active UNC-8 channels induce cholinergic cell death

Based on previous findings that constitutively active DEG/ENaC proteins induce neuronal death, we examined a *C. elegans* strain with an UNC-8 dominant mutation (Brenner 1974; E. C. Park & Horvitz 1986; Shreffler et al. 1995). The *unc-8d n491* mutation is a single nucleotide substitution that results in a glycine to glutamate substitution (G387E, **Figure 6.1A**). We confirmed previous reports that *unc-8d* L1

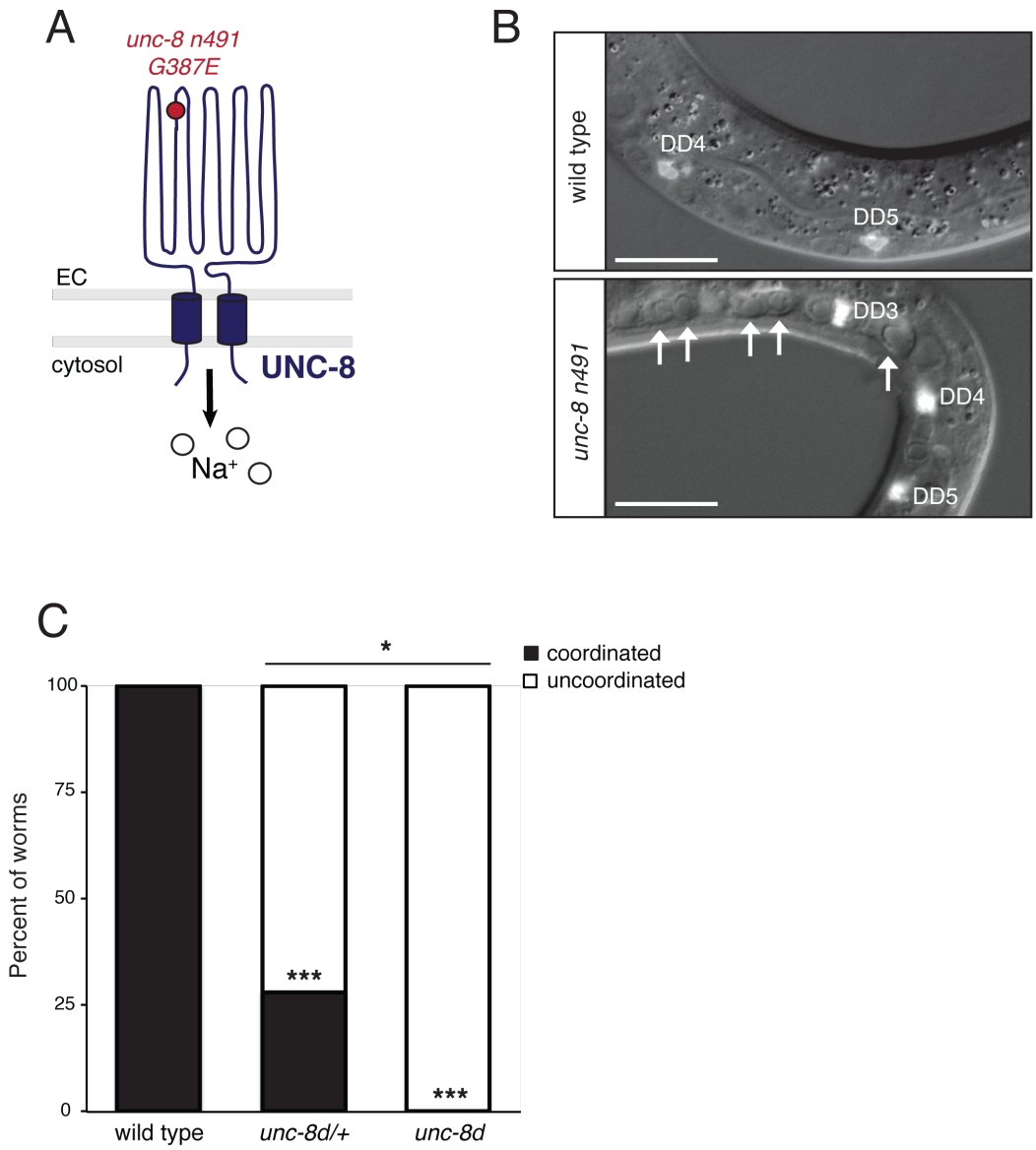

Figure 6.1: Constitutive activation of the DEG/ENaC protein UNC-8 induces cholinergic motor neuron swelling and uncoordinated locomotion. A. Schematic of the UNC-8 DEG/ENaC subunit. The *unc-8 (n491)* point mutation, G387E renders the channel constitutively active. EC is extracellular. **B.** Representative images of wild type (top) and *unc-8 (n491)* L1 animals. DD GABAergic motor neurons are fluorescently labeled with *punc-25::GFP* and are annotated in the figure. Swollen cholinergic motor neurons are present only in the *unc-8 (n491)* animals and are indicated by arrows. Scale bar is 5 um. **C.** Adult wild type, *unc-8 (n491/+)* and *unc-8 (n491)* animals were analyzed for movement defects (see **Methods**). Wild-type animals do not exhibit coiling behavior when tapped on the head with a platinum wire pick; however, a significant number of *unc-8 (n491/+)* and *unc-8 (n491)* animals coil (***p<0.001 compared to wild type, *p<0.05 *unc-8 (n491/+)* compared to *unc-8 (n491)*, Fisher's Exact Test, n= 10(wild type), 25 (*unc-8 (n491/+)*), 21(*unc-8 (n491)*).

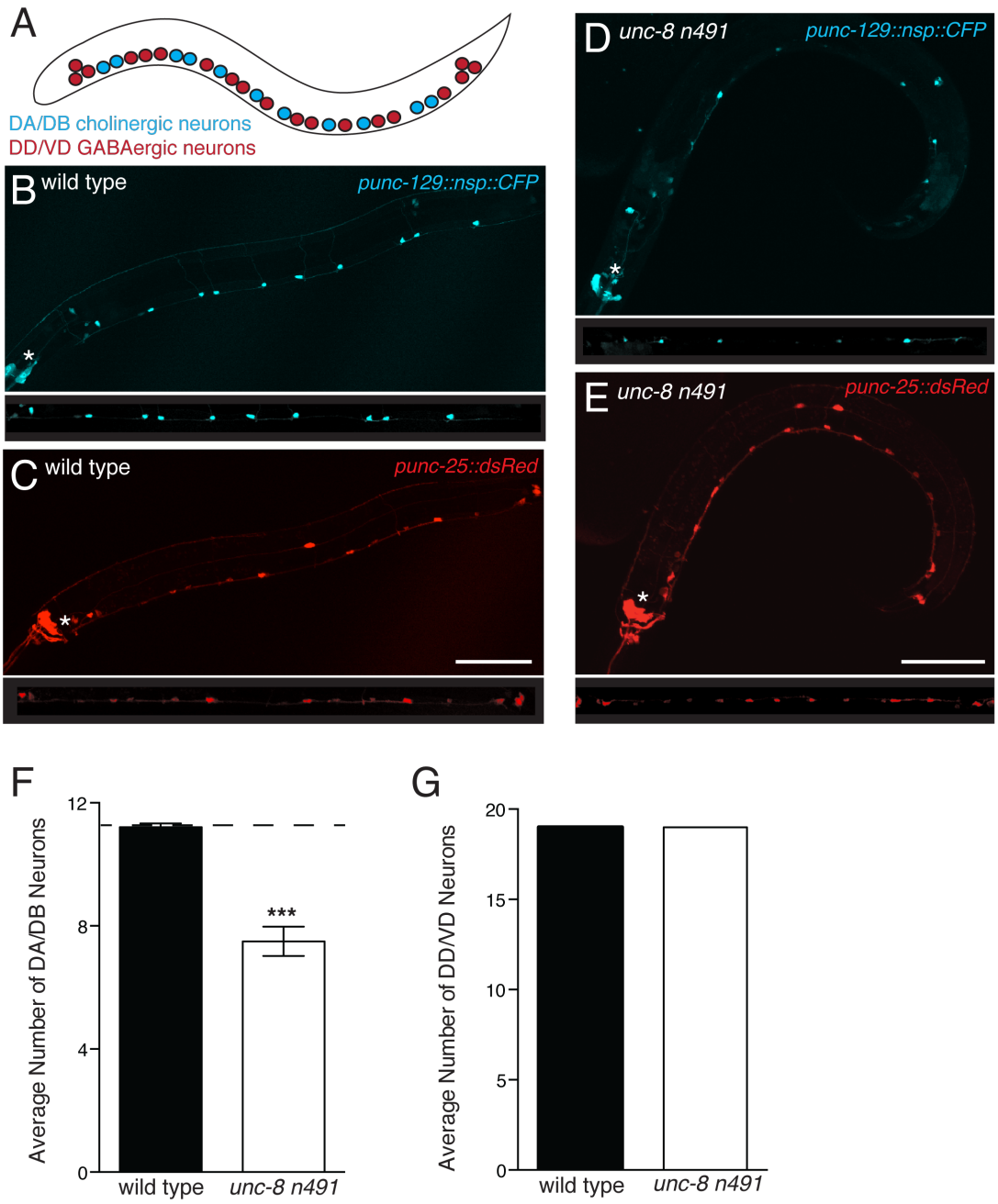

Figure 6.2: Chronic UNC-8 channel activation selectively degenerates cholinergic motor neurons. A. Schematic of the DA/DB cholinergic motor neurons (blue) and the DD/VD GABAergic motor neurons (red). DA/DB and DD/VD neurons were counted between DD1 and DD6. **B/C.** Representative images of a wild type animal expressing *punc-129::nsp::CFP* (cyan: DA/DB neurons) and *punc-25::dsRed* (red: DD/VD neurons). Insets below images show straightened ventral nerve cords. **D/E.** Representative images of DA/DB(cholinergic/cyan) and DD/VD (GABAergic/red) neurons in *unc-8 (n491)* animals. Insets below images show straightened ventral nerve cords, scale bars are 25 μm, asterisks annotate the head. **F/G.** Quantification of the number of DA/DB and DD/VD neurons for each genotype. *unc-8 (n491)* adult animals have a significant loss of

cholinergic DA/DB motor neurons, while GABAergic DD/VD neurons are unaffected (***p<0.001, Student's t-test, dotted line indicates wild type number of DA/DB neurons, n=24 (wild type),14 (*unc-8 n491*), data are mean ± SEM).

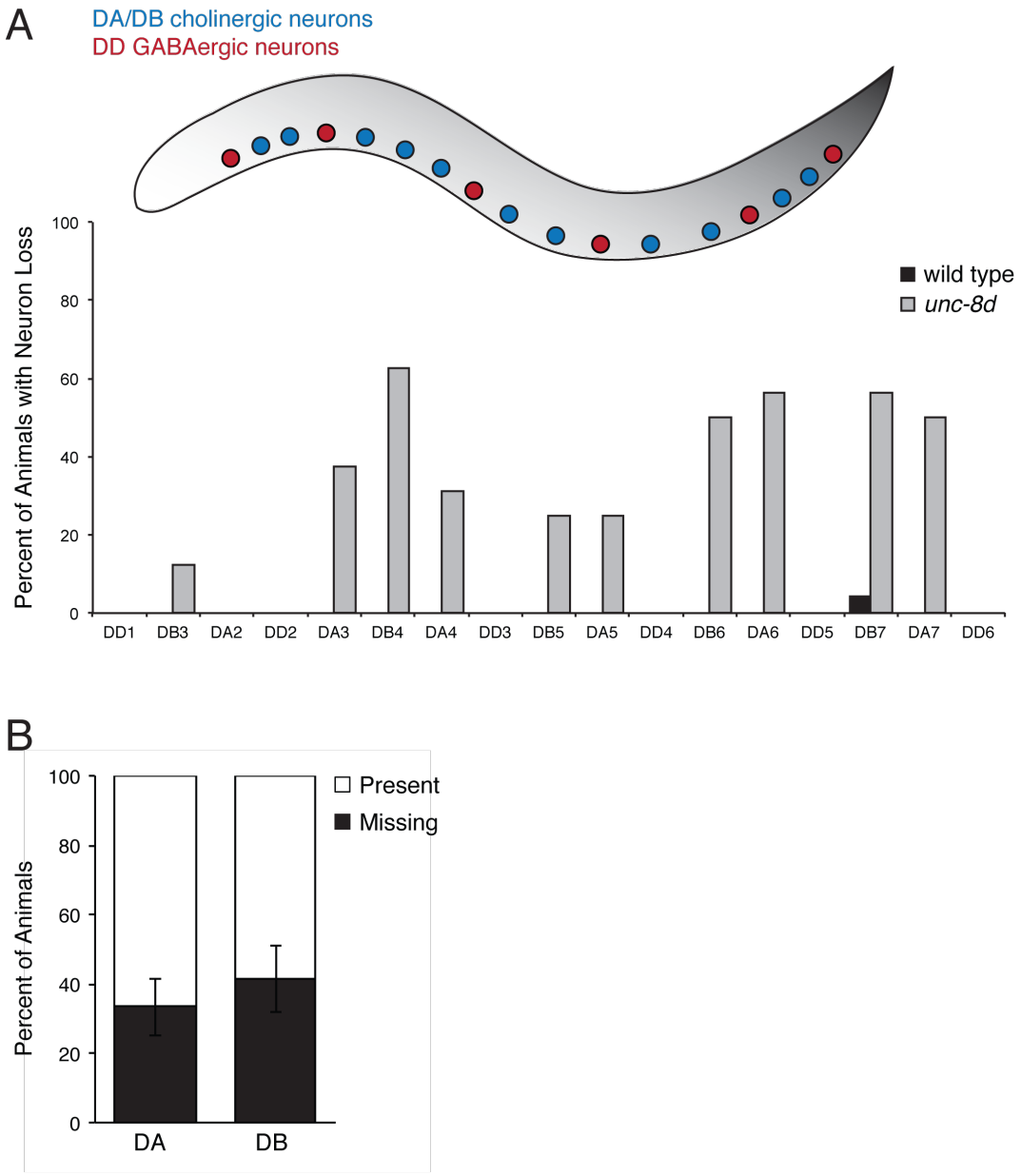

Figure 6.3: Loss of cholinergic motor neurons in *unc-8 n491* animals equally affects DA and DB cells. A. Schematic of DA/DB and DD neurons in *C elegans.* Loss of DA/DB (blue) and DD (red) neurons was quantified by analyzing the percent of animals missing each individual DA, DB, or DD cell in wild-type and *unc-8 (n491)* adult worms. Wild-type animals rarely exhibit loss of DA/DB or DD cells. *unc-8 (n491)* animals show a severe loss of all DA/DB neurons. **B.** Quantification of the percent of animals missing DA or DB neurons in the *unc-8 (n491)* mutants. Neuron loss in *unc-8 (n491)* mutants does not preferentially affect DA or DB neurons (no significant difference between DA and DB, p=0.35 Fisher's exact test, n= 10 animals, data are mean ± SEM).

animals have severe neuronal swelling visualized by light microscopy, while neighboring neurons appeared unaffected (**Figure 6.1B**). To determine the affected cells, we labeled GABAergic motor neurons with a genetically encoded fluorescent marker (*punc-25::GFP*). This strategy revealed that swelling was restricted to the cholinergic motor neurons; whereas, no GABAergic motor neurons were swollen. This result was surprising, as we had previously found that *unc-8* is expressed in cholinergic and GABAergic motor neurons. Additionally, we validated that adult animals exhibited highly uncoordinated movement; adult animals coil and fail to move backward (Shreffler et al. 1995). This effect is dependenton *unc-8d* gene dosage, as heterozygous *unc-8d* animals exhibit a partially uncoordinated phenotype compared to the severe uncoordination observed in the *unc-8d* homozygotes (**Figure 6.1C**).

We predicted that the adult *unc-8d* animals might show a loss of embryonic cholinergic motor neurons, consistent with the swelling visualized in young L1 larval animals that is correlated with a severe uncoordinated Unc-8 phenotype. We labeled DA/DB neurons with the cholinergic marker, *punc-129::nsp::CFP* and DD/VD GABAergic neurons with *punc-25::dsRed*. Consistent with our prediction, adult *unc-8d* animals showed significantly fewer DA/DB cholinergic neurons compared to wild-type controls, whereas, the normal DD/VD GABAergic cell number was unchanged (**Figure 6.2**).

To determine whether specific DA/DB cholinergic neurons are more sensitive to *unc-8d*-induced degeneration, we monitored the distribution of missing cells in the *unc-8d* animals. While wild-type animals rarely exhibit any missing cells, *unc-8d* animals are missing several DA and DB neurons along the length of the entire nerve cord, with no apparent bias (**Figure 6.3A**). We also determined there was no apparent bias for neuronal degeneration of DA versus DB cholinergic neurons. These results suggest that DA and DB motor neurons are equally likely to degenerate in *unc-8d* mutant animals and

their position along the ventral nerve cord is not correlated with degeneration (**Figure 6.3B**).

Reconstituted UNC-8 G387E channel is inhibited by extracellular calcium

As described in the **Introduction**, we expressed the constitutively active UNC-8 G387E channel in *Xenopus* oocytes and found that channel activity was blocked by extracellular calcium; UNC-8 G387E currents recorded in physiological solution were small; however, currents recorded in physiological solution containing the calcium chelating agent EGTA showed enhanced current traces (Y. Wang et al. 2013). Based on these results, we predicted that treatment of *unc-8d* animals with EGTA might enhance neurodegeneration in the DA/DB cholinergic cells. To test this hypothesis, we grew wild-type and *unc-8d* animals on plates containing EGTA. We quantified the number of DA/DB neurons and examined locomotion, but found no differences between animals grown on control or EGTA plates (**Figure 6.4**). Because we were unable to determine whether sufficient EGTA was able to penetrate the outer cuticle of the worm, these results are difficult to interpret. More work would be needed to examine the effects of *in vivo* calcium concentrations on neuronal degeneration in *C. elegans*.

Accessory proteins mediate DEG/ENaC protein function

Heterologous expression of UNC-8 G387E protein in oocytes yielded detectable current that was blocked by Amiloride, Benzamil, and extracellular calcium; however, expression of the wild-type UNC-8 protein resulted in no detectable current. Previous studies have found that DEG/ENaC function can require co-expression with accessory proteins. Examples include the MEC-4 channel that requires the stomatin-like protein

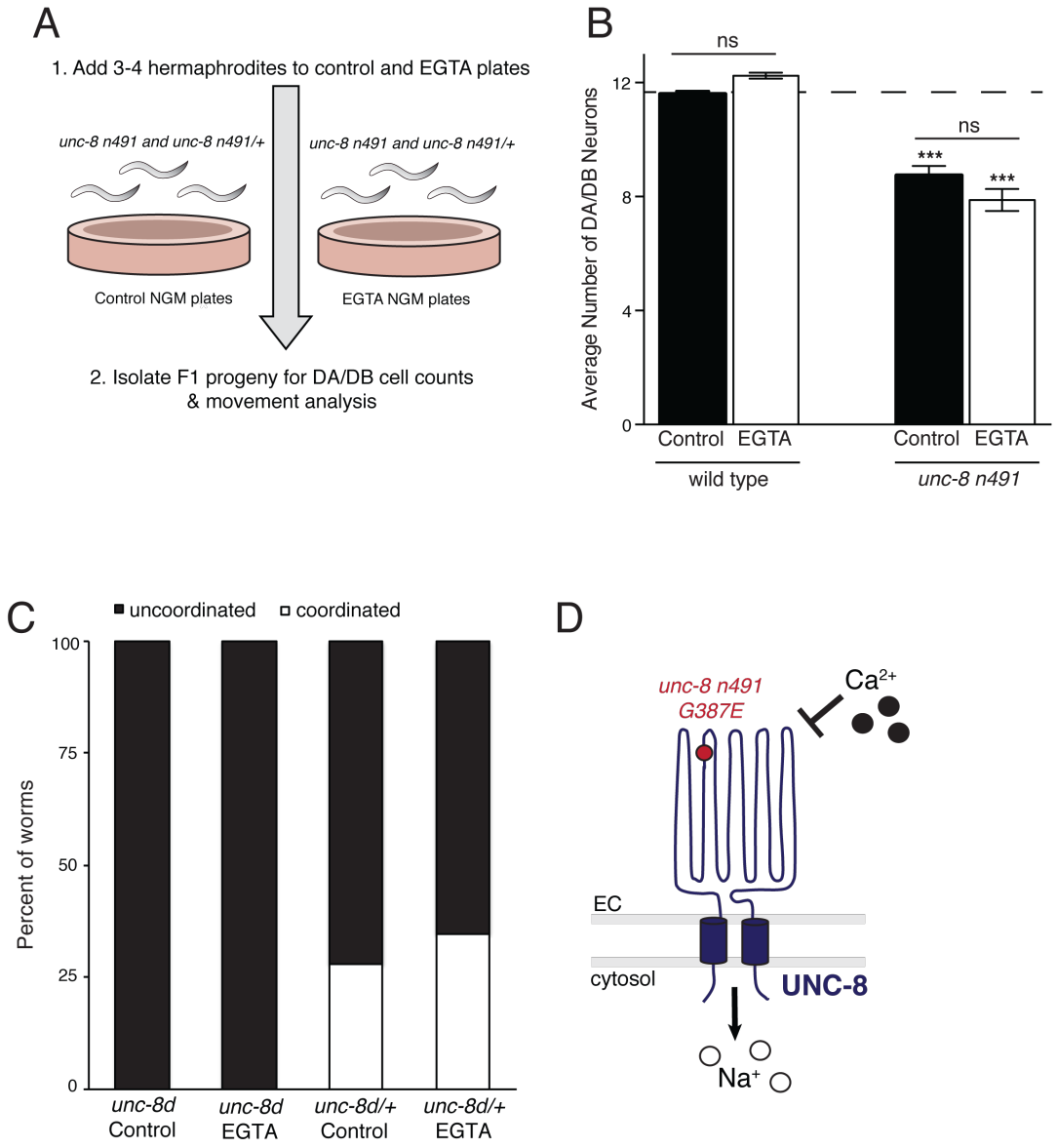

Figure 6.4: EGTA treatment does not affect UNC-8d-mediated cell death or movement defects. A. Schematic describing the treatment of wild-type, *unc-8 (n491/+)*, and *unc-8 (n491)* worms with 500 µM EGTA. **B.** Quantification of DA/DB cell number in wild-type and *unc-8 (n491)* worms on control or 500 µM EGTA plates. Treatment of worms with EGTA has no effect on DA/DB cell number (***$p < 0.001$, ns is not significant, One Way ANOVA with Bonferroni correction, $n \geq 23$ animals per genotype and condition, data are mean ± SEM, dotted line is number of wild-type DA/DB neurons between DD1 and DD6). **C.** Quantification of tapping assay for *unc-8 (n491/+)* and *unc-8 (n491)* mutants grown on control or 500 µM EGTA plates. Treatment with EGTA has no affect on locomotive behaviors in *unc-8 (n491/+)* or *unc-8 (n491)* mutants ($p > 0.05$, Fisher's Exact Test, $n \geq 21$ animals per genotype and condition). **D.** *In vitro* expression of UNC-8 G387E in *Xenopus* oocytes show that UNC-8 channel activity is strongly inhibited by extracellular calcium. EC is extracellular.

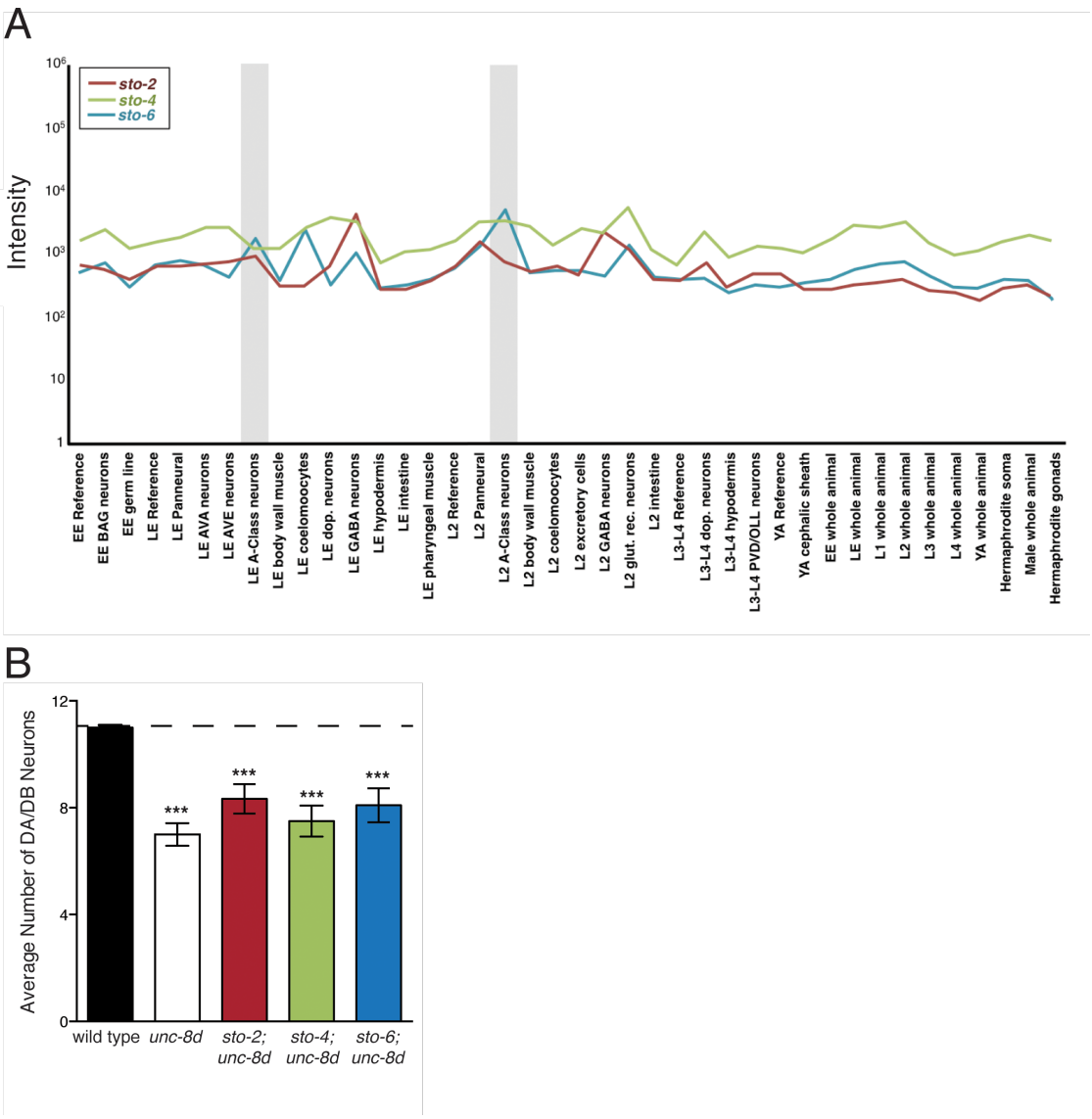

Figure 6.5: Stomatin proteins are not required for UNC-8d-mediated cell death. A. Expression data of stomatin genes (*sto-2*/red, *sto-4*/green, and *sto-6*/blue) from WormViz (reference). Stomatin gene expression in A-class motor neurons is highlighted in gray. Stomatin proteins are also enriched in several additional neuronal cell types. **B.** Quantification of DA/DB cell number. *unc-8 (n491)* animals show significantly fewer DA/DB motor neurons than wild-type (11 DA/DB cells between DD1 and DD6 in the ventral nerve cord), but DA/DB cells are notrestored in double mutants of *unc-8 (n491)* with *sto-2, sto-4,* or *sto-6.* (***$p < 0.001$, One Way ANOVA with Bonferroni correction, $n \geq 10$ animals per genotype, data are mean ± SD).

MEC-2 for proper function in *C. elegans*. Stomatin-like proteins are also required for ASIC channel function in mammals (Price et al. 2004; M. Huang et al. 1995). Therefore, we predicted that reconstitution of functional wild-type UNC-8 channels may require co-expression of accessory proteins in *Xenopus* oocytes. To identify potential UNC-8 accessory proteins, we utilized WormViz to identify genes enriched in A class cholinergic neurons, as these cells swell and degenerate in *unc-8d* animals (**Figure 6.1-6.3**) and are therefore likely to provide accessory proteins that promote UNC-8 function (see **Chapter 2**). WormViz is an open access online tool for accessing whole-genome profiles from specific *C. elegans* cells during distinct developmental stages (see **Methods,** (Spencer et al. 2011)). Using this approach identified three stomatin proteins; STO-2, STO-4, and STO-6, which are enriched in A-class cholinergic cells (**Figure 6.5A**). We predicted that loss of accessory proteins required for UNC-8 channel function in *unc-8d* animals, should suppress neurodegeneration in *unc-8d* cholinergic neurons. However, quantification of the double mutants of *unc-8d* with *sto-2, sto-4,* or *sto-6* did not detect significant rescue in comparison to *unc-8d* (**Figure 6.5B**). This result suggests that the stomatin proteins we evaluated do not regulate UNC-8 channel function; however, we cannot rule out the possibility that these channels function redundantly. This possibility could be tested by constructing the quadruple mutant *unc-8d; sto-2; sto-4; sto-6*.

The *unc-8* dominant gene has no effect on GABAergic synapse removal

Based on the findings that UNC-8 channel activity promotes synapse removal and that forced expression of *unc-8* is sufficient to drive synapse elimination in GABAergic neurons, we tested whether the constitutive activity of *unc-8d* is sufficient to accelerate DD remodeling. For this experiment, we used a fluorescent presynaptic marker to monitor the removal of ventral DD synapses and their formation on the dorsal

side in wild-type and *unc-8d* animals. We observed that *unc-8d* animals remove ventral DD puncta prematurely compared to wild-type, but this effect was limited to the earliest time point (6 hours **Figure 6.6**) and therefore may not be indicative an *unc-8d*-dependent effect for remodeling. Based on our findings that *unc-8d* does not induce GABA neuron swelling or induce precocious synaptic remodeling, we predict that the wild-type UNC-8 and UNC-8 G387E protein may be functioning differently in the GABAergic and cholinergic neurons.

Genetic screens to elucidate the mechanism of DEG/ENaC-induced neurodegeneration have detected additional proteins that mediate the process. *mec-6* encodes a paraoxonase that is required for MEC-4d channel expression in *C. elegans*. *mec-6* mutants suppress the uncoordinated coiling phenotype of *unc-8d* animals, suggesting that MEC-6 is also required for *unc-8d* function (Chelur et al. 2002). Based on our finding that wild-type UNC-8 channel activity drives synapse removal, we asked whether *mec-6* mutants are defective in synapse elimination. This experiment did not detect a delay in the removal of ventral GABAergic presynaptic puncta in *unc-55; mec-6* double mutants; however, this result is consistent with the idea that wild-type UNC-8 and UNC-8 G387E proteins diferentially regulated in GABAergic versus cholinergic ventral cord motor neurons (**Figure 6.7**).

ASIC proteins do not regulate synapse removal

Acid-sensing ion channels (ASICs) are members of the DEG/ENaC family of proteins and have been implicated in mammalian models of synaptic plasticity (Coryell et al. 2008; Kreple et al. 2014). We predicted that since the DEG/ENaC subunit UNC-8 promotes synapse removal, it is possible that another DEG/ENaC subunit ASIC-1 may

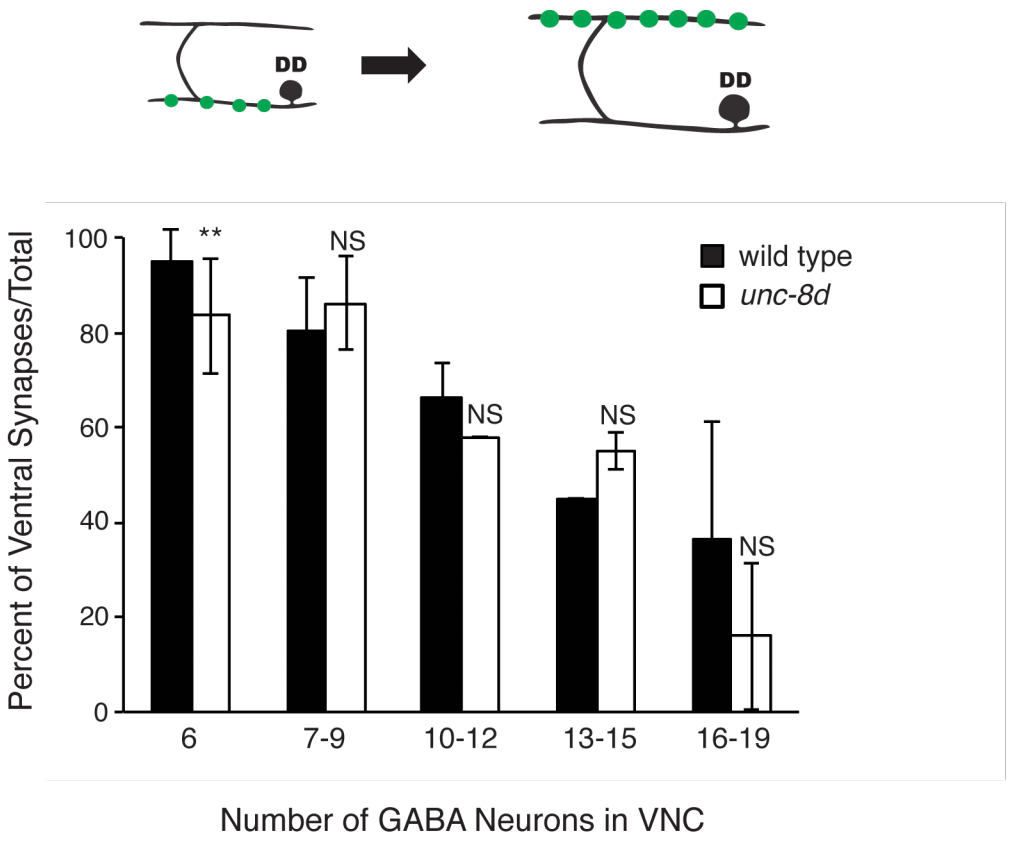

Figure 6.6: UNC-8d has minimal effects on the timing of GABAergic synapse removal. The timing of DD synapse remodeling was observed in wild type and *unc-8d n491* animals. Synchronized larvae were normalized by developmental age by counting the number of GABAergic neurons in ventral nerve cord. *unc-8d* animals show significantly fewer ventral synapses compared to wild type animals; however, these effects are only seen at the earliest developmental window (**p < 0.01, NS is not significant, Student's t-test, n= 55 wild type and 51 *unc-8d* animals, data are mean ± SEM).

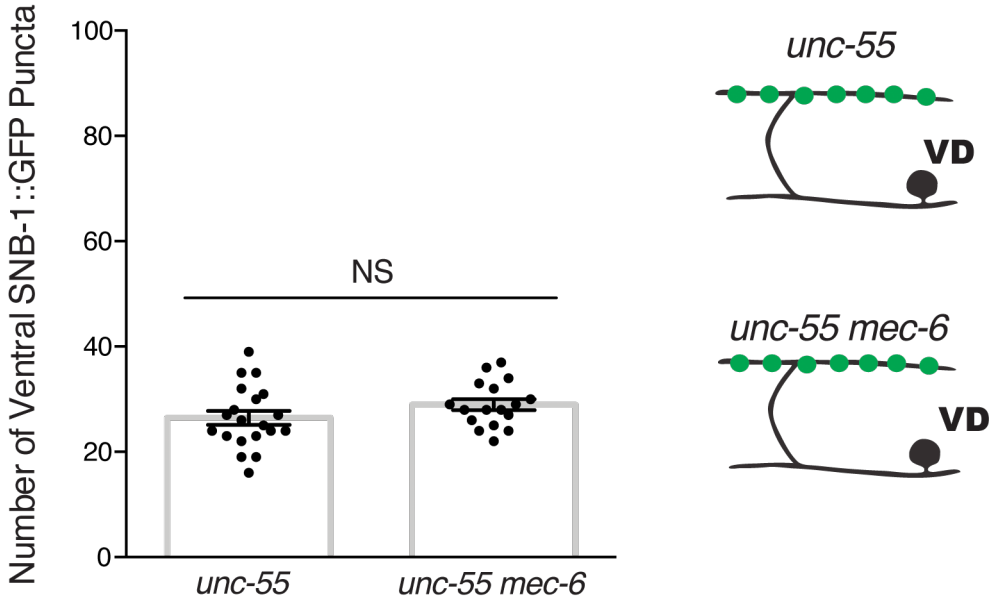

Figure 6.7: The UNC-8 channel accessory protein MEC-6 has no effect on GABAergic synapse removal. Loss of *mec-6 lb84* in *unc-55* animals has no effect on ventral GABAergic synapse removal (NS is not significant, Student's t-test, n ≥ 17, data are mean ± SEM).

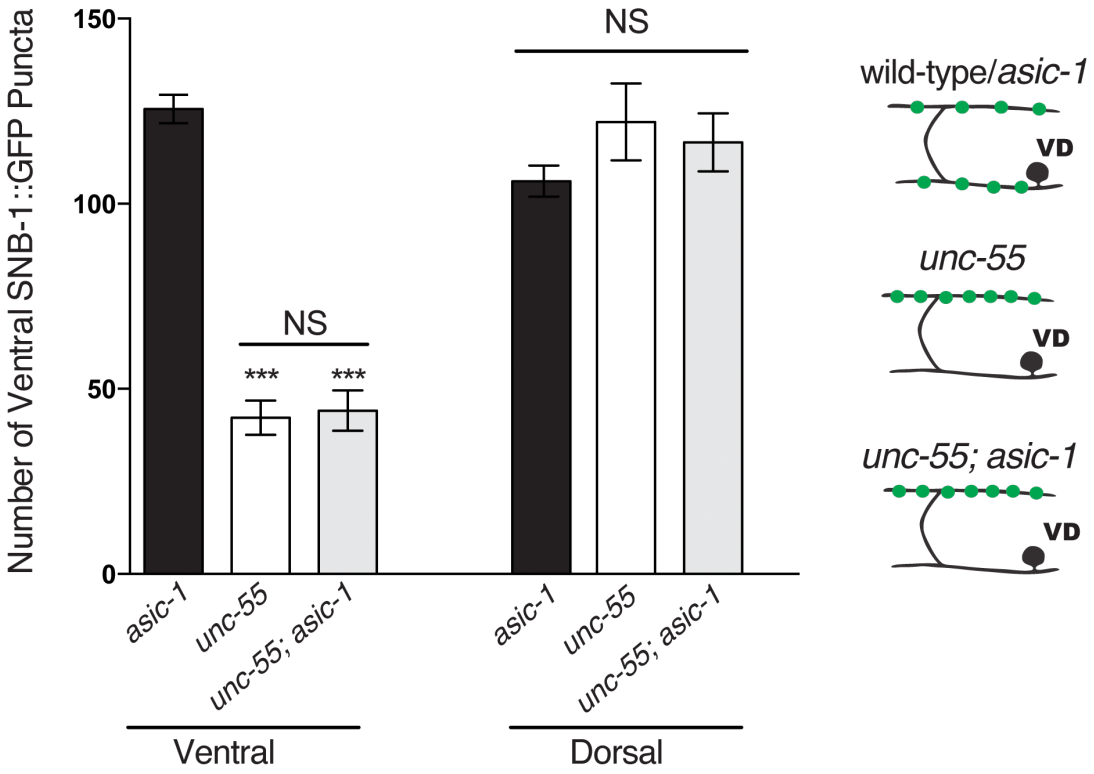

Figure 6.8: The DEG/ENaC family protein ASIC-1 has no effect on GABAergic synapse removal. The loss-of-function allele *asic-1 (ok415)* has no effect on ventral synapse removal or dorsal synapse formation in *unc-55* animals (***p< 0.001, NS is not significant, One Way ANOVA with Bonferroni correction, n ≥ 10, data are mean ± SEM).

also drive this process. To test this idea, dorsal and ventral GABAergic puncta were examined in *unc-55* and *unc-55 asic-1* animals. There was no detectable difference in presynaptic number, suggesting that ASIC-1 does not regulate synaptic remodeling (**Figure 6.8**). Importantly, *asic-1* is localized to the presynaptic regions of dopaminergic neurons in *C. elegans*, where it promotes dopaminergic signaling in an associative learning paradigm (Voglis & Tavernarakis 2008). This result suggests that although we saw no effect of *asic-1* in GABAergic plasticity, it is likely important for synaptic stability and neurotransmission in other classes of neurons.

Discussion

Neurodegeneration of specific neuronal subtypes

We show here that cholinergic motor neurons selectively degenerate in *unc-8d* animals, while neighboring GABAergic neurons are unaffected. This result was surprising, as we had previously shown that *unc-8* is expressed in both GABAergic DD neurons and cholinergic cells (**Chapter 2**). This finding parallels a hallmark of many neurodegenerative diseases, where a selective population of neurons die. Examples of this include Parkinson's Disease which causes neurodegeneration of the dopaminergic neurons in the substantia nigra and motor neuron-specific death in amyotrophic lateral sclerosis (ALS) (Bird et al. 1983; Obeso et al. 2008). The underlying mechanism of why some neurons are more vulnerable than others is not well understood, but there are some common characteristics that may shed light on this cell type-specific hypersensitization. Comparison of diseased and resistant neurons from specific brain areas found differences in mitochondrial function, oxidative stress, calcium signaling,

and energy production (Hedlund et al. 2010; C. Y. Chung et al. 2005; X. Wang & Michaelis 2010). While this work provides clues for this inherent cell vulnerability; the relationship is correlational and the mechanisms driving these cellular changes in some cells and not others is unclear.

UNC-8 channels have distinct roles in different cell types

In the previous chapters, we established a role for the UNC-8 channel in promoting synapse removal in GABAergic neurons. Here, we find an additional role for the constitutively active UNC-8 G387E channel for inducing neurodegeneration in cholinergic neurons. These findings suggest that the wild-type and dominant forms of the UNC-8 channel regulate distinct processes in different cells. In support of this idea, the dominant UNC-8 channel does not appear to accelerate GABA synapse remodeling, although *unc-8* is clearly expressed in these cells. Based on the findings that DEG/ENaC proteins can form either homotrimers or heterotrimers, we can postulate that UNC-8 may be assembling with different channel subunits and accessory proteins in a cell-specific manner that results in divergent roles for GABAergic and cholinergic motor neurons (Askwith et al. 2004; Chelur et al. 2002; Lingueglia 2007; M. B. Goodman et al. 2002). To test this idea, we examined whether loss-of-function mutations in three different stomatin proteins could suppress *unc-8d*-mediated cholinergic neuronal degeneration. However, we were unable to detect significant differences in these double mutants compared to *unc-8d* animals. Additionally, we considered the possibility that *unc-8* may be forming a heteromeric channel with the DEG/ENaC subunit *asic-1*; however, loss of *asic-1* has no effect on *unc-8d* neurotoxicity (data not shown) and *asic-1* has no detectable role in GABAergic neuron removal (**Figure 6.8**). Therefore, we expect that

UNC-8 channels in cholinergic and GABAergic neurons may be regulated by different subsets of accessory proteins and DEG/ENaC subunits.

DEG/ENaC-mediated sodium influx may contribute to necrotic cell death

Hyperactive DEG/ENaC-mediated neurotoxicity has been contributed to calcium influx through these channels, which activates calpains and cathepsins to mediate necrotic cell death (Xu et al. 2001; Syntichaki et al. 2002). While MEC-4 and ASIC1a channels mediate calcium influx, some DEG/ENaCs, including UNC-8, are calcium impermeable, raising the possibility that these channels may promote neurotoxic effects that do not arise from direct gating of calcium (Y. Wang et al. 2013). In support of this idea, cellular swelling and apoptotic death have been observed to result from sodium ion influx (Banasiak et al. 2004; Hains et al. 2004; Sheldon et al. 2004). Additionally, we found that the UNC-8 G387E preferentially gates sodium and UNC-8-mediated neurotoxicity was blocked by inhibiting channel activity (Y. Wang et al. 2013). In collaboration with the Bianchi lab, we have further investigated the effects of calcium permeability and sodium influx on neurotoxicity. Expression of UNC-8 G387E channels in the absence of extracellular sodium rescued the neurotoxicity observed in EGTA-treated oocytes (Matthewman et al. 2016). Interestingly, similar results were found for the MEC-4d protein and for UNC-8d/MEC-4d chimeric channel, both of which show calcium permeability. These results indicate that either calcium or sodium influx can contribute to cell death in different DEG/ENaCs. Calcium mediates neurotoxicity in MEC-4d-expressing cells; whereas, sodium influx through UNC-8d channels can also promote cell death (Matthewman et al. 2016).

Author Contributions

All images and analyses in this chapter were performed by Tyne Miller-Fleming. Patrick M. Meyers constructed the *unc-55 mec-6* recombinant strain in **Figure 6.7** under the mentorship of Tyne Miller-Fleming and David M. Miller. Under the guidance of Laura Bianchi, Ying Wang and Cristina Matthewman performed the all of the *Xenopus* oocyte experiments described in this chapter.

Acknowledgments

The *asic-1 ok415* mutant strain was a gift from Andrew Hardaway in the laboratory of Randy Blakely. Some strains used in this study were provided by the CGC, which is funded by the NIH Office of Research Infrastructure Programs (P40 OD010440). This work was supported by NIH grants RO1NS26115 and R21MH077302 (DMM) and the Vanderbilt Silvio O. Conte Center grant MH078078 (TMF). The images and data in **Figures 6.1**, **6.2**, and **6.3** were adapted from previous publications (Matthewman et al. 2016; Y. Wang et al. 2013).

CHAPTER VII

GABAERGIC SIGNALING DRIVES SYNAPTIC REMODELING

Summary

GABAergic signaling drives circuit pruning in several regions of the nervous system of vertebrate and invertebrate species. One classic example of GABA-mediated pruning occurs in the mammalian visual system during the acquisition of binocular vision. Initially, neural connections from both eyes innervate overlapping regions in the lateral geniculate nucleus and visual cortex. Binocular stimulation, or light exposure to both eyes, results in activity-dependent pruning of the neural connections into distinct compartments within the brain. This period of synaptic plasticity is controlled by GABA signaling; depletion of GABA synthesis blocks the onset of the visual system critical period and treatment with the GABA receptor agonist, benzodiazepine, rescues this effect (Hensch et al. 1998). In another example of GABA-mediated plasticity in mammals, dendritic $GABA_A$ receptors mediate pruning in the hippocampus (Afroz et al. 2016). Interestingly, this effect is limited to female mice and is initiated at the onset of puberty, providing an additional example of GABA-mediated refinement of neural circuitry that is confined to a specific developmental period and sex. Additional evidence from mouse interneurons reveals that reduction of GABA release results in smaller, immature synapses; however, complete genetic ablation of GABA synthesis leads to overgrown axons and defects in synapse elimination. Thus, this study identifies multiple roles for GABA signaling, including in the maturation of GABAergic synapses, as well as the efficient pruning of redundant synaptic connections (Wu et al. 2012).

GABA signaling has also been implicated in the refinement of neural circuitry in invertebrate species, suggesting that these mechanisms are likely conserved. For example, in *Drosophila* GABAergic signaling has been shown to shape the visual and olfactory systems, and GABAergic signaling is dysfunctional in *Drosophila* models of Fragile X syndrome (Sugie et al. 2015; Wilson & Treisman 1988; Gatto et al. 2014). Because the molecular pathways that mediate neurotransmission are highly conserved in *C. elegans*, we can utilize these organisms as model systems to identify fundamental regulators of synaptic plasticity. The DD/VD GABAergic motor neurons in *C elegans* innervate muscles and receive input from cholinergic motor neurons. These GABAergic neurons undergo a synaptic remodeling event in which ventral DD presynaptic compartments are removed and relocated to more distal regions located in dorsal segments of each DD neuron. Using powerful genetic and optogenetic tools for *C. elegans*, we examined the role of neuronal activity during synapse removal and formation.

These studies have revealed that GABAergic neurotransmission promotes synaptic remodeling; genetic mutations that impair GABA synthesis, packaging or release impede GABAergic synapse removal. An important role for GABA receptor function is suggested by the finding that mutations in the metabotropic $GABA_B$ receptors GBB-1 and GBB-2 also perturb the removal of presynaptic components in remodeling GABAergic neurons. Surprisingly, mutations that disable the ionopropic GABAA receptor UNC-49, result in the opposite effect of enhancing *unc-55* synapse remodeling. Together, these results suggest that GABA-dependent regulation of synaptic remodeling is likely complex and may be modulated by the opposing roles of separate classes of GABA receptors. Additionally, we confirmed our genetic findings by utilizing optogenetic tools to activate cells of the *C. elegans* motor circuit. Collectively, our findings suggest

that GABA signaling is required for synaptic removal in a complex network that is regulated by both GABAergic and cholinergic neurons, in addition to postsynaptic muscle cells.

Materials and Methods

Strains and Genetics

C. elegans strains were cultured at 20° C as previously described on standard nematode growth medium seeded with OP50 (Brenner 1974). The mutant alleles and strains used in this study are outlined in **Tables 7.1** and **7.2**.

Microscopy

Animals were immobilized on 2% agarose pads with 15mM levamisole as previously described (C. J. Smith et al. 2012). Images and timecourse analysis of L1 animals (**Figures 7.2**, **7.3, 7.8,** and **7.9**) were collected with a Zeiss Axioplan inverted microscope using ImageJ Micro-Manager software and a 63x oil objective (camera ORCA; Hammamatsu). L1 animals were synchronized by placing 100 gravid adult hermaphrodites onto plates and allowing them to lay eggs for one hour. The midpoint of the hour was considered T_0. After the hour all adults were removed and plates were incubated at 23° C unless stated otherwise. At 18 hours post-laying (T=18), L1 larval animals were imaged and analyzed. Images of young adults (**Figure 7.7**) were collected on a Zeiss Axioplan inverted microscope using a 63x oil objective. Fluorescently-labeled synapses from GABAergic DD/VD neurons were counted between DD1 and DD6 in L1

animals or VD3 to VD11 in young adult animals using the 63X objective on a Zeiss Axioplan inverted microscope. The examiner was blinded to genotype.

Pharmacology

Pregnenolone sulfate sodium salt (PS, Sigma, #P162) stock solution was prepared in ethanol (2 mg/ml) and stored at 4°C. A final concentration of 1 mM (high PS) and 100 μM (low PS) diluted in OP50 bacteria was seeded on NGM plates. Control NGM plates contained the same volume of ethanol added to OP50. Plates were stored at 4°C for up to one week. Five adult hermaphrodites were placed on either high PS, low PS, or control plates at room temperature and progeny examined at the young adult stage (**Figure 7.5**). The number of ventral puncta was counted using a Zeiss Axiovert microscope (63X oil objective). The examiner was blinded to genotype and treatment condition.

Optogenetics

A 100 mM stock of all-*trans* retinal (ATR, Sigma, #R2500) was dissolved in ethanol and stored at -20°C. 300 µM of ATR or ethanol (control) was added to OP50 bacteria and seeded onto NGM plates. Plates were protected from light and were stored at 4°C for up to one week. 100 adult hermaphrodites laid eggs on ATR or control plates for 1 hour and were then removed. The midpoint of this hour is considered T_0. Plates were exposed to 470-nm LED light pulses (#M470L2, Thor Labs, Newton, NJ) for 13 to 15 hours as indicated (0.5 Hz, 2 mW/mm2 measured with Solartech Inc. Solar Meter 9.4 radiometer). Light stimulation was controlled using NI Max software through TTL signals generated by a digital function generator (National Instruments, Austin, TX). 13 or 15 hours after

egg laying, animals were assayed for DD remodeling by counting the number of dorsal or ventral presynaptic SNB-1::GFP puncta. The examiner was blinded to the treatment.

Feeding RNA Interference Experiments

Knockdown by feeding RNAi in **Figure 7.6** was performed as previously described (S. C. Petersen et al. 2011). Bacteria producing either double-stranded RNA or containing the RNAi empty vector (EV) were seeded on NGM plates and stored at 4°C for up to 1 week. Four L4 animals were grown on each single RNAi plate at 23°C until progeny reached the L4 stage, or about 3-4 days. Progeny were picked to fresh RNAi plates and imaged at the young adult stage.

Table 7.1. Mutant alleles and genotyping primers used in this study.

Allele	Source	Genotyping Primer Sequences
snf-11 ok156 V	CGC	GATCCCCAAGATTTGCCTAC
		TTGATTTCAATGTCGGGTCG
gbb-1 tm1466 X	NBRP	TCACTATCCTCATCGGGGCA
		GGCCCTTTTCAGCTTAGCCT
gbb-2 tm1165 IV	NBRP	AGGACTCCTTTGACTGCATA
		GCCGGCGATGTCTGGAATGA
unc-47 e307 III	CGC	GCAGAGTTGATTGCTCTGAG
		TGTTTTCGGCTACACATCTC
unc-49 e407 III	CGC	GGAACATGACCAAGGTTAGG
		TACTGTAGCCGTCTGAAAGC
unc-55 e1170 I	CGC	TAAGGACTACACGGATCCTG
		CCCAAGAAGAAAAGAGAGGT
unc-8 tm5052 IV	NBRP	TGGGGCCCTAATAATTTCGA
		CCTGGCTTCATACTGTCACT
eri-1 mg366 IV	CGC	CATGCAATTTCAATGCCTTTTA
		TGCATCATCCAATCCACTATGT
tom-1 ok2437 I	CGC	CGATTTCAAAGTCTGATGGT
		CGCTGTGTGTAATTTTTCAA
lgc-35 tm1444 II	E. Jorgensen lab, Utah	CTAGCTTGCCGTCTGCAATA
		ATAGGGGAGAAGAGACGCAG

Table 7.2. Strains used in this study.

Strain	Genotype
CZ333	*juIs1 [punc-25::SNB-1::GFP; lin-15+] IV*
CB1170	*unc-55 (e1170) I*
NC1851	*unc-55 (e1170); juIs1 IV*
CB156	*unc-25 (e156) III*
NC2839	*unc-55 (e1170) I ; unc-25 (e156) III ; juIs1 IV*
CB307	*unc-47(e307) III*
NC2584	*unc-47 (e307) III; juIs1 IV*
NC2641	*unc-55 (e1170) I ; unc-47 (e307) III; juIs1 IV*
FX05052	*unc-8 (tm5052) IV*
NC2387	*unc-8 (tm5052) juIs1 IV*
NC2388	*unc-55 (e1170) I; unc-8 (tm5052) juIs1 IV*
NC2837	*unc-55 (e1170) I ; unc-8 (tm5052) juIs1 IV ; unc-47 (e307) III*
NC2585	*wyIs202 [pflp-13::gfp::rab-3, pflp-13::mcherry; podr-1::dsRed] X*
NC2713	*unc-47 (e307) III; wyIs202 X*
NC2859	*unc-47 (e307) III; punc-47::mCherry I; wyIs202 X*
CB407	*unc-49 (e407) III*
NC2682	*unc-49 (e407) III; juIs1 (IV)*
NC2722	*unc-49 (e407) III; unc-55 (e1170) I; juIs1 IV*
NC2892	*gbb-1 (tm1466) X*
NC3050	*gbb-1(tm1466) X; unc-49 (e407) III; unc-55 (e1170) I; juIs1 IV*
EG4787	*lgc-35 (tm1444) II*
NC3023	*lgc-35 (tm1444) II; juIs1 IV*
NC3024	*unc-55 (e1170) I; lgc-35 (tm1444) II; juIs1 IV*
KP5348	*nuIs279 [punc-25::UNC-57::GFP; punc-25::mCherry::RAB-3]*
NC2984	*unc-55 (e1170) I; nuIs279*
NC2905	*gbb-2 (tm1165) IV*
NC2890	*gbb-2 (tm1165) IV; nuIs279*
NC2871	*unc-55 (e1170) I; gbb-2 (tm1165) IV; nuIs279*
NC1852	*unc-55 (e1170) I; eri-1 (mg366) juIs1 IV*
RM2710	*snf-11 (ok156) V*
NC2901	*snf-11 (ok156) V; juIs1 IV*
NC2891	*unc-55 (e1170) I; snf-11 (ok156) V; juIs1 IV*
EG5025	*oxIs351 [punc-47:ChR2::mCherry; lin-15+] X*
NC2893	*oxIs351 X; juIs1 IV*
CZ2060	*juIs137 [pflp-13::SNB-1::GFP] II*
NC3084	*oxIs351 X; juIs137 II*
NC3054	*unc-25 (e156) III; juIs1 IV; oxIs351 X*
EG5027	*oxIs353 [myo-3p::channelrhodopsin::mCherry + lin-15(+)] V*
NC3142	*oxIs353 V; juIs137 II*
NC3051	*ufIs53 [punc-17::ChR2::mCherry; pelt-2::GFP]; juIs1 IV*
CB113	*unc-17(e113) IV*
NC2985	*unc-17 (e113) IV; nuIs279*
NC2902	*unc-55 (e1170) I ; unc-17 (e113) IV; nuIs279*
RB1887	*tom-1 (ok2437) I*
NC2616	*tom-1(ok2437) I; juIs1 IV*
NC2787	*tom-1 (ok2437) I; unc-47 (e307) III; juIs1 IV*

Results

The GABAergic signaling pathway is highly conserved from invertebrate to vertebrate species (**Figure 7.1**). The glutamic acid decarboxylase (GAD) homolog, UNC-25 synthesizes GABA from glutamate. GABA is then packaged into synaptic vesicles via the vesicular GABA transporter, VGAT/UNC-47 for release. Extracellular GABA activates the ionotropic inhibitory $GABA_A$ receptor UNC-49 on postsynaptic muscle cells, or the excitatory ionotropic $GABA_A$ receptors EXP-1 and LGC-35, at the synaptic region or perisynaptically (Bamber et al. 1999; Bamber et al. 2005; Jobson et al. 2015; Beg & Jorgensen 2003). Additionally, GABA can activate the metabotropic $GABA_B$ receptor dimer GBB-1/GBB-2, which inhibits signaling from nearby cholinergic motor neurons (Dittman & Kaplan 2008). *C. elegans* also encode a GABA transporter, GAT/SNF-11 that has been shown to be expressed on postsynaptic muscle cells and some neurons (Schultheis et al. 2011; Gendrel et al. 2016). Based on our findings that DD GABAergic synapse removal is activity-dependent, we sought to delineate the source of activity that drives this process.

GABA release and synthesis promote synapse removal

To determine whether GABA release is required for DD synaptic remodeling, we examined the timing of dorsal synapse formation with a DD-specific presynaptic marker, DD::SNB-1::GFP. In comparison to wild-type, animals containing a loss-of-function mutation in the vesicular GABA transporter VGAT/*unc-47* exhibited a significantly fewer DD::SNB-1::GFP puncta during intermediate periods of the remodeling program in L1 larvae. This effect was not detectable in late L1 larvae at the end of remodeling (16-18 cell stage); *unc-47* mutants eventually catch up with the wild-type controls (**Figure 7.2**).

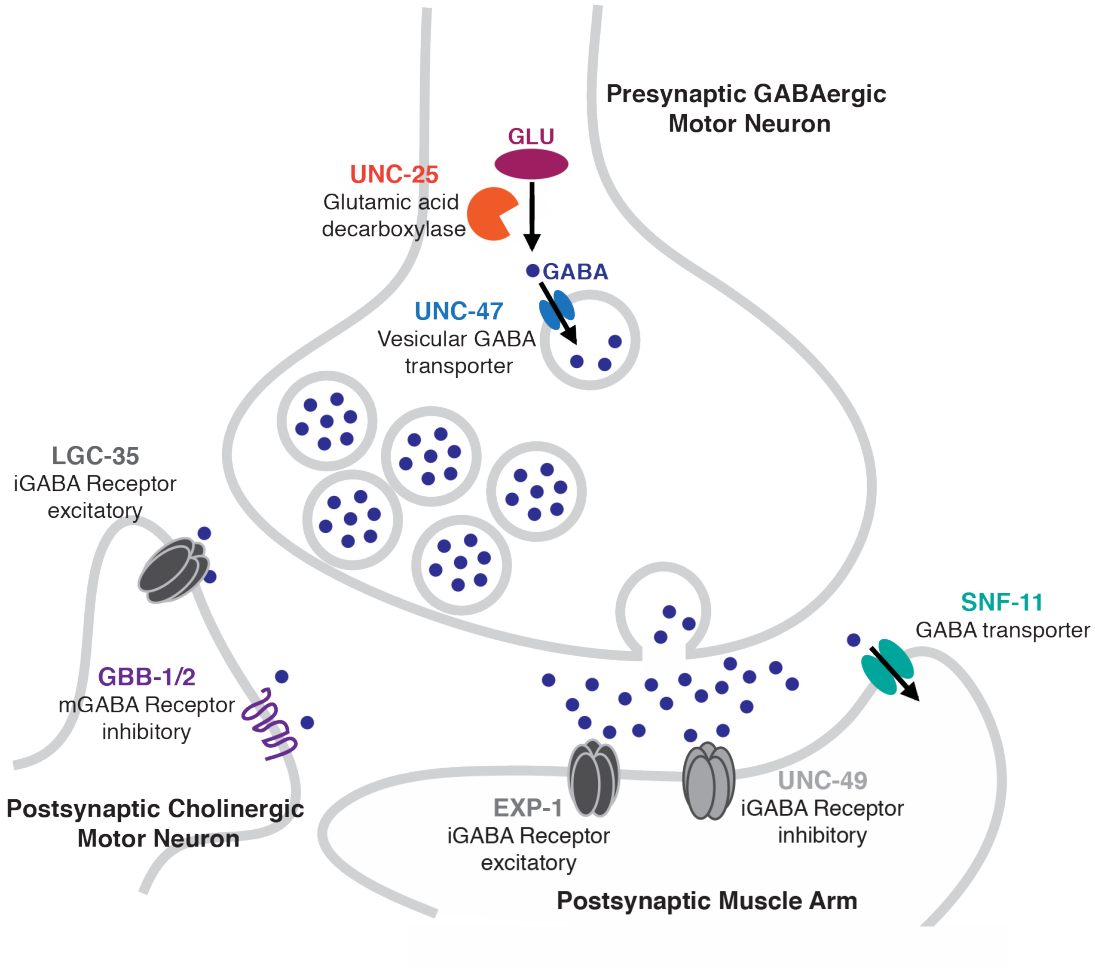

Figure 7.1: GABAergic neurotransmission pathways are conserved in *C. elegans.* Schematic depicting the GABAergic neurotransmission pathway, including the proteins required to synthesize (UNC-25) and package (UNC-47) GABA for release into the synaptic cleft. Additionally, multiple ionotropic (UNC-49, EXP-1, LGC-35) and metabotropic GABA receptors (GBB-1/GBB-2) are known to mediate GABA signaling. GABA can also be recycled from the extracellular space by the GABA transporter, SNF-11.

Previous work in *C. elegans* found that loss-of-function mutations in *tom-1,* a gene that normally antagonizes neurotransmitter release, results in premature formation of dorsal DD synapses. We asked whether this effect is GABA-dependent. Examination of the *tom-1; unc-47* double mutants revealed strong suppression of the *tom-1* precocious phenotype at the latest time point observed (10-12 cell stage, **Figure 7.3**), but not at earlier stages. These results suggest that GABA release may not be required in the initial period of dorsal synapse assembly, but is necessary for achieving the full complement of dorsally located DD presynaptic domains. As an additional test, we examined whether GABA release also regulates the removal of ventral DD synapses. We found that ventral DD synapse removal is significantly delayed for the first half of remodeling (6, 7-9, and 10-12 cell stages); however, towards the end of remodeling, the *unc-47* mutants become indistinguishable from wild type (**Figure 7.2**).

Results from **Chapter 3** indicated that both DD and VD synapses are removed in *unc-55* animals and this effect can be visualized later in development at the young adult stage (S. C. Petersen et al. 2011). We examined ventral synapse removal in *unc-55; unc-47* double mutants and found a significant deficit in the elimination of ventral SNB-1::GFP. Interestingly, this effect was also found with mutations in the GABA biosynthetic enzyme, *unc-25*; loss of *unc-25* in *unc-55* animals also exhibited the failure to remove ventral synapses (**Figure 7.4**). These effects were much more penetrant than those observed in remodeling DD cells; furthermore, this result correlates with a previous study showing that ablation of GABA signaling mediates synapse maintenance and pruning, but has no effect on synapse formation (Thompson-Peer et al. 2012; Wu et al. 2012; Jin et al. 1999). We concluded that GABA synthesis and release are required for the proper removal of ventral GABAergic synapses; however, whether there is a transient role for GABA in dorsal DD synapse formation is unclear. To further delineate the role of

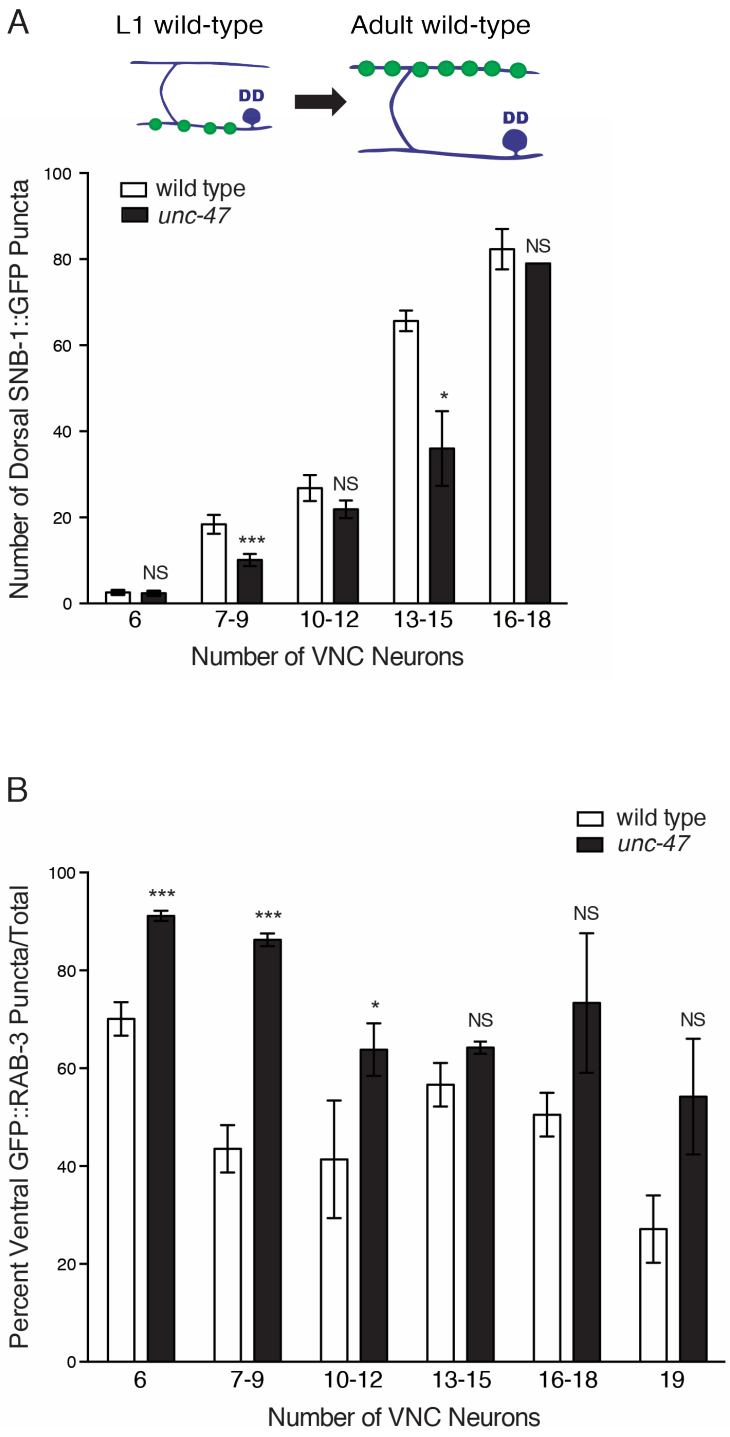

Figure 7.2: GABA release promotes GABAergic synapse elimination in remodeling DD neurons. A. Loss of the vesicular GABA transporter UNC-47 delays dorsal DD synapse formation (measured by counting the number of dorsal GABA::SNB-1::GFP puncta between DD1 and DD6); however this effect is not significant at all time points examined. Student's t-test performed for wild type versus *unc-47* at each time point (N= 57 wild type and N= 172 *unc-47* animals). **B.** Removal of ventral DD::GFP::RAB-3

puncta is significantly delayed in *unc-47* animals. *unc-47* mutants exhibit delayed synapse removal during early time points; however, this effect is lost at later time points and the *unc-47* mutants recover to wild type levels. Student's t-test performed for wild type versus *unc-47* at each time point (N= 229 wild type and N=170 *unc-47* animals). For A-B, puncta number are normalized to the number of VD neurons in the ventral nerve cord to control for the overall developmental delay in *unc-47* animals. All data are represented at mean ± SEM. NS is not significant, $*p < 0.05$, $**p < 0.01$, $***p < 0.001$.

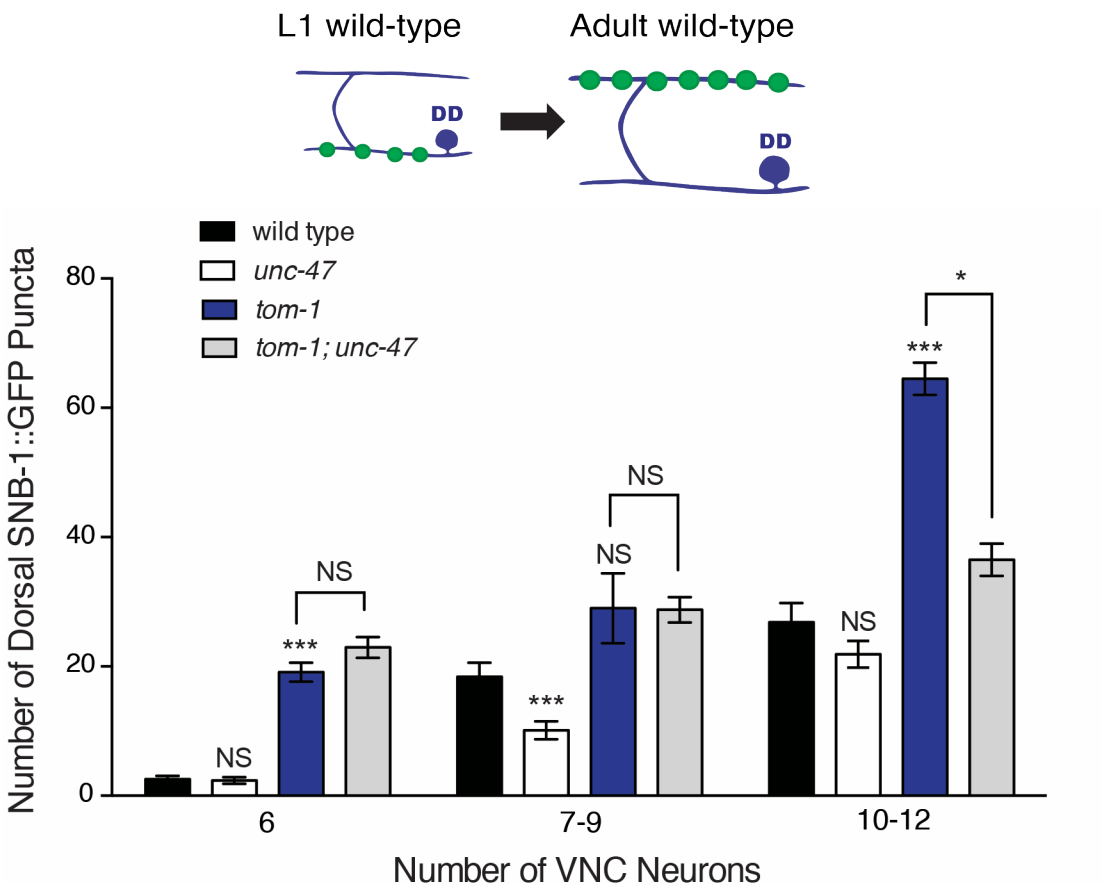

Figure 7.3: Precocious remodeling in *tom-1* mutants partially requires GABA release. Dorsal DD synapse formation was measured by counting the number of dorsal GABA::SNB-1::GFP puncta between DD1-DD6 over time. Puncta number are normalized to the number of VD neurons in the ventral nerve cord to control for the overall developmental delay in *unc-47* animals. Previous studies show that *tom*-1 animals have hyperactive neurotransmission and exhibit precocious DD remodeling. Here we show that this effect is partially mediated by GABA release, as loss of *unc-47*/VGAT suppresses precocious DD remodeling of *tom-1* mutants at the last time point measured (10-12 cell stage). These results suggest that GABA release may not be required for the initial effects of *tom-1*-mediated precocious remodeling, but plays an important role at later stages of development. All data are represented as mean ± SEM. Student's t-test was performed for each genotype versus wild type, and for *tom-1* versus *tom-1; unc-47*. N = 45 wild type, N = 168 *unc-47,* N= 39 *tom-1,* and N= 45 *tom-1; unc-47* animals. NS is not significant, $*p < 0.05$, $**p < 0.01$, $***p < 0.001$.

GABAergic signaling in this pathway, it would be helpful to ablate GABA synthesis and release specifically in the DD and VD motor neurons, as there appear to be more GABAergic neurons in *C. elegans* than originally thought (Gendrel et al. 2016).

Based on our findings that GABA signaling does appear to be required for synapse elimination, we tested whether the DEG/ENaC protein UNC-8 drives removal in the same genetic pathway. We evaluated the *unc-55; unc-47; unc-8* triple mutants and found that this triple mutant did not enhance the *unc-55; unc-8* removal defects; however, the triple mutant has a significantly weaker effect than the *unc-55; unc-47* double mutants (**Figure 7.4**). This finding reveals a complex genetic relationship between GABA release and UNC-8 activity, including the possibility that loss of *unc-8* antagonizes *unc-47*-induced removal defects. These findings are difficult to interpret, as *unc-8* expression (or lack thereof) in cholinergic motor neurons could contribute the suppression of *unc-55; unc-47* removal defects by regulating cholinergic neuronal activity. This is also supported by our finding that cholinergic signaling likely promotes GABAergic synapse removal (see below).

Ionotropic and metabotropic GABA receptors have opposite roles in regulating synapse removal

Our finding that GABA synthesis and release mediate ventral synapse elimination predicted that GABA receptor activity is required for synaptic removal. To test this prediction, we treated wild type, *unc-8*, *unc-55,* and *unc-55; unc-8* animals with the $GABA_A$ receptor antagonist pregnenolone sulfate (PS, **Figure 7.5**). This drug has been used to block the ionotropic GABA receptors in several model systems (Bamber et al.

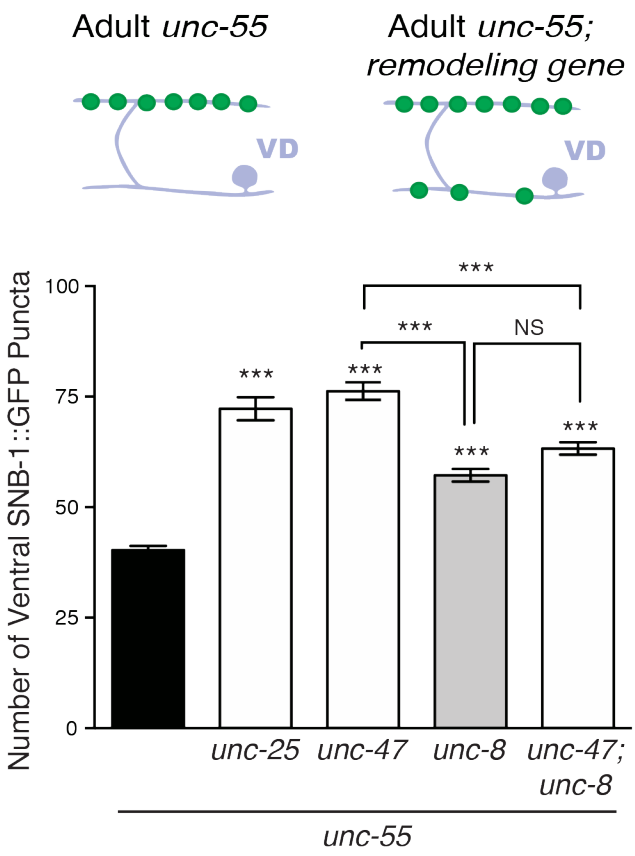

Figure 7.4: GABA release promotes synapse removal in the *unc-8* pathway. The number of ventral GABAergic presynaptic puncta were counted from VD3 to VD11 for each genotype. *unc-55* animals exhibit a loss of ventral synapses due to endogenous DD neuron remodeling and ectopic VD neuron remodeling. This effect is significantly suppressed upon elimination of the GABA biosynthetic enzyme GAD/UNC-25 and the vesicular GABA transporter VGAT/UNC-47. Previously, we have shown that loss of the DEG/ENaC protein UNC-8 also suppresses this phenotype. Genetic loss of *unc-47* and *unc-8* significantly suppresses the *unc-55* removal phenotype; however, this effect is weaker than the *unc-47; unc-55* mutant phenotype, suggesting there may be a complex genetic relationship between *unc-8* and *unc-47*. One Way ANOVA and Tukey's correction for multiple comparisons (N ≥ 41 animals per genotype).

2005; Majewska et al. 1988). We observed that treatment with low (100 μM) or high (1 mM) PS had no effect on the number of synapses in wild type animals. Interestingly, treatment of *unc-8* animals increased the number of ventral synapses to that of wild type levels. Perhaps most importantly, we found that treatment of the *unc-55; unc-8* mutants with 1 mM PS rescued the *unc-55; unc-8* removal defect. This result was surprising as it suggests that $GABA_A$ receptor activity normally acts to stabilize the presynaptic apparatus in *unc-55; unc-8* animals; and thus blocking $GABA_A$ receptors in *unc-55; unc-8* animals restores removal (**Figure 7.5**).

Because PS has also been shown to block NMDA receptors, we took a genetic approach to directly test the role of individual GABA receptors during synapse removal. Utilizing the *unc-55* removal paradigm, we quantified the number of ventral GABAergic synaptic puncta in ionotropic and metabotropic GABA receptor mutants. Loss of the ionotropic GABA receptor *unc-49* showed a significant decrease in ventral synapses compared to the *unc-55* mutant alone (**Figure 7.6**). This finding is consistent with our pharmacological experiment and suggests that the ionotropic $GABA_A$ receptors normally function to stabilize the presynaptic apparatus. We tested additional $GABA_A$ receptors in *C. elegans* (*lgc-35, gab-1, exp-1, lgc-50*), which have been shown to be either excitatory or inhibitory, but saw no effect on *unc-55*-mediated synapse removal (Beg & Jorgensen 2003; Jobson et al. 2015; Gendrel et al. 2016; Feng et al. 2002). In contrast, mutations that disable the metabotropic $GABA_B$ receptor homolog *gbb-2* significantly suppressed *unc-55*-driven synapse elimination, suggesting the GABA signaling through metabotropic receptors is important for this process. We also found that the *unc-55; gbb-1; unc-49* triple mutant enhanced the *unc-55; gbb-2* and the *unc-55; unc-49* phenotypes, raising the possibility that multiple pathways of GABAergic signaling regulate the synapse

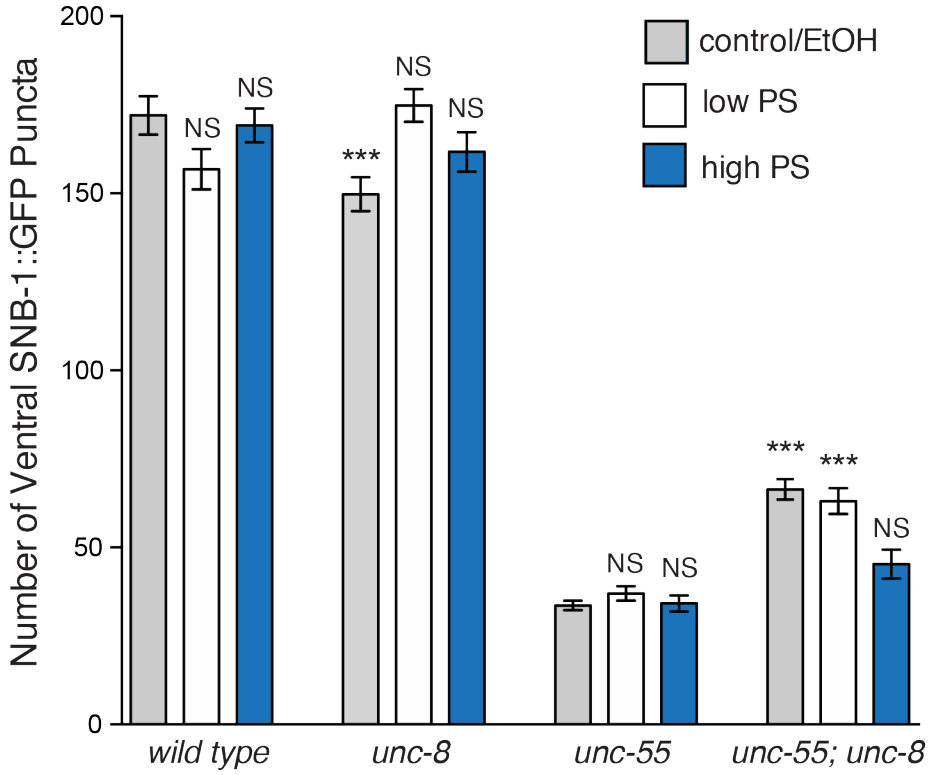

Figure 7.5: The pharmacological $GABA_A$ receptor antagonist pregnenolone sulfate promotes GABAergic synapse removal in *unc-55; unc-8* animals. Ventral GABA::SNB-1::GFP puncta were counted from VD3-VD11. Animals from each genotype were seeded on plates containing ethanol (control), 100 μM pregnenolone sulfate (low PS), or 1 mM pregnenolone sulfate (high PS). One-way ANOVA with Dunnett's multiple comparison tests were performed, comparing wild type and *unc-8* animals in each treatment group to wild type animals on control plates. *unc-55* and *unc-55; unc-8* animals treated with each condition were compared to *unc-55* animals on control plates. All data are represented at mean ± SEM. N ≥ 10 animals per genotype). NS is not significant, $*p < 0.05$, $**p < 0.01$, $***p < 0.001$.

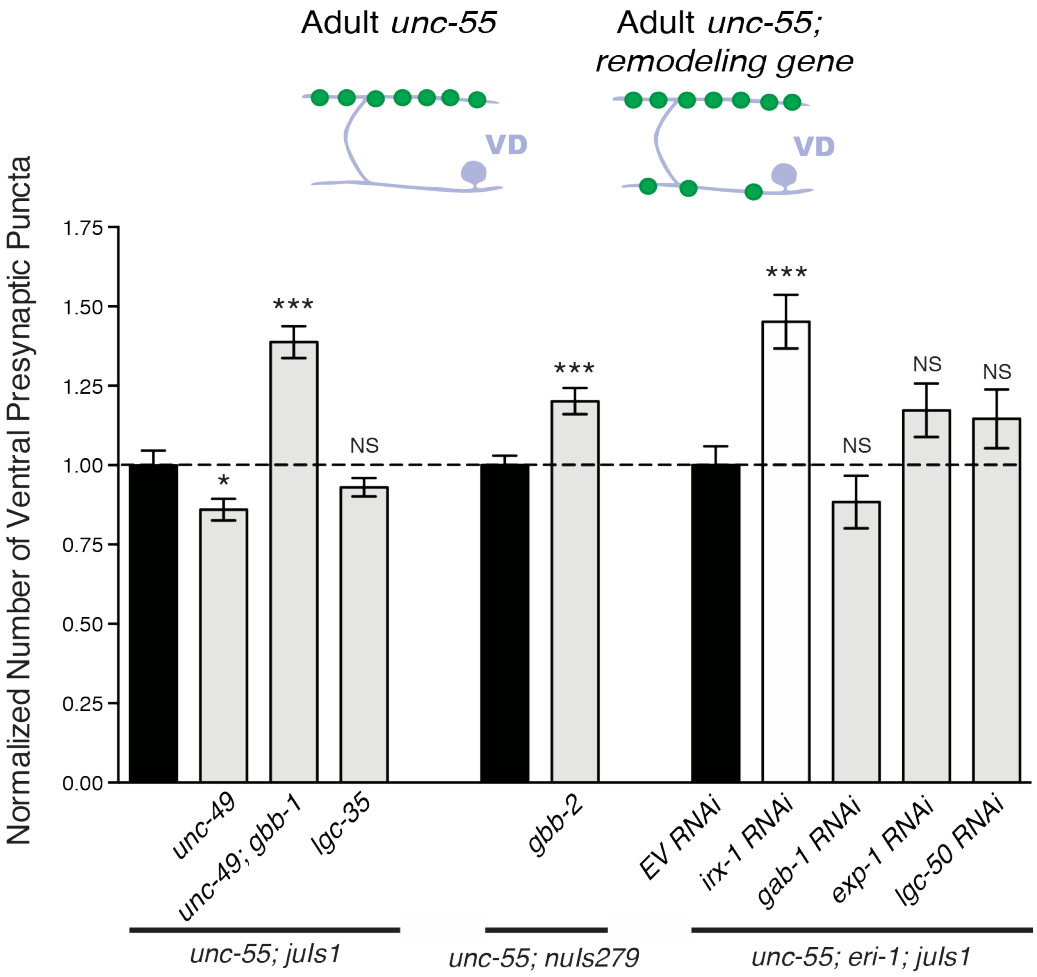

Figure 7.6: Metabotropic $GABA_B$ receptors GBB-1/GBB-2 promote remodeling; whereas, the ionotropic $GABA_A$ receptor UNC-49 may antagonize GABAergic synapse removal. Presynaptic GABA::SNB-1::GFP (*juls1*) or GABA::UNC-57::GFP (*nuls279*) puncta were counted between VD3-VD11. Data were normalized to *unc-55* or *unc-55* on empty vector (EV) RNAi levels for each respective marker, which is annotated by the dotted line. Genetic loss of the ionotropic $GABA_A$ receptor UNC-49 enhances *unc-55* synapse removal; whereas, genetic loss of the metabotropic $GABA_B$ receptors GBB-1/GBB-2 significantly suppresses *unc-55* removal. Genetic loss of the excitatory $GABA_A$ receptor *lgc-35,* and knockdown of the $GABA_A$ receptors *gab-1, exp-1, or lgc-50* by RNAi have no effect on *unc-55* synapse removal. These results suggest that GABAergic signaling via UNC-49 antagonizes synapse removal, whereas signaling through metabotropic GABA receptors GBB-1/GBB-2 promotes synapse removal. RNAi against *irx-1* was used as a positive control. All data are represented at mean ± SEM. One Way ANOVA and Bonferroni's correction for multiple comparisons (N ≥ 10 animals per genotype). NS is not significant, $*p < 0.05$, $**p < 0.01$, $***p < 0.001$.

removal process and ionotropic versus metabotropic signaling have opposite effects (**Figure 7.6**).

GABA reuptake promotes synapse elimination

Transporters are critical for the reuptake and recycling of neurotransmitters. Based on our findings that GABA release promotes synapse removal, we predicted that GABA reuptake via the GABA transporter homolog GAT/SNF-11 would play a role in synapse removal. A recent publication suggests that the only known GAT in *C. elegans,* SNF-11, is expressed in the body wall muscle (Gendrel et al. 2016). From this information, we predicted that loss of *snf-11* may result in a phenotype opposite to that of the *unc-49* mutation. We suspected that in the *snf-11* mutants, excess GABA would be in the synaptic terminal, resulting in enhanced activation of the local $GABA_A$ receptor, UNC-49. Consistent with our finding that *unc-49* stabilizes the presynaptic complex, we confirmed that *unc-55*; *snf-11* animals retain significantly more ventral synapses compared to *unc-55* (**Figure 7.7**). This result suggests that GABA reuptake via SNF-11 promotes the disassembly of presynaptic structures.

Optogenetic activation of the motor circuit drives GABAergic synaptic remodeling

Our findings argue that GABA signaling and thus GABA neuronal activity modulate synaptic remodeling. To test this idea, we used a GABA neuron-specific promoter to express channelrhodopsin (ChR2) in DD neurons (Q. Liu et al. 2009). Blue light exposure of these GABA::ChR2 transgenic animals evoked muscle relaxation with immediate cessation of locomotion as expected for a treatment that enhances

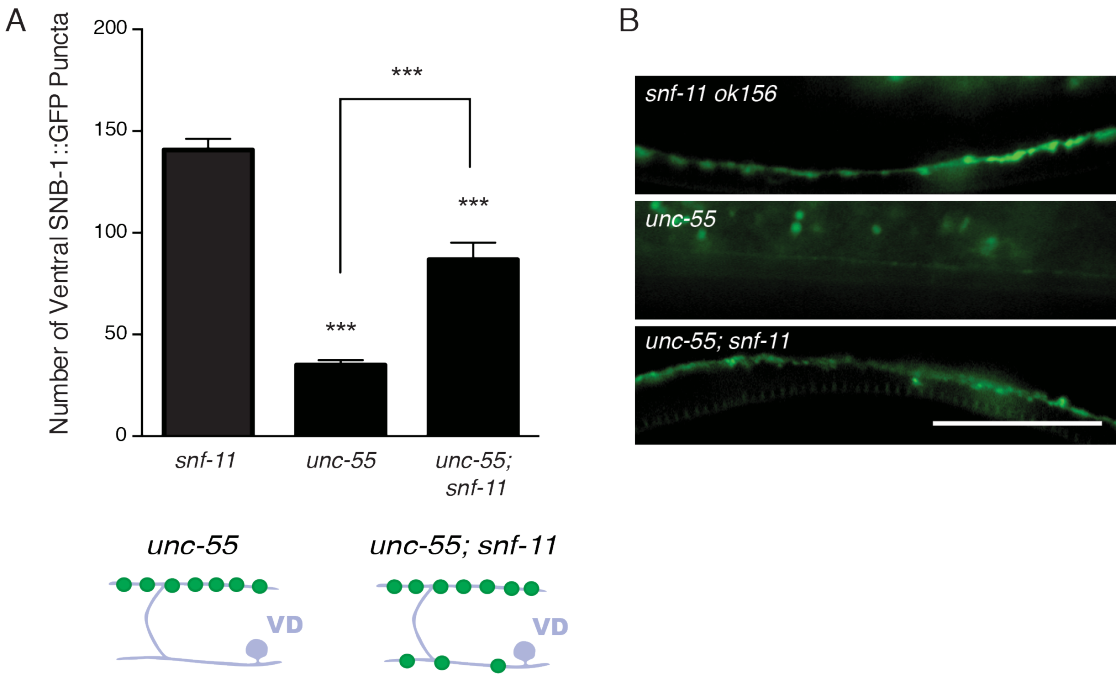

Figure 7.7: The GABA transporter SNF-11 promotes GABAergic synapse removal. **A.** Ventral GABA::SNB-1::GFP puncta were counted from VD3-VD11. Loss of the GABA transporter *snf-11* significantly suppresses *unc-55* ventral synapse removal. One Way ANOVA and Bonferroni's correction for multiple comparisons (N ≥ 10 animals per genotype). All data are represented at mean ± SEM. NS is not significant, *$p < 0.05$, **$p < 0.01$, ***$p < 0.001$. **B.** Representative images of the ventral nerve cords labeled with GABA::SNB-1::GFP. *unc-55* animals show a loss of ventral fluorescence, which is restored in the *unc-55; snf-11* animals. Scale bar is 10 μm.

GABA release (Figure 7.8A, (Schuske et al. 2004)). Synchronized populations of GABA::ChR2 animals were exposed to blue light at 0.5 Hz for 13 or 15 hours. DD neurons were assayed for precocious remodeling by counting the number of dorsal SNB-1::GFP puncta at the end of this period. The results for this experiment show that optogenetic activation of GABA neurons accelerates DD remodeling and that both blue light and exogenous all-*trans* retinal (ATR) are required for this effect; DD neurons that express ChR2 (GABA::ChR2) remodel earlier with significantly more dorsal puncta after 13 or 15 hours of light exposure in comparison to controls (**Figure 7.8C** and **7.9A**, respectively, (Miller-Fleming et al. 2016)). This finding argues that neuronal activity in DD neurons is sufficient to drive synaptic remodeling.

The motor circuit in *C elegans* is well defined (see **Introduction**, (White et al. 1986)). Cholinergic and GABAergic motor neurons innervate body wall muscle to cause contraction and relaxation on opposing sides of the worm, while cholinergic axons also synapse with GABAergic dendrites to regulate locomotor behavior. Therefore, we predicted that stimulation of cholinergic neurons would also regulate GABAergic synapse removal. Similar to the channelrhodopsin (ChR2) experiment outlined above, we expressed ChR2 in cholinergic motor neurons (pACh::ChR2) and exposed synchronized embryos to blue light at 0.5 Hz for 15 hours. At the end of this period, we examined the number of GABAergic dorsal synaptic puncta in animals grown on control plates (no ATR) or plates containing the obligate ChR2 co-factor, ATR. The average number of puncta was greater in the worms grown on ATR compared to controls, however, the population exhibited high variability and the differences were not statistically significant (**Figure 7.9E**). As an additional test of this model, we used a genetic approach to examine the role of acetylcholine in synapse removal. *unc-17* is the *C. elegans* homolog of vesicular acetylcholine transporter (VAChT) and is critical for

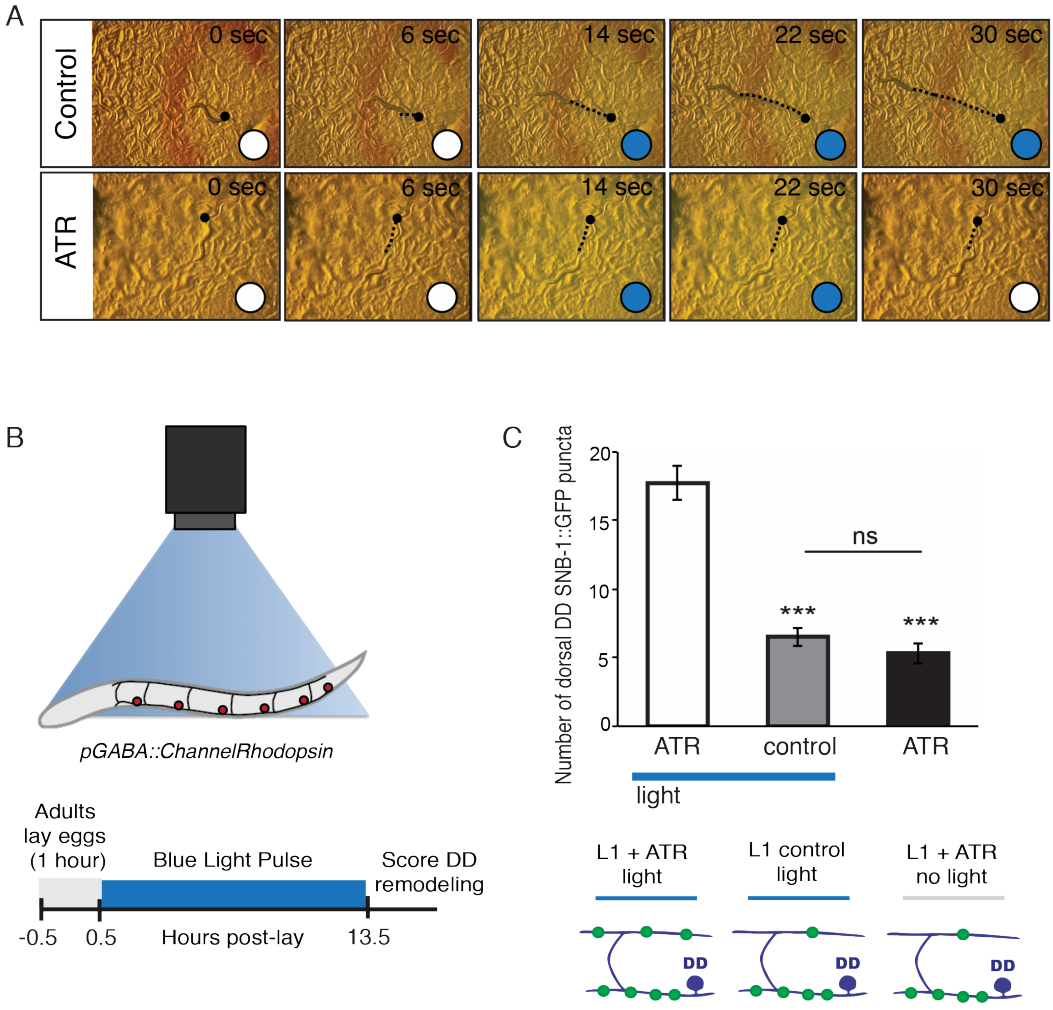

Figure 7.8: Optogenetic activation of GABAergic motor neurons drives precocious DD remodeling. A. Animals expressing fluorescently-labeled channelrhodopsin (ChR2) in GABA neurons were grown on control (ethanol) or all trans-retinal (ATR) plates. ATR is required for activation of the ChR2 cation channel in response to blue light. Upon light stimulation, animals on control plates continue to move forward, unaffected by the light. Animals on the ATR plates become paralyzed in response to blue light exposure. Time stamp is located in the upper right corner of each image, white circle denotes blue light is OFF, blue circle denotes blue light is ON. Black circle annotates starting position of each worm and dotted line traces the movements between frames. Consistent with previous findings, we see that optogenetic activation of GABA neurons induces paralysis **B.** 100 adult worms were placed on control or ATR plates and laid eggs for 1 hour. The midpoint of this hour is considered T_0. After the hour all the adults were removed from

the plates. Embryos were exposed to 470 nm light pulses (0.5 Hz) for 13 hours. After 13 hours, hatched larval worms were imaged and GABA::SNB-1::GFP puncta were quantified. **C.** Optogenetic activation of GABAergic motor neurons induces precocious dorsal DD synapse formation. All data are represented at mean ± SEM. One Way ANOVA and Bonferroni's correction for multiple comparisons (N ≥ 18 animals per genotype). NS is not significant, $*p < 0.05$, $**p < 0.01$, $***p < 0.001$.

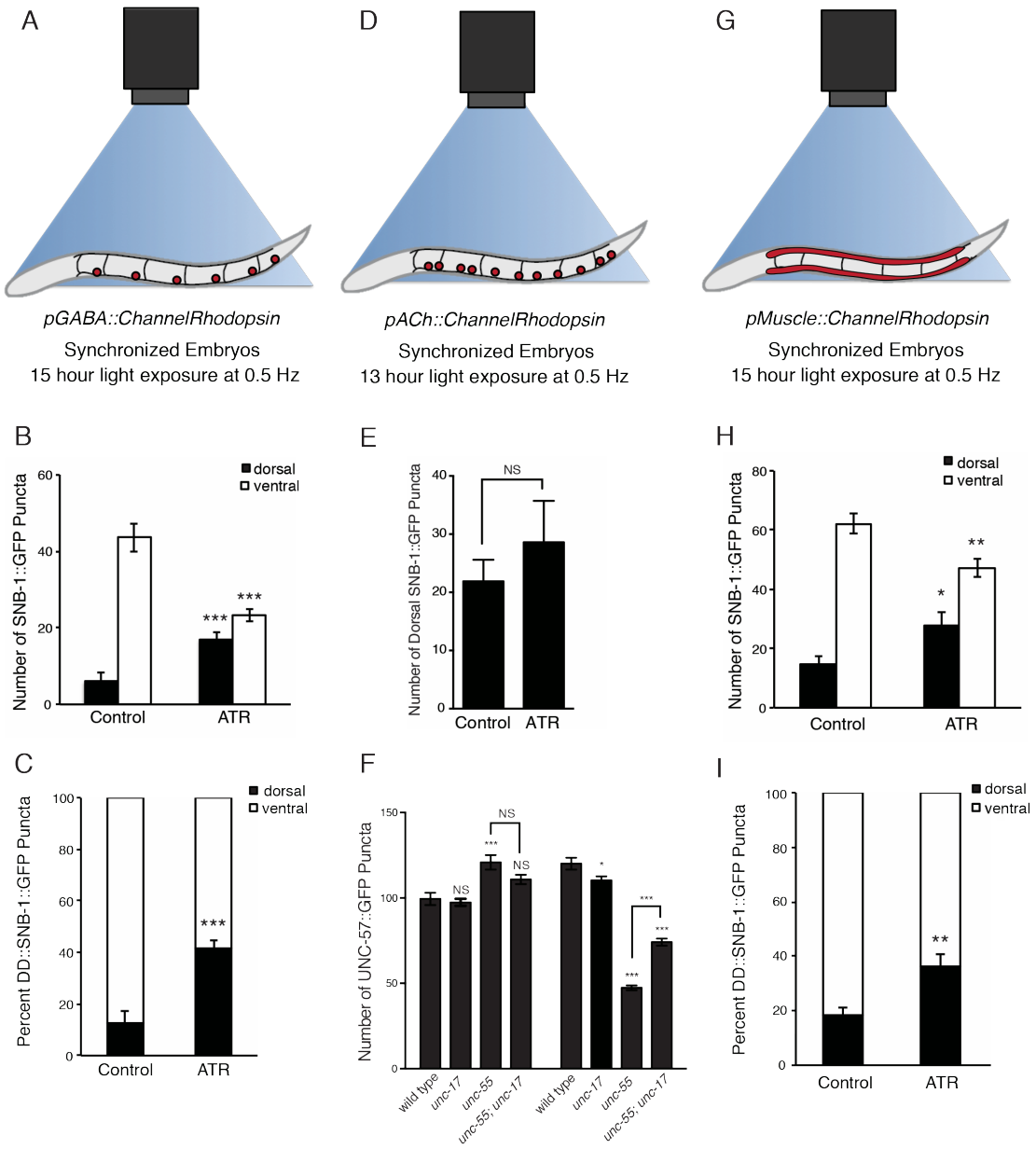

Figure 7.9: Optogenetic activation of GABAergic motor neurons and body wall muscles promote GABAergic synapse removal. A. Synchronized embryos expressing GABA::ChR2 were grown on control and ATR plates. After 15 hours of blue light (470nm) exposure (0.5 Hz), dorsal and ventral DD::SNB-1::GFP puncta were counted between DD1-DD6. **B/C.** Activation of GABAergic motor neurons induces precocious remodeling. The number of dorsal puncta is significantly increased and the number of ventral puncta is significantly decreased, suggesting GABA activity promotes both dorsal DD synapse formation and ventral DD synapse removal. Student's t-test was performed for ATR versus wild type, (N= 5 control and N=8 ATR) **D.** Synchronized embryos expressing ChR2 in cholinergic motor neurons were grown on control and ATR plates. After 15 hours of blue light (470nm) exposure (0.5 Hz), dorsal GABA::SNB-1::GFP puncta were counted between DD1-DD6. **E.** Surprisingly, activation of cholinergic neurons did not elicit a strong effect on remodeling. Student's t-test was

performed for ATR versus wild type, (N= 9 control, N= 5 ATR). **F.** As an additional test to determine whether cholinergic signaling is important during remodeling, we examined the effects of genetic ablation of the vesicular acetylcholine transporter (VAChT/UNC-17) on GABA neuron remodeling. Loss of *unc-17* in *unc-55* animals significantly suppresses the *unc-55* remodeling phenotype on the dorsal (left 4 bars) and ventral nerve cord (right 4 bars), implicating cholinergic signaling during GABA neuron remodeling. One Way ANOVA and Tukey's correction for multiple comparisons, (N ≥ 16 animals per genotype). NS is not significant, $*p < 0.05$, $**p < 0.01$, $***p < 0.001$. All data are represented at mean ± SEM.). **G.** Synchronized embryos expressing Muscle::ChR2 were grown on control and ATR plates. After 15 hours of blue light (470nm) exposure (0.5 Hz), dorsal and ventral DD::SNB-1::GFP puncta were counted between DD1-DD6. **H/I.** Hyperpolarization of muscles resulted in precocious dorsal DD synapse formation and ventral DD synapse removal. Student's t-test was performed for ATR versus wild type, (N= 7 control, N= 7 ATR).

loading acetylcholine into synaptic vesicles for release. The *unc-55; unc-17* double mutants significantly suppress the dorsal and ventral remodeling defects in *unc-55* animals, implicating cholinergic signaling in both the formation of dorsal DD synapses and the removal of ventral DD synapses (**Figure 7.9F**).

Having established a role for GABAergic and cholinergic signaling in remodeling, we next tested the possibility that muscle activity also regulates this process. Using optogenetic tools, we expressed channelrhodopsin in the body wall muscles of *C. elegans* (*pMuscle::ChR2*). Again, we exposed a population of synchronized embryos to blue light at 0.5 Hz for 15 hours. We examined the number of dorsal and ventral GABAergic puncta after the 15-hour exposure and found that animals treated with ATR exhibited precocious ventral synapse removal and premature dorsal synapse assembly (**Figure 7.9H-I**). These findings suggest that depolarization of the postsynaptic body wall muscle can also promote synaptic remodeling. Overall, these experiments confirm previous work that showed an important role for neuronal activity during synapse remodeling in *C. elegans* (Thompson-Peer et al. 2012). Interestingly, while GABA activity plays an important role in synapse elimination, activation of cholinergic neurons and muscle also contribute to the remodeling process (**Figure 7.10**).

Discussion

UNC-8 promotes synapse elimination in the GABA-signaling pathway

In **Chapters 2** through **5** we demonstrate a critical role for the DEG/ENaC protein UNC-8 in the removal of ventral presynaptic components in GABAergic neurons. We show that UNC-8 promotes this process in an activity-dependent pathway that requires

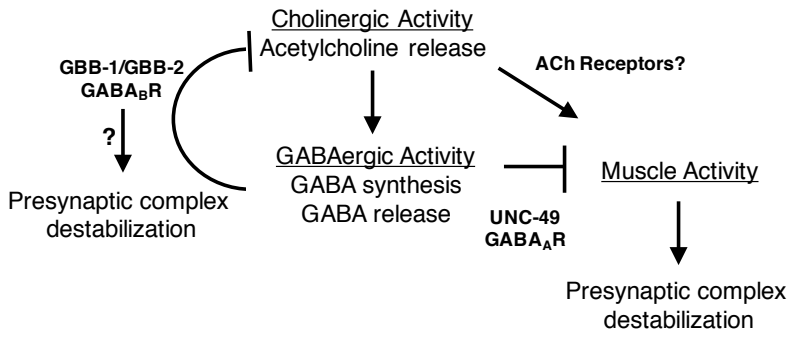

Figure 7.10: Model for activity-driven GABAergic synapse disassembly. GABAergic signaling through ionotropic GABA receptors antagonizes removal of presynaptic GABAergic synapses, whereas signaling through metabotropic GABA receptors promotes GABA synapse disassembly. Metabotropic receptors inhibit cholinergic activity and additionally drive removal via an unknown mechanism. Cholinergic activity and muscle depolarization promote remodeling; however, we have not tested the cholinergic receptor(s) required for this effect. This model also predicts the presence of a retrograde signal from muscle that regulates presynaptic complex stabilization.

neurotransmitter release. In this chapter, we set out to uncover the origin of this neuronal activity. Utilizing genetic and optogenetic approaches, we found that GABA synthesis, acetylcholine release, and muscle activity promote remodeling. Interestingly, we found that GABA activity has much stronger affects on synapse elimination, rather than dorsal DD synapse formation (defects in dorsal DD synapse formation were weaker than the effects of ventral DD and VD synapse removal in *unc-55* animals). Similar results were reported in a study of GABAergic interneurons in mice (Wu et al. 2012).

We examined the *unc-55; unc-47; unc-8* triple mutant and found that these animals do not enhance the *unc-55; unc-8* defect, suggesting that DEG/ENaC/UNC-8 promotes synapse removal in the GABA signaling pathway (**Figure 7.4**). While we have previously shown that UNC-8 mediates this effect in a cell-autonomous mechanism (**Chapter 3**), our finding that loss of *unc-8* partially suppresses the *unc-55; unc-47* removal defect suggests that these genes may have a more complex interaction. This genetic result predicts that GABA release *(unc-47)* promotes remodeling in the *unc-8* pathway, but likely plays additional roles.

Different roles for ionotropic and metabotropic GABA receptors in synapse elimination

Our findings that GABA synthesis and release promote synapse removal are complicated by our results that different GABA receptors can elicit opposite effects on synapse removal. Genetic and pharmacological block of the ionotropic $GABA_A$ receptor UNC-49 improves *unc-55*-mediated synapse removal; whereas, genetic ablation of the GABAB receptors GBB1/GBB2 suppress *unc-55*-mediated removal. Additionally, the loss-of-function mutation in the GABA transporter *snf-11* suppresses removal in *unc-55* animals, consistent with the idea that the *snf-11* mutation likely enhances UNC-49

signaling. The UNC-49 $GABA_A$ receptor is expressed on muscles at sites that co-localize with the presynaptic GABAergic terminal.

Genetic ablation of the metabotropic $GABA_B$ receptor dimer *gbb-1/gbb-2* suppressed GABAergic synapse removal, exhibiting the opposite effect of the $GABA_A$ receptor, UNC-49. The GBB-1/GBB-2 receptor pair are G-protein coupled receptors (GPCRs) that bind GABA and inhibit cholinergic neurons in *C. elegans* (Dittman & Kaplan 2008). This function mirrors the metabotropic $GABA_B$ receptors in mammals that are expressed extrasynaptically and inhibit neuronal excitability (Isaacson 1993, Dittman Regehr 1997). Our findings suggest that ionotropic $GABA_A$ receptors at the NMJ, neuro-muscular junction stabilize the presynaptic complex, possibly through the indirect activation of cholinergic cells; however, this effect is counter-balanced by the activation of the extrasynaptic metabotropic $GABA_B$ receptor (GBB-1/GBB-2) that silences cholinergic signaling and thus destabilizes the presynaptic complex of GABA neurons (**Figure 7.10**). These findings suggest that the optogenetic stimulation of cholinergic and GABAergic cells might mediate synapse removal through the activation of the $GABA_B$ receptors, rather than the $GABA_A$ receptors. Additionally, we found that depolarization of the post-synaptic muscle cells induces precocious removal and relocation of GABAergic synapses. This effect is consistent with the idea of UNC-49-mediated synaptic stabilization, which hyperpolarizes the muscle; whereas, muscle depolarization by channelrhodopsin may shift the balance in favor of synapse disassembly. Future experiments will evaluate which GABA receptors mediate the effects of our optogenetic assays by combining genetic and pharmacological block of GABA receptor subtypes, while stimulating different populations of cells by optogenetics. Additionally, there are likely to be retrograde signals from muscle that mediate the remodeling process.

Conserved roles for GABA signaling in synapse elimination

Here, we provide evidence that GABA synthesis and release promote the removal of synaptic connections. Similarly, genetic ablation of the GABA synthesizing enzyme GAD of the vesicular GABA transporter VGAT in mouse interneurons yields strikingly similar results (Wu et al. 2012). In this scenario, interneuron connections that are normally pruned become stabilized. This finding and our results correlate well with the extensive pruning observed in the visual system that is activated and maintained by GABA signaling (Hensch et al. 1998).

Author Contributions

The experiments performed in this chapter (strain construction, image collection, and synapse quantifications) were completed by Tyne Miller-Fleming.

Acknowledgments

We thank E. Jorgensen for EG5025 *oxIs351[punc-47::ChR2::mCherry]* and EG4787 *lgc-35 (tm1444).* Some strains used in this study were provided by the CGC, which is funded by the NIH Office of Research Infrastructure Programs (P40 OD010440). We also received strains from the Japanese National BioResource Project. This work was supported by NIH grants 5R01NS081259 (DMM), and 1F31NS084732 (TWM). The GABAergic channelrhodopsin experiment in **Figure 5.8** was published in *eLife* (Miller-Fleming et al. 2016).

CHAPTER VIII

DISCUSSION AND FUTURE DIRECTIONS

The work in this dissertation defines a role for the Degenerin/Epithelial Sodium Channel (DEG/ENaC) protein UNC-8 during GABAergic synapse elimination. We propose that calcium influx through voltage-gated calcium channels (VGCCs) mediates the activation of UNC-8 in a mechanism that requires the conserved calcium-dependent phosphatase calcineurin. We predict that UNC-8, under the transcriptional regulation of UNC-55, mediates synapse removal by driving calcium influx through the depolarization of the presynaptic membrane and subsequent activation of local VGCCs. Furthermore, the rise of intracellular calcium may activate the canonical apoptotic proteins (including CED-4), and likely disassembles the presynaptic scaffolds of GABAergic motor neurons through the F-actin severing protein gelsolin. This model of synapse removal shares characteristics with previously established pathways that destabilize synaptic connections, including calcium-dependent pruning and long-term depression models in mammalian neurons and activity-dependent remodeling in *Drosophila* photoreceptors (Beattie et al. 2000; Ertürk et al. 2014; Sugie et al. 2015; Hashimoto et al. 2011). Our work provides evidence that the non-ASIC members of the DEG/ENaC protein family, which are conserved across species, play a role in neuronal refinement and offers a foundation for future studies to understand synapse stability during development and in disease. Here, I outline the key contributions of this work and discuss future directions to elucidate the mechanisms of synapse stability.

UNC-8 Dismantles the Presynaptic Apparatus in an Activity-Dependent Pathway

Calcium signaling promotes GABAergic synapse removal

We find that UNC-2, the P/Q-type VGCC Alpha 1A subunit in *C. elegans*, is required for the removal of ventral GABAergic synapses, suggesting that calcium signaling is likely a conserved mechanism for synapse elimination. We found that calcium signaling mediates GABAergic synapse removal through the activation of the neuronal phosphatase calcineurin, which promotes this process upstream of UNC-8 channel activity. In our proposed model, initial calcium influx through VGCCs activates calcineurin, which may promote UNC-8 channel activity. Sodium influx through UNC-8 will depolarize the presynaptic membrane, sustaining the activity of local VGCCs. Our model predicts that the VGCC/UNC-2 functions upstream and downstream of UNC-8. This prediction could be tested genetically by knocking out *unc-2* in the transgenic strain that overexpresses UNC-8 (*pttr-39::UNC-8cDNA*, **Figure 3.7**). We see that forced expression of UNC-8 leads to ventral synapse removal (Miller-Fleming et al. 2016). If this effect is mediated by the downstream activation of VGCCs, we would expect this effect to be suppressed upon the loss of *unc-2.* We could further validate our model using a calcium-imaging approach. Expression of fluorescent calcium indicators, such as the GCAmP6, have been successfully used in *C. elegans* (S. H. Chung et al. 2013; Chen et al. 2013). To confirm that UNC-8 channel activity functions in the calcium pathway, we could determine whether treatment of neurons with the DEG/ENaC inhibitors Benzamil and Amiloride or genetic knock out of *unc-8* (*unc-8 tm5052*) blocks

calcium transients as we would expect. Additionally, we would expect to see prolonged calcium transients in *unc-8* gain-of-function animals.

Calcineurin removes synapses upstream of UNC-8 channel activity

Activation of the calcium and calmodulin-dependent protein phosphatase, calcineurin (CaN), promotes the weakening of synaptic connections during LTD. Low and prolonged influx of calcium ions through postsynaptic NMDA receptors may initially activate CaN, rather than the opposing kinases such as CaMKII, because CaN has a much higher affinity for calcium and calmodulin (Van Eldik & Watterson 2012; Bito et al. 1997). Additionally, stronger and repetitious bursts of postsynaptic calcium influx activate CaMKII over CaN (Bito et al. 1996; Deisseroth et al. 2003). Interestingly, we see opposing functions for CaN/TAX-6 and CaMKII/UNC-43 in the GABAergic synaptic remodeling paradigm; genetic loss of CaN and gain-of-function mutations in CaMKII/UNC-43 both block removal (**Figures 4.6, 4.7,** and **4.9**). Additionally, we found that constitutive activation of CaN induces precocious removal and this effect requires UNC-8 channel activity (**Figure 4.8,** Miller-Fleming et al. 2016). These results led us to predict that UNC-8 may be a direct target of CaN phosphatase activity. This prediction is supported by a previous study of the DEG/ENaC family ASIC protein showing that phosphorylation of ASIC1a by CaMKII regulates channel activity (Gao et al. 2005).

Future studies will address whether UNC-8 is a direct target of CaN/TAX-6 and CaMKII/UNC-43. Initially, we would need to confirm that UNC-8 and UNC-43 regulate removal in the same genetic pathway by building the *unc-8 tm5052; unc-43gf* (gain-of-function) double mutant and looking for enhanced defects. If we find that UNC-8 and UNC-43 are in the same genetic pathway (no enhancement), we can perform

biochemical experiments to identify potential phosphorylation sites in UNC-8. These *in vitro* experiments can be performed by purifying the intracellular N and C termini of UNC-8, incubating with purified CaMKII and running the sample on a Western blot. As an alternative approach, specific serine/threonine target sites could be evaluated *in vivo* by utilizing the genome editing tool CRISPR to generate phosphomimetic and phospho-dead versions of UNC-8. Our current model suggests that UNC-8 is activated by dephosphorylation; therefore, we would predict that the phosphomimetic UNC-8 would delay synapse removal, whereas the phospho-dead UNC-8 would induce precocious removal. These findings would determine whether UNC-8 is a direct or indirect target of calcineurin signaling and further characterize the novel calcineurin-mediated pathway that promotes synapse removal through UNC-8 activation.

CED pathway proteins drive synapse destabilization, without inducing cell death

We were able to link the UNC-2/calcineurin/UNC-8-mediated removal pathway to a downstream mechanism that utilizes the cell death (CED) proteins to eliminate the presynaptic structure (Miller-Fleming et al. 2016). Future work should validate this model by confirming calcium signaling is upstream of the CED proteins. For example, calcium-imaging using the GCaMP6 reporter in GABA neurons could be performed in wild type and in CED mutants. Our model predicts that loss of CED proteins should not alter the upstream calcium transients. Additionally, we could perform genetic assays to confirm that CED proteins are functioning downstream of UNC-8 and calcium signaling; CED loss-of-function mutants should suppress the precocious removal effects of *unc-8* overexpression, *unc-2 gf*, and *tax-6 gf*.

Work from the Yan lab and others demonstrates that the canonical cell death machinery can mediate synapse elimination, without killing the neuron (Meng et al. 2015; Ertürk et al. 2014). This is thought to be achieved by the proteasome, which may limit the localization of the cell death proteins to distinct synaptic regions during removal (Ertürk et al. 2014). Presynaptic localization of the cell death pathway gene CED-3 in *C. elegans* further supports this hypothesis (Meng et al. 2015). To confirm that CED proteins are active during synapse removal, we could express fluorescently-tagged CED-3 and CED-4 in GABAergic neurons and examine their synaptic localization during synapse removal. Additionally, loss of proteasome activity (blocking the proteasome genetically or pharmacologically), should result in the spreading of fluorescently-labeled CED proteins and DD cell death.

Multiple Pathways Regulate GABAergic Synaptic Remodeling

Transcriptional pathways control active zone composition and stability

The Miller lab previously identified 19 *unc-55* target genes that promote synaptic remodeling in *C. elegans* GABAergic cells (S. C. Petersen et al. 2011). This list encodes a diverse array of proteins, including transcription factors, channel proteins, G-protein signaling components, cytoskeletal regulators, and metalloproteases. Additional studies have identified other *unc-55*-regulated proteins, including the hunchback homolog, HBL-1 and the IG domain-containing protein OIG-1, and *unc-55*-independent components (dynamic microtubules, CDK-5, cyclin/CYY-1, kinesin/UNC-104, and chloride transporters) (Thompson-Peer et al. 2012; He et al. 2015; Kurup et al. 2015; M. Park et

al. 2011; Han et al. 2015). These findings suggest that GABAergic neuron remodeling is complex and requires the coordination of many distinct pathways.

In this dissertation, we confirm that the Iroquois transcription factor IRX-1 drives GABAergic synapse remodeling in a parallel pathway to the DEG/ENaC protein UNC-8. The Miller lab previously found that IRX-1 is necessary and sufficient for the removal of ventral DD synapses and the formation of dorsal DD synapses (S. C. Petersen et al. 2011). Interestingly, we find that IRX-1, but not UNC-8, drives the removal of the vesicular priming protein UNC-13L (long isoform, **Figure 5.10**). These findings suggest that at least two distinct pathways regulate the removal of ventral GABAergic synapses, and that these two pathways may differentially regulate the stability of specific components of the presynaptic active zone, including UNC-13.

Our findings suggest that transcriptional activity of IRX-1 can control the presynaptic localization of UNC-13L at active zone scaffolds. While much work has been done to characterize the core proteins that make up the active zone, it remains unclear how these proteins are targeted there initially and how they are removed. Our work could shed light on the upstream regulatory mechanisms of individual active zone proteins. Dissection of the IRX-1-dependent and UNC-8-independent mechanisms of UNC-13L removal may also identify novel pathways for regulating the presynaptic active zone. Specifically, future studies will examine whether other fluorescently-tagged active zone proteins, including SYD-1, ELKS-1, or the short isoform of UNC-13 (UNC-13S) are differentially stabilized by UNC-8 and IRX-1. This may be especially important in light of recent studies showing that immature synapses contain UNC-13S recruited by SYD-1 and SYD-2, while mature synaptic connections localize UNC-13L with RIM and RIM-binding proteins (Böhme et al. 2016). Differential localization of the UNC-13S and UNC-13L has also been shown to regulate synaptic function, thus confirming that the

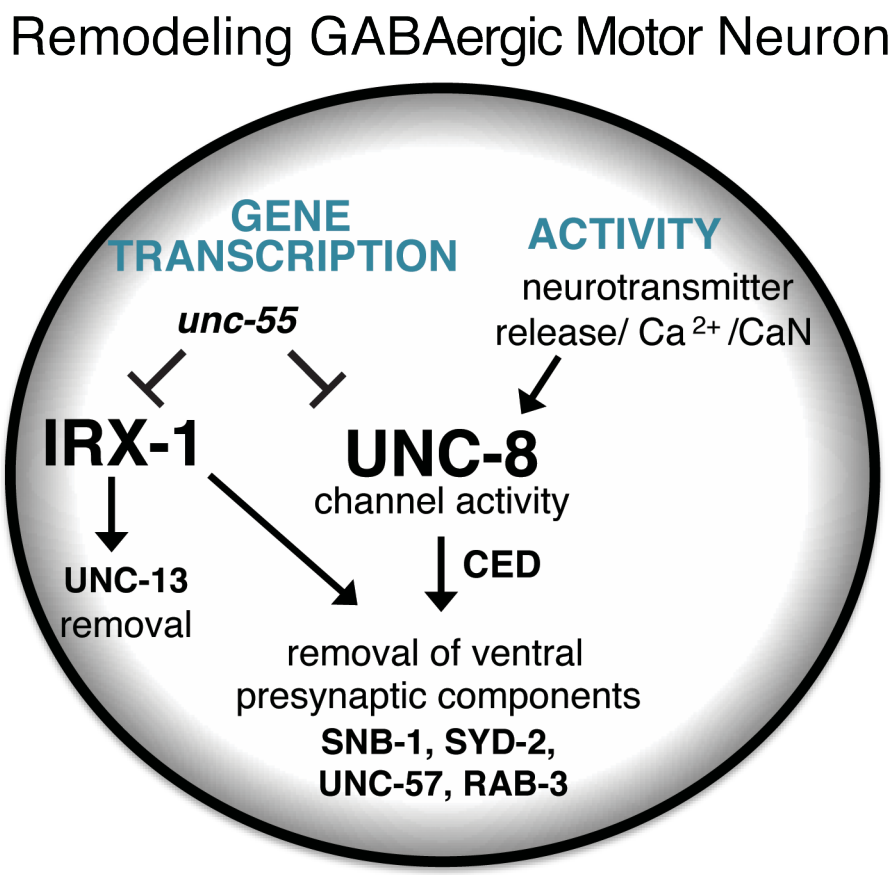

Figure 8.1: UNC-8/DEG/ENaC and IRX-1/Iroquois are UNC-55 targets that promote ventral synapse elimination. Schematic summarizing the UNC-8 and IRX-1 genetic interactions defined in this thesis. UNC-8 serves as a link between the UNC-55 genetic program and the activity-dependent synapse removal pathway. Calcium signaling through VGCCs and calcineurin (CaN) promote synapse removal upstream of UNC-8 channel activity. The cell death (CED) pathway also mediates the elimination of ventral GABAergic synaptobrevin/SNB-1, liprin-alpha/SYD-2, endophillin/UNC-57, and the vesicular GTPase RAB-3. IRX-1 functions in an UNC-8-independent pathway and promotes the removal of all of the presynaptic proteins we examined, including the long isoform of UNC-13/Munc13.

structural changes at the presynaptic active zone directly effect synapse function (Hu et al. 2013; K. Zhou et al. 2013; Böhme et al. 2016). Additionally, we will examine the genetic releationship between IRX-1 and the proteasome, as proteasomal activity has been shown to regulate UNC-13 localization at the synapse (Aravamudan & Broadie 2003; Speese et al. 2003).

GABAergic signaling drives synapse elimination

GABAergic activity drives synaptic pruning in the mammalian nervous system. GABA synthesis is required to initiate refinement of the optic connections that innervate the lateral geniculate nucleus and visual cortex, which results in binocular vision. Loss of GABA synthesis in this paradigm blocks synaptic pruning until the exogenous addition of the GABA receptor agonist benzodiazepine (Hensch et al. 1998). A similar effect was found in GABAergic interneurons when GABA synthesis was blocked; genetic ablation of GABA synthesis leads to overgrown axons and defects in synapse elimination. Interestingly, reduction of GABA release in these same interneurons results in smaller, immature synapses, suggesting that levels of GABA synthesis are important for determining the outcome of synaptic connections (Wu et al. 2012). Here, we found that GABA synthesis and vesicular packaging promote GABAergic synapse elimination. This data supported a role for GABA signaling in synapse elimination; however, loss of the ionotropic $GABA_A$ receptor homolog, UNC-49 does not block synapse elimination, it actually improves the process (**Figure 7.6**). This finding was surprising, as it suggests that muscle inactivation by $GABA_A$ receptors actually stabilizes the presynaptic complex. We next examined the effects of the metabotropic $GABA_B$ receptor mutant, *gbb-2*. Loss of *gbb-2* significantly suppressed *unc-55* synapse removal (**Figure 7.6**). These findings

support a model in which GABAergic signaling through the $GABA_A$ receptor UNC-49 contributes to stabilization of the presynaptic complex; whereas, the $GABA_B$ receptor promotes synapse removal.

As an additional test of this prediction, we examined the effects of depolarizing GABAergic neurons, cholinergic neurons, or muscle cells with the light-activated cation channel CHR2 (channelrhodopsin). We found that activation of GABAergic neurons accelerates DD remodeling, which supports our genetic data (**Figures 7.8**). Additionally, depolarization of body wall muscles induced precocious DD removal, which is consistent with our finding that $GABA_A$ receptor activity, and thus muscle hyperpolarization, stabilizes ventral presynaptic complexes. Therefore, our genetic and optogenetic data suggest that GABA signaling through UNC-49/$GABA_A$ receptors blocks removal by hyperpolarizing muscles, whereas, GABA signaling through GBB-2/$GABA_B$ receptors promotes synapse elimination. These findings are complicated by our result that optogenetic activation of cholinergic cells also accelerates remodeling (**Figure 7.9**). Although this finding supports our prediction that depolarization of muscle cells drives synapse removal, this result is inconsistent with our findings that the $GABA_B$ receptor activity promotes elimination, as GBB-1/GBB-2 are expressed in cholinergic cells to inhibit them (Dittman & Kaplan 2008). Future studies can combine optogenetic techniques and cell-specific mutations to dissect these interactions. Specifically, it would be informative to know whether the precocious remodeling effects seen upon activation of cholinergic neurons requires GABA release. This can be tested by knocking out GABA synthesis in animals expressing the cholinergic CHR2 construct. Additionally, it has been shown that retrograde signals for muscles can modulate presynaptic function in *C. elegans* and *Drosophila* (Doi & Iwasaki 2002; T. Wang et al. 2014). This possibility

could be addressed by knocking down GABA or acetylcholine synthesis and release in animals expressing CHR2 in muscle cells.

UNC-8 serves as link between genetic and activity-dependent pathways that drive synapse removal

DEG/ENaC family proteins, including the mammalian ASIC proteins are thought to strengthen synaptic connections in an activity-dependent mechanism, where presynaptic neurotransmitter release drives ASIC function (Wemmie et al. 2002). Sodium influx through ASIC proteins are predicted to depolarize the postsynaptic membrane, strengthening the synaptic connection. We find that the DEG/ENaC UNC-8 functions in an activity-dependent pathway that has the opposite effect, by destabilizing the presynaptic apparatus. Our genetic data suggest that calcium signaling and activation of the calcium-dependent phosphatase calcineurin mediate UNC-8 channel activity (**Figures 4.4, 4.7, 4.8,** Miller-Fleming et al. 2016). Loss of *unc-8* results in the defective removal of ventral GABAergic synapses that can be observed as electron-dense active zones by EM.

Interestingly, we find that overexpression of UNC-8 cDNA in VD motor neurons is sufficient to induce ventral synapse removal in neurons that normally retain ventral connections (Miller-Fleming et al. 2016). This result demonstrates that all of the components needed to dismantle the presynaptic apparatus are already expressed in VD neurons; however, removal is prohibited in these cells because *unc-8* expression is blocked by the transcription factor UNC-55. Overcoming this transcriptional repression is the only modification needed to induce ectopic ventral synapse removal, supporting our prediction that UNC-8 functions as a link between a developmental genetic program and

activity-dependent synapse stability. These experiments were performed by overexpressing UNC-8 cDNA (UNC-8 OE) in wild type animals and examining the localization of fluorescently-tagged synaptobrevin/SNB-1 in GABAergic neurons (**Figure 3.7**). Future experiments could examine whether UNC-8 overexpression is also capable of removing other components of the presynaptic complex (such as SYD-2/liprin-alpha, SYD-1, ELKS-1, endophilin/UNC-57, RAB-3). Our result that UNC-13L removal is UNC-8-independent, predicts that fluorescently-tagged UNC13L may still be properly localized to the ventral nerve cords of UNC-8 OE animals. It would also be interesting to test whether the loss of ventral synapses in UNC-8 OE animals results in a loss of presynaptic function. These experiments could be accomplished by examining movement and spontaneous ventral GABA activity with electrophysiology. We would predict that the UNC-8 OE animals would exhibit backward locomotor defects and a loss of spontaneous ventral GABA activity, similar to the phenotype seen in *unc-55* animals.

The DEG/ENaC Protein UNC-8 Regulates Different Processes in Cholinergic and GABAergic neurons

Hyperactive UNC-8 channels induce neurotoxicity in cholinergic motor neurons

Degenerin family proteins were initially identified for their capacity to induce neurodegeneration when constitutively active (Driscoll & Chalfie 1991). Examples of this include the MEC-4 and ASIC1a channels that induce neurotoxicity due to calcium influx and consequent activation of the necrotic cell death pathway in the cells in which they are expressed (Driscoll & Chalfie 1991; Canessa et al. 1993; García-Añoveros et al.

1995). We find that expression of a constitutively active UNC-8 channel in *Xenopus* oocytes induces cell death; however, this channel is blocked by extracellular calcium ions. Additionally, UNC-8 selectively transports sodium ions into oocytes, which is still sufficient to induce neurodegeneration (Y. Wang et al. 2013). These findings suggest that both calcium and sodium influx through hyperactive DEG/ENaC proteins can induce neurodegeneration.

We examined the constitutively active *unc-8 (n491)* allele *in vivo*. Consistent with previous reports, we find that *unc-8 (n491)* animals exhibit cholinergic neuron swelling in larval animals that eventually leads to cell death. Although we found that *unc-8* is expressed in both GABAergic and cholinergic motor neurons, only the cholinergic cells are sensitive to hyperactive UNC-8 activity. Additionally, we did not see any GABAergic synapse removal defects in *unc-8 (n491)* animals. Cholinergic degeneration in *unc-8 (n491)* animals requires expression of *mec-6*, the *C. elegans* homolog to the human paraoxonase gene (PON1, Chelur et al. 2002); however, *mec-6* has no effect on GABAergic synapse elimination (**Figure 6.7**). These findings raise the possibility that UNC-8 may associate with unique DEG/ENaC subunits to form heterotrimers or interact with different accessory proteins in GABAergic and cholinergic neurons to mediate synapse removal and cell death, respectively. Additionally, UNC-8 is regulated by distinct mechanisms in GABAergic and SAB cholinergic cells (**Figure 8.2**), which include the COUP TFII transcription factor UNC-55 and the COE transcription factor UNC-3, respectively.

Future experiments will identify the interacting partners of UNC-8 in GABAergic and cholinergic motor neurons. We can use a genetic approach to identify mutations in DEG/ENaC subunits and proteins that suppress *unc-8 n491* neurodegeneration or block *unc-8 (tm5052)*-mediated ventral synapse removal defects in cholinergic and GABAergic

neurons, respectively. These findings can be confirmed by expressing UNC-8 and interacting proteins in *Xenopus* oocytes to evaluate the effects on channel function. Additionally, we can generate an UNC-8 antibody and use mass spectrometry to identify proteins that co-immunoprecipitate with UNC-8, including DEG/ENaC subunits and accessory proteins.

UNC-8–containing channels drive synapse removal in GABAergic motor neurons

Previous studies of neuronal DEG/ENaC proteins demonstrate a role for these channels in stabilizing synaptic connections. In one example of this, the non-ASIC DEG/ENaC protein pickpocket drives homeostatic plasticity at the *Drosophila* neuromuscular junction (Younger et al. 2013). Similar to our findings, in this paradigm the ENaC subunit homolog functions in a calcium-signaling pathway to enhance presynaptic neurotransmitter release and compensate for a loss of postsynaptic receptor function. The presynaptic DEG/ENaC protein enhances neurotransmission by activating local VGCCs and increasing VGCC transcription (Younger et al. 2013). In another DEG/ENaC model of plasticity, postsynaptic ASIC proteins detect presynaptic vesicle release (by sensing the drop in pH), and promote postsynaptic sodium ion influx, thus enhancing the postsynaptic response (Askwith et al. 2004; Benson et al. 2002; Wemmie et al. 2002; Wemmie et al. 2003; Ziemann et al. 2009). In both of these paradigms, DEG/ENaC proteins stabilize synaptic connectivity by enhancing neurotransmission. We find, however, that the DEG/ENaC protein UNC-8 utilizes similar mechanisms to destabilize synaptic connections and promote synapse elimination. Therefore, it appears

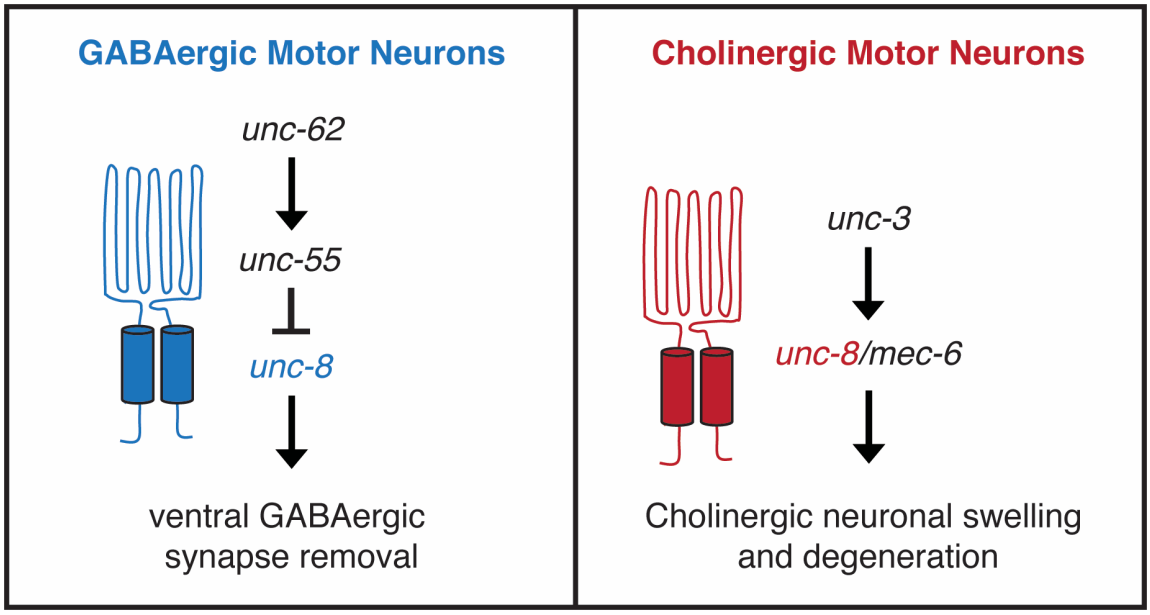

Figure 8.2: UNC-8/DEG/ENaC has distinct roles in GABAergic and cholinergic neurons. Schematic depicting the *unc-8* pathways in GABAergic (left) and cholinergic (right) cells. *unc-55* expression is regulated by the Meis homeodomain protein UNC-62 and transcriptionally represses *unc-8* in GABAergic neurons. In cholinergic cells, hyperactive UNC-8 and accessory protein MEC-6 promote cell swelling and death. The COE-type transcription factor promotes UNC-8 expression in SAB cholinergic cells.

that DEG/ENaC proteins can function to both stabilize and destabilize synaptic connections.

Based on the DEG/ENaC data from *Drosophila*, mice, and *C. elegans*, it is clear that DEG/ENaC family proteins regulate diverse neuronal processes in the cells in which they are expressed. Therefore, it is likely that these channels not only interact with many different accessory proteins, but they also activate different downstream pathways. In the future, it would be beneficial to examine why sodium influx through different DEG/ENaC proteins, such as pickpocket and UNC-8 can activate similar downstream targets, such as calcium channels (VGCCs), and how calcium influx ultimately results in two opposite outcomes: synapse stabilization and synapse elimination, respectively.

Conclusions

The research outlined in this thesis uncovers a mechanism of GABAergic synapse removal that requires (1) calcium influx through VGCCs/UNC-2, (2) activation of the phosphatase calcineurin/TAX-6, (3) sodium influx through the DEG/ENaC UNC-8, and (4) downstream remodeling of the presynaptic active zone through activation of the canonical CED pathway. Our findings provide a link between genetic programs and activity-dependent neuronal circuit reorganization that may advance our understanding of nervous system development and diseases arising from synaptic dysfunction.

REFERENCES

Afroz, S. et al., 2016. Synaptic pruning in the female hippocampus is triggered at puberty by extrasynaptic GABAA receptors on dendritic spines. *eLife*, 5:e15106.

Ahmari, S.E., Buchanan, J. & Smith, S.J., 2000. Assembly of presynaptic active zones from cytoplasmic transport packets. *Nature Neuroscience*, 3(5), pp.445–451.

Antonini, A. & Stryker, M.P., 1996. Plasticity of geniculocortical afferents following brief or prolonged monocular occlusion in the cat. *The Journal of comparative neurology*, 369(1), pp.64–82.

Antonini, A. et al., 1998. Morphology of single geniculocortical afferents and functional recovery of the visual cortex after reverse monocular deprivation in the kitten. *The Journal of neuroscience : the official journal of the Society for Neuroscience*, 18(23), pp.9896–9909.

Aravamudan, B. & Broadie, K., 2003. Synaptic Drosophila UNC-13 is regulated by antagonistic G-protein pathways via a proteasome-dependent degradation mechanism. *Journal of Neurobiology*, 54(3), pp.417–438.

Askwith, C.C. et al., 2004. Acid-sensing ion channel 2 (ASIC2) modulates ASIC1 H+-activated currents in hippocampal neurons. *The Journal of biological chemistry*, 279(18), pp.18296–18305.

Augustin, I. et al., 1999. Munc13-1 is essential for fusion competence of glutamatergic synaptic vesicles. *Nature*, 400(6743), pp.457–461.

Åstrand, A.B.M. et al., 2015. Linking increased airway hydration, ciliary beating, and mucociliary clearance through ENaC inhibition. *American journal of physiology. Lung cellular and molecular physiology*, 308(1), pp.L22–32.

Bamber, B.A. et al., 1999. The Caenorhabditis elegans unc-49 locus encodes multiple subunits of a heteromultimeric GABA receptor. *The Journal of neuroscience : the official journal of the Society for Neuroscience*, 19(13), pp.5348–5359.

Bamber, B.A. et al., 2005. The composition of the GABA receptor at the Caenorhabditis elegansneuromuscular junction. *British Journal of Pharmacology*, 144(4), pp.502–509.

Banasiak, K.J., Burenkova, O. & Haddad, G.G., 2004. Activation of voltage-sensitive sodium channels during oxygen deprivation leads to apoptotic neuronal death. *Neuroscience*, 126(1), pp.31–44.

Beattie, E.C. et al., 2000. Regulation of AMPA receptor endocytosis by a signaling mechanism shared with LTD. *Nature Neuroscience*, 3(12), pp.1291–1300.

Beg, A.A. & Jorgensen, E.M., 2003. EXP-1 is an excitatory GABA-gated cation channel. *Nature Neuroscience*, 6(11), pp.1145–1152.

Bellemer, A. et al., 2011. Two types of chloride transporters are required for GABA(A) receptor-mediated inhibition in C. elegans. *The EMBO Journal*, 30(9), pp.1852–1863.

Bennett, M.K., Calakos, N. & Scheller, R.H., 1992. Syntaxin: a synaptic protein implicated in docking of synaptic vesicles at presynaptic active zones. *Science*, 257(5067), pp.255–259.

Benson, C.J. et al., 2002. Heteromultimers of DEG/ENaC subunits form H+-gated channels in mouse sensory neurons. *Proceedings of the National Academy of Sciences of the United States of America*, 99(4), pp.2338–2343.

Bianchi, L. & Driscoll, M., 2002. Protons at the gate: DEG/ENaC ion channels help us feel and remember. *Neuron*, 34(3), pp.337–340.

Bird, T.D. et al., 1983. Alzheimer's disease: choline acetyltransferase activity in brain tissue from clinical and pathological subgroups. *Annals of neurology*, 14(3), pp.284–293.

Bito, H., Deisseroth, K. & Tsien, R.W., 1997. Ca2+-dependent regulation in neuronal gene expression. *Current Opinion in Neurobiology*, 7(3), pp.419–429.

Bito, H., Deisseroth, K. & Tsien, R.W., 1996. CREB phosphorylation and dephosphorylation: a Ca(2+)- and stimulus duration-dependent switch for hippocampal gene expression. *Cell*, 87(7), pp.1203–1214.

Blaesse, P. et al., 2009. Cation-chloride cotransporters and neuronal function. *Neuron*, 61(6), pp.820–838.

Böhme, M.A. et al., 2016. Active zone scaffolds differentially accumulate Unc13 isoforms to tune Ca(2+) channel-vesicle coupling. *Nature Neuroscience*, 19(10), pp.1311–1320.

Brenner, S., 1974. The genetics of Caenorhabditis elegans. *Genetics*, 77(1), pp.71–94.

Brose, N. et al., 1995. Mammalian homologues of Caenorhabditis elegans unc-13 gene define novel family of C2-domain proteins. *The Journal of biological chemistry*, 270(42), pp.25273–25280.

Brose, N. et al., 1992. Synaptotagmin: a calcium sensor on the synaptic vesicle surface. *Science*, 256(5059), pp.1021–1025.

Buffelli, M. et al., 2003. Genetic evidence that relative synaptic efficacy biases the outcome of synaptic competition. *Nature*, 424, pp.430-434.

Bury, L.A.D. & Sabo, S.L., 2016. Building a Terminal: Mechanisms of Presynaptic Development in the CNS. *The Neuroscientist*, 22(4), pp.372–391.

Bury, L.A.D. & Sabo, S.L., 2011. Coordinated trafficking of synaptic vesicle and active zone proteins prior to synapse formation. *Neural development*, 6, p.24.

Calavia, M.G. et al., 2010. Differential localization of Acid-sensing ion channels 1 and 2 in human cutaneus pacinian corpuscles. *Cellular and molecular neurobiology*, 30(6), pp.841–848.

Calderone, V., 2002. Large-conductance, ca(2+)-activated k(+) channels: function, pharmacology and drugs. *Current medicinal chemistry*, 9(14), pp.1385–1395.

Canessa, C.M., Horisberger, J.D. & Rossier, B.C., 1993. Epithelial sodium channel related to proteins involved in neurodegeneration. *Nature*, 361(6411), pp.467–470.

Cavodeassi, F., Modolell, J. & Gómez-Skarmeta, J.L., 2001. The Iroquois family of genes: from body building to neural patterning. *Development*, 128(15), pp.2847–2855.

Chelur, D.S. et al., 2002. The mechanosensory protein MEC-6 is a subunit of the C. elegans touch-cell degenerin channel. *Nature*, 420(6916), pp.669–673.

Chen, Y. et al., 2013. Structural insight into enhanced calcium indicator GCaMP3 and GCaMPJ to promote further improvement. *Protein & cell*, 4(4), pp.299–309.

Cheung, Z.H. & Ip, N.Y., 2007. The roles of cyclin-dependent kinase 5 in dendrite and synapse development. *Biotechnology journal*, 2(8), pp.949–957.

Cheung, Z.H., Fu, A.K.Y. & Ip, N.Y., 2006. Synaptic roles of Cdk5: implications in higher cognitive functions and neurodegenerative diseases. *Neuron*, 50(1), pp.13–18.

Chung, C.Y. et al., 2005. Cell type-specific gene expression of midbrain dopaminergic neurons reveals molecules involved in their vulnerability and protection. *Human molecular genetics*, 14(13), pp.1709–1725.

Chung, S.H., Sun, L. & Gabel, C.V., 2013. In vivo neuronal calcium imaging in C. elegans. *Journal of visualized experiments : JoVE*, (74).

Cohen, L.D. et al., 2013. Metabolic turnover of synaptic proteins: kinetics, interdependencies and implications for synaptic maintenance. *PLoS ONE*, 8(5), p.e63191.

Colledge, M. et al., 2003. Ubiquitination regulates PSD-95 degradation and AMPA receptor surface expression. *Neuron*, 40(3), pp.595–607.

Coryell, M.W. et al., 2008. Restoring acid-sensing ion channel-1a in the amygdala of knock-out mice rescues fear memory but not unconditioned fear responses. *The Journal of neuroscience : the official journal of the Society for Neuroscience*, 28(51), pp.13738–13741.

Culican, S.M., Nelson, C.C. & Lichtman, J.W., 1998. Axon withdrawal during synapse elimination at the neuromuscular junction is accompanied by disassembly of the postsynaptic specialization and withdrawal of Schwann cell processes. *The Journal of neuroscience : the official journal of the Society for Neuroscience*, 18(13), pp.4953–4965.

Cull-Candy, S.G., Miledi, R. & Uchitel, O.D., 1980. Diffusion of acetylcholine in the synaptic cleft of normal and myasthenia gravis human endplates. *Nature*, 286(5772), pp.500–502.

Dai, Y. et al., 2006. SYD-2 Liprin-α organizes presynaptic active zone formation through ELKS. *Nature Neuroscience*, 9(12), pp.1479–1487.

Darboux, I. et al., 1998. dGNaC1, a gonad-specific amiloride-sensitive Na+ channel. *The Journal of biological chemistry*, 273(16), pp.9424–9429.

Davis, G.W. & Goodman, C.S., 1998. Synapse-specific control of synaptic efficacy at the terminals of a single neuron. *Nature*, 392(6671), pp.82–86.

Davis, G.W. & Müller, M., 2015. Homeostatic control of presynaptic neurotransmitter release. *Annual Review of Physiology*, 77, pp.251–270.

Davletov, B.A. & Südhof, T.C., 1993. A single C2 domain from synaptotagmin I is sufficient for high affinity Ca2+/phospholipid binding. *The Journal of biological chemistry*, 268(35), pp.26386–26390.

Deisseroth, K. et al., 2003. Signaling from synapse to nucleus: the logic behind the mechanisms. *Current Opinion in Neurobiology*, 13(3), pp.354–365.

Dickinson, D.J. et al., 2013. Engineering the Caenorhabditis elegans genome using Cas9-triggered homologous recombination. *Nature methods*, 10(10), pp.1028–1034.

Ding, M. et al., 2007. Spatial Regulation of an E3 Ubiquitin Ligase Directs Selective Synapse Elimination. *Science*, 317(5840), pp.947–951.

Dittman, J.S. & Kaplan, J.M., 2008. Behavioral impact of neurotransmitter-activated G-protein-coupled receptors: muscarinic and GABAB receptors regulate Caenorhabditis elegans locomotion. *The Journal of neuroscience : the official journal of the Society for Neuroscience*, 28(28), pp.7104–7112.

Doi, M. & Iwasaki, K., 2002. Regulation of retrograde signaling at neuromuscular junctions by the novel C2 domain protein AEX-1. *Neuron*, 33(2), pp.249–259.

Dresbach, T. et al., 2006. Assembly of active zone precursor vesicles: obligatory trafficking of presynaptic cytomatrix proteins Bassoon and Piccolo via a trans-Golgi compartment. *The Journal of biological chemistry*, 281(9), pp.6038–6047.

Driscoll, M. & Chalfie, M., 1991. The mec-4 gene is a member of a family of Caenorhabditis elegans genes that can mutate to induce neuronal degeneration. *Nature*, 349(6310), pp.588–593.

Du, J. et al., 2014. Protons are a neurotransmitter that regulates synaptic plasticity in the lateral amygdala. *Proceedings of the National Academy of Sciences*, 111(24), pp.8961–8966.

Earls, L.R. et al., 2010. Coenzyme Q protects Caenorhabditis elegans GABA neurons from calcium-dependent degeneration. *Proceedings of the National Academy of Sciences*, 107(32), pp.14460–14465.

Easley-Neal, C. et al., 2013. Late recruitment of synapsin to nascent synapses is regulated by Cdk5. *Cell reports*, 3(4), pp.1199–1212.

Ehlers, M.D., 2003. Activity level controls postsynaptic composition and signaling via the ubiquitin-proteasome system. *Nature Neuroscience*, 6(3), pp.231–242.

Ehmann, N., Sauer, M. & Kittel, R.J., 2015. Super-resolution microscopy of the synaptic active zone. *Frontiers in cellular neuroscience*, 9, p.7.

Ertürk, A., Wang, Y. & Sheng, M., 2014. Local Pruning of Dendrites and Spines by Caspase-3-Dependent and Proteasome-Limited Mechanisms. *Journal of Neuroscience*, 34(5), pp.1672–1688.

Etchberger, J.F. et al., 2007. The molecular signature and cis-regulatory architecture of a C. elegans gustatory neuron. *Genes & Development*, 21(13), pp.1653–1674.

Fagiolini, M. & Hensch, T.K., 2000. Inhibitory threshold for critical-period activation in primary visual cortex. *Nature*, 404(6774), pp.183–186.

Falet, H. et al., 2002. Importance of free actin filament barbed ends for Arp2/3 complex function in platelets and fibroblasts. *Proceedings of the National Academy of Sciences of the United States of America*, 99(26), pp.16782–16787.

Farboud, B. & Meyer, B.J., 2015. Dramatic enhancement of genome editing by CRISPR/Cas9 through improved guide RNA design. *Genetics*, 199(4), pp.959–971.

Feng, X.-P. et al., 2002. Study of the nematode putative GABA type-A receptor subunits: evidence for modulation by ivermectin. *Journal of neurochemistry*, 83(4), pp.870–878.

Fenster, S.D. et al., 2000. Piccolo, a presynaptic zinc finger protein structurally related to bassoon. *Neuron*, 25(1), pp.203–214.

Frank, C.A. et al., 2006. Mechanisms underlying the rapid induction and sustained expression of synaptic homeostasis. *Neuron*, 52(4), pp.663–677.

Friese, M.A. et al., 2007. Acid-sensing ion channel-1 contributes to axonal degeneration in autoimmune inflammation of the central nervous system. *Nature medicine*, 13(12), pp.1483–1489.

Fujita, Y. et al., 1998. Tomosyn: a syntaxin-1-binding protein that forms a novel complex in the neurotransmitter release process. *Neuron*, 20(5), pp.905–915.

Fukuda, M., 2003. Distinct Rab binding specificity of Rim1, Rim2, rabphilin, and Noc2. Identification of a critical determinant of Rab3A/Rab27A recognition by Rim2. *The Journal of biological chemistry*, 278(17), pp.15373–15380.

Fukunaga, K., 1993. [The role of Ca2+/calmodulin-dependent protein kinase II in the cellular signal transduction]. *Nihon yakurigaku zasshi. Folia pharmacologica Japonica*, 102(6), pp.355–369.

Gao, J. et al., 2005. Coupling between NMDA receptor and acid-sensing ion channel contributes to ischemic neuronal death. *Neuron*, 48(4), pp.635–646.

Garcia, L.R., Mehta, P. & Sternberg, P.W., 2001. Regulation of distinct muscle behaviors controls the C. elegans male's copulatory spicules during mating. *Cell*, 107(6), pp.777–788.

García-Añoveros, J., Ma, C. & Chalfie, M., 1995. Regulation of Caenorhabditis elegans degenerin proteins by a putative extracellular domain. *Current biology : CB*, 5(4), pp.441–448.

Gatto, C.L., Pereira, D. & Broadie, K., 2014. GABAergic circuit dysfunction in the Drosophila Fragile X syndrome model. *Neurobiology of disease*, 65, pp.142–159.

Gendrel, M., Atlas, E.G. & Hobert, O., 2016. A cellular and regulatory map of the GABAergic nervous system of C. elegans. *eLife*, 5:e17686.

Gengyo-Ando, K. & Mitani, S., 2000. Characterization of mutations induced by ethyl methanesulfonate, UV, and trimethylpsoralen in the nematode Caenorhabditis elegans. *Biochemical and biophysical research communications*, 269(1), pp.64–69.

Geppert, M. et al., 1994. Synaptotagmin I: a major Ca2+ sensor for transmitter release at a central synapse. *Cell*, 79(4), pp.717–727.

Ghatta, S. et al., 2006. Large-conductance, calcium-activated potassium channels: structural and functional implications. *Pharmacology & therapeutics*, 110(1), pp.103–116.

Giese, K.P. et al., 1998. Autophosphorylation at Thr286 of the alpha calcium-calmodulin kinase II in LTP and learning. *Science*, 279(5352), pp.870–873.

Giraldez, T. & Domínguez, J., 2013. ENaC in the Brain-Future Perspectives and Pharmacological Implications. *Current molecular pharmacology*, 6(1), pp. 44-49.

Goodman, M.B. et al., 2002. MEC-2 regulates C. elegans DEG/ENaC channels needed for mechanosensation. *Nature*, 415(6875), pp.1039–1042.

Gómez-Skarmeta, J.L. & Modolell, J., 2002. Iroquois genes: genomic organization and function in vertebrate neural development. *Current Opinion in Genetics & Development*, 12(4), pp.403–408.

Gracheva, E.O. et al., 2010. Differential Regulation of Synaptic Vesicle Tethering and Docking by UNC-18 and TOM-1. *Frontiers in Synaptic Neuroscience*, 2.

Gracheva, E.O. et al., 2008. Direct interactions between C. elegans RAB-3 and Rim provide a mechanism to target vesicles to the presynaptic density. *Neuroscience Letters*, 444(2), pp.137–142.

Gracheva, E.O. et al., 2006. Tomosyn inhibits synaptic vesicle priming in Caenorhabditis elegans. *PLoS Biology*, 4(8), p.e261.

Gribkoff, V.K., Starrett, J.E. & Dworetzky, S.I., 1997. The pharmacology and molecular biology of large-conductance calcium-activated (BK) potassium channels. *Advances in pharmacology (San Diego, Calif.)*, 37, pp.319–348.

Hains, B.C. et al., 2004. Sodium channel blockade with phenytoin protects spinal cord axons, enhances axonal conduction, and improves functional motor recovery after contusion SCI. *Experimental neurology*, 188(2), pp.365–377.

Hall, D.H. & Hedgecock, E.M., 1991. Kinesin-related gene unc-104 is required for axonal transport of synaptic vesicles in C. elegans. *Cell*, 65(5), pp.837–847.

Hallam, S.J. & Jin, Y., 1998. lin-14 regulates the timing of synaptic remodelling in Caenorhabditis elegans. *Nature*, 395(6697), pp.78–82.

Hallam, S.J. et al., 2002. SYD-1, a presynaptic protein with PDZ, C2 and rhoGAP-like domains, specifies axon identity in C. elegans. *Nature Neuroscience*, 5(11), pp.1137–1146.

Han, B., Bellemer, A. & Koelle, M.R., 2015. An Evolutionarily Conserved Switch in Response to GABA Affects Development and Behavior of the Locomotor Circuit of Caenorhabditis elegans.

Hanover, J.L. et al., 1999. Brain-derived neurotrophic factor overexpression induces precocious critical period in mouse visual cortex. *Journal of Neuroscience*, 19(22), p.RC40.

Hanukoglu, I. & Hanukoglu, A., 2016. Epithelial sodium channel (ENaC) family: Phylogeny, structure-function, tissue distribution, and associated inherited diseases. *Gene*, 579(2), pp.95–132.

Hashimoto, K. et al., 2011. Postsynaptic P/Q-type Ca2+ channel in Purkinje cell mediates synaptic competition and elimination in developing cerebellum. *Proceedings of the National Academy of Sciences*, 108(24), pp.9987–9992.

He, S. et al., 2015. Transcriptional Control of Synaptic Remodeling through Regulated Expression of an Immunoglobulin Superfamily Protein. *Current Biology*, 25(19), pp.2541–2548.

Hedlund, E. et al., 2010. Global gene expression profiling of somatic motor neuron populations with different vulnerability identify molecules and pathways of degeneration and protection. *Brain : a journal of neurology*, 133(Pt 8), pp.2313–2330.

Hensch, T.K. et al., 1998. Local GABA circuit control of experience-dependent plasticity in developing visual cortex. *Science*, 282(5393), pp.1504–1508.

Hernández-González, E.O. et al., 2006. Sodium and epithelial sodium channels participate in the regulation of the capacitation-associated hyperpolarization in mouse sperm. *The Journal of biological chemistry*, 281(9), pp.5623–5633.

Hitomi, Y. et al., 2009. Immunohistochemical detection of ENaCbeta in the terminal Schwann cells associated with the periodontal Ruffini endings of the rat incisor. *Biomedical research*, 30(2), pp.113–119.

Hodgkiss, J.P. & Kelly, J.S., 1995. Only “de novo” long-term depression (LTD) in the rat hippocampus in vitro is blocked by the same low concentration of FK506 that blocks LTD in the visual cortex. *Brain research*, 705(1-2), pp.241–246.

Holderith, N. et al., 2012. Release probability of hippocampal glutamatergic terminals scales with the size of the active zone. *Nature Neuroscience*, 15(7), pp.988–997.

Hong, K. & Driscoll, M., 1994. A transmembrane domain of the putative channel subunit MEC-4 influences mechanotransduction and neurodegeneration in C. elegans. *Nature*, 367(6462), pp.470–473.

Hu, Z., Tong, X.-J. & Kaplan, J.M., 2013. UNC-13L, UNC-13S, and Tomosyn form a protein code for fast and slow neurotransmitter release in Caenorhabditis elegans. *eLife*, 2, p.e00967.

Huang, M. et al., 1995. A stomatin-like protein necessary for mechanosensation in C. elegans. *Nature*, 378(6554), pp.292–295.

Huang, Z.J. et al., 1999. BDNF regulates the maturation of inhibition and the critical period of plasticity in mouse visual cortex. *Cell*, 98(6), pp.739–755.

Hubel, D.H. & Wiesel, T.N., 1970. The period of susceptibility to the physiological effects of unilateral eye closure in kittens. *The Journal of Physiology*, 206(2), pp.419–436.

Hubel, D.H. & Wiesel, T.N., 1963. Receptive fields of cells in striate cortex of very young, visually inexperienced kittens. *Journal of Neurophysiology*, 26(6), pp.994–1002.

Huttenlocher, P.R. & de Courten, C., 1987. The development of synapses in striate cortex of man. *Human neurobiology*, 6(1), pp.1–9.

Jasti, J. et al., 2007. Structure of acid-sensing ion channel 1 at 1.9 A resolution and low pH. *Nature*, 449(7160), pp.316–323.

Jiao, S. & Li, Z., 2011. Nonapoptotic function of BAD and BAX in long-term depression of synaptic transmission. *Neuron*, 70(4), pp.758–772.

Jin, Y. et al., 1999. The Caenorhabditis elegans gene unc-25 encodes glutamic acid decarboxylase and is required for synaptic transmission but not synaptic development. *The Journal of neuroscience : the official journal of the Society for Neuroscience*, 19(2), pp.539–548.

Jobson, M.A. et al., 2015. Spillover Transmission Is Mediated by the Excitatory GABA Receptor LGC-35 in C. elegans. *The Journal of neuroscience : the official journal of the Society for Neuroscience*, 35(6), pp.2803–2816.

Johnson, E.L., Fetter, R.D. & Davis, G.W., 2009. Negative regulation of active zone assembly by a newly identified SR protein kinase. *PLoS Biology*, 7(9), p.e1000193.

Kaczorowski, G.J. et al., 1996. High-conductance calcium-activated potassium channels; structure, pharmacology, and function. *Journal of bioenergetics and biomembranes*, 28(3), pp.255–267.

Kaeser, P.S. et al., 2011. RIM proteins tether Ca2+ channels to presynaptic active zones via a direct PDZ-domain interaction. *Cell*, 144(2), pp.282–295.

Kalla, S. et al., 2006. Molecular dynamics of a presynaptic active zone protein studied in Munc13-1-enhanced yellow fluorescent protein knock-in mutant mice. *Journal of Neuroscience*, 26(50), pp.13054–13066.

Kelleher, J.F., Atkinson, S.J. & Pollard, T.D., 1995. Sequences, structural models, and cellular localization of the actin-related proteins Arp2 and Arp3 from Acanthamoeba. *The Journal of Cell Biology*, 131(2), pp.385–397.

Kennedy, S., Wang, D. & Ruvkun, G., 2004. A conserved siRNA-degrading RNase negatively regulates RNA interference in C. elegans. *Nature*, 427(6975), pp.645–649.

Kim, S., Violette, C.J. & Ziff, E.B., 2015. Reduction of increased calcineurin activity rescues impaired homeostatic synaptic plasticity in presenilin 1 M146V mutant. *Neurobiology of aging*, 36(12), pp.3239–3246.

Kittelmann, M. et al., 2013. Liprin-α/SYD-2 determines the size of dense projections in presynaptic active zones in C. elegans. *The Journal of Cell Biology*, 203(5), pp.849–863.

Klaavuniemi, T., Yamashiro, S. & Ono, S., 2008. Caenorhabditis elegans gelsolin-like protein 1 is a novel actin filament-severing protein with four gelsolin-like repeats. *The Journal of biological chemistry*, 283(38), pp.26071–26080.

Kleyman, T.R. & Cragoe, E.J., 1988. Amiloride and its analogs as tools in the study of ion transport. *The Journal of membrane biology*, 105(1), pp.1–21.

Kratsios, P. et al., 2015. Transcriptional coordination of synaptogenesis and neurotransmitter signaling. *Current biology : CB*, 25(10), pp.1282–1295.

Kreple, C.J. et al., 2014. Acid-sensing ion channels contribute to synaptic transmission and inhibit cocaine-evoked plasticity. *Nature Neuroscience*, 17(8), pp.1083–1091.

Kuo, C.T. et al., 2006. Identification of E2/E3 ubiquitinating enzymes and caspase activity regulating Drosophila sensory neuron dendrite pruning. *Neuron*, 51(3), pp.283–290.

Kurup, N. et al., 2015. Dynamic microtubules drive circuit rewiring in the absence of neurite remodeling. *Current biology : CB*, 25(12), pp.1594–1605.

Lai, K.-O. & Ip, N.Y., 2009. Recent advances in understanding the roles of Cdk5 in synaptic plasticity. *Biochimica et biophysica acta- Molecular basis of disease*, 1792(8), pp.741–745.

Lee, H.K. et al., 1998. NMDA induces long-term synaptic depression and dephosphorylation of the GluR1 subunit of AMPA receptors in hippocampus. *Neuron*, 21(5), pp.1151–1162.

Lee, R.Y. et al., 1997. Mutations in the alpha1 subunit of an L-type voltage-activated Ca2+ channel cause myotonia in Caenorhabditis elegans. *The EMBO Journal*, 16(20), pp.6066–6076.

Li, C. et al., 1995. Ca(2+)-dependent and -independent activities of neural and non-neural synaptotagmins. *Nature*, 375(6532), pp.594–599.

Li, Z. et al., 2010. Caspase-3 activation via mitochondria is required for long-term depression and AMPA receptor internalization. *Cell*, 141(5), pp.859–871.

Lichtman, J.W. & Purves, D., 1983. Activity-mediated neural change. *Nature*, 301(5901), p.563.

Lingueglia, E., 2007. Acid-sensing ion channels in sensory perception. *The Journal of biological chemistry*, 282(24), pp.17325–17329.

Lisman, J., Schulman, H. & Cline, H., 2002. The molecular basis of CaMKII function in synaptic and behavioural memory. *Nature Reviews Neuroscience*, 3(3), pp.175–190.

Liu, K.S.Y. et al., 2011. RIM-binding protein, a central part of the active zone, is essential for neurotransmitter release. *Science*, 334(6062), pp.1565–1569.

Liu, Q., Hollopeter, G. & Jorgensen, E.M., 2009. Graded synaptic transmission at the Caenorhabditis elegans neuromuscular junction. *Proceedings of the National Academy of Sciences*, 106(26), pp.10823–10828.

Liu, Z., Kanzawa, N. & Ono, S., 2011. Calcium-sensitive Activity and Conformation of Caenorhabditis elegans Gelsolin-like Protein 1 Are Altered by Mutations in the First Gelsolin-like Domain. *The Journal of biological chemistry*, 286(39), p.34051–34059.

Lo, Y.J. & Poo, M.M., 1991. Activity-dependent synaptic competition in vitro: heterosynaptic suppression of developing synapses. *Science*, 254(5034), pp.1019–1022.

Lonze, B.E. & Ginty, D.D., 2002. Function and regulation of CREB family transcription factors in the nervous system. *Neuron*, 35(4), pp.605–623.

Maas, C. et al., 2012. Formation of Golgi-derived active zone precursor vesicles. *Journal of Neuroscience*, 32(32), pp.11095–11108.

Mabb, A.M. & Ehlers, M.D., 2010. Ubiquitination in postsynaptic function and plasticity. *Annual review of cell and developmental biology*, 26, pp.179–210.

Maeder, C.I. & Shen, K., 2011. Genetic dissection of synaptic specificity. *Current Opinion in Neurobiology*, 21(1), pp.93–99.

Mahoney, R.E., Rawson, J.M. & Eaton, B.A., 2014. An age-dependent change in the set point of synaptic homeostasis. *Journal of Neuroscience*, 34(6), pp.2111–2119.

Majewska, M.D., Mienville, J.M. & Vicini, S., 1988. Neurosteroid pregnenolone sulfate antagonizes electrophysiological responses to GABA in neurons. *Neuroscience Letters*, 90(3), pp.279–284.

Malhotra, V. et al., 1988. Role of an N-ethylmaleimide-sensitive transport component in promoting fusion of transport vesicles with cisternae of the Golgi stack. *Cell*, 54(2), pp.221–227.

Mansuy, I.M. et al., 1998. Restricted and regulated overexpression reveals calcineurin as a key component in the transition from short-term to long-term memory. *Cell*, 92(1), pp.39–49.

Maruyama, I.N. & Brenner, S., 1991. A phorbol ester/diacylglycerol-binding protein encoded by the unc-13 gene of Caenorhabditis elegans. *Proceedings of the National Academy of Sciences of the United States of America*, 88(13), pp.5729–5733.

Matkovic, T. et al., 2013. The Bruchpilot cytomatrix determines the size of the readily releasable pool of synaptic vesicles. *The Journal of Cell Biology*, 202(4), pp.667–683.

Matthewman, C. et al., 2016. The role of Ca2+ permeability and Na+ conductance in cellular toxicity caused by hyperactive DEG/ENaC channels. *American journal of physiology. Cell physiology*, p.ajpcell.00247.2016.

Matz, J. et al., 2010. Rapid structural alterations of the active zone lead to sustained changes in neurotransmitter release. *Proceedings of the National Academy of Sciences*, 107(19), pp.8836–8841.

Meng, L. et al., 2015. The Cell Death Pathway Regulates Synapse Elimination through Cleavage of Gelsolin in Caenorhabditis elegans Neurons. *Cell reports*, 11(11), pp.1737–1748.

Miller-Fleming, T.W. et al., 2016. The DEG/ENaC cation channel protein UNC-8 drives activity-dependent synapse removal in remodeling GABAergic neurons. *eLife*, 5:e14599.

Mittelstaedt, T. & Schoch, S., 2007. Structure and evolution of RIM-BP genes: identification of a novel family member. *Gene*, 403(1-2), pp.70–79.

Miyazaki, T. et al., 2004. P/Q-type Ca2+ channel alpha1A regulates synaptic competition on developing cerebellar Purkinje cells. *Journal of Neuroscience*, 24(7), pp.1734–1743.

Monier, S. et al., 2002. Characterization of novel Rab6-interacting proteins involved in endosome-to-TGN transport. *Traffic (Copenhagen, Denmark)*, 3(4), pp.289–297.

Mulkey, R.M. et al., 1994. Involvement of a calcineurin/inhibitor-1 phosphatase cascade in hippocampal long-term depression. *Nature*, 369(6480), pp.486–488.

Mullins, R.D., Heuser, J.A. & Pollard, T.D., 1998. The interaction of Arp2/3 complex with actin: nucleation, high affinity pointed end capping, and formation of branching networks of filaments. *Proceedings of the National Academy of Sciences of the United States of America*, 95(11), pp.6181–6186.

Müller, M. et al., 2012. RIM controls homeostatic plasticity through modulation of the readily-releasable vesicle pool. *Journal of Neuroscience*, 32(47), pp.16574–16585.

Müller, M., Genç, Ö. & Davis, G.W., 2015. RIM-binding protein links synaptic homeostasis to the stabilization and replenishment of high release probability vesicles. *Neuron*, 85(5), pp.1056–1069.

Naka, H. et al., 2008. Requirement for COUP-TFI and II in the temporal specification of neural stem cells in CNS development. *Nature Neuroscience*, 11(9), pp.1014–1023.

Nakata, T. et al., 1999. Fusion of a novel gene, ELKS, to RET due to translocation t(10;12)(q11;p13) in a papillary thyroid carcinoma. *Genes, chromosomes & cancer*, 25(2), pp.97–103.

Nakayama, H. et al., 2012. GABAergic inhibition regulates developmental synapse elimination in the cerebellum. *Neuron*, 74(2), pp.384–396.

Nieratschker, V. et al., 2009. Bruchpilot in ribbon-like axonal agglomerates, behavioral defects, and early death in SRPK79D kinase mutants of Drosophila. *PLoS genetics*, 5(10), p.e1000700.

Niles, W.D. & Smith, D.O., 1982. Effects of hypertonic solutions on quantal transmitter release at the crayfish neuromuscular junction. *The Journal of Physiology*, 329, pp.185–202.

Obeso, J.A. et al., 2008. Functional organization of the basal ganglia: therapeutic implications for Parkinson's disease. *Movement disorders : official journal of the Movement Disorder Society*, 23 Suppl 3, pp.S548–59.

Ohno, T. et al., 2010. Specific involvement of postsynaptic GluN2B-containing NMDA receptors in the developmental elimination of corticospinal synapses. *Proceedings of the National Academy of Sciences*, 107(34), pp.15252–15257.

Ohtsuka, T. et al., 2002. Cast: a novel protein of the cytomatrix at the active zone of synapses that forms a ternary complex with RIM1 and munc13-1. *The Journal of Cell Biology*, 158(3), pp.577–590.

Oray, S., Majewska, A. & Sur, M., 2004. Dendritic spine dynamics are regulated by monocular deprivation and extracellular matrix degradation. *Neuron*, 44(6), pp.1021–1030.

Owald, D. et al., 2010. A Syd-1 homologue regulates pre- and postsynaptic maturation in Drosophila. *The Journal of Cell Biology*, 188(4), pp.565–579.

Oyler, G.A. et al., 1989. The identification of a novel synaptosomal-associated protein, SNAP-25, differentially expressed by neuronal subpopulations. *The Journal of Cell Biology*, 109(6 Pt 1), pp.3039–3052.

Park, E.C. & Horvitz, H.R., 1986. Mutations with dominant effects on the behavior and morphology of the nematode Caenorhabditis elegans. *Genetics*, 113(4), pp.821–852.

Park, M. et al., 2011. CYY-1/Cyclin Y and CDK-5 Differentially Regulate Synapse Elimination and Formation for Rewiring Neural Circuits. *Neuron*, 70(4), pp.742–757.

Patel, M.R. & Shen, K., 2009. RSY-1 is a local inhibitor of presynaptic assembly in C. elegans. *Science*, 323(5920), pp.1500–1503.

Patel, M.R. et al., 2006. Hierarchical assembly of presynaptic components in defined C. elegans synapses. *Nature Neuroscience*, 9(12), pp.1488–1498.

Paul, M.M. et al., 2015. Bruchpilot and Synaptotagmin collaborate to drive rapid glutamate release and active zone differentiation. *Frontiers in cellular neuroscience*, 9, p.29.

Peled, E.S., Newman, Z.L. & Isacoff, E.Y., 2014. Evoked and spontaneous transmission favored by distinct sets of synapses. *Current biology : CB*, 24(5), pp.484–493.

Perin, M.S. et al., 1990. Phospholipid binding by a synaptic vesicle protein homologous to the regulatory region of protein kinase C. *Nature*, 345(6272), pp.260–263.

Petersen, S.A. et al., 1997. Genetic analysis of glutamate receptors in Drosophila reveals a retrograde signal regulating presynaptic transmitter release. *Neuron*, 19(6), pp.1237–1248.

Petersen, S.C. et al., 2011. A Transcriptional Program Promotes Remodeling of GABAergic Synapses in Caenorhabditis elegans. *Journal of Neuroscience*, 31(43), pp.15362–15375.

Petersen, S.C. 2011. A transcriptional program remodels GABAergic synapses in *C. elegans*. Vanderbilt University electronic dissertation, pp.1–249; 3674304.

Petzoldt, A.G., Lützkendorf, J. & Sigrist, S.J., 2016. Mechanisms controlling assembly and plasticity of presynaptic active zone scaffolds. *Current Opinion in Neurobiology*, 39, pp.69–76.

Pi, H.J. et al., 2010. Autonomous CaMKII can promote either long-term potentiation or long-term depression, depending on the state of T305/T306 phosphorylation. *Journal of Neuroscience*, 30(26), pp.8704–8709.

Plomp, J.J., van Kempen, G.T. & Molenaar, P.C., 1992. Adaptation of quantal content to decreased postsynaptic sensitivity at single endplates in alpha-bungarotoxin-treated rats. *The Journal of Physiology*, 458, pp.487–499.

Price, M.P. et al., 2004. Stomatin modulates gating of acid-sensing ion channels. *The Journal of biological chemistry*, 279(51), pp.53886–53891.

Purves, D. & Lichtman, J.W., 1980. Elimination of synapses in the developing nervous system. *Science*, 210(4466), pp.153–157.

Purves, D., Augustine, G.J., Fitzpatrick, D., Katz, L.C., LaMantia, A.-S., McNamara, J.O. & Williams, S.M., 2001a. Chemical Synapses.

Purves, D., Augustine, G.J., Fitzpatrick, D., Katz, L.C., LaMantia, A.-S., McNamara, J.O. & Williams, S.M., 2001b. Synaptic Transmission.

Raj, A. et al., 2008. Imaging individual mRNA molecules using multiple singly labeled probes. *Nature methods*, 5(10), pp.877–879.

Reinchisi, G. et al., 2012. COUP-TFII expressing interneurons in human fetal forebrain. *Cerebral cortex*, 22(12), pp.2820–2830.

Ressad, F. et al., 1999. Control of actin filament length and turnover by actin depolymerizing factor (ADF/cofilin) in the presence of capping proteins and ARP2/3 complex. *The Journal of biological chemistry*, 274(30), pp.20970–20976.

Richmond, J.E. & Jorgensen, E.M., 1999. One GABA and two acetylcholine receptors function at the C. elegans neuromuscular junction. *Nature Neuroscience*, 2(9), pp.791–797.

Rivera, C. et al., 1999. The K+/Cl- co-transporter KCC2 renders GABA hyperpolarizing during neuronal maturation. *Nature*, 397(6716), pp.251–255.

Rostaing, P. et al., 2004. Preservation of immunoreactivity and fine structure of adult C. elegans tissues using high-pressure freezing. *The journal of histochemistry and cytochemistry : official journal of the Histochemistry Society*, 52(1), pp.1–12.

Roy, A. et al., 2010. Diffusion pathways of oxygen species in the phototoxic fluorescent protein KillerRed. *Photochemical & photobiological sciences : Official journal of the*

European Photochemistry Association and the European Society for Photobiology, 9(10), pp.1342–1350.

Sabo, S.L. & McAllister, A.K., 2003. Mobility and cycling of synaptic protein-containing vesicles in axonal growth cone filopodia. *Nature Neuroscience*, 6(12), pp.1264–1269.

Saeki, S., Yamamoto, M. & Iino, Y., 2001. Plasticity of chemotaxis revealed by paired presentation of a chemoattractant and starvation in the nematode Caenorhabditis elegans. *The Journal of experimental biology*, 204(Pt 10), pp.1757–1764.

Saheki, Y. & Bargmann, C.I., 2009. Presynaptic CaV2 calcium channel traffic requires CALF-1 and the α2δ subunit UNC-36. *Nature Neuroscience*, 12(10), pp.1257–1265.

Sanderson, J.L. et al., 2012. AKAP150-anchored calcineurin regulates synaptic plasticity by limiting synaptic incorporation of Ca2+-permeable AMPA receptors. *Journal of Neuroscience*, 32(43), pp.15036–15052.

Schultheis, C. et al., 2011. Optogenetic analysis of GABAB receptor signalling in Caenorhabditis elegans motor neurons. *Journal of Neurophysiology,* 106(2), pp.817-827.

Schuske, K., Beg, A.A. & Jorgensen, E.M., 2004. The GABA nervous system in C. elegans. *Trends in Neurosciences*, 27(7), pp.407–414.

Schuske, K.R. et al., 2003. Endophilin is required for synaptic vesicle endocytosis by localizing synaptojanin. *Neuron*, 40(4), pp.749–762.

Seeburg, D.P. et al., 2008. Critical role of CDK5 and Polo-like kinase 2 in homeostatic synaptic plasticity during elevated activity. *Neuron*, 58(4), pp.571–583.

Selkoe, D.J., 2002. Alzheimer's disease is a synaptic failure. *Science*, 298(5594), pp.789–791.

Shan, G. et al., 2005. Convergent genetic programs regulate similarities and differences between related motor neuron classes in Caenorhabditis elegans. *Developmental Biology*, 280(2), pp.494–503.

Shapira, M. et al., 2003. Unitary assembly of presynaptic active zones from Piccolo-Bassoon transport vesicles. *Neuron*, 38(2), pp.237–252.

Sheldon, C. et al., 2004. Sodium influx pathways during and after anoxia in rat hippocampal neurons. *Journal of Neuroscience*, 24(49), pp.11057–11069.

Shen, K. & Bargmann, C.I., 2003. The immunoglobulin superfamily protein SYG-1 determines the location of specific synapses in C. elegans. *Cell*, 112(5), pp.619–630.

Shen, K., Fetter, R.D. & Bargmann, C.I., 2004. Synaptic specificity is generated by the synaptic guidepost protein SYG-2 and its receptor, SYG-1. *Cell*, 116(6), pp.869–881.

Shreffler, W. et al., 1995. The unc-8 and sup-40 genes regulate ion channel function in Caenorhabditis elegans motorneurons. *Genetics*, 139(3), pp.1261–1272.

Siebert, M. et al., 2015. A high affinity RIM-binding protein/Aplip1 interaction prevents the formation of ectopic axonal active zones. *eLife*, 4:e06935.

Silva, A.J., Paylor, R., et al., 1992. Impaired spatial learning in alpha-calcium-calmodulin kinase II mutant mice. *Science*, 257(5067), pp.206–211.

Silva, A.J., Wang, Y., et al., 1992. Alpha calcium/calmodulin kinase II mutant mice: deficient long-term potentiation and impaired spatial learning. *Cold Spring Harbor symposia on quantitative biology*, 57, pp.527–539.

Smith, C.J. et al., 2012. Netrin (UNC-6) mediates dendritic self-avoidance. *Nature Neuroscience*, 15(5), pp.731–737.

Smith, C.J. et al., 2013. Sensory neuron fates are distinguished by a transcriptional switch that regulates dendrite branch stabilization. *Neuron*, 79(2), pp.266–280.

Spangler, S.A. et al., 2013. Liprin-α2 promotes the presynaptic recruitment and turnover of RIM1/CASK to facilitate synaptic transmission. *The Journal of Cell Biology*, 201(6), pp.915–928.

Speese, S.D. et al., 2003. The ubiquitin proteasome system acutely regulates presynaptic protein turnover and synaptic efficacy. *Current biology : CB*, 13(11), pp.899–910.

Spencer, W.C. et al., 2011. A spatial and temporal map of C. elegans gene expression. *Genome Research*, 21(2), pp.325–341.

Stevens, B. et al., 2007. The classical complement cascade mediates CNS synapse elimination. *Cell*, 131(6), pp.1164–1178.

Sugie, A. et al., 2015. Molecular Remodeling of the Presynaptic Active Zone of Drosophila Photoreceptors via Activity-Dependent Feedback. *Neuron*, 86(3), pp.711–725.

Sugiyama, S. et al., 2008. Experience-dependent transfer of Otx2 homeoprotein into the visual cortex activates postnatal plasticity. *Cell*, 134(3), pp.508–520.

Südhof, T.C., 2012. The presynaptic active zone. *Neuron*, 75(1), pp.11–25.

Südhof, T.C. et al., 1989. A synaptic vesicle membrane protein is conserved from mammals to Drosophila. *Neuron*, 2(5), pp.1475–1481.

Syntichaki, P. et al., 2002. Specific aspartyl and calpain proteases are required for neurodegeneration in C. elegans. *Nature*, 419(6910), pp.939–944.

Tang, Y. et al., 2013. Fast vesicle transport is required for the slow axonal transport of synapsin. *Journal of Neuroscience*, 33(39), pp.15362–15375.

Tanis, J.E. et al., 2009. The potassium chloride cotransporter KCC-2 coordinates development of inhibitory neurotransmission and synapse structure in Caenorhabditis elegans. *Journal of Neuroscience*, 29(32), pp.9943–9954.

Tao-Cheng, J.-H., 2007. Ultrastructural localization of active zone and synaptic vesicle proteins in a preassembled multi-vesicle transport aggregate. *Neuroscience*, 150(3), pp.575–584.

Taru, H. & Jin, Y., 2011. The Liprin homology domain is essential for the homomeric interaction of SYD-2/Liprin-α protein in presynaptic assembly. *Journal of Neuroscience*, 31(45), pp.16261–16268.

Teruyama, R. et al., 2012. Epithelial Na^+ sodium channels in magnocellular cells of the rat supraoptic and paraventricular nuclei. *American journal of physiology. Endocrinology and metabolism*, 302(3), pp.E273–85.

Thompson-Peer, K.L. et al., 2012. HBL-1 Patterns Synaptic Remodeling in *C. elegans*. *Neuron*, 73(3), pp.453–465.

Torii, N. et al., 1995. An inhibitor for calcineurin, FK506, blocks induction of long-term depression in rat visual cortex. *Neuroscience Letters*, 185(1), pp.1–4.

Trimble, W.S., Cowan, D.M. & Scheller, R.H., 1988. VAMP-1: a synaptic vesicle-associated integral membrane protein. *Proceedings of the National Academy of Sciences of the United States of America*, 85(12), pp.4538–4542.

Tsuriel, S. et al., 2009. Exchange and redistribution dynamics of the cytoskeleton of the active zone molecule bassoon. *Journal of Neuroscience*, 29(2), pp.351–358.

Turney, S.G. & Lichtman, J.W., 2012. Reversing the outcome of synapse elimination at developing neuromuscular junctions in vivo: evidence for synaptic competition and its mechanism. *PLoS Biology*, 10(6), p.e1001352.

Tursun, B. et al., 2009. A toolkit and robust pipeline for the generation of fosmid-based reporter genes in C. elegans. *PLoS ONE*, 4(3), p. e4625.

Van Eldik, L.J. & Watterson, D.M., 2012. *Calmodulin and Signal Transduction*, Academic Press.

Varoqueaux, F. et al., 2002. Total arrest of spontaneous and evoked synaptic transmission but normal synaptogenesis in the absence of Munc13-mediated vesicle priming. *Proceedings of the National Academy of Sciences of the United States of America*, 99(13), pp.9037–9042.

Vergo, S. et al., 2011. Acid-sensing ion channel 1 is involved in both axonal injury and demyelination in multiple sclerosis and its animal model. *Brain : a journal of neurology*, 134(Pt 2), pp.571–584.

Voglis, G. & Tavernarakis, N., 2008. A synaptic DEG/ENaC ion channel mediates learning in C. elegans by facilitating dopamine signalling. *The EMBO Journal*, 27(24), pp.3288–3299.

Waites, C.L., Craig, A.M. & Garner, C.C., 2005. Mechanisms of vertebrate synaptogenesis. *Annual review of neuroscience*, 28, pp.251–274.

Waldeck, W. et al., 2011. Positioning effects of KillerRed inside of cells correlate with DNA strand breaks after activation with visible light. *International journal of medical sciences*, 8(2), pp.97–105.

Waldmann, R. et al., 1995. Molecular cloning and functional expression of a novel amiloride-sensitive Na+ channel. *The Journal of biological chemistry*, 270(46), pp.27411–27414.

Walsh, M.K. & Lichtman, J.W., 2003. In vivo time-lapse imaging of synaptic takeover associated with naturally occurring synapse elimination. *Neuron*, 37(1), pp.67–73.

Walthall, W.W. & Plunkett, J.A., 1995. Genetic transformation of the synaptic pattern of a motoneuron class in Caenorhabditis elegans. *The Journal of neuroscience : the official journal of the Society for Neuroscience*, 15(2), pp.1035–1043.

Wang, J.-Y. et al., 2014. Caspase-3 Cleavage of Dishevelled Induces Elimination of Postsynaptic Structures. *Developmental Cell*, 28(6), pp.670–684.

Wang, T. et al., 2014. Endostatin is a trans-synaptic signal for homeostatic synaptic plasticity. *Neuron*, 83(3), pp.616–629.

Wang, X. & Michaelis, E.K., 2010. Selective neuronal vulnerability to oxidative stress in the brain. *Frontiers in aging neuroscience*, 2, p.12.

Wang, X. et al., 1999. Aczonin, a 550-kD putative scaffolding protein of presynaptic active zones, shares homology regions with Rim and Bassoon and binds profilin. *The Journal of Cell Biology*, 147(1), pp.151–162.

Wang, Y. et al., 2002. A family of RIM-binding proteins regulated by alternative splicing: Implications for the genesis of synaptic active zones. *Proceedings of the National Academy of Sciences of the United States of America*, 99(22), pp.14464–14469.

Wang, Y. et al., 2008. A glial DEG/ENaC channel functions with neuronal channel DEG-1 to mediate specific sensory functions in C. elegans. *The EMBO Journal*, 27(18), pp.2388–2399.

Wang, Y. et al., 2013. Neurotoxic unc-8 mutants encode constitutively active DEG/ENaC channels that are blocked by divalent cations. *The Journal of general physiology*, 142(2), pp.157–169.

Wang, Y. et al., 1997. Rim is a putative Rab3 effector in regulating synaptic-vesicle fusion. *Nature*, 388(6642), pp.593–598.

Wang, Y., Sugita, S. & Südhof, T.C., 2000. The RIM/NIM family of neuronal C2 domain proteins. Interactions with Rab3 and a new class of Src homology 3 domain proteins. *The Journal of biological chemistry*, 275(26), pp.20033–20044.

Watanabe, S. et al., 2011. Protein localization in electron micrographs using fluorescence nanoscopy. *Nature methods*, 8(1), pp.80–84.

Weimer, R.M., 2006. UNC-13 and UNC-10/Rim Localize Synaptic Vesicles to Specific Membrane Domains. *Journal of Neuroscience*, 26(31), pp.8040–8047.

Wemmie, J.A. et al., 2003. Acid-sensing ion channel 1 is localized in brain regions with high synaptic density and contributes to fear conditioning. *Journal of Neuroscience*, 23(13), pp.5496–5502.

Wemmie, J.A. et al., 2002. The Acid-Activated Ion Channel ASIC Contributes to Synaptic Plasticity, Learning, and Memory. *Neuron*, 34(3), pp.463–477.

Wemmie, J.A., Price, M.P. & Welsh, M.J., 2006. Acid-sensing ion channels: advances, questions and therapeutic opportunities. *Trends in Neurosciences*, 29(10), pp.578–586.

White, J.G. et al., 1986. The structure of the nervous system of the nematode Caenorhabditis elegans. *Philosophical transactions of the Royal Society of London. Series B, Biological sciences*, 314(1165), pp.1–340.

White, J.G., Albertson, D.G. & Anness, M.A., 1978. Connectivity changes in a class of motoneurone during the development of a nematode. *Nature*, 271(5647), pp.764–766.

Wiesel, T.N. & Hubel, D.H., 1963. Effects of visual deprivation on morphology and physiology of cells in the cats lateral geniculate body. *J Neurophysiol*, 26, pp.978–993.

Williams, D.W. et al., 2006. Local caspase activity directs engulfment of dendrites during pruning. *Nature Neuroscience*, 9(10), pp.1234–1236.

Wilson, T. & Treisman, R., 1988. Removal of poly(A) and consequent degradation of c-fos mRNA facilitated by 3' AU-rich sequences. *Nature*, 336(6197), pp.396–399.

Winder, D.G. et al., 1998. Genetic and Pharmacological Evidence for a Novel, Intermediate Phase of Long-Term Potentiation Suppressed by Calcineurin. *Cell*, 92(1), pp.25–37.

Wu, X. et al., 2012. GABA signaling promotes synapse elimination and axon pruning in developing cortical inhibitory interneurons. *Journal of Neuroscience*, 32(1), pp.331–343.

Xiong, Z.-G. et al., 2004. Neuroprotection in Ischemia. *Cell*, 118(6), pp.687–698.

Xu, K., Tavernarakis, N. & Driscoll, M., 2001. Necrotic cell death in C. elegans requires the function of calreticulin and regulators of Ca(2+) release from the endoplasmic reticulum. *Neuron*, 31(6), pp.957–971.

Yamada, J. et al., 2004. Cl- uptake promoting depolarizing GABA actions in immature rat neocortical neurones is mediated by NKCC1. *The Journal of Physiology*, 557(Pt 3), pp.829–841.

Yamamura, H. et al., 2004. Protons activate the delta-subunit of the epithelial Na+ channel in humans. *The Journal of biological chemistry*, 279(13), pp.12529–12534.

Yang, S. & Kimmelman, A.C., 2011. A critical role for autophagy in pancreatic cancer. *Autophagy*, 7(8), pp.912–913.

Yeh, E., 2005. Identification of Genes Involved in Synaptogenesis Using a Fluorescent Active Zone Marker in Caenorhabditis elegans. *Journal of Neuroscience*, 25(15), pp.3833–3841.

Younger, M.A. et al., 2013. A presynaptic ENaC channel drives homeostatic plasticity. *Neuron*, 79(6), pp.1183–1196.

Yuan, J. & Horvitz, H.R., 1992. The Caenorhabditis elegans cell death gene ced-4 encodes a novel protein and is expressed during the period of extensive programmed cell death. *Development*, 116(2), pp.309–320.

Zeng, H. et al., 2001. Forebrain-specific calcineurin knockout selectively impairs bidirectional synaptic plasticity and working/episodic-like memory. *Cell*, 107(5), pp.617–629.

Zhang, W. et al., 2008. Intersubunit interactions between mutant DEG/ENaCs induce synthetic neurotoxicity. *Cell Death and Differentiation*, 15(11), pp.1794–1803.

Zhen, M. & Jin, Y., 1999. The liprin protein SYD-2 regulates the differentiation of presynaptic termini in C. elegans. *Nature*, 401(6751), pp.371–375.

Zhou, H.M. & Walthall, W.W., 1998. UNC-55, an orphan nuclear hormone receptor, orchestrates synaptic specificity among two classes of motor neurons in Caenorhabditis elegans. *The Journal of neuroscience : the official journal of the Society for Neuroscience*, 18(24), pp.10438–10444.

Zhou, K. et al., 2013. Position of UNC-13 in the active zone regulates synaptic vesicle release probability and release kinetics. *eLife*, 2, p.e01180.

Ziemann, A.E. et al., 2009. The Amygdala Is a Chemosensor that Detects Carbon Dioxide and Acidosis to Elicit Fear Behavior. *Cell*, 139(5), pp.1012–1021.

Ziv, N.E. & Fisher-Lavie, A., 2014. Presynaptic and postsynaptic scaffolds: dynamics fast and slow. *The Neuroscientist*, 20(5), pp.439–452.

APPENDIX A

GENE EXPRESSION PROFILING OF THE NEUROSECRETORY MOTOR NEURONS (NSM) VALIDATES THE SEQCEL METHOD

Summary

The simple, yet well-characterized nervous system of *C. elegans* has been established as an ideal model system to study neural circuitry. With the recent completion of the neuronal connectome, we now have a foundation to investigate circuit-level complexities of the nervous system. While this connectivity map can be extremely helpful to study neuronal networks, a deeper understanding of each individual cell will be critical to discern the molecular framework of the nervous system. Based on the Kuhn cell dissociation method, we have established the SeqCeL (RNA-Seq of *C. elegans* cells) technique to isolate individual neurons and generate cell-specific transcript profiles (Zhang et al. 2011). This information can be used for the identification of novel genes and verification of previously described genes. We isolated the serotonergic neuron pair, NSM and performed RNA sequencing to construct a complete transcript profile of this cell. Below, we reveal NSM-specific transcripts identified by SeqCel and validate the strength of this method to isolate and characterize the complete transcriptome of individual neurons in *C. elegans*.

Materials and Methods

Strains and Genetics

C. elegans strains were cultured at 20° C as previously described on standard nematode growth medium seeded with OP50 (Brenner 1974). The strains used in this study are outlined in **Tables A.1**.

Microscopy

Animals were immobilized on 2% agarose pads with 15mM levamisole as previously described (Smith et al. 2012). Images were collected (**Figures A.1** and **A.2**) on a Leica SP5 confocal microscope using a 63x oil objective (1 um/step). Single-plane projections were generated with the Leica Application Suite Advanced Fluorescence software (LAS-AF). Expression patterns of strains carrying GFP-reporters were visualized with a Zeiss Axioplan inverted microscope using ImageJ Micro-Manager software and a 63x oil objective (camera ORCA; Hammamatsu). Expression of GFP reporters in NSM was evaluated by the stereotyped position of the NSM neurons in the anterior bulb of the pharynx and neurite processes that extend posteriorly.

Table A.1: Strains used in this study.

Strain	Genotype
LX837	*vsIs45 [ptph-1::GFP]*
BC12468	*dpy-5(e907) I; sEx12468 [rCesF56F3.6::GFP + pCeh361]*
BC14934	*dpy-5(e907) I; sEx14934 [rCesZC317.3::GFP + pCeh361]*
BC13337	*dpy-5(e907) I; sIs12928 [rCesY39B6A.19::GFP + pCeh361]*
BC12693	*dpy-5(e907) I; sIs12693 [rCesF41E7.3::GFP + pCeh361]*
SD1614	*dpy-20(e1282) X; unc-119(ed3) III; ccIs4251 [pmyo-3::GFP::LacZ::NLS + pmyo-3p::mitoGFP + dpy-20(+)] I; stIs10447 [ceh-34p::HIS-24::mCherry + unc-119(+)]*
OH134	*otEx57 [ttx-3fl::GFP; pBx]; pha-1(e2123)III*

Results

Isolation and RNA sequencing of fluorescently-labeled NSM neurons reveals regulators of serotonergic signaling.

We developed a method for neuron isolation and RNA sequencing termed SeqCeI to collect neuronal transciptomes from single cells. We expanded on an established method to isolate *C. elegans* neurons by fluorescence activated cell sorting (FACS). Previously, the Kuhn lab isolated viable cells from *C. elegans* using a cell dissociation approach; however, this method consistently yielded low numbers of neurons (Zhang et al. 2011). In the Kuhn lab protocol, cell media is changed 24 hours after sorting; however, we found that at this stage, neurons are not adhered to the plate and are therefore discarded if washed within 1 day in culture. In our hands, neuronal isolation is robust and yields a high number of cells (Spencer et al. 2014). We applied the SeqCeI method to analyze the transcriptome of serotonergic NSM neurons.

NSM cells are paired sensory neurons (NSML and NSMR) found in the head of *C. elegans*. These neurons are serotonergic and are thought to alert the animal of the presence of food (Horvitz et al. 1982). In support of this role, ablation of NSM causes defects in the enhanced slowing response, the stereotypical decrease in movement seen when worms encounter food in their environment (Sawin et al. 2000). We obtained an NSM-specific fluorescent reporter (*pTPH-1::GFP*), to selectively label NSML and NSMR in larval (L1) animals (**Figure A.1**,(Nelson & Colón-Ramos 2013)). NSM neurons were collected from dissociated animals by FACS and RNA was extracted. Additionally, reference RNA was collected from all cells in larval (L1) animals to serve as a control (Spencer et al. 2014).

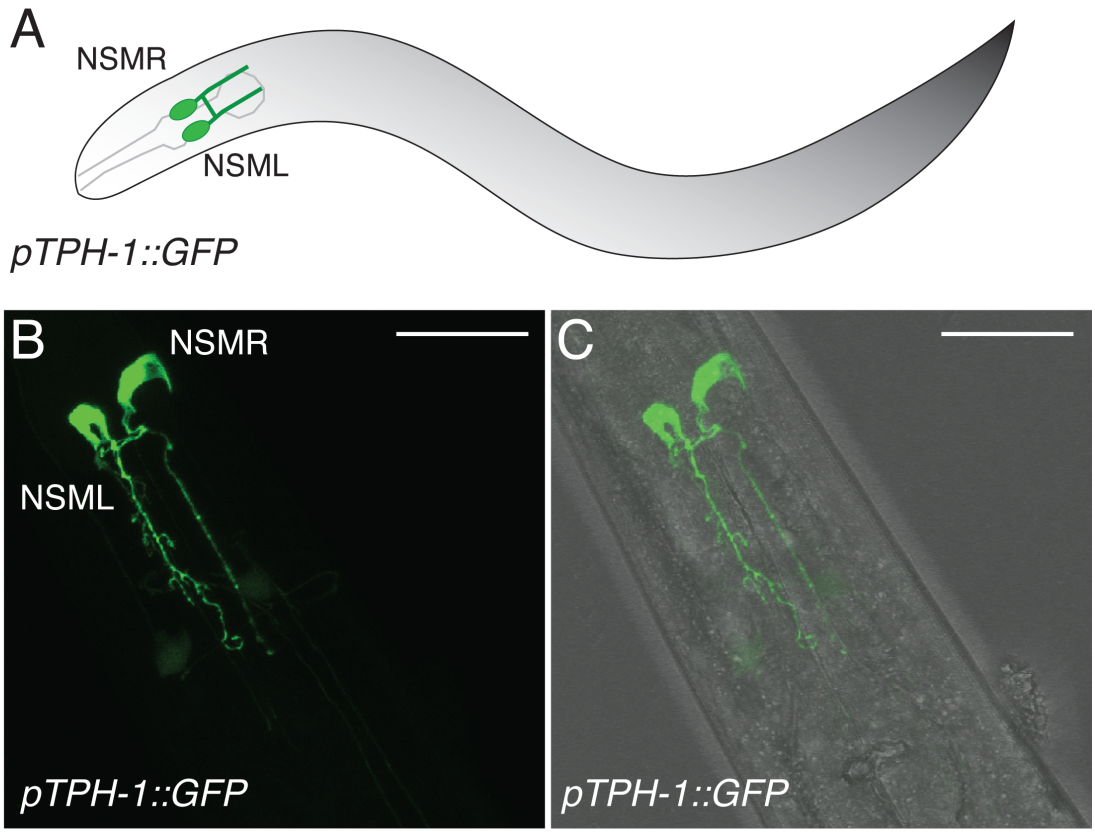

Figure A.1: A modified *pTPH-1::GFP* reporter is expressed in NSML and NSMR neurons in *C. elegans*. A. Schematic showing *pTPH-1::GFP* expression in NSML and NSMR. NSM cell bodies are located in the anterior bulb of the pharynx and send neurite processes posteriorly. Anterior is to the left, ventral is down. **B.** Z-stack confocal image of the NSML and NSMR neurons in adult animals labeled with *pTPH-1::GFP*. **C.** DIC and GFP overlay of *pTPH-1::GFP* adult. Scale bars are 20 µm.

We identified > 1,000 NSM enriched transcripts, compared to transcripts from all L1 larval cells (Q value ≤ 0.05,(Spencer et al. 2014)). To validate this list of enriched genes, we examined whether known regulators of serotonergic signaling were represented in our list. As expected, we found that several serotonergic transcripts were highly enriched in our data set (**Table A.2**). As an independent verification of our dataset, we identified several NSM-enriched transcripts that have not been previously reported to function in serotonergic neurons. We obtained transcriptional GFP reporters to examine whether these genes are expressed in NSM neurons. Indeed, we found that of the reporter genes we examined, most were expressed in NSM or in clusters of head neurons that are likely to include NSM (**Table A.3** and **Figure A.2**). These results validate the SeqCel method as a new technique to isolate and collect the transcriptome of individual neurons in *C. elegans*.

Table A.2: Serotonergic genes enriched in the NSM data set.

Gene Name	Gene Function	Fold Enrichment
mod-5	Serotonin transporter	5.56
tph-1	Tryptophan hydroxylase	4.89
cat-1	Vesicular monoamine transporter	4.29
bas-1	Aromatic amino acid decarboxylase	3.66
dop-5	Dopamine/serotonin receptor	3.17
dop-4	Dopamine receptor	2.60
unc-86	POU-homeodomain protein	2.26
mod-1	Serotonin-gated chloride channel	2.20
ser-4	Metabotropic serotonin receptor	1.98
ser-7	Metabotropic serotonin receptor	1.73

Discussion

Uncovering the transcriptome of every neuron in *C. elegans* will provide a foundation to understand individual neuron behavior, and further dissect neural circuit function. This information will be crucial to advance our understanding of how neurons work and how neurological diseases arise. In this chapter we validate the SeqCel method to isolate and generate transcript profiles of specific neurons.

Table A.3: GFP-reporter results for candidate genes enriched in the NSM profile.

GFP Reporter	Gene	Gene Function	GFP Expression
F56F3.6::GFP	*ins-17*	Insulin-like peptide	8-10 head neurons, VNC, DNC
Y39B6A.19::GFP	*twk-46*	Potassium channel	NSM, 15 head neurons, 22 VNC neurons, PDE
F41E7.3::GFP	*npr-6*	Neuropeptide receptor	NSM, 14-16 head neurons, 5 VNC neurons
C10G8.6::GFP	*ceh-34*	Homeodomain protein	NSM, additional head neurons
C40H5.5::GFP	*ttx-3*	LIM homeodomain protein	Multiple head neurons
ZC317.3::GFP	*glc-3*	Glutamate-gated chloride channel	12-14 head neurons, 1 tail neuron

SeqCel method generates transcriptome profiles of individual neurons

Previous methods to isolate RNA from specific cells in *C. elegans* included microdissection and mRNA-tagging. Microdissection, including laser microdissection and pressure catapulting (LMPC) involves using a pulsed laser to isolate individual cells from the surrounding tissue (Burgemeister 2005). While this technique provides very pure

samples for subsequent analysis, it is technically challenging and requires high accessibility to the cell type of interest. It is also unclear if this technique can be used to isolate the interconnected neurons of *C. elegans*, many of which send out long neurite processes throughout the body of the worm. Alternatively, the mRNA-tagging method can be used to isolate mRNA from specific *C. elegans* neurons as previously described (Petersen et al. 2011). This technique requires transgenic expression of a tagged poly-A binding protein, expressed only in the cells of interest. Unfortunately, construction and proper expression of these transgenes can be problematic and immunoprecipitation of the tagged-mRNA can pull down non-specific targets. Here, we validate the SeqCel method which isolates individual neurons using cell-specific fluorescent markers and FACS. The cell-specific fluorescent markers are already widely available for most neurons in *C. elegans*; additionally, a combination of multiple markers can be used to label and isolate specific subsets of cells (i.e,. GFP and RFP). Lastly, this technique should be applicable for animals of all ages, and can be used to monitor transcript level changes throughout development.

Analyzing neuronal transcriptomes to understand neurological disease

Neurological disorders, such as Schizophrenia and Alzheimer's Disease, affects many people in the world. Unfortunately, we understand very little about the origin of most neurological diseases, and therefore, there is a lack of available treatments. Developing a complete transcriptome map of multiple neuronal cells type will allow us to identify patterns of neuronal dysfunction, especially since many of these disorders likely arise from a genetic predisposition. One example of this includes the DISC-1 (disrupted

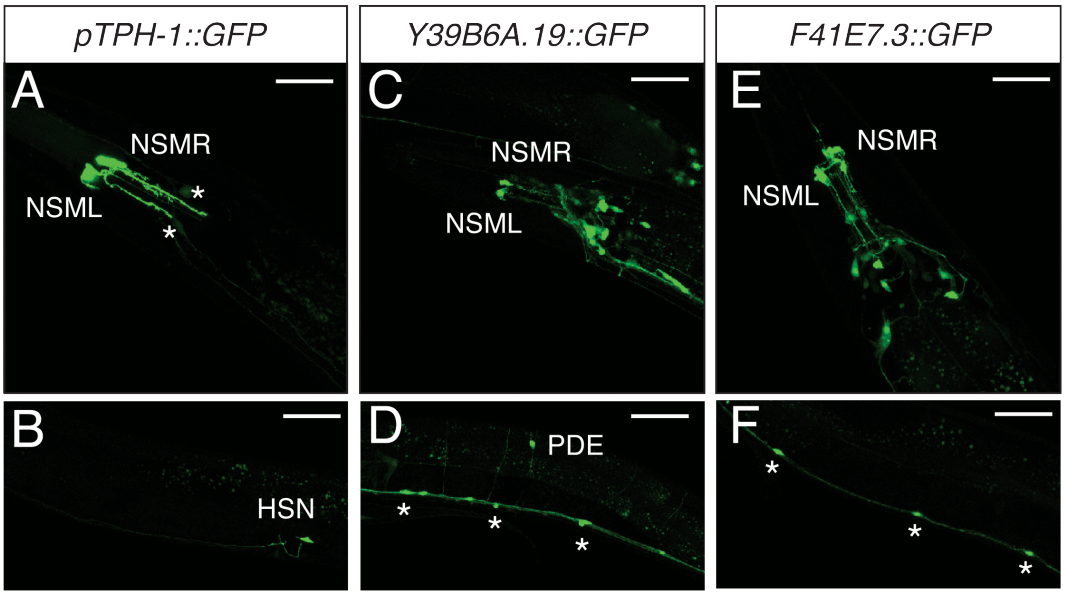

Figure A.2: GFP reporter strains validate the NSM gene expression profile. A/B. Bright GFP (*pTPH-1::GFP*) labels NSML/R (**A**), and HSN (**B**) in adult animals; however, early larval (L1) expression is limited to the NSML/R neurons. Very dim expression is also seen in ADFL and ADFR sensory neurons, annotated with asterisks (**A**). **C-F**. The *Y39B6A.19/twk-46* and *F41E7.3/npr-6* genes were significantly enriched in the NSM data set. GFP reporters for these genes show expression in NSML and NSMR, in addition to multiple other neurons. **C**. GFP reporter expression for *Y39B6A.19/twk-46* shows strong expression in NSML/R and 15 other head neurons. **D.** GFP expression is also seen in 22 ventral nerve cord neurons (asterisks) and the sensory neuron PDE. **E.** Reporter expression for *F41E7.3/npr-6* shows strong GFP fluorescence in NSML/R and 14-16 other head neurons. Additionally, GFP is expressed in 5 ventral nerve cord neurons (asterisks). Scale bars are 20 μm.

in schizophrenia 1) gene in schizophrenia. DISC-1 was identified in a family with a high incidence rate of schizophrenia, and was found to be deleted in all of the affected family members (Margolis & Ross 2010). Further investigation into the mechanism of DISC-1 function has identified it as an important regulator of signaling pathways, (including Wnt and Rac) which dictate axon guidance, neuronal migration, and synapse formation (Mao et al. 2010; Komiya & Habas 2008). Although this mutation was originally isolated in humans, the implicated pathways are highly-conserved in *C. elegans*; transgenic expression of DISC-1 in *C. elegans* induces axon guidance defects and ectopically activates the Rac signaling pathway (Chen et al. 2011). Evaluating the complete transcriptome of normal and damaged neurons, such as those expressing DISC-1 in *C. elegans*, will reveal novel effectors of neurological diseases and provide potential therapeutic targets.

Author Contributions

NSM neurons were extracted by Rebecca McWhirter, and the fluorescent cells were isolated by Fluorescence-Activated-Cell-Sorting (FACS) at the Vanderbilt Flow Cytometry Core. Rebecca collected RNA from the sorted NSM cells and RNA sequencing was performed by the Vanderbilt Sequencing Core. The RNA sequencing data was analyzed by Clay Spencer, David Miller, Owen Thompson, and LaDeana W. Hillier. Tyne Miller-Fleming imaged fluorescent reporters for genes that were enriched in the NSM dataset and collected the images shown in this chapter.

Acknowledgments

We thank D. Colon-Ramos for LX837 *vsIs45 [ptph-1::GFP].* Some strains used in this study were provided by the CGC, which is funded by the NIH Office of Research Infrastructure Programs (P40 OD010440). This work was supported by the Vanderbilt Silvio O. Conte Center grant MH078028 (TMF) and NIH Grants R01 NS26115 (DMM) and U01 HG004263 (RHW/DMM). The images and tables from this chapter were adapted from a previously published study (Spencer et al. 2014).

Appendix B: Plasmids used/generated for these studies.

Plasmid Name	Made by	Selection	Description
pTWM1	TM	Amp	pttr-39::GFP::utrophin
pTWM2	TM	Amp	punc-25::GFP::utrophin
pTWM3	TM	Amp	pttr-39::GFP::utrophin; unc-119+
pTWM4	TM	Amp	punc-25::GFP::utrophin; unc-119+
pTWM5	TM	Spec	GFP::act-1 in pCR8
pTWM6	Invitrogen	Spec	pCR8
pTWM7	TM	Amp	punc-25::GFP::act-1
pTWM8	Invitrogen	Amp	pCR2.1
pTWM10/pRRF207	P. Roy	Amp	him-4p::GFP::act-1
pTWM13	TM	Amp	pttr-39::ARX-5 F csRNAi; unc-119+
pTWM14	TM	Amp	pttr-39::ARX-5 R csRNAi; unc-119+
pTWM15	TM	Amp	pttr-39::ARX-5 R csRNAi; punc-25::mCherry
pTWM16	TM	Amp	punc-25::act-1::GFP; unc-119+
pTWM17	TM	Spec	ARX-5 in pCR8
pTWM18/pCJS93	C. Smith	Amp	pF49h12.4::unc-40::GFP
pTWM19/pCJS04	C. Smith	Amp	pF49h12.4::mCherry
pTWM20		Amp	L4440
pTWM21	TM		arx-1 in pCR8
pTWM22/pMLH35	M. Hacker	Amp	punc-25::TOM-20::mRFP
pTWM23/pMLH40	M. Hacker	Amp	punc-25::TOM-20::mRFP; unc-119+
pTWM24/pMLH132	M. Hacker	Amp	punc-25::mCherry
pTWM25/pSA47	S.Petersen	Amp	pttr-39::irx-1 F csRNAi; unc-119+
pTWM26/pSA49	S.Petersen	Amp	pttr-39::irx-1 R csRNAi; punc-25::mCherry
pTWM27/pSA57	S.Petersen	Amp	punc-25::dys-1::YFP
pTWM28/pSA76	S.Petersen	Amp	pttr-39::unc-8; unc-119+
pTWM29/pSA79	S.Petersen	Amp	punc-25::rab-3::mCherry
pTWM30/pG2M19	O. Hobert	Amp	ceh-22::GFP
pTWM31/pBX	M. Granato	Amp	pha-1+
pTWM32	Y. Jin	Amp	punc-25::GFP
pTWM33/pRF4	C. Mello	Amp	rol-6
pTWM34	TM	Amp	arx-5 RNAi clone
pTWM35	TM	Amp	pttr-39::ARX-5::GFP
pTWM36	TM	Amp	pttr39::ARX-5::mCherry
pTWM37	TM	Amp	pttr-39::ARX-5::GFP; unc-119+
pTWM38	TM	Amp	pttr-39::ARX-5::mCherry; unc-119+
pTWM39	TM	Amp	arx-5 F csRNAi in pCR2.1
pTWM40	TM	Amp	arx-5 R csRNAi in pCR2.1
pTWM41	TM	Amp	pttr-39::arx-5 F csRNAi; unc119+
pTWM42	TM	Amp	pttr-39::arx-5 R csRNAi; u119+
pTWM43	TM	Amp	
pTWM44	TM	Amp	pttr-39::arx-5 R csRNAi; punc-25::mCherry
pTWM45	TM	Amp	pflp-13 in pCR2.1
pTWM46	TM	Amp	pflp-13::rab-3::mCherry
pTWM47	Stratagene	Amp	pBlueScript II
pTWM49/pMLH221	M. Hacker	Amp	pMLH221 pttr39::membrane bound::mCherry
pTWM50/pG2M17	O. Hobert	Amp	pelt-2::GFP
pTWM51	TM	Amp	punc-25::UNC-47
pTWM52/pG2M20	Colon-Ramos	Amp	pUNC122::GFP coelmocytes::GFP

pTWM54	Invitrogen	Amp	TOPO Blunt end vector
pTWM55/X	C.Bargmann	Amp	punc25::GFP::UNC2
pTWM56/pSA30	S. Petersen	Amp	UNC8::GFP; unc-119+ UNC8 fosmid
pTWM57	S. He	Amp	pflp-13::3xflagmCherry::RAB3
pTWM59/pCL32	M. Francis	Amp	pflp-13::ACR12::GFP
pTWM60	L. Bianchi	Amp	UNC-8 cDNA in pSGEM
pTWM61	L. Bianchi	Amp	UNC-8 G387E cDNA in pSGEM
pTWM62	TM	Amp	punc-25::UNC-8::GFP
pTWM63	TM	Amp	punc-25::UNC-8G387::GFP
pTWM64	TM	Amp	punc-25::UNC-8::mCherry
pTWM65	TM	Amp	punc-25::UNC-8G387::mCherry
pTWM66/pCFJ601	E.Jorgensen	Amp	peft-3::MOSASE
pTWM67/pCFJ90	E.Jorgensen	Amp	pmyo-2::mCherry
pTWM68/pGH8	E.Jorgensen	Amp	prab-3::mCherry
pTWM69/pCFJ104	E.Jorgensen	Amp	pmyo-3::mCherry
pTWM70/pCFJ151	E.Jorgensen	Amp	
pTWM71/pCFJ352	E.Jorgensen	Amp	R and L recombinase; unc-119+
pTWM72			
pTWM73	L. Bianchi	Amp	UNC-8 cDNA D693A in pGEM
pTWM74	L. Bianchi	Amp	UNC-8 cDNA D693C in pGEM
pTWM75	L. Bianchi	Amp	UNC-8 cDNA D693G in pGEM
pTWM76/pMA122	AddGene	Amp	hsp::PEEL-1
pTWM77/pDD162	AddGene	Amp	peft-3::Cas9 empty sgRNA
pTWM78/pDD104	AddGene	Amp	peft-3::Cre
pTWM79/pEVL26	B. Ackley	Amp	punc-25::mCherry::RAB-3
pTWM80/pBA109	B. Ackley	Amp	punc-25::SNB-1::dsRED
pTWM81/pCCM935	AddGene	Kan	peft-3::Cas9 unc-22 sgRNA
pTWM82	TM	Amp	peft-3::Cas9 unc-8 sgRNA2
pTWM83	L. Bianchi	Amp	UNC-8 G387E cDNA/MEC-4 TM2 in pGEM
pTWM84	TM	Amp	peft-3::Cas9 unc-8 sgRNA3
pTWM85	TM	Amp	peft-3::Cas9 unc-8 sgRNA4
pTWM86	TM	Amp	peft-3::Cas9 unc-8 sgRNA5
pTWM87	TM	Amp	peft-3::Cas9 unc-8 sgRNA6
pTWM88	J. Kaplan	Amp	punc-129::UNC-13L::mCherry
pTWM89	J. Kaplan	Amp	psnib::UNC-13S
pTWM90	TM	Amp	punc-25::UNC-13LcDNA::GFP
pTWM91	TM	Amp	pttr-39::UNC-8cDNA::GFP
pTWM92	TM	Amp	pttr-39::UNC-8cDNA
pTWM93	TM	Amp	pacr-2::UNC-8cDNA::GFP
pTWM94	TM	Amp	pacr-2::UNC-8cDNA
pTWM95	TM	Amp	punc8::GFP wild type
pTWM96/pAK049	I. Mori	Amp	pgcy-8::TAX-6 cDNA::GFP
pTWM97/pAK050	I. Mori	Amp	pgcy-8::TAX-6gf cDNA::GFP
pTWM98	TM	Amp	punc-8::GFP: mutated unc55 binding site
pTWM99	TM	Amp	punc-25::TAX-6cDNA::GFP
pTWM100/pN6HSII	VAPR	Kan	N-terminal His tagging vector from VAPR
pTWM101/pAT108a	VAPR	Kan	N-terminal MBP tagging vector from VAPR
pTWM102/pAT108b	VAPR	Kan	N-terminal MBP tagging vector from VAPR
pTWM103	TM	Kan	2.61 MBP::UNC-8 ECD
pTWM104	TM	Kan	2.67 MBP::UNC-8 ECD
pTWM105	TM	Kan	3.61 MBP::UNC-8 ECD

pTWM106	TM	Kan	3.62 MBP::UNC-8 ECD
pTWM107	TM	Spec	UNC-8 ECD in pCR8 (BamH1/EcoR1)
pTWM108	TM	Kan	6NHIS::UNC-8 ECD (BamH1/EcoR1)
pTWM109	TM	Amp	punc-25::3xflagmCherry::OIG-1
pTWM110	TM/A.Beers	Amp	punc-25::3xflagmCherry::UNC-8cDNA
pTWM111	TM	Amp	peft-3::Cas9::LGC-36 sgRNA
pTWM112	TM	Amp	peft-3::Cas9::LGC-37 sgRNA
pTWM113	TM	Amp	peft-3::Cas9::LGC-38 sgRNA
pTWM114	TM	Amp	pttr-39::3xflagmCherry::UNC-8 cDNA
pTWM115	TM	Kan	6NHISMBP::UNC-8 ECD

Appendix References

Brenner, S., 1974. The genetics of Caenorhabditis elegans. *Genetics*, 77(1), pp.71–94.

Burgemeister, R., 2005. New aspects of laser microdissection in research and routine. *The journal of histochemistry and cytochemistry : official journal of the Histochemistry Society*, 53(3), pp.409–412.

Chen, S.-Y., Huang, P.-H. & Cheng, H.-J., 2011. Disrupted-in-Schizophrenia 1-mediated axon guidance involves TRIO-RAC-PAK small GTPase pathway signaling. *Proceedings of the National Academy of Sciences*, 108(14), pp.5861–5866.

Horvitz, H.R. et al., 1982. Serotonin and octopamine in the nematode Caenorhabditis elegans. *Science*, 216(4549), pp.1012–1014.

Komiya, Y. & Habas, R., 2008. Wnt signal transduction pathways. *Organogenesis*, 4(2), pp.68–75.

Mao, W., Wordinger, R.J. & Clark, A.F., 2010. Focus on molecules: SFRP1. *Experimental eye research*, 91(5), pp.552–553.

Margolis, R.L. & Ross, C.A., 2010. Neuronal signaling pathways: genetic insights into the pathophysiology of major mental illness. *Neuropsychopharmacology : official publication of the American College of Neuropsychopharmacology*, 35(1), pp.350–351.

Nelson, J.C. & Colón-Ramos, D.A., 2013. Serotonergic neurosecretory synapse targeting is controlled by netrin-releasing guidepost neurons in Caenorhabditis elegans. *Journal of Neuroscience*, 33(4), pp.1366–1376.

Petersen, S.C. et al., 2011. A Transcriptional Program Promotes Remodeling of GABAergic Synapses in Caenorhabditis elegans. *Journal of Neuroscience*, 31(43), pp.15362–15375.

Sawin, E.R., Ranganathan, R. & Horvitz, H.R., 2000. C. elegans locomotory rate is modulated by the environment through a dopaminergic pathway and by experience through a serotonergic pathway. *Neuron*, 26(3), pp.619–631.

Smith, C.J. et al., 2012. Netrin (UNC-6) mediates dendritic self-avoidance. *Nature Neuroscience*, 15(5), pp.731–737.

Spencer, W.C. et al., 2014. Isolation of specific neurons from C. elegans larvae for gene expression profiling. *PLoS ONE*, 9(11), pp.e112102–e112102.

Zhang, S., Banerjee, D. & Kuhn, J.R., 2011. Isolation and culture of larval cells from C. elegans. *PLoS ONE*, 6(4), p.e19505.